SOME ASPECTS OF ION MOTION IN LIQUID HELIUM : THE STUDY OF MOBILITY DISCONTINUITIES IN SUPERFLUID HELIUM (AND LIQUID NITROGEN), AND THE INFLUENCE OF GRIDS ON THE TRANSMISSION OF AN ION BEAM

Christopher S. M. Doake

A Thesis Submitted for the Degree of PhD
at the
University of St. Andrews

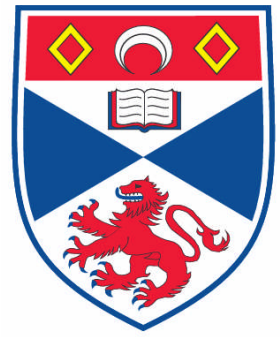

1972

SOME ASPECTS OF
ION MOTION IN LIQUID HELIUM

The study of mobility discontinuities in superfluid helium (and liquid nitrogen), and the influence of grids on the transmission of an ion beam.

A Thesis

presented by

Christopher S.M. Doake, B.Sc.

to the

University of St. Andrews

in application for the Degree

of Doctor of Philosophy.

CERTIFICATE

I certify that Christopher S.M. Doake, B.Sc., has spent nine terms at research work in the School of Physical Sciences, St. Andrews University, under my direction, that he has fulfilled the conditions of Ordinance No. 16 (St. Andrews) and he is qualified to submit the accompanying thesis in application for the Degree of Doctor of Philosophy.

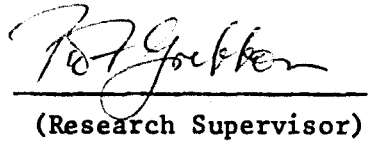

(Research Supervisor)

CAREER

I first matriculated in the University of St. Andrews in October 1962. I studied Mathematics and Physics, and obtained a First Class B.Sc. Honours in Physics in 1966.

In October 1966, following the award of an S.R.C. Research Studentship, I was enrolled as a research student under Ordinance 12, and was transferred to Ordinance 16 in October 1967 as a candidate for the degree of Ph.D.

ACKNOWLEDGEMENTS

I should like to express my deep gratitude to Dr. P.W.F. Gribbon for his unflagging interest, patient guidance and help while supervising this work.

I would also like to thank Professor J.F. Allen for the excellent facilities available for doing research, and his interest in the work.

The technical staff were invaluable, especially Mr. J. McNab for his advice and encouragement while designing and building the cryostat, and Mr. R.H. Mitchell for providing an ample supply of liquid helium.

CONTENTS

ABSTRACT

INTRODUCTION

CHAPTER 1

I Microscopic Theory 1

II Tisza and Landau Theories 4

III Hydrodynamic Equations 6

IV Vorticity 7

V Mutual Friction and Turbulence 8

CHAPTER 2

Structure and Properties of Ions

A. Structure

I Positive Ions 14

II Negative Ions 14

B. Properties

I Low Field Mobility

1. Temperature Dependence 17

2. Pressure Dependence 19

II High Field Behaviour 20

III Interaction with Vorticity 25

CHAPTER 3

Experimental Detail

I Velocity Measurement

(a) Triode 28

(b) Gate Spectrometer 31

II Experimental Equipment

(a) Pulse Generator 32

(b) Other Electronics 34

(c) Temperature Measurement 35

(d) Cryostat 35

(e) Ion Cell 36

CHAPTER 4

Mobility Discontinuities

I History

A. Reported Discontinuities 38

B. Temperature Dependence of v_c 41

C. Absence of Discontinuities 43

D. Comment on Velocity Measurement 44

E. Theories of Discontinuities 51

I Vortex Ring Production Theories

(a) Huang and Olinto 52

(b) Di Castro 56

(c) Jones 58

Summary of Theories

1. Circulation $n > 1$ 61

2. Criterion for Vortex Shedding 64

3. Criteria for Periodicity of v_c 66

Summary 70

II Vibrating Ion Theory 71

F. Experimental Results 75

G. Summary 80

II Results

A. Velocity Measurement 82

B. Representation of Results 87

C. Theoretical Curves 91

D. Discussion 96

E. Summary 101

CHAPTER 5

D.C. Characteristics

I Introduction 102

II Ideal Grid

(a) Theory 104

(b) Transmission Coefficient 105

III Results

(a) Introduction 108

(b) Low Field Results 112

(c) High Field Results 115

(i) Negatively Charged Vortex Rings 116

Properties of E_{max}

1. Temperature Dependence 117

2. Vortex Ring Velocity at E_{max} 118

3. Pressure Dependence 118

4. Properties of I_{max} 121

5. Peak Shape 122

(ii) Positively Charged Vortex Rings 124

IV Comparison of High Field Results with Second Sound Attenuation 125

V Discussion of High Field Results

(a) Formation of Vorticity 131

(b) Influence of the Extracting Field 135

(c) High Field ($>E_{max}$) Behaviour 137

(d) Behaviour of I_{max} 139

(e) Criticism and Conclusions 143

VI Fast Ions

(a) Introduction 146

(b) Fast Ion Models

1. Ion Trapping in Grid Vorticity 147

2. High Energy Vortex Rings 148

3. Ion Trapping in Decaying Turbulence 150

(c) Photoejection evidence for fast ions 154

(d) Conclusion 155

VII Negative Conductance

(a) Introduction 159

(b) High Field Domain Formation 160

(c) Relevance to Liquid Helium 161

CHAPTER 6

Ion Motion in Liquid Nitrogen

I Introduction 163

II D.C. Characteristics 165

(a) Triode 165

(b) Multiple Grid 166

III A.C. Results

1. Introduction 167

2. Interpretation of the Current-Frequency Curves 168

3. Comparison of I_o with D.C. Characteristics 169

4. Mobility Results 169

5. Comparison with other Reported Results 171

6. Liquid Motion 172

7. Variation of Mobility with Field 175

8. Analysis of Results 176

9. Discussion 178

10. Relation to Mobility Discontinuities 181

APPENDIX I

APPENDIX II

APPENDIX III

SUMMARY

~~SUGGESTIONS FOR FURTHER WORK~~

FIGURE CAPTIONS

REFERENCES

ABSTRACT

We were unable to verify the existence of ion mobility discontinuities in either superfluid helium at 1 K or liquid nitrogen. The velocity-field dependence in helium was described by an increased interaction with the normal fluid, due to an increase in the roton number density close to the ion surface. The mobility results in nitrogen were interpreted as being due to liquid motion, following a theory by Kopylov.

The D.C. results showed that the effect of a grid on the transmission of an ion beam could be described by a field dependent grid transmission coefficient, independent of the ion velocity. The vortex ring transmission through a grid was a complex function of vorticity being captured by the grid, the capture and escape probabilities of the bare ions by vorticity, and the onset for vorticity propagating throughout the ion cell.

INTRODUCTION

For the past decade the study of ion motion in liquid helium has provided a powerful technique for investigating superfluid flow. Negative ions have been used as microscopic probes for detecting vorticity in turbulent flow, and both signs of ion produce quantized vorticity in the form of vortex rings. These vortex rings have been shown to follow the classical hydrodynamic description, with modifications to allow for the vortex core. The binding of ions to vorticity has been explained, but not the initial formation and growth of the ring.

The low field ion mobility is interesting in that the existence of mobility discontinuities occuring at periodic intervals of a critical ion drift velocity cannot be explained by present theories of superfluid hydrodynamics. The discovery of these discontinuities in classical liquids confuses the issue, as do the reports denying the existence of discontinuities.

This work was started to test one of the ideas put forward to explain discontinuities in superfluid helium (the vibrating ion theory by Cope and Gribbon). We were however unable to measure a discontinuity in either helium or liquid nitrogen. In the belief that the electrode arrangement, and in particular the grid through which the ion beam was transmitted, had some affect on the current that might explain the phenomenon we carried out extensive work under D.C. conditions. This led on to examining the effect of the grid on the transmission of high energy vortex rings.

CHAPTER 1

The purpose of this chapter is to outline the background theory of liquid helium so as to provide the relevant equations and concepts for a proper appreciation of the results contained in the later chapters. In particular, the purpose is to introduce the concepts of a vortex line, vorticity and turbulence because much of the work in Chapters 4 and 5 is concerned with the vorticity produced by ions in HeII.

MICROSCOPIC THEORY

I. The macroscopic quantum effects seen in liquid HeII can be related to the idea of a condensate wave function. The theory is based on a phenomenological approach in which a 'condensation' of particles in an ideal Bose gas takes place into a single particle quantum energy state. This condensation can occur below some critical temperature in any fluid system of interacting particles in which there is an absence of order in configurational space. The main effect of the particle interactions is to restrict the fraction of condensed particles to some value less than unity as the temperature tends to zero.

The condensate in a single particle energy state may be described by a mean value condensate wave function

$$\langle\psi(r,t)\rangle = f(r,t)\ \exp(i\phi(r,t)) \qquad (1)$$

which has phase coherence throughout the system. The condensate is in a state with momentum $h\nabla\phi$, and if the momentum does not

alter rapidly with position $\underline{r}$ and time $\underline{t}$, then $f(r,t)$ is constant. This corresponds to a superflow with a velocity $V_s(r)$ given by

$$V_s(r) = \frac{\hbar}{m} \cdot \nabla\phi \ . \qquad (2)$$

If the flow is uniform then $V_s(r)$ is constant in space, and it can be identified with a particle velocity V_s. The whole condensate is then in a state with particle momentum $m V_s$ and mass density ρ_s, and there is a mass flow $\rho_s V_s$ in the system. If the momentum is large or varies rapidly with position, V_s is still defined by (2) but the mass flow must be corrected for the dependence of ρ_s on velocity.

In a superfluid the velocity field is irrotational in a simply-connected region of the fluid : there is no vorticity or $\nabla \times V_s = 0$, and the phase ϕ in (1) is single-valued. However in a multiply-connected region, ϕ need only return to its original value $\pm 2n\pi$ on traversing a path round a nonsuperfluid obstacle:

$$\oint \nabla\phi.dr = 2n\pi,$$

and using (2)
$$\oint V_s(r).dr = \frac{nh}{m} \qquad (3)$$

This expresses the quantisation of the circulation in a superfluid. It is a'macroscopic' quantum effect because it depends on a large number of atoms having each the same quantised angular momentum.

In an ideal Bose gas in equilibrium the energy of a particle in the condensate is the chemical potential μ per

particle in the system. If this is true for any superfluid system then firstly, (1) will be modified by an additional factor,

$$\langle\psi(r,t)\rangle = f(r,t)\ \exp(i(\phi(r) - \tfrac{\mu t}{\hbar}))$$

and, secondly, if there is a potential difference $\mu_1 - \mu_2$ between two points 1 and 2 in the system then the phases ϕ_1 and ϕ_2 must change with time to produce a motion of quantised circulation or vortices between 1 and 2, according to

$$\langle \mu_1 - \mu_2 \rangle_{av} = h \langle \frac{dn}{dt} \rangle_{av}$$

where $\langle\ \rangle_{av}$ denotes time average, and $\frac{dn}{dt}$ is the rate of motion of the vortices. This concept is of general validity, and forms a useful basis for the discussion of dynamic effects such as the various Josephson experiments in a superfluid system.

The ability of an ideal Bose gas to exhibit superfluid flow $\rho_s V_s$ depends on the velocity dependence of ρ_s. If there are weak interactions between particles then at a certain critical velocity V_c, ρ_s goes to zero and superflow is destroyed. This happens when the temperature falls to zero, so the ideal Bose gas picture fails to account for superfluidity. However when the interacting particles are no longer considered to be free classical particles with energies $\varepsilon = p^2/2m$, but rather to be particles with an excitation spectrum, that has been modified

by the interactions then the critical velocity $V_c = \frac{dE}{dp}$ is finite. The lowest energy excitations in the modified spectrum are phonons and will be discussed in II.

Superfluidity is connected therefore not only with the presence of a condensate but also with the interactions between the atoms. Any system of interacting boson particles with no configurational order would show superfluidity below a critical temperature : in practice, only liquid He^4 and superconducting electron pairs behave in this way.

II. Tisza and Landau Theories

The properties of superfluid helium have been explained adequately by Tisza's two-fluid model. In the model there is a viscous 'normal' fluid component of density ρ_n, and a superfluid component of density ρ_s, such that the total density $\rho = \rho_n + \rho_s$. Each component has its own independent low velocity field V_n and V_s: the total momentum density $j = \rho_n V_n + \rho_s V_s$ can lead to a counterflow in the two fluids. The superfluid has zero viscosity and has no entropy. ρ_s varies with temperature, such that ρ_s/ρ is zero at the critical temperature, or the λ-point, and increases to unity as the temperature goes to zero. It should be pointed out that a simple connection does not exist between ρ_s and the fraction of particles in the condensate (I).

The thermodynamic properties of liquid helium depend on the energy spectrum of the excitations. The distribution function n(p) for a system obeying Bose statistics is given by

$$n(p) = \frac{1}{h^3} \int (e^{\frac{\varepsilon(p)}{kT}} - 1)^{-1}.$$

The spectrum proposed by Landau consisted of phonons with low energy $\varepsilon = pc$ and rotons with energies $\varepsilon = \Delta + \frac{(p - p_o)^2}{2\mu_o}$ above the energy gap Δ at a minimum in the ε- p spectrum.[o] These energies apply in a frame of reference moving with the background superfluid at a velocity V_s. The energy $\varepsilon(p)$ in the function n(p) is however the energy of the excitations in a frame of reference that moves with the excitations, so that n(p) has to be modified by a Galilean transformation into

$$n(p) = \frac{1}{h^3} \int (e^{\frac{\varepsilon - p.V}{kT}} - 1)^{-1}$$

where $V = V_n - V_s$ is the relative velocity between the two frames of reference.

This means, for example, that the average momentum density, given by

$$j = \int p.n(\varepsilon - p.V)\ d^3p,$$

can be reduced and equated to the excitation density ρ_n by $j = \rho_n V$ at small velocities to give the expression

$$\rho_n = \frac{4\pi}{3} \int \frac{dn}{d\varepsilon} . p^4\ dp$$

This example emphasises that ρ_n depends on the statistical nature of the system, and on the form of the energy spectrum. Any microscopic theory therefore must produce the Landau excitation spectrum from first principles to have any weight, since this spectrum has served as a successful method of explaining ~~in~~ many of the properties of superfluid helium.

III. Hydrodynamic Equations

The flow of HeII can be described by the appropriate hydrodynamic equations of motion which for the two fluid model are similar to those classical fluids. For a perfect fluid with zero viscosity the conservation of momentum is given by Euler's equation

$$\rho \frac{DV}{Dt} = f$$

in which f is the force per unit volume in the fluid. For the superfluid component of HeII this becomes

$$\rho_s \frac{DV_s}{Dt} = -\frac{\rho_s}{\rho} \nabla P + \rho_s S\nabla T \qquad (4)$$

and for the normal fluid component

$$\rho_n \frac{DV_n}{Dt} = -\frac{\rho_n}{\rho} \nabla P - \rho_s S\nabla T + \eta_n \nabla^2 V_n \qquad (5)$$

where $$\frac{DV}{Dt} = \frac{\partial V}{\partial t} + (V.\nabla)V$$

The mass continuity equation is

$$\frac{\partial \rho}{\partial t} + \nabla.J = 0 \qquad (6)$$

where $$J = \rho_s V_s + \rho_n V_n \qquad (7)$$

and the conservation of entropy equation is

$$\frac{\partial}{\partial t}(\rho S) + \nabla.(\rho S V_n) = 0 \qquad (8)$$

IV. Vorticity

The above equations (4) - (8) hold only for low velocities. Superfluid vortices are formed at high flow velocities where their production is energetically more favoured than that of phonons and rotons. Since the circulation of a vortex line is quantised in units of $\frac{h}{m}$ we have

$$V_s(r) = \frac{n\,h}{m} \cdot \frac{1}{r} \quad .$$

The energy per unit length of a vortex line or the kinetic energy of the fluid rotating about a core of radius 'a' of atomic dimensions in a vessel of radius 'b' is

$$E = \int_a^b \tfrac{1}{2}\rho_s V^2 . 2\pi r . dV = \pi\rho_s \frac{h^2}{m^2} . \ell n \frac{b}{a} \quad .$$

Classically a vortex must have its ends on a boundary or be bent into a closed loop or ring. The energy of such a ring of radius R is given by

$$E_R \simeq 2\pi^2 \rho_s \frac{h^2}{m^2} . R . \ell n(\frac{R}{a})$$

or more exactly

$$E_R = \tfrac{1}{2}\rho_s \kappa^2 R . \ell n(\frac{8R}{a} - \frac{7}{4}) \qquad (9)$$

where κ is the circulation of the ring. The velocity of the ring is

$$V_R = \frac{\kappa}{4\pi R} . \ell n(\frac{8R}{a} - \frac{1}{4}) \qquad (10)$$

A vortex ring carries no net linear momentum, but when a ring is formed there is a change in momentum of the system equal to the impulse of the ring (P), (Lin 1963), given by

$$P = \pi \rho_s \kappa R^2 .$$

This leads for a channel of width 'd' to a critical velocity

$$V_{crit} = \frac{E}{P} \simeq \frac{\kappa}{\pi} \cdot \frac{1}{d} \cdot \ell n\left(\frac{d}{2a}\right) . \qquad (11)$$

This velocity is only of the order of a few cms sec^{-1} for $d \simeq 10^{-3}$ cm, and is much smaller than the velocity $\simeq 60$ m sec^{-1} necessary to create rotons at the minimum of the Landau $\varepsilon - p$ spectrum.

V. Mutual Friction and Turbulence

When a classical fluid is rotated at an angular frequency Ω in a container, the profile of the fluid surface is a parabola given by

$$y = \frac{\Omega^2 . r^2}{2g} \qquad (12)$$

The fluid rotates like a solid body, since $V = \Omega . r$, and $\nabla \times V = 2\Omega$. If $\nabla \times V_s = 0$ in liquid helium, then on rotation the profile should alter to

$$y = \frac{\rho_n}{\rho} \cdot \frac{\Omega^2 r^2}{2g} \qquad (13)$$

with only the normal fluid involved in the rotation. It was found however that liquid helium obeyed the classical result (12). This can be explained if it is assumed that a vortex

line density n_ℓ is formed in the superfluid with $\nabla \times V_s = 0$ everywhere, except in a path round a vortex core. The total circulation round a curve enclosing the total number of lines N is

$$\oint V_s(r).dr = N.\frac{h}{m}$$

and

$$\nabla \times V_s = n_\ell.\frac{h}{m} = 2\Omega \qquad (14)$$

This means that in rotating helium a uniform density of vortex lines is built up, given by

$$n_\ell = \frac{2\Omega}{\kappa}$$

The normal fluid can be scattered by vortex lines, as shown by Hall and Vinen (1956), to give on a vortex line of velocity V_L a Magnus force

$$f = \rho_s(V_L - V_s) \times \kappa$$

so that the line moves relative to the superfluid. This provides an effective interaction between the normal and superfluid. It adds to the hydrodynamic equations a 'mutual friction' term

$$F_{sn} = \frac{B\rho_s\rho_n}{\rho}.\Omega(V_s - V_n)$$

where B is a mutual friction constant.

Vinen (1957) in his experiments on the attentuation of second sound in the presence of a heat flow in a channel also showed that the increased resistance to flow above the critical velocity was caused by a tangled mass of quantised vortex lines

which formed turbulence in the superfluid.

The growth of superfluid turbulence can be explained by the role of the mutual friction force in building up the individual lines, while the decay process occurs in a way similar to that of a classical fluid. In a steady heat current Vinen (1957) arrived at an equation for the time rate of change of the equilibrium length of vortex line 'L' per unit volume given by

$$\frac{dL}{dt} = \chi_1 \frac{B}{2} \frac{\rho_n}{\rho} V L^{3/2} - \chi_2 \frac{\hbar}{m} L^2 - \chi_3 \frac{B}{2} \frac{\rho_n}{\rho} V \frac{L}{d} + \gamma V^{5/2} = 0 \qquad (15)$$

where χ_1, χ_2, χ_3 are constants, γ a temperature-dependent parameter, d the channel width, $V = (V_s - V_n)$, and the terms represent the growth, decay, perturbing wall effects and nucleation of turbulence respectively.

The analysis of such non-linear effects has been extended so that the normal fluid also exhibits a transition into a turbulent state above another higher critical velocity.

There are therefore three flow regions:-

(i) a subcritical flow in which there is no energy dissipation in the flow of the superfluid,

(ii) a flow with turbulence in the superfluid, and related to its coupling with the normal fluid, and

(iii) a turbulent flow of both the normal and superfluid.

The transition to a normal fluid turbulence (iii) can be characterised by a critical Reynolds number,

$$R = \frac{\rho V_n d}{\eta_n} \qquad (16)$$

This number is a function of the mutual friction coupling between the two fluids and of their velocities. The importance of the mutual friction and the stability of perturbations in the normal fluid flow can be denoted by a dimensionless number ρdAV, where A has the dimensions of reciprocal viscosity. ~~is a temperature-dependent experimental constant~~. The onset of turbulence in the normal fluid can be described by a universal function

$$R_c = R_c(g)$$

where $g = \frac{\rho dAV}{1 + \rho dAV}$ is an appropriate coupling parameter.

R_c has its classical value for small g and low temperatures and decreases with an increase in g. For a flow where $R_c < R < 2R_c$ there is a transition between laminar and turbulent flow for the normal fluid, and there is additional viscosity due to the growth of velocity perturbations in the laminar flow given by

$$\eta_{ne} = \beta(R - R_c)^{\frac{1}{2}}$$

where β is a temperature and geometry-dependent parameter. The existence of this eddy viscosity gives an extra normal fluid force F_n in the hydrodynamical equations. This effect also occurs in region (ii), when there is turbulence in the superfluid only and the normal fluid flow is laminar, so that there is a superfluid eddy viscosity caused by vortex line interaction which gives a superfluid force F_s in the equations. The equations are modified therefore to

$$\rho_s \frac{DV_s}{Dt} = -\frac{\rho_s}{\rho} \nabla P + \rho_s S\nabla T + F_{sn} + F_s \qquad (4^1)$$

and $$\rho_n \frac{DV_n}{Dt} = \frac{\rho_n}{\rho} \nabla P - \rho_s S\nabla T + \eta_n \nabla^2 V_n - F_{sn} + F_n \qquad (5^1)$$

in which $$F_{sn} = A\,\rho_s\rho_n(|V_s-V_n|^2-V_o^2)(V_s-V_n) \qquad (17)$$

where V_s and V_n are velocities greater than the appropriate critical velocities, V_o is a small constant velocity, and (V_s-V_n) and $|V_s-V_n|$ denote the instantaneous and time average of the relative velocity V_s-V_n.

Measurements on the temperature and pressure gradients in thermal counterflow show that F_s and F_n have the form

$$F_s = \alpha(V - V_o)V \qquad (18)$$

where α is a constant, $V = V_s-V_n$, and V_o is the critical superfluid velocity, and $$F_n = \frac{0.133}{R^{\frac{1}{4}}} \cdot \frac{\rho V_n}{d} \qquad (19)$$

Both F_n and R contain the total density ρ rather than ρ_n due to the coupling of the normal fluid to the superfluid to involve all the liquid in the transition. There is reasonable agreement with many experimental measurements using equations (17)-(19), but a further refinement has been made by Chase (1966) by an adjustment of the critical Reynolds number (16) to take account of the superfluid effective viscosity η_s. Empirically (16) becomes

$$R = \rho d\left(\frac{V_n}{\eta_n} + \frac{V_s}{\eta_s}\right) \qquad (16^1)$$

where $\eta_s = \xi\,\rho\frac{h}{m}\,DL_o^{\frac{1}{2}}$, in which D is the ratio of the channel area to its perimeter, ξ is an adjustable parameter, and L_o is the equilibrium length of vortex line in unit volume, given by

(15). This number (16^1) has less variation with temperature compared with (16), and can be considered as a more satisfactory definition of the critical Reynolds number, while the expression proposed for η_s is in good agreement with the experimental values observed by Brewer and Edwards (1961).

The current situation in the origin and behaviour of the different flow regions in most conditions can therefore be considered to show a satisfactory agreement in both experiment and theory.

CHAPTER 2

STRUCTURE AND PROPERTIES OF IONS

A. STRUCTURE

I. Positive Ions

The charge is concentrated on a helium atom complex, He_n^+, where n is a small number, (He_2^+ is known to be stable). The electric field of the charge polarizes the surrounding helium, such that the pressure increases towards the ion. Atkins (1959), treating the helium as a continuum so that macroscopic relationships like the equation of state are valid, expressed the density of helium as a function of distance from the charge.

$$\int_{\rho_o}^{\rho} V \, d\rho = \frac{N_o \alpha e^2}{2\varepsilon^2 r^4}$$

where α is the atomic polarizability, ε the dielectric constant. It is found that the melting point occurs at $r \simeq 6.3$ Å, giving a solid core radius 6.3 Å, and an excess density outside this region falling as r^{-4}.

The mass of the positive ion consists of three parts (1) the mass of the solid core, (2) the mass due to the excess density outside the core, and (3) when the ion is moving, its hydrodynamic mass $\frac{1}{2} \cdot 4/3 \, \pi \, r^3 . \rho$, where ρ is the total density of the unperturbed fluid. These total about 70 helium atom masses.

II Negative Ions

The different properties of negative and positive ions suggest different structures. There is no known stable helium ion of the

form He^-_n, at least for small n, to localize the electron to atomic size, so we would not expect a solid structure similar to the positive ion. This would also rule out an impurity ie. O^-, as the core - a solid structure - would again be formed. The other alternative is a bare electron, the structure of the ion then being determined by the lowest energy state in which it can exist in liquid helium.

The electron-helium atom interaction consists of a strong short range repulsion, arising from the Pauli exclusion principle, and a weak long range polarization attraction. The repulsive force is seen as an energy barrier for the injection of electrons into liquid helium. This has been measured by Sommer (1964) and Woolf and Rayfield (1965) to be about 1.1 eV. Burdick has calculated the electron energy needed to propagate without attenuation through the liquid, regarded as a lattice, finding the lowest energy to be again about 1.1 eV.

A lower energy state is found when the electron is considered to be confined to a cavity whose surface is formed by polarized helium atoms (the 'bubble' state). The total energy of the ion is then (1) the kinetic energy of an electron in a potential well (2) the surface energy of the bubble and (3) the work required to form the cavity. The polarization energy, responsible for the positive ion structure is ignored, decreasing with increasing distance. The equilibrium bubble size is found by minimizing the total energy, E_T. For a spherical square well,

$$E_T = \frac{\hbar^2 k^2}{2m_e} + 4\pi\sigma R^2 + \frac{4}{3}\pi R^3 . P$$

where k is a solution of the equation

$$k \cot kR = -(k_o^2 - k^2)^{\frac{1}{2}},$$

where k is related to the well depth $V_o = \frac{\hbar k_o^2}{2m_e}$, σ is the surface tension, and P is the external pressure. If it is assumed that V_o = 1.1eV for an electron within a bubble of radius of about 16Å, then this gives a minimum energy of 0.16eV. However the electron is still a free particle in low density helium gas, although Levine and Sanders (1967) have shown that increasing the density of the gas produces also a stable 'bubble' state of low energy similar to those produced within the liquid.

The mass of the negative ion totals about 250 helium masses, and this is made up of an excess density of helium atoms outside the bubble and held there by polarisation forces, and of its attached hydrodynamic mass associated with its motion through the liquid. The only measurements of the effective masses of ions in liquid helium have been made in a microwave reflection cavity by Dahm and Sanders (1966). At 1.2°K they found a temperature-dependent positive ion mass of about $40M_{He}$ and a negative ion mass of about $200M_{He}$.

Further evidence for the bubble model comes from photoejection experiments: Northby and Sanders measured the cross section for the ejection of electrons from their ions by radiation of near infra-red wavelengths. Their results were compatible with the model in which the electron is bound in a well of a certain radius and depth. However their results quantitatively are open to further interpretation, and this will be discussed in a later chapter.

It is expected that the radius of a negative ion should be pressure dependent, and this has provided a very accurate way of finding the

by its interaction with vorticity.

B. PROPERTIES

I. Low Field Mobility

1. Temperature dependence

The motion of positive and negative ions under the influence of an electric field is normally analysed using Kinetic theory, for temperatures not too near the λ point. This is feasible, the ions interacting with the normal fluid quasiparticles, phonons and rotons, and the ion-quasiparticle mean free path is greater than the ion dimensions. Above about $1.9^{\circ}K$, when the mean free path becomes comparable with ion size, the liquid may be regarded as a normal viscous fluid. Normal kinetic theory gives for the low field mobility, equating the loss of momentum by an ion in a collision, with the energy gained from the field, as

$$mV = e\,E\,\tau$$

$$\text{ie} \quad \mu = \frac{V}{E} = \frac{e}{m} \cdot \tau$$

where τ is the mean time between collisions of the ion with a quasiparticle. If the ion velocity is not zero after a collision (i.e. persistence of velocity), and letting 'f' be the mean fraction of momentum lost by the ion in each collision, then

$$\mu = \frac{e}{m} \cdot \tau \cdot \frac{1}{f}$$

$$= \frac{e}{m} \cdot \frac{1}{f} \cdot \frac{1}{N\sigma V}$$

where the collision probability τ^{-1} is the product of the total number of scattering centres N, the collision cross section σ, and the mean

relative thermal velocity $V = (V_{ion}^2 + V_q^2)^{\frac{1}{2}}$.

For temperatures above .9 K, the important scattering centres are rotons, whose dispersion relationship is

$$\varepsilon = \Delta + \frac{(p - p_o)^2}{2\mu_o}$$

The number of rotons is given by

$$N = 2(2\pi)^{3/2} h^{-3} (\mu_o kT)^{\frac{1}{2}} p_o \exp(\frac{-\Delta}{kT})$$

and the relative ion-roton velocity is

$$V = (\frac{3kT}{M} + \frac{kT}{\mu_o})^{\frac{1}{2}}$$

$$\simeq (\frac{kT}{\mu_o})^{\frac{1}{2}} \text{ for } M >> \mu_o$$

$$\text{hence } \mu = \frac{3}{4}(2\pi)^{3/2} h^3 (\frac{e}{M})(\frac{1}{kT\sigma}) \frac{1}{p_o^2} \exp(\Delta/kT) \qquad (1)$$

where f $\simeq$2/3, from Meyer and Reif (1961).

The scattering cross section, assuming a hard sphere interaction, is

$$\sigma = \pi(r_{ion} + r_{roton})^2$$

for high energy scattering ($k(r_{ion} + r_{roton}) >> 1$) and the roton radius is taken to be ~4 Å (Kuper 1961).

We do not expect to be able to obtain accurate absolute values of either the mass or size of the ions from these formulae, being essentially statistical in nature; but the functional dependence of the mobility on various parameters (e.g. temperature and pressure) should be obeyed. Meyer and Reif (1961), have shown the temperature dependence of the low field mobility of positive and negative ions to be given by (1) up to about 1.9°K, but with a slightly lower value

for Δ for negative ions.

Above 1.9°K Dahm and Sanders have shown that the low field mobility for positive ions follows that found from Stokes law,

$$\mu = \frac{e}{6\pi\mu R}$$

where R is given by

$$R = \frac{(\varepsilon - 1)e^2}{8\pi\varepsilon^2(P_m - P_o)}^{\frac{1}{4}}$$

P_m is the melting pressure and P_o the ambient pressure. These equations also account for the observed positive ion mobility in HeI.

2. Pressure dependence

The pressure dependence of the positive ion low field mobility has been shown by Meyer and Reif to depend on the pressure dependence of P_o and Δ in equation (1), and assuming a constant effective mass and scattering cross section. This unexpected behaviour must throw doubt on the correctness of the detailed structure of the positive ion.

The negative ion low field mobility is approximately half that of the positive ion at the saturated vapour pressure, because of its higher effective mass and scattering cross section. Increasing pressure at constant temperature increases the negative ion mobility, until at 7 atmospheres it has the same value as the positive ion. Thereafter, it either has the same mobility (Meyer and Reif 1961) or a higher mobility then the positive ion (Cunsolo and Mazzoldi 1961). The increase in mobility with pressure can be qualitatively explained by a decrease in the bubble size, lowering its scattering cross section. Above 7 atmospheres, according to the data of Meyer and Reif, the

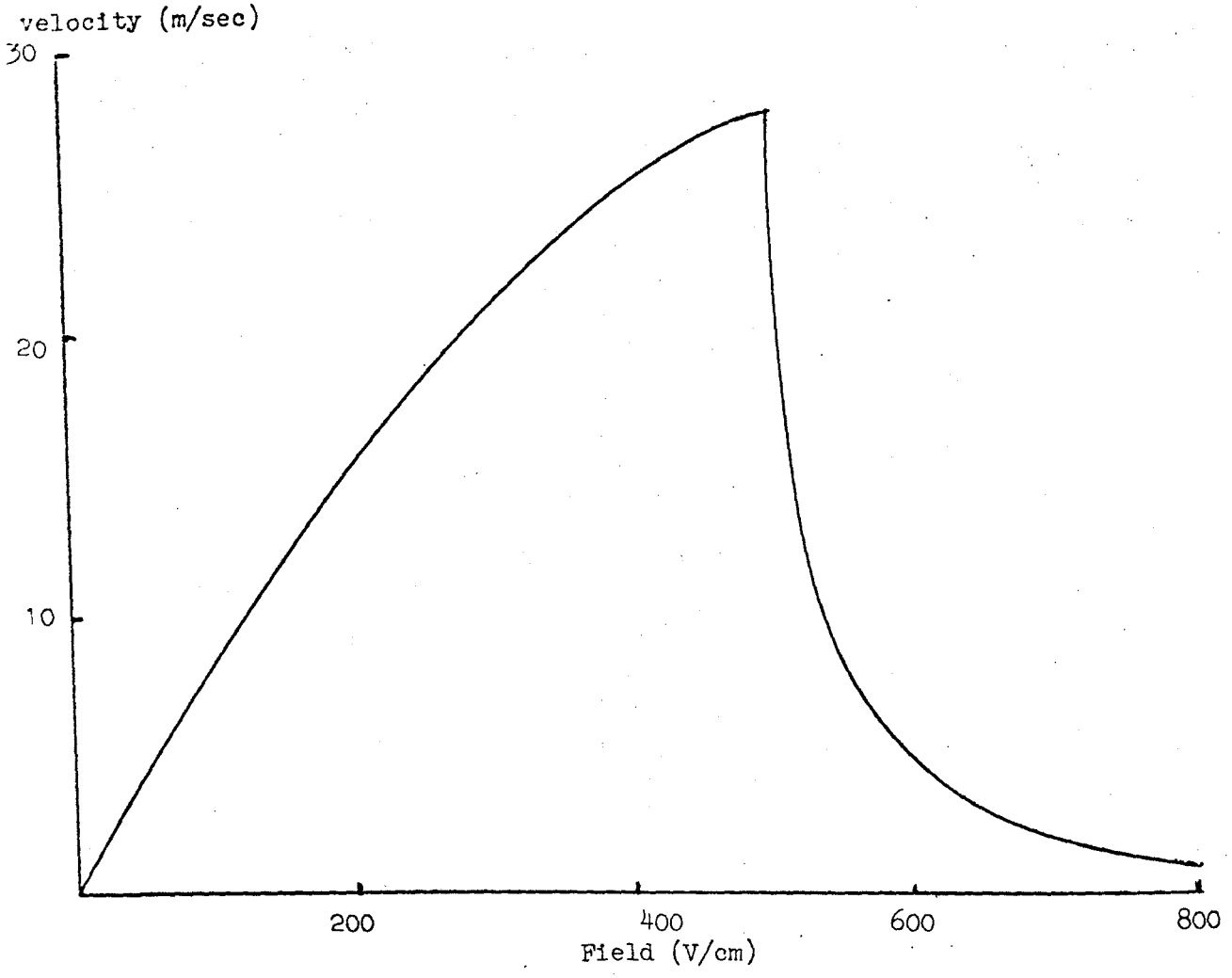

Fig 2.1 Drift velocity versus electric field (negative ions, T = 0.94°K)

product of the effective mass M and the scattering cross section σ ~~must be~~ are the same for positive and negative ions, and ~~must be~~ are constant, independent of pressure.

II. High Field Behaviour

Simple Kinetic theory is applicable for ion motion when the energy gained from the field in one mean free path (ℓ) is less than the thermal energy of the ion. The ion drift velocity is then proportional to the applied field, with a field independent mobility. This is described by the criterion

$$eE\ell < \frac{3}{2} kT.$$

For high fields, where this does not hold, one would expect a region where the drift velocity is proportional to the square root of the field. Wannier (1953) has shown in this case

$$V = \left(\frac{2}{M^2}\right)^{\frac{1}{4}} (e\ell E)^{\frac{1}{2}}$$

A plot of drift velocity against field is shown in fig (1). The same qualitative behaviour is shown by positive and negative ions at all temperatures and pressures, but with interesting differences in detail.

For low fields, $V_D \propto E$ as expected. At higher fields the mobility drops, until at a critical velocity of the ion there is a sudden fall in velocity with increased field. Measurements in this region at low temperatures ($\sim.2^{\circ}K$) where there is very little energy loss due to quasiparticle scattering, gives the relation $V_D \times E \simeq$ constant where E, the applied field, is now a direct measure of the energy of

the ion complex. This unusual behaviour can be explained by considering the ion trapped to a vortex ring which then dominates the ion's motion. As shown in Chapter I, V x E ≈ constant for a vortex ring. The experiments by Rayfield and Reif (1964) were the first to show quantum effects on a macroscopic scale. Using the classical expressions for a vortex ring, the best fit to their data was given by the circulation κ being equal to one quantum $\kappa_o = \frac{h}{m}$, and the core radius of the order 1 Å.

At higher temperatures, where quasiparticle scattering by the vortex becomes important, there are energy losses due to a frictional force F acting on the vortex.

$$F = \alpha(T) \quad \ell n\left(\frac{8R}{a} - \tfrac{1}{4}\right) \qquad (2)$$

where $\alpha(T)$ is a temperature dependent attenuation constant, depending on the roton-vortex line scattering cross section σ_{rv} as

$$\alpha(T) = \frac{3\pi^2}{8} \frac{k}{h^3} p_o^4 \sigma_{rv} e^{-\Delta/kT}$$

For equilibrium motion

$$eE = \alpha(T) \quad \ell n\left(\frac{8R}{a} - \tfrac{1}{4}\right)$$

using $$V = \frac{\kappa}{4\pi R} \quad \ell n\left(\frac{8R}{a} - \tfrac{1}{4}\right)$$

we get, eliminating R

$$\ell n\left(\frac{V}{E}\right) = \ell n\left(\frac{2\kappa e}{\pi a \ \alpha(T)}\right) - \tfrac{1}{4} - \frac{eE}{\alpha(T)}$$

The velocity V_g where the ion is trapped by a vortex ring, at saturated vapour pressure, has been calculated by Huang and Olinto using the stability criterion from the viscous forces acting on the charged vortex ring. The total viscous force is given by

$$F(V,T) = F_1(V,T) + F_2(V,T)$$

where F_1 is the frictional force on a vortex ring given by equation (2) and F_2 is the frictional force on the ion bound to the vortex ring. Steady state motion is possible if

$$eE = F$$

For temperature around 1.0°K, this gives a temperature independent V_g = 32 m/sec for positive ions and 26 m/sec for negative ions, in agreement with experiment. Bruschi et al (1968) find a temperature dependent V_g for positive ions above 1.1°K, falling for increasing temperature. Due to the finite life time for an ion bound to a vortex ring, which is very small for positive ions in high fields and temperatures above 1.1°K, the velocity-field characteristic shows a marked change. The curve goes through a minimum in the vortex ring velocity, then asymptotically approaches V_g at very high electric fields. This is interpreted as meaning the ion forms a vortex ring at the critical velocity V_g. For higher fields, because of the large escape probability, the ion will break away from the vortex ring and form and bind to another vortex ring. At very high fields, the ion continuously creates rings, while never being trapped. Negative ions do not show this behaviour, being more strongly bound to the vortex ring. This is very strong evidence for the velocity V_g being that necessary for an ion to form a vortex ring, and then be trapped by it. This is very important when we discuss the fine structure in the mobility at low fields.

For temperatures below .9°K, the Huang-Olinto stability criteria gives a lower velocity than the experimentally found V_g. Rayfield (1968) has found a temperature independent V_g for positive and negative ions below .7°K, a pressure dependent V_g for negative ions, and a pressure independent V_g for positive ions. He also found that a larger electric field was needed to create a vortex ring than that necessary to support a charged vortex ring which had already been formed. The pressure dependence of V_g for the negative ion (an increase in V_g with pressure), can be explained by the change in bubble size, until at about 15 atmospheres the ion velocity is limited by roton emission at the Landau critical velocity.

This behaviour can be understood if we assume V_g is the velocity at which the ion creates a vortex ring. Then taking a suitable path in the superfluid velocity field V_s around the ion, we have below V_g

$$\oint \underline{V}_s . d\underline{\ell} = 0$$

and just above V_g

$$\oint \underline{V}_s . d\underline{\ell} = \frac{h}{m}$$

Taking $\underline{V}_s$ to be proportional to V_g, the ion drift velocity, and $d\underline{\ell}$ proportional to the ion radius R, gives

$$V_g \times R = \text{constant}$$

Rayfield, using the pressure dependence of V_g, then calculated the relative change in bubble radius with pressure. Taking $R = 16$ Å at the vapour pressure gave similar curves to these found by Springett, obtained from the trapping of negative ions by

vortex lines in rotating HeII. Rayfield's results show that at 15 atmospheres, R = 10.5 Å.

The relationship between positive and negative ion radii and V_g,

$$\frac{R+}{R-} = \frac{V_g^-}{V_g^+} \qquad (3)$$

does not appear to hold, giving $\frac{R_+}{R_-}$ varying from 0.85 at 0.5°K to about 1 at 1.4°K, much higher than the value .38 taking R_+ = 6.3 Å and R_- = 16 Å. This exposes our basic ignorance of how a vortex ring is formed, also a problem in classical hydrodynamics. Presumably the completely different boundary conditions for the two ions play an important role.

Taking a path in the superfluid velocity field outside the ion is more meaningful, and it is interesting that at these velocities, the diameter of a classical vortex ring would be about the same as the diameter of an ion. This we would expect, from the analagous situation of vortex formation is a classical fluid, which may be studied directly (Prandtl, 1952).

Classically, a stationary vortex ring is formed behind a sphere at a Reynolds number of 8. There is no anomaly in the drag coefficient for the sphere, showing the creation of the ring to be a smooth transition from a laminar flow pattern.

Thus $$R_e = \frac{\rho_n}{\mu_{eff}} \cdot R\, V$$

$$\text{i.e.} \quad R.V = \frac{\mu_{eff} R_e}{\rho_n}$$

which gives the same relationship between positive and negative ion radii as equation (3). Due to the non-applicability of viscous hydrodynamics to the motion of ions below 1.9°K one can make no comparison for absolute values of R and V_g.

III. Interaction with Vorticity

It is found that negative ions are trapped by vortex lines present in rotating HeII. The current perpendicular to the axis of rotation is attenuated as

$$I = I_o \exp\ (-2\Omega\ m\sigma h^{-1}.n)$$

where $2\Omega mh^{-1}$ is the number of vortex lines per cm., σ the capture cross section and n the distance travelled by the ion. For constant electric field, σ first increases slowly with temperature then shows a sudden 'cut off' at 1.7 K at the vapour pressure. The 'cut off' is described by

$$\sigma = \sigma_o \exp(-P.t)$$

where P is the escape probability of the ion from the line, and t a characteristic time for the ion to remain on the vortex. Donnelly and Roberts (1967), by considering the ions to be in a potential well formed by the ion replacing the rotating fluid near the vortex core, have calculated P, with only the radius of the ion as the unknown. Measurements of the mean trapped lifetime of the ion on a vortex at the vapour pressure give $R \simeq 16$ Å. Springett (1967) by considering σ as a function of pressure has then been able to measure the negative ion radius as a function of

pressure. σ is also a decreasing function for increasing electric field -because a lowering of the potential well occurs.

As the positive ion is smaller, it is less strongly bound to the vortex line. An estimate of the binding energy is given by the kinetic energy of the rotating fluid replaced by the ion:

$$E_B = \frac{1}{2} m\bar{V}^2$$
$$= \rho_s \frac{2}{3} \pi . R^3 . \bar{V}^2$$

and since the velocity field for a vortex varies as

$$V = \frac{h}{m} \cdot \frac{1}{r}$$

then $$E_B \simeq \frac{2}{3}\pi \left(\frac{h}{m} \right)^2 \rho_s . R$$

This is proportional to R, the radius of the ion, and will be smaller for the positive ion. It is found that the escape probability for the positive ion is such that above 0.8K no trapping is expected.

The potential well for negative ions at 1.0°K is U = 50 kT, and at 1.8°K, U = 19 kT. For positive ions at 1.0°K, U = 19 kT.

Sitton and Moss (1969) have shown that negative ions are trapped by turbulence caused by a supercritical heat current. The vorticity in the turbulence is identical to that in rotation, except for the line configuration.

In Springett's work on the pressure dependence of the negative ion radius, he showed the mobility can be explained by the pressure dependence of the term $N_r\sigma$, N_r being the roton number density and

σ the ion-roton cross section. But here, as with the positive ion, we must assume a constant effective mass, independent of pressure. This is surprising for the negative ion, as the major contribution to its effective mass should come from the hydrodynamic part, $\frac{1}{2} \times \frac{4}{3} \pi R^2 . \rho$, which is very pressure dependent through R.

CHAPTER 3

EXPERIMENTAL DETAIL

I. VELOCITY MEASUREMENT

a. Triode

The simplest method of measuring an ion velocity is by the square wave method of Cunsolo (1961). An electric field between the source S and grid G extracts the required type of ion, which passes into the grid collector space. A square wave electric field is applied to the grid G, so that the ions are drawn towards the collector C for one half of the cycle, and are drawn back to the grid G for the reverse half of the cycle. The frequency of the square wave is increased until the ion flight time from the grid to the collector is greater than the half cycle period of the square wave, allowing no current to be collected. The equation for the current collected at C is

$$I = I_o(\frac{1}{2} - \frac{df}{V_D})$$

where f is the square wave frequency, d the grid collector distance, and V_D the drift velocity of the ion.

A plot of I against f is a straight line, cutting the frequency axis at I = 0 at f_c. Then $V_D = 2\ d\ f_c$.

When the field in the grid collector space is reversed, changing from one half cycle to the other of the square wave, the ion must take a certain time τ, of the order of the mean free time between collisions, to reverse its direction of travel. τ must be

much less than the ion transit time, $\frac{1}{2f_c}$, for this method to give sensible results. τ is of the order 10^{-11} secs at 1 K, while the ion transit time, for grid collector spacings of a few millimetres, is of the order 10^{-3} secs. The quality of the method may be estimated by the linearity of the plot of current against frequency, and the sharpness of the cut off near f_c. It is commonly found that at low currents, ie. the frequency near the cut off f_c, a small tail appears. This could be an indication of a spread in the ion beam's velocity, due to electric field inhomogeneity or misalignment of the grid and collector. Space charge build up at the grid would also cause a low current tail. The currents used are of the order 10^{-11} amps, in a beam about 1 cm in diameter. This gives a charge density of about 10^5 ions/cc. The field distortion due to the space charge may be roughly estimated from

$$\nabla.\underline{E} = \frac{\rho}{\varepsilon_o}$$

$$E \simeq \frac{\rho.d}{\varepsilon_o}$$

$$\simeq 10^{-2} \text{ volts/cm}$$

which is negligible compared with a normal applied field at 10^2 volts/cm. The displacement current, due to the motion of the ions between the grid and collector, will average out to zero and is ignored.

$$j = \varepsilon_o.\frac{dE}{dt} = \varepsilon_o.\nabla E.V = \rho V$$

Trouble can be caused at very low frequencies by the change

of field from one half of the square wave to the other half. This results in a large capacitive pick - up causing oscillation of the electrometer, while still averaging to zero. This 'pick up' can be reduced by screening the collector (which is connected directly to the electrometer) by another grid called the Frisch grid. This is not normally necessary in helium, the square wave frequency being much larger than the response time of the electrometer, which then just acts as a current integrator over a period of about 10 seconds.

Field penetration at the grid should be negligible - Verster, 1963 gives a value of 10^{-5} cm. If we assume field distortion up to a distance d_o comparable with the grid mesh size, we get for a 60 line per inch grid

$$d_o \simeq .4 \text{ mm}$$

which is 10% of a grid collector distance of 4 mm. The amount of distortion will be zero when the fields on each side of the grid are equal, so we can define an effective distance for field distortion as

$$d = d_o(1 - \frac{E_1}{E_2})$$

where E_1 and E_2 are the fields on each side of the grid, with $E_2 > E_1$. Most velocity measurements are carried out with $E_1 \sim E_2$, so field penetration is small.

If there are a number of different types of ion present, then a current v frequency plot would be a superposition of the curves for each separate type, assuming no interaction between them.

For large radius, high energy but slow moving vortex rings, the time taken to reach equilibrium velocity can be of the same order as, or larger than, the transit time. A current v frequency graph will not be a straight line, and will not have a sharp cut off. This method cannot therefore be used to measure low vortex ring velocities.

b. Gate Spectrometer

By using two pairs of closely spaced grids as gates, separated by a distance more than five times the gate spacing, a variety of different pulse methods may be used for velocity measurements. This is essentially the classic arrangement for finding gaseous ion velocities eg. Tyndall and Powell (1930). The pulses are applied across the two gates, leaving a uniform field between them in the drift space. The current collected is a function of frequency, showing a number of peaks at certain harmonics of the fundamental transit time frequency. This is the method used at low temperatures by Meyer and Reif, and Rayfield, who found as many as ten distinct peaks, showing great homogeneity in the ion beam velocity. Here again, the current is collected as a function of frequency, and may thus be integrated over a large number of cycles.

Pulse methods have also been used (Bruschi and Santini 1970), in which the transit time is found from analysing the current pulse shape. This requires the response time of the current measuring instrument to be much less than the transit time i.e. a wide

Fig 3.1 Square wave generator for frequencies 10 c/s - 10 kc/s

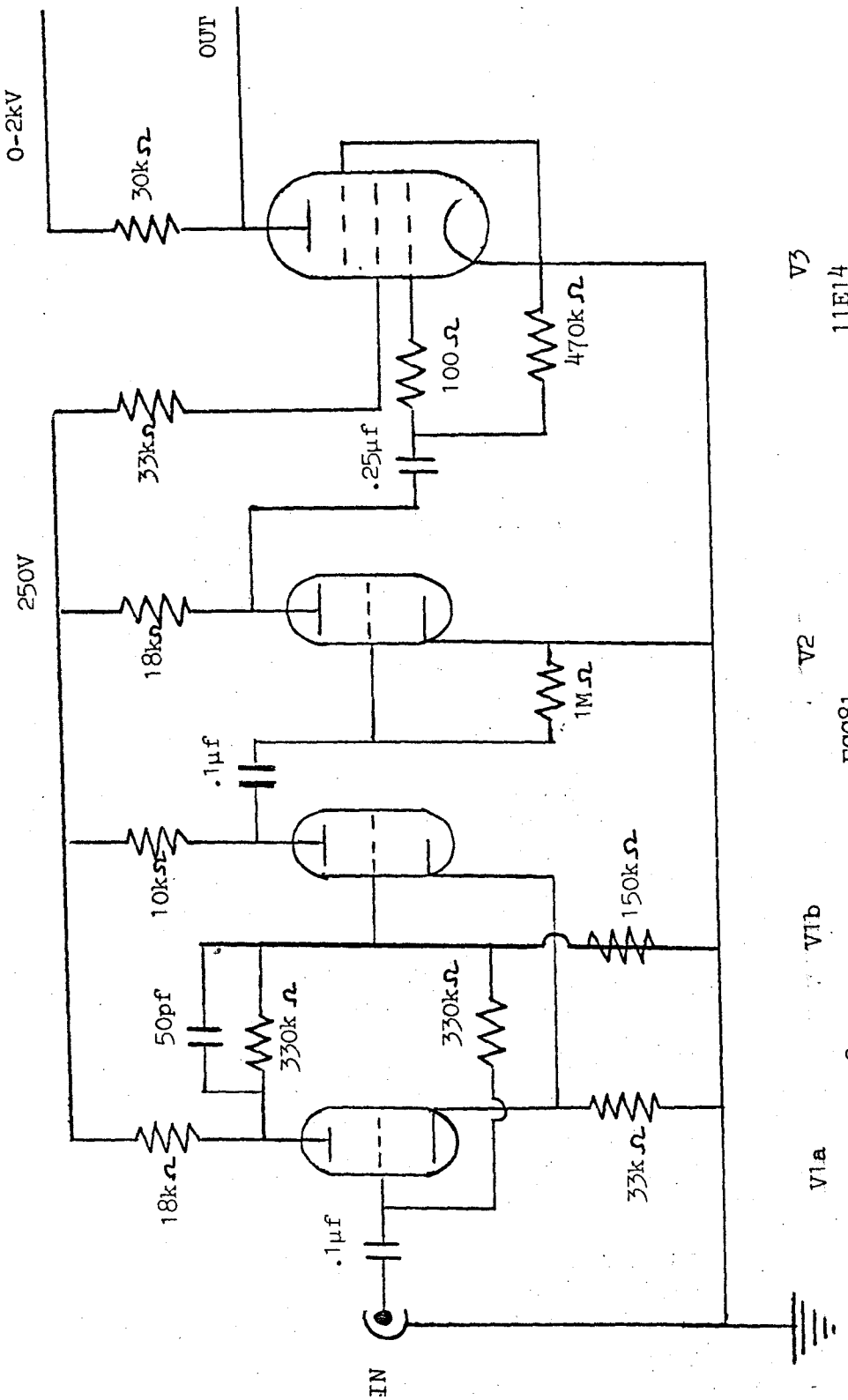

bandwidth amplifier with associated noise, and thus the use of a waveform analyser. In principle this is a more fundamental method for measuring velocities as the transit time is measured directly.

The gate spectrometer suffers from needing a number of grids with associated disturbances in the ion beam and bulk fluid. However, in the main drift space, there is only one way traffic. With the triode, the ions move in both directions in the measuring space, though not simultaneously. If there is any interaction between the ions and the bulk fluid, this can lead to hysteresis effects. There also tends to be charge bunching at the grid on the reverse half of the square wave. These effects are all eliminated in the pulse method, which is ~~therefore~~ however much more expensive to set up.

II. EXPERIMENTAL EQUIPMENT

a. Pulse Generator

In the two methods used, mainly the triode but also the gate spectrometer, a high voltage square wave is needed, which is applied to the grids with appropriate D.C. Bias voltages.

The square wave generator built is shown in Fig. (1). A low voltage triggering square wave is applied to a Schmidt trigger, and the output amplified and fed to the grid of a high voltage valve. The output from the anode alternates between the applied anode potential when the valve is non conducting, to zero potential when it is switched on. The rise time of the output is a few micro-seconds, in a pulse width of commonly 10^4 microseconds. The amplitude

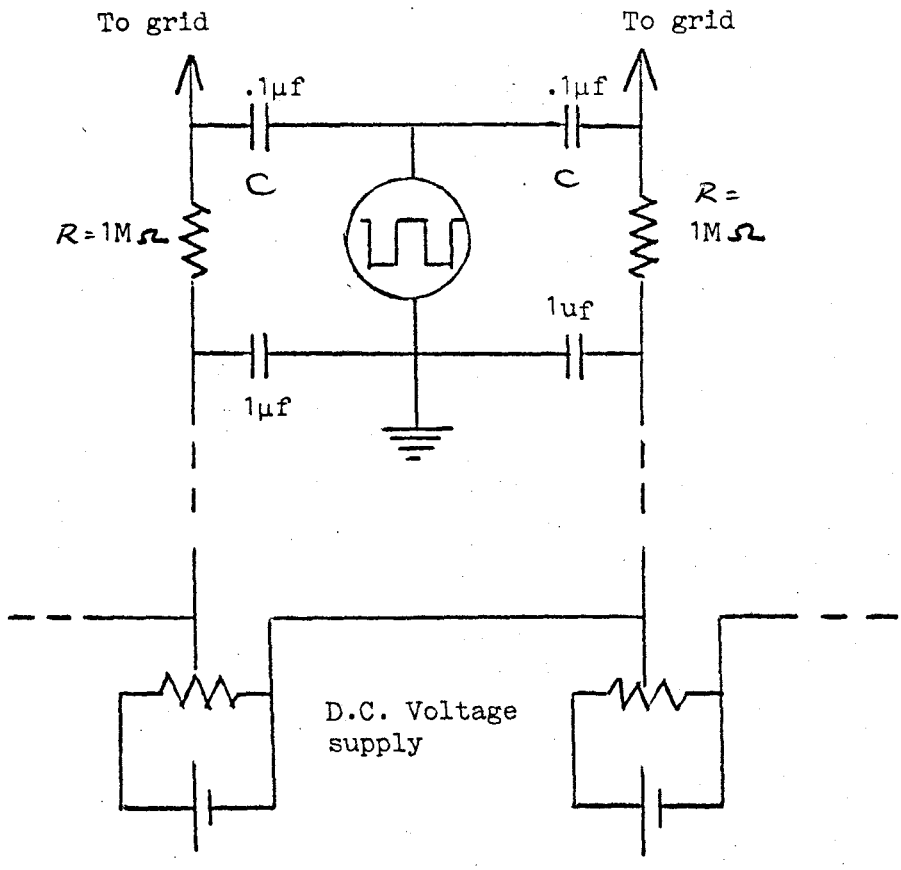

Fig 3.2 D.C. Biasing circuit

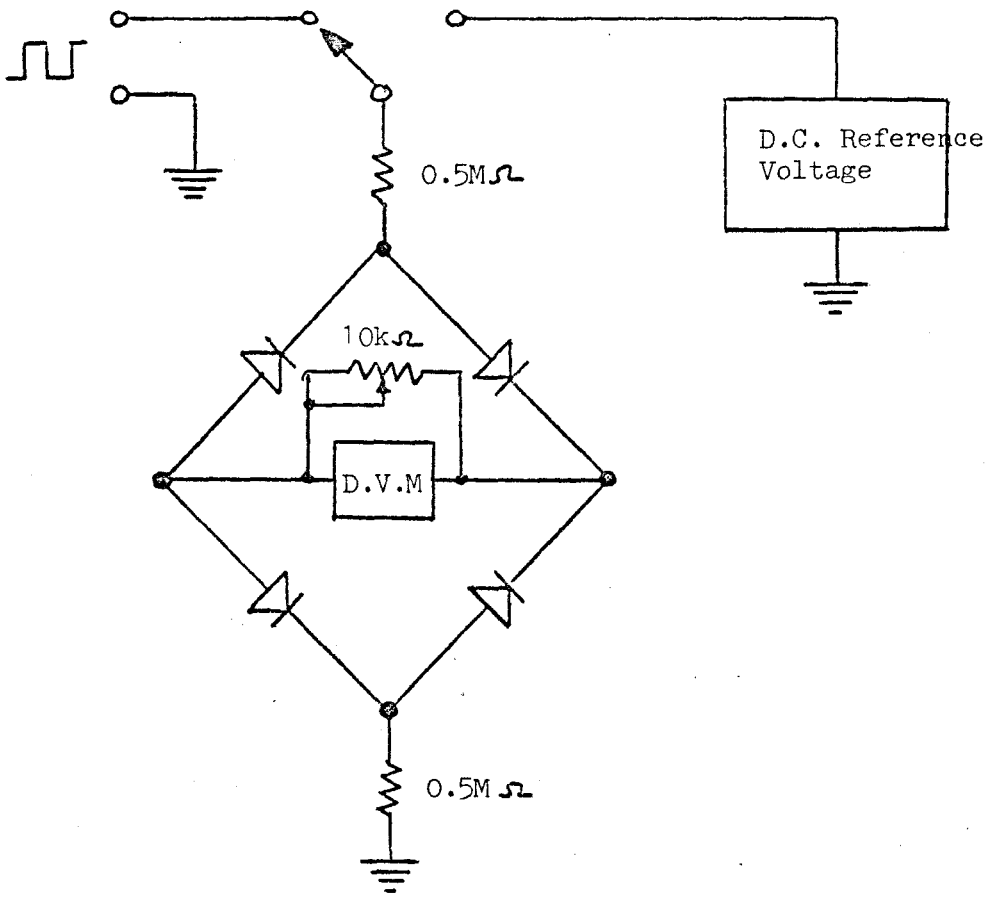

Fig 3.3 Four diode bridge for measuring the square wave amplitude (from Bruschi et al 1966)

of the output is a few percent less than the applied anode potential, due to the finite anode resistance of the valve.

The circuit for applying the square wave and D.C. biases to the grids is shown in Fig (2). By bringing the anode output through a capacitor C, the mean voltage is brought down to zero, ie. it is symmetric about the half amplitude voltage at zero potential. A D.C. Bias through the resistor R brings the mean level to this D.C. voltage. The values of C and R are chosen so that the square wave pulse width τ is much less than the product CR.

The square wave amplitude can be calibrated against a known anode potential either by measuring it on an oscilloscope, allowing for the input impedance, or using a four diode bridge. The diode bridge circuit used is similar to that of Bruschi et al (1968), Fig (3) in which a reference D.C. voltage giving the same deflection on the ammeter as the square wave is one half the square wave amplitude.

The square wave frequency was measured on a Hewlett Packard 5233L Electronic Counter. To avoid overloading the counter, and distorting the square wave, a small inductance coil was wound round the cryostat leads carrying the square wave, and used as the counter input signal.

The square wave generator could give amplitudes from 0 to 2000 volts peak to peak, and frequencies from about 20 c/s to about 8 kc/s. The upper and lower frequency limits depend on the

Fig 3.4 Square wave generator for frequencies 1 to 15 c/s

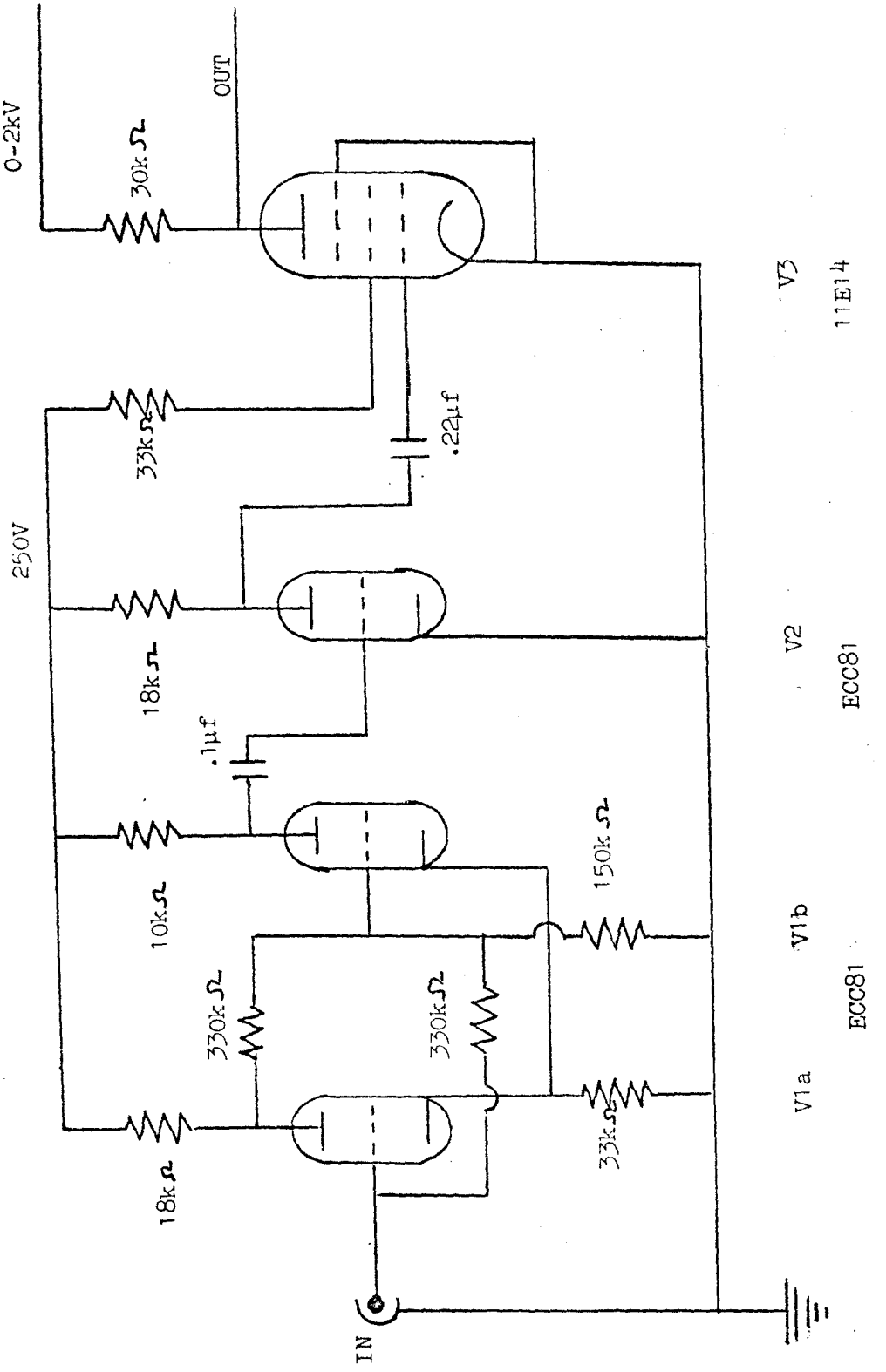

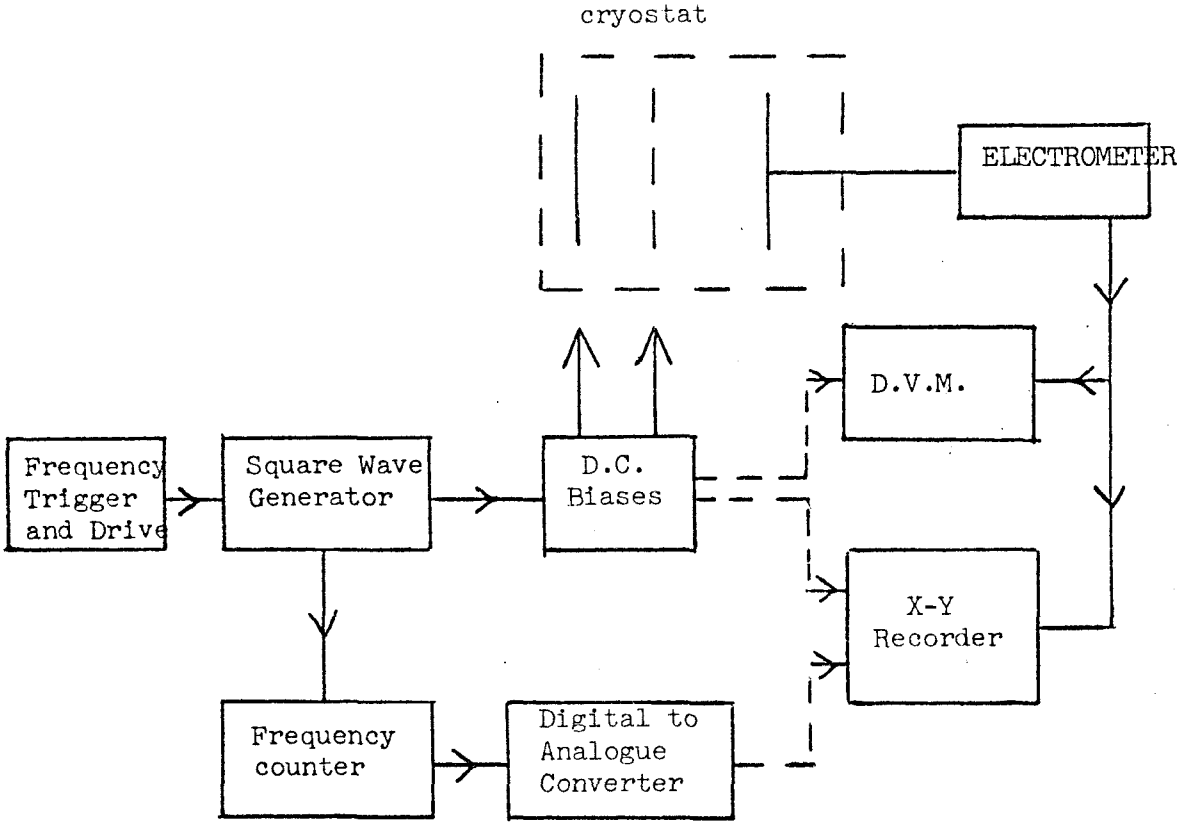

Fig 3.5 Block circuit diagram

square wave rise time, giving distorted pulses at high frequencies, and the time constants of the generator.

A modified square wave generator Fig(4) was built to allow longer pulse times, up to 1 sec pulse width, for work with liquid nitrogen. The first stage was a bistable multivibrator, triggered by pulses from a Tektronix pulse generator. The resulting square wave output was amplified as before, but with different circuit time constants. The rise time was of the order 50 μsec, negligible in a pulse width of 10^{-1}secs.

b. Other Electronics

A typical circuit used is shown in Fig (5). The ion current was measured on a Wayne Kerr electrometer, which could give a range of 10^{-15} to 10^{-8} amps full scale for the appropriate input resistance. It was normally used on the 10^{10} ohm input resistance, giving a time constant of about 1 sec. The output was read on a Dynamco Digital Voltmeter, allowing a resolution to .1% of the electrometer current scale. The output was also connected to the Y axis of an X-Y recorder. The X axis of the recorder could read either the square wave frequency, from an Hewlett Packard digital-analogue converter connected to the counter, or one of the grid bias voltages when measuring the D.C. characteristics. The square wave triggering generator was attached to a drive motor, allowing automatic measurements of the current v frequency curves. The square wave potential was taken from a Fluke power supply. Grid

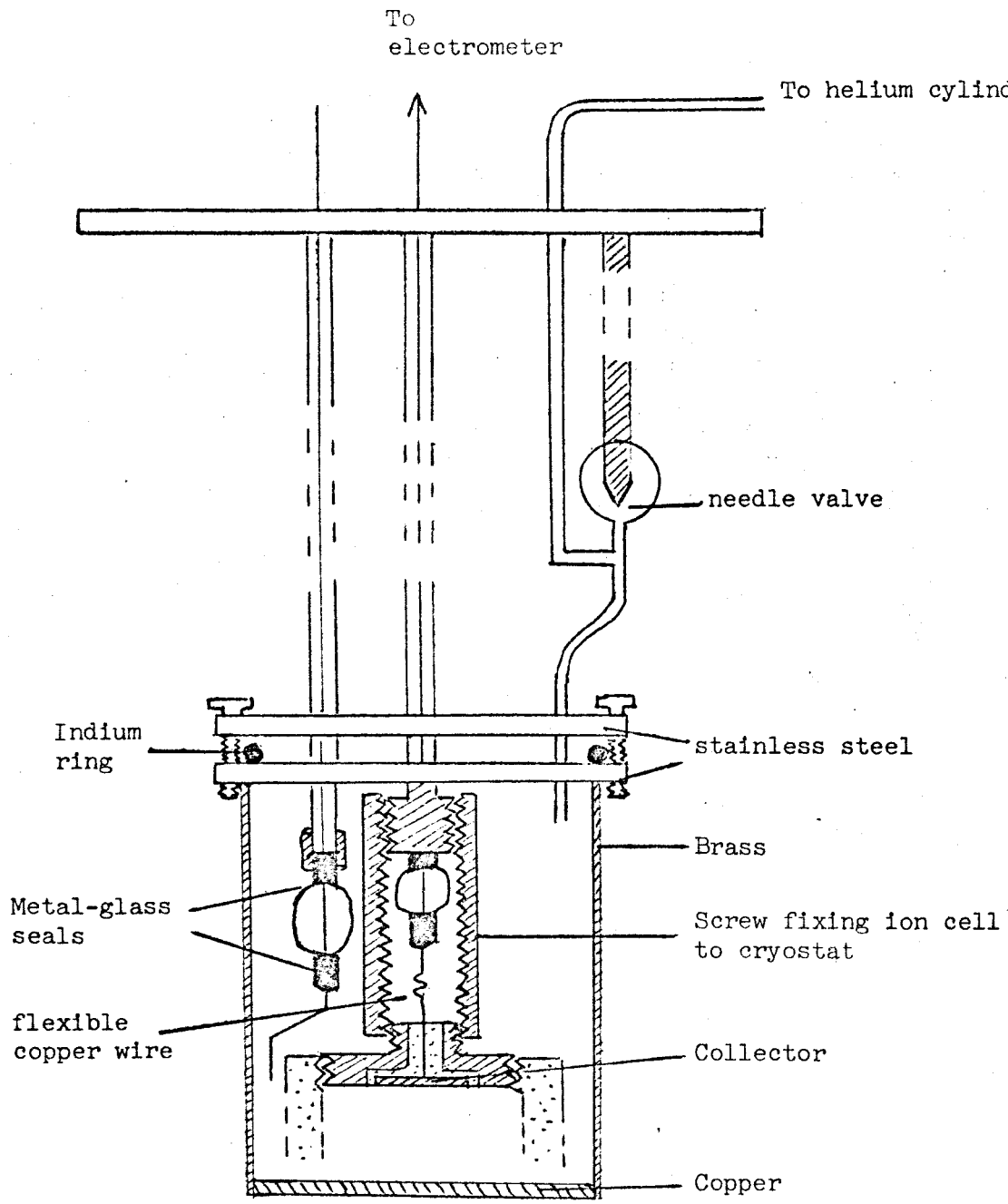

Fig 3.6 Cryostat and Pressure Cell

biases were from either another Fluke power supply or batteries. The Digital Voltmeter could also read the D.C. grid bias voltages.

c. Temperature Measurement and Control

The resistance of a Cryocal doped Germanium resistor was measured on an A.C. Bridge. The resistor was calibrated against the vapour pressure of He^3 down to .9°K. The sensitivity was such that a change of 1 millidegree could be detected at that temperature. The bridge had a feedback circuit for automatic temperature control, but it required a typical heat input of a few milliwatts to keep the temperature constant, at an off balance reading of the bridge. It was found that varying the pumping speed of the Booster pump gave a very delicate control, and was always used.

A Kinney backing pump, with a capacity of 3000 litres/min was used down to 1.2°K. Below this, an Edwards 9B3 Booster pump, with a pumping speed of 800 litres/min was used to around .9°K. A mercury manometer was used at high temperatures.

d. Cryostat

A schematic diagram of the cryostat used for pressure measurements is shown in Fig (6). The electrometer lead, and other grid voltage leads were made from 5 cm o.d. cryogenic quality stainless steel tubing - ordinary stainless steel tubing was found to perforate after a number of low temperature cycles. Ordinary commercial metal glass seals took the electrical leads at the top of the cryostat, and special seals were made for the bottom end. These had to have a high insulation resistance, and stand up

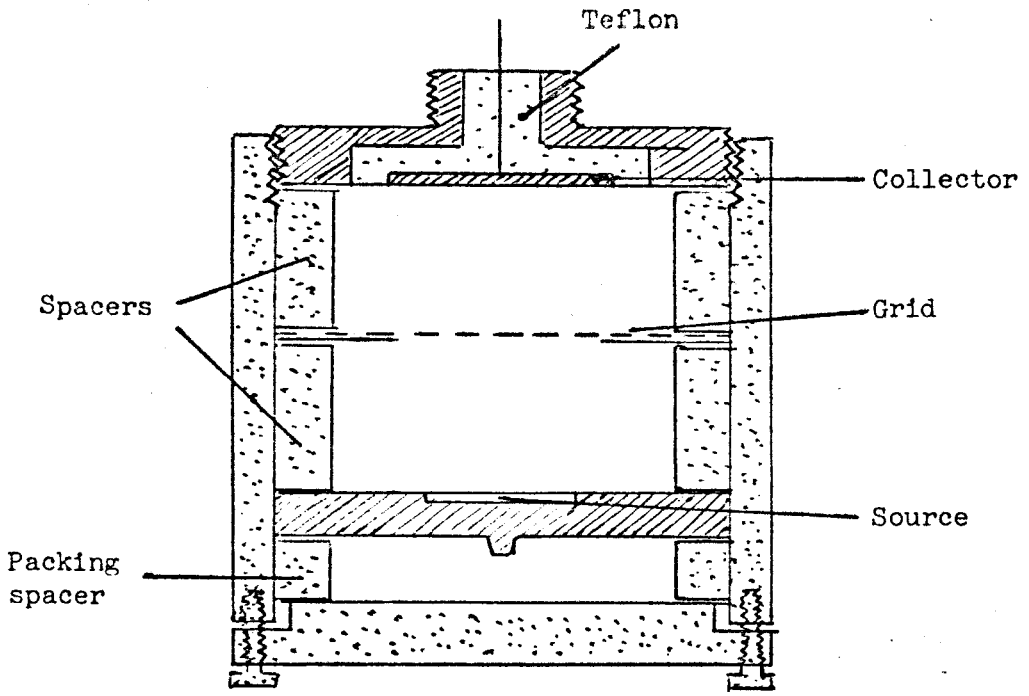

Fig 3.7 Ion cell

to a pressure differential of about 30 atmospheres at 1 K, being vacuum tight as well. The electrical leads were 40 swg constantan, insulated by glass tubing. The leads were kept under vacuum, to keep their insulation resistance of the order 10^{12} ohms.

The pressure can was made of brass, with a copper bottom for good thermal contact between the bath and helium inside the can. The top was stainless steel, sealed by an indium ring. The can was filled through a 1 mm o.d. stainless steel tube; a needle valve allowed the bath helium to fill the can, and the pressure then applied from a cylinder of high pressure pure helium gas. The pressure in the system was read on a Wallace and Tiernen gauge, the dial calibrated up to 500 lbs/in^2 in $\frac{1}{2}$ lb/in^2 degrees.

e. Ion Cell

This is shown in Fig (7). The cell was made of perspex, with the collector assembly screwed in. The collector consisted of a brass guard ring, insulated by teflon from the gold plated brass collector plate. The collector lead was soldered onto the electrometer lead, and a screw coupling used for both electrical shielding and holding the cell onto the cryostat. The grids were made from electroformed nickel mesh 60, 110, 250 and 500 lines per inch, supplied by Buckbee Mears. Mesh discs were soldered onto annular nickel rings, $\sim$2 mm thick, and gold plated. The ions were produced by α-particles from a 200 μC Am^{241} source, prepared by the Radiochemical Centre, Amersham. The 5 Mev α-particles produce

a region of intense ionisation within about .2 mm from the source and the required sign of ion is extracted by suitable electric field. The heat input from the source is about 1 μwatt. The source and grids are separated by perspex spacers.

The radioactive area on the source is 1 cm diameter. The perspex spacers are 2 cm inside diameter, and the grids are 1 cm diameter. The collector is 1 cm diameter. Any beam spreading is contained by the grids, and only the central part of the ion beam falls on the collector. This ensures that the effects of stray fields are minimized.

CHAPTER 4

MOBILITY DISCONTINUITIES

I. HISTORY

A. Reported Discontinuities

Careri, Cunsolo and Mazzoldi (1964) measured the drift velocity of positive and negative ions, using the time of flight technique in a triode. They worked at temperatures around 1 K, and at low electric fields i.e. for ion velocities up to the giant discontinuity at about 30 m/sec. By displaying their results in the form of ion mobility plotted against ion drift velocity, they interpreted the apparent dependence of the mobility on the applied field by discrete constant mobility levels, changing abruptly at integer multiples of a critical velocity, v_c. The value of v_c was 5.2 ± 0.2 m/sec for positive ions, and 2.4 ± 0.1 m/sec for negative ions; v_c was independent of the temperature in the range $0.88^\circ K < T < 1^\circ K$. The change $\frac{\Delta\mu}{\mu}$ between successive mobility levels was of the order 6%, such that the mobility always decreased with increasing field.

At low temperatures ($T \simeq 0.88^\circ K$) the fall from one mobility level to another was not as sharp as at higher temperatures: the lower level would be reached at an ion velocity of $v_D = v_c + \Delta v$, where Δv could be about 2 → 3 m/sec for positive ions at $T = .88^\circ K$ decreasing to about ½ m/sec at $T = 1.0^\circ K$. A common feature of the data is the absence of a discontinuity at a critical velocity. Indeed, for negative ions, Careri et al, never found the first

discontinuity i.e. at v_D = 2.4 m/sec; the value of v_C = 2.4 m/sec was inferred from discontinuities at higher drift velocities. The results in their paper (their Fig. 7) for negative ions show a maximum of one discontinuity up to $v_D \simeq 12$ m/sec, implying the mobility changes by only 6% at the most up to this velocity.

Positive ions were more consistent in showing mobility changes. But not only were some discontinuities absent, but others had an anomalously high mobility gap i.e. $\frac{\Delta\mu}{\mu} \sim 6\%$.

Careri et al estimated their error in an absolute mobility measurement to be 4.5%, with a lower error for the relative mobility values taken in one run when only the electric field was changed.

Further evidence for a mobility discontinuity at 5.2 m/sec for positive ions came from Careri, Cunsolo and Vicentini - Missoni (1964), who measured the deflection of a beam of positive ions by a thermally induced two fluid counterflow perpendicular to the current. They kept the heat current and temperature constant, increased the D.C. electric field (E), and measured the change in current on a central electrode to give the beam deflection (α). Their results showed a discontinuity in the plot of tan α against $\frac{1}{E}$, at a field E_C corresponding to an ion drift velocity of 4.9 $\pm$ 0.3 m/sec.

Cope (1966) has reported mobility discontinuities with both positive and negative ions using a time of flight triode. He showed

the mobility drop $\Delta\mu/\mu$ depended on the source grid extracting field E_{SG} such that for $E_{SG} < E_c$ (the field of the first discontinuity) $\Delta\mu/\mu \sim 8\%$, decreasing as E_{SG} increased. By using low enough extracting fields he saw the first discontinuity for negative ions at $v_D = 2.4$m/sec.

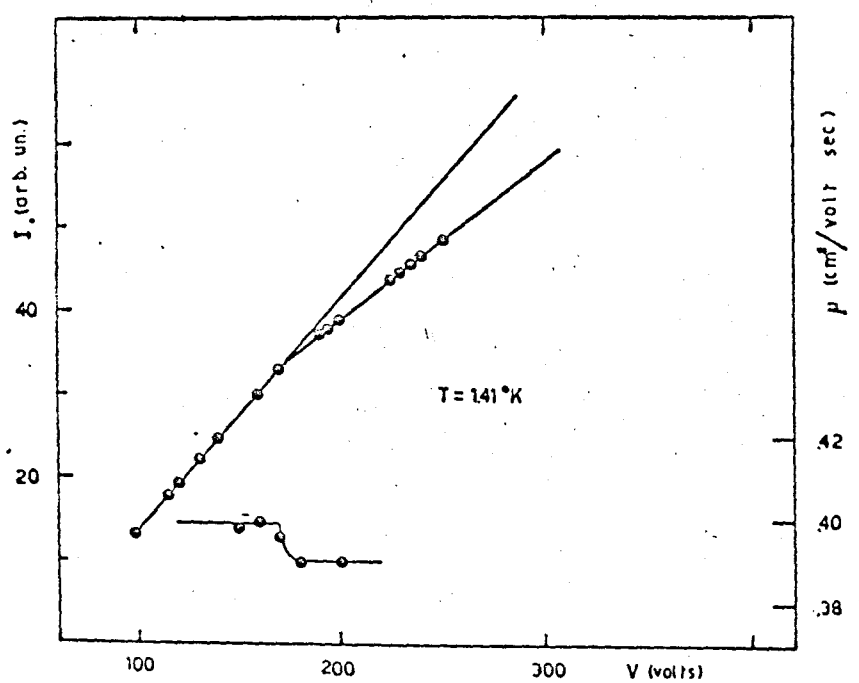

FIG. 3. The mean current collected at the receiving electrode at various square-wave voltages. The frequency of the SW is fixed at 50 cps. A change in the slope occurs at the same value of the voltage at which the mobility falls to the second level. In the lower part of the figure are reported five values of the mobility measured around the discontinuity.

Fig 4.1 From Bruschi et al (1968)

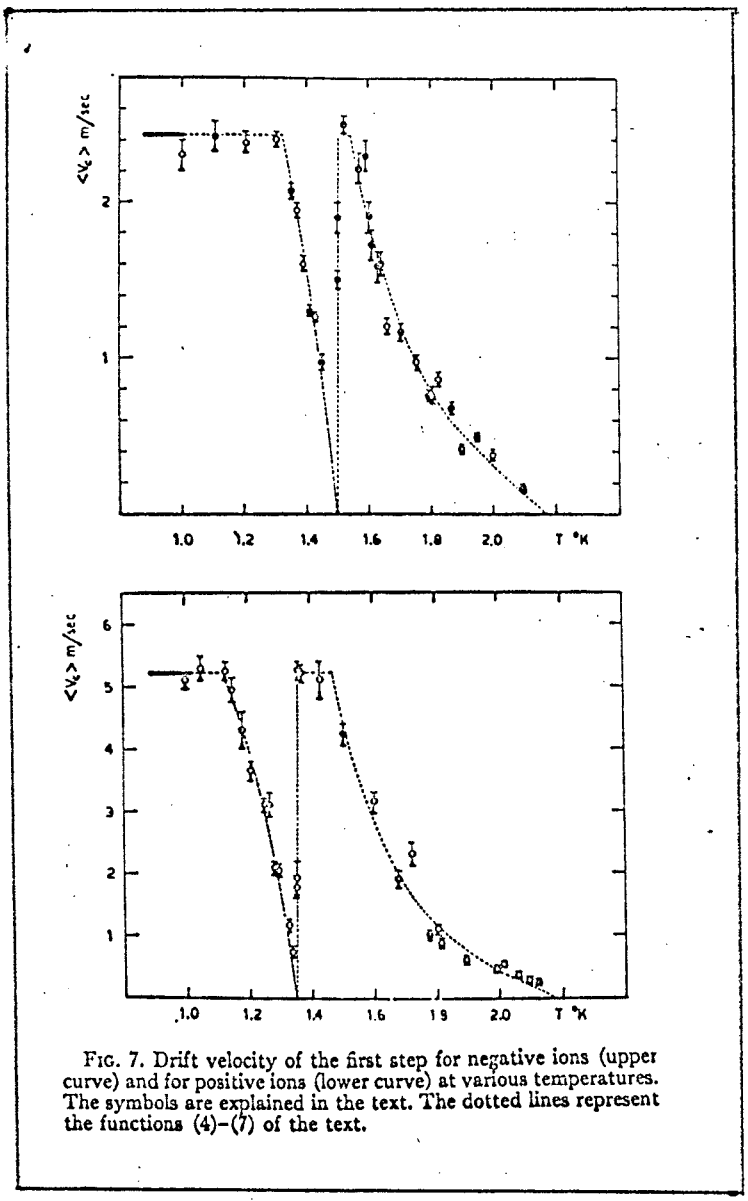

FIG. 7. Drift velocity of the first step for negative ions (upper curve) and for positive ions (lower curve) at various temperatures. The symbols are explained in the text. The dotted lines represent the functions (4)–(7) of the text.

Fig 4.2 From Bruschi et al 1968. Temperature dependence of the critical velocity for the first discontinuity

B. Temperature Dependence of v_c

Bruschi Mazzoldi and Santini (1968) have reported the temperature dependence of the critical velocity v_c for the first mobility discontinuity for positive and negative ions from T = 1°K to 2.3°K, using a time of flight triode.

They first report the results of keeping the square wave frequency constant, and measuring the current as a function of the square wave amplitude. Their Fig.3 (our Fig.1) shows a change in slope at a critical field E_c, which is also the critical field for the first mobility discontinuity. This effect was sometimes used for finding the critical velocity v_c, although they claim an incomplete understanding of the phenomenon, and this will be critically examined later.

Their results for the temperature dependence of v_c are shown in Fig. 2. Discontinuities are seen up to the λ point, but not at higher temperatures. Above the λ point the velocity range investigated was from 20 cm/sec to 100 cm/sec, and so does not exclude a critical velocity outside these limits. (Bruschi, Mazzoldi and Santini (1970) have reported a positive ion critical velocity of 180 cm/sec in HeI at 4.2°K). Up to the λ point, the periodic nature of the discontinuities is preserved, and the size of the first discontinuity $\frac{\Delta\mu}{\mu}$ appears to be constant, independent of the temperature. For positive ions they give $\frac{\Delta\mu}{\mu} \sim$ 5% and for negative ions $\frac{\Delta\mu}{\mu} \sim$ 4%, each with an error of ±50%.

The fall in v_c for $T \sim 1.3^{\circ}K$ is linear with $\frac{\rho_n}{\rho}$, where ρ_n is the normal fluid density, for both positive and negative ions. They deduce

$$v_c = v_1 - a(\frac{\rho_n}{\rho} - b)$$

where v_1, a, b are constants, with different values for positive and negative ions.

At low temperatures ($T \sim 1$ K) v_c is constant, as previously found.

The high temperature fall in v_c is fitted by v_c being proportional to the ratio of the superfluid and normal fluid densities

$$v_c = k.(\frac{\rho_s}{\rho_n})$$

where k is a constant, with a different value for positive and negative ions.

Fig 4.3 From Schwartz (1970). Showing no sign of mobility discontinuities

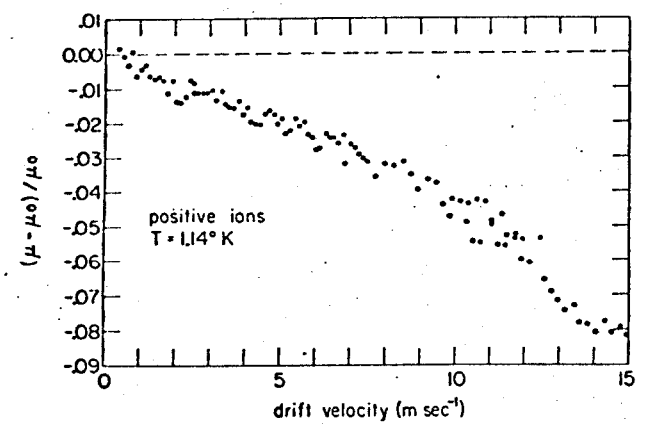

FIG. 2. Fractional deviation of the mobility from its zero-field value, for positive ions at 1.14°K.

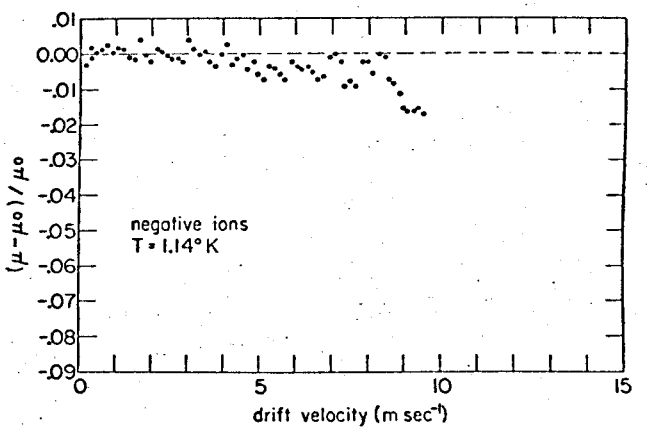

FIG. 3. Fractional deviation of the mobility from its zero-field value, for negative ions at 1.14°K.

C. Absence of Discontinuities

Schwarz (1970) has examined the drift velocity of positive and negative ions at a temperature of 1.14°K, using a pulse technique. He represented his results in the form $\frac{\Delta\mu}{\mu_o}$ against v_D, where μ_o is the zero field mobility, $\Delta\mu = \mu(\text{measured}) - \mu_o$, v_D the ion drift velocity, and they are shown in Fig. 3. There is no sign of a discontinuity in the mobility for either sign of ion, which would be shown by a drop of 3 to 10 divisions at v_c. The error in the results is of the order ½%.

Further, Reif and Meyer (1960) have not reported discontinuities using a double gate technique which had comparable accuracy and resolution with later work.

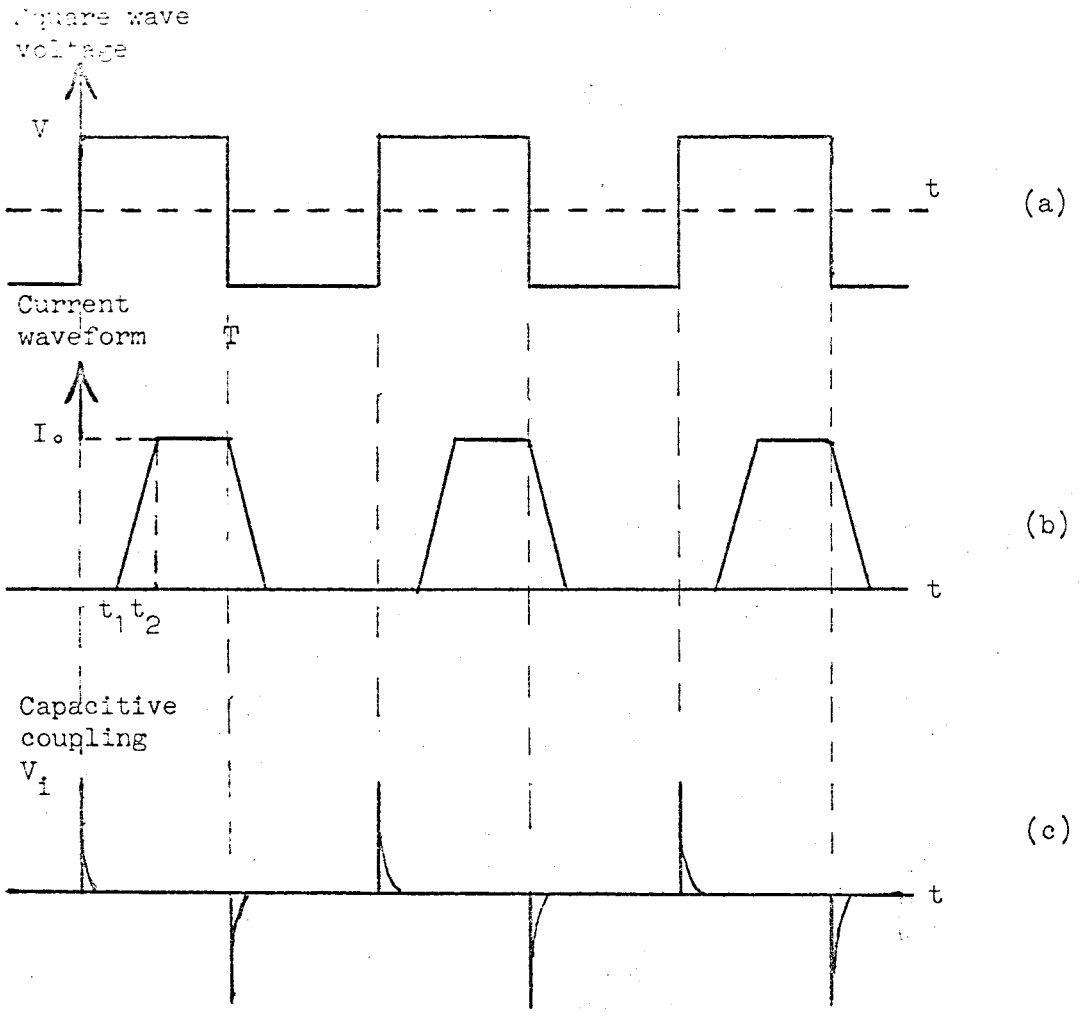

Fig 4.4 Theoretical current waveforms in a triode; for gating the source-grid space

D. Comment on Velocity Measurement

We see there are two opposing ~~results~~ views for the existence of the mobility discontinuities. The obvious difference between the experiments is the velocity measuring technique. The pulse method allows the current waveform to be examined, and any spurious shapes can be analyzed and the source of error identified. With the triode, the D.C. electrometer integrates the received pulses over a period of time, with the hope that spurious signals average out to zero.

We will give a theoretical analysis of the expected waveforms for various electrode configurations. Consider a triode system, but with a square wave applied between the source and grid, keeping the grid collector field constant. Then ions will periodically be injected into the grid collector region. Ignoring diffusion and beam spreading, the signal received at the collector will have a trapezoidal shape, as shown in Fig. 4. At time t = 0 the square wave passes ions from the source to the grid. After a time t_1 the charge passes the grid and enters the collecting space, inducing a current on the electrometer. When the ion beam reaches the collector at t_2 , the current has reached a constant value. After time T the square wave reverses the source grid field, cutting off the ion beam. The trailing edge of the beam still has to pass through the drift space, giving a falling current until all the ions have reached the collector.

Consider the circuit composed of the grid and collector, electrometer and D.C. power supply to grid. When we have a number of charges $n.d\Omega$ in volume $d\Omega$ moving from the grid to the collector with velocity v in an electric field E, the current di flowing in the electrometer circuit is given by

$$V_g.di = nev.E\ d\Omega$$

where V_g is the potential of the grid with respect to the collector.

Thus the current is

$$I = e\int_\Omega \frac{nvE}{V_g}\, d\Omega$$

If the field across the drift space is constant, we have

$$E = \frac{V_g}{d}$$

so

$$I = \frac{ev}{d}\int_\Omega n\, d\Omega \qquad (1)$$

$$= \frac{ev}{d}\, N(r)$$

where $N(r) = \int_\Omega n\, d\Omega$ is the total charge in the drift volume at time t. As the charge enters the drift space, N increases with time as

$$N(r) = nAvt$$

so $$I = \frac{nev^2At}{d} \qquad (2)$$

The current I reaches its steady value I_o when the charge reaches the collector

$$I_o = nevA \qquad (3)$$

If the charge pulse is now cut off, changing the time to be at t = 0, we now have

$$I = \frac{nevA}{d}\,(d - vt) \qquad (4)$$

Thus the waveform in Fig. 4(b) is given by equations 2, 3 and 4.

By measuring the time t_2 for the current either to reach its equilibrium value I_o, or to fall from I_o to zero on the off pulse, the drift velocity is easily calculated, knowing the drift distance d.

$$V_D = \frac{d}{t_2}$$

The pulse method used by Schwarz consisted of a source, a gating grid 2 mm from the source, a 1.9 cm drift space, a guard grid 1 mm in front of the collector. He measured the time taken by the trailing edge of a pulse of ions when the beam was cut off by a suitable voltage between the source and gating grid, with current in the rest of the cell. If the pulse was cut off at time t = 0, a constant current is collected until time t_1 when the trailing edge of the pulse reached the guard grid. The current then fell to zero in time t_2, the time taken for the ions to reach the collector from the guard grid.

Schwarz could identify effects which could cause error when using a D.C. electrometer. Incomplete guarding of the collector by the grid was shown by a gradual change in current while the on pulse was propagating between the grids. A sharp peak in the collected currents when the current was turned on was due to an increased ion concentration near the source during the off pulse. Both these effects could be eliminated by using a finer mesh grid, and higher source voltages. At low temperatures, when there could be ions and vortex rings present, complicated pulse shapes could be obtained due

Fig 4.5 (i) Theoretical current waveforms in a triode; for gating the grid collector space

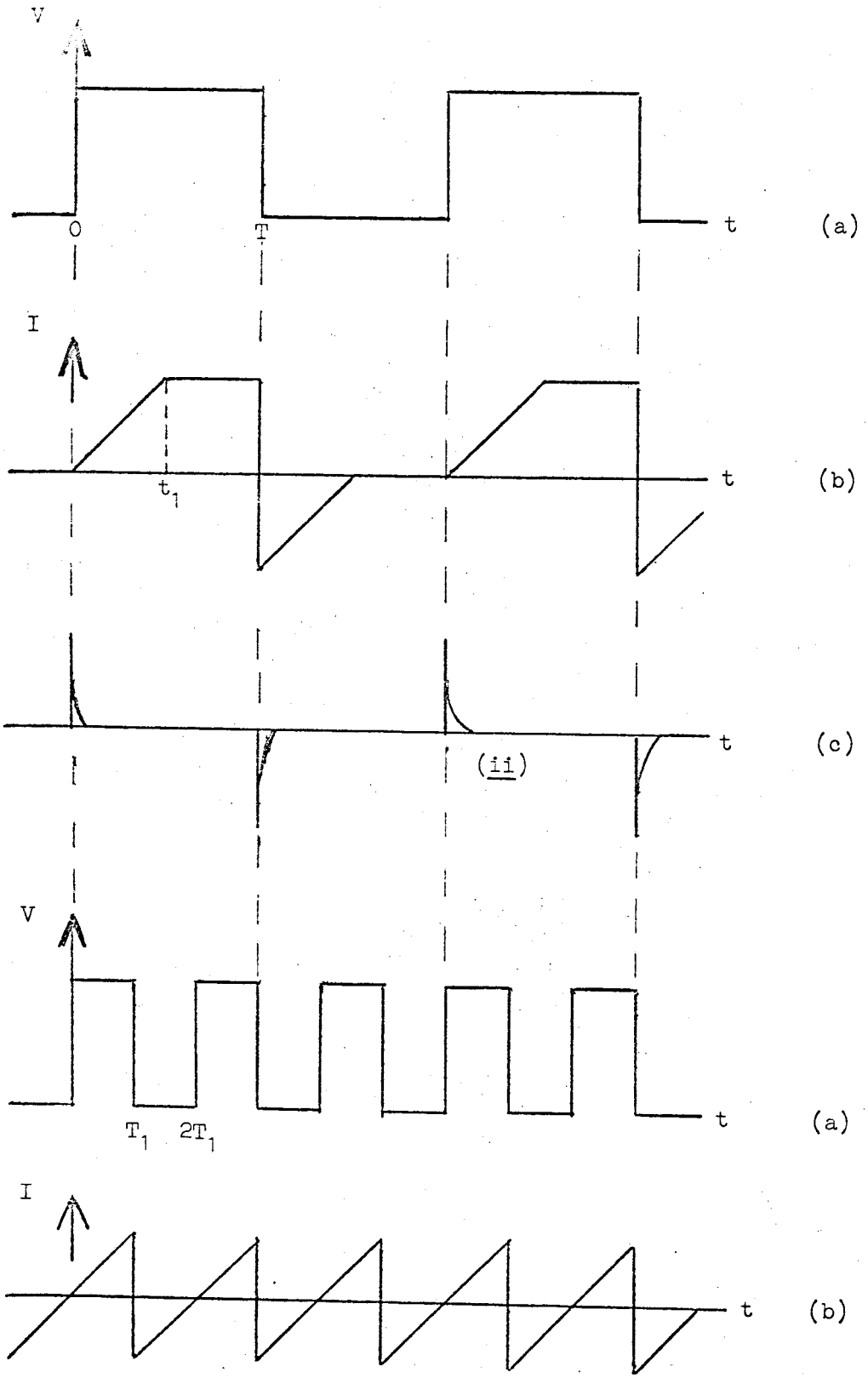

to a variety of effects. The limiting drift velocity of 4.8 m/sec for negative ions forming vortex rings below .53 K found by Cunsolo, Maraviglia and Ricci (1968) was found to be spurious, as pure negative ion currents were found at much higher velocities and lower temperatures. Diffusion and a spread in the ion beam velocity were shown to have a negligible effect on the pulse shape.

Capacitance coupling between the source and collector will result in an input waveform as in Fig. 4(c). If the stray capacitance between S and C is C_S, the input capacitance of the electrometer C_i, V_S the source voltage then the input spike voltage i.e. V_i is given by

$$C_i V_i = \frac{C_S C_i}{C_S + C_i} V_S$$

$$\text{i.e.} \quad V_i = \left(\frac{C_S}{C_S + C_i} \right) V_S$$

and decays exponentially according to the input time constant $t = C_i R$. Normally $C_i \gg C_S$, so

$$V_i \simeq \frac{C_S}{C_i} \cdot V_S$$

where C_S depends on how well the collector is shielded from the source.

The triode square wave method of measuring ion velocities depends on averaging a large number of current pulses. Fig 5 shows the expected waveforms integrated by the electrometer. When the square wave frequency is low enough to allow the ions starting

from the grid to reach the collector, the current waveform will look like Fig. 5(i) (b). At time t = 0 the square wave changes to allow the cell to conduct current. The front edge of the charge pulse produces the rising portion of the current waveform in (b) until at time t_1 the ions reach the collector. A constant current will be read until time T when the square wave reverses, drawing the ions in the drift space back to the grid. This produces the negative part of the current waveform, falling to zero at time $T + t_2$ when all the ions have been collected by the grid. Obviously, for an ideal set up, $t_1 = t_2$. As the collector has no shielding from the grid to which the square wave is applied, the pick up will be large, and of the form shown in Fig. 5(i) (c).

If the frequency of the square wave is increased, so that the ions never reach the collector, the current waveform should look like Fig. 5(ii) (b). From time t = 0 to T_1 the leading edge of the ion pulse travels towards the collector, giving an increase in current with time. At time T_1 the square wave reverses the field in the drift space, reversing the direction of motion of the ions, giving the negative part of the waveform. This should be zero at time t = 2T, when the grid has collected the ions. The maximum current amplitude is a decreasing function of the square wave frequency, as opposed to 5(i) (b) where the flat top portion of the current pulse is constant with frequency. For these ideal waveforms the capacitance spikes and the rising and falling parts

of the current waveform average to zero. In fig 5(i) (b) the current is then proportional to $I_o(T-t_1)$: i.e. $q_c \simeq I_o(\frac{1}{2f} - t_1)$

but $$I_c = q_c f$$

i.e. $$I_c = I_o(\tfrac{1}{2} - ft_1) \qquad (5)$$

where f is the frequency of the applied square wave and t_1 is the transit time for the ions across the drift space. As f is increased, I_c falls linearly to zero at $t_1 = \frac{1}{2}f_c$. Knowing the drift space distance d we then know the ion velocity by

$$V_D = 2f_c\, d \qquad (6)$$

When $f > f_c$ the current waveform in Fig. 5(ii) (b) averages to zero. We have then justified the triode operating equations 5 and 6, for the case of ideal behaviour of the ions.

In practice, a number of errors can creep in. The above analysis has depended on

(1) the ions reaching their steady velocity in a time much shorter than the transit time;

(2) there ~~is~~ being no field distortion, due to misalignment of the grids, stray fields, space charge at the grids, or the ions themselves;

(3) the square wave rise and fall time being much smaller than the ion transit time;

(4) there ~~is~~ being no charge bunching at the grid during the reverse cycle of the square wave;

(5) ~~that~~ the effective distance between the collector and grid for ion injection remains~~s~~ -ing constant;

(6) during the reverse cycle of the square wave, the ions ~~do~~ not interacting with the helium, causing hysteresis effects in a full cycle;

(7) the electrometer itself ~~has~~ having no frequency dependence.

For low field, low velocity measurements when the ion transit time is long, we expect most of the above errors to be significant only when it is near f_c i.e. as I tends to zero. In this case, extrapolating the low frequency part of the curve should give a reasonable estimate of f_c. At higher fields, close to the vortex ring transition, there could well be a mixture of bare ions and vortex rings present (Donnelly and Roberts, 1969) giving a complicated pulse shape and a non linear current against frequency graph. High energy vortex rings take a long time to reach a steady velocity, of the order of the transit time, and again a non linear graph is expected.

If any of the above effects leads to a distorted pulse shape, especially in the rising and falling sections, then a time average will not give zero current at $f = f_c$. Thus care must be taken when analysing the current frequency graphs when determining an ion velocity by the triode square wave method.

E. Theories of Discontinuities

The experimental results, on which the theories are based, may be summarized as follows.

(1) the phenomenon is unique to a superfluid system; reports by Henson (1964) of discontinuities in liquid nitrogen, unconfirmed by other experimentalists confuse the situation (see Chap. 6). Bruschi et al (1970) and Santini (private communication 1970) report discontinuities in 4 classical liquids, at temperatures up to 300 K; but existing theories have been based on the superfluid postulate.

(2) the discontinuities occur at periodic integer intervals of a critical velocity v_c: i.e. v_c, $2v_c$, $3v_c$ etc.

(3) the change in mobility $\frac{\Delta\mu}{\mu}$ is $\sim$ 6% at a discontinuity; the mobility is constant between discontinuities

(4) the critical velocity is independent of the ion beam density, or cell geometry

(5) v_c is different for positive and negative ions; i.e. the ion size determines the onset of the phenomenon.

(6) the extra dissipation suffered by the ion complex above v_c is due to an increased interaction with the normal fluid (from the 'heat flush' measurements)

(7) the temperature dependence of v_c is a complex function of the temperature, below $\sim 1^{\circ}$K, v_c is temperature independent.

(8) the thermal velocity of an ion at 1°K is around 6 m/sec;

depending on the value used for the ion's effective mass (Dahm and Sanders, 1966)

The proposed phenomenological theories, which only apply for $T \sim 1^{\circ}K$, fall into 2 groups; creation of vortex rings (Huang and Olinto 1965, Di Castro 1966, and Jones 1969), and excitation of vibrational states of the ion (Cope and Gribbon 1970). The temperature dependence of v_c has been explained by Bruschi et al (1968) by considering the superfluid velocity field around the ion. No theory covers both the multiple discontinuity phenomenon and the temperature dependence.

I. Vortex ring production theories

These are all based on the hypothesis that the ion, at the nth discontinuity, creates a vortex ring with quantized circulation $n\kappa$. The ion-ring complex is unstable, and breaks up. When the ion velocity is $\sim$30 m/sec it forms a vortex ring and binds to it, giving the fall in velocity with increasing field. We will examine each theory, showing their basic similarity, and how each one attempts to overcome a former difficulty.

(a) Huang and Olinto neglect fluctuations in the ion's velocity, and consider only steady state motion of the ion. They justify this by the fact that at $T \sim 1^{\circ}K$ the ion roton mean free path is the same order as the ion radius. Thus the drift velocity consists of a high frequency 'trembling' motion, and a slower

average drift velocity. Then, at a critical drift velocity v given by the empirical formula $6\pi R\, v = n\kappa$, where R is the radius of the ion, $\kappa = \frac{h}{m_{He}}$ is the circulation, n = 1, 2, 3, a vortex ring with circulation $n\kappa$ is created. The motion of an ion in an electric field E is described by an equation

$$M_{ion} \left(\frac{dv}{dt}\right)_{ion} = eE - F \qquad (7)$$

where F is the viscous force felt by the ion due to quasiparticle collisions, dominated by rotons for $T > 0.9^{\circ}K$. The ion accelerates to the velocity $v_{ion} = v_c$, where it stays at this constant velocity by feeding energy gained from the electric field into superfluid turbulence and forming a vortex ring with n = 1. The velocity of the vortex ring is assumed to be the same as the ion velocity i.e. v_c. For positive ions v_c = 5.2 m/sec and the size of a vortex ring with this velocity is $\sim$100 Å. For negative ions v_c $\sim$2.4 m/sec giving a vortex ring with a radius $\sim$250 Å. The time taken to form a vortex ring is calculated from equation (7) i.e. the rate at which energy is being transferred to the superfluid turbulence is $(eE - F)v_c$, and when this equals the energy of a vortex ring with velocity v_c the process is complete. If the electric field E is less than the critical electric field for the ion to bind to the vortex ring E_c, the viscous force on the ring causes it to lose energy and decay. The ion then accelerates in the electric field to a velocity $2v_c$, where it remains until a ring with circulation n=2 has been formed. This continues until the right hand side of equation (7) is zero, the ion has then reached its equilibrium velocity for the applied

electric field.

The critical field E_c for an ion to form a stable charged vortex ring, is found from considering the viscous force acting on an ion bound to a vortex ring. Huang and Olinto reduce this to form

$$F = n\alpha(T)\ (\eta - \tfrac{1}{4} - \frac{\ell n(1-\frac{v}{v_o})}{n}) \qquad (8)$$

where $\eta = \ell n(\frac{8R}{a})$. $\alpha(T)$ is the frictional force on an uncharged vortex ring , v_o = 58 m/sec = Landau critical velocity.

Stable motion is possible only if $F = eE$,

$$\text{i.e.} \qquad eE = n\alpha(T)\ (\eta - \tfrac{1}{4} - \frac{\ell n(1-\frac{v}{v_o})}{n}) \qquad (9)$$

The right hand side has a minimum value at $v = v_1$, so equation (7) cannot be satisfied unless $E > E_c$ where E_c is given by

$$eE_c = n\alpha(T)\ (\eta_1 - \tfrac{1}{4} - \frac{\ell n(1-\frac{v_1}{v_o})}{n})$$

For $E > E_c$ the charged vortex ring will adjust its velocity to that required by equation (9). For $E < E_c$, the charged vortex ring will always be suffering energy loss, which tends to accelerate the vortex ring and slow down the ion, pulling them apart.

When $E > E_c$, the motion of an ion is an acceleration to v_c according to equation (7), where a vortex ring, with velocity v_c and $n = 1$, is formed. The ion is trapped by the ring, and the velocity of the complex adjusts to fit equation (9).

On this theory, the velocity measured is the time average of the various critical velocities and the terminal velocity of the ion, giving an apparent mobility discontinuity when the terminal velocity reaches and passes a critical velocity. There is thus an explicit dependence of the size of the mobility discontinuity on the drift length of the ion in the electric field. The time for the ion to accelerate to a critical velocity, and the decay time for the break up of an unstable charged vortex ring are assumed negligible compared with the time of formation of a vortex ring at a critical velocity.

Quantitatively, the measured drift velocity v_D is given by

$$v_D = v_\infty \left(1 + \frac{g_n}{L}\right)^{-1} \tag{10}$$

where L is the length of the drift space, and

$$g_n = \frac{\varepsilon_o v_\infty}{eEv_c} \sum_{\ell=1} \frac{\ell\left(1-\ell\frac{v_c}{v_\infty}\right)}{1 - \frac{E_\ell}{E}} \tag{11}$$

ε_o is the energy of the vortex ring at the first critical velocity v_c, E_ℓ is the electric field at a critical velocity needed to satisfy equation (7), E the applied electric field and v_∞ the terminal velocity of the bare ion. The shape of the velocity field dependence is crudely interpolated by

$$v_\infty = v_o\left(1 - \exp\left(-\frac{E}{E_o}\right)\right) \tag{12}$$

where v_o is the Landau roton creation velocity, and E_o is given by $E_o = \frac{v_o}{\mu_o}$ where μ_o is the zero field mobility.

Using equation (12), E_ℓ is given by

$$E_{\ell} = - E_o \ln\left(1 - \frac{\ell v_c}{v_o}\right)$$

The validity of this theory obviously does not depend on the exact functional form of equation (12), which only describes the smoothed velocity-field characteristic needed for an estimate of the time taken to create a vortex ring.

(b) Di Castro postulated that an ion could create many vortex rings, above a critical velocity, instead of just one required by Huang and Olinto. The size of the step ($\Delta\mu$) is determined by the number of vortices formed during the transit time. The equation of motion for an ion is taken as

$$\frac{dP}{dt} = eE = \frac{M_i}{\tau} v_i \qquad (13)$$

where M_i is the ion mass, τ the relaxation time to reach a steady state velocity in the applied electric field E. When the ion exceeds the critical velocity, vortices may be formed; the necessary energy coming from the electric field, so that $\frac{dP}{dt} \neq 0$ in equation (13). The vortex which is formed is of a fixed size, and therefore velocity (depending only on the ion size and circulation); thus the impulse P_r of the ring is constant. Taking the time average of equation (13) we get

$$\dot{N} \; P_r = \Delta v \frac{M_i}{\tau} \qquad (14)$$

where $\dot{N}$ is the average creation rate of vortices; $\Delta v = v_o - v_i$ where $v_o = \mu_o E$, μ_o being the zero field mobility, and $v_i = \mu E$ thus $\Delta v = \Delta\mu . E$

and $$\dot{N} \cdot P_r = \Delta\mu \cdot E \cdot \frac{M_i}{\tau} \quad . \qquad (15)$$

Taking $\dot{N} \alpha E$ gives $\Delta\mu \sim$ constant.

For the second discontinuity, vortex rings with n = 2 are formed; from equation (15) $(\Delta\mu)_2 \alpha P_{r2} = 2P_{r1} \alpha 2(\Delta\mu)$, where P_{r1} is the impulse of the vortex rings formed at the first critical velocity. So the discontinuities are approximately the same size.

Euqation (14) can be written as

$$\dot{N} \cdot \tau = \frac{\Delta v \cdot M_i}{P_r}$$

or $$\frac{\tau}{t_r} = \frac{\Delta v M_i}{P_r} \simeq 10^{-4}$$

where $t_r = \frac{1}{\dot{N}}$ is the creation time of a vortex ring.

t_r is the characteristic time involved in the process responsible for the discontinuities; as it is much longer than τ, the thermal relaxation time, the process will depend on the average drift velocity of the ion, and not the instantaneous velocity - the thermal fluctuations may be ignored.

Again, a vortex ring of radius $\sim$ 100 Å is formed at a critical velocity by an ion of radius $\sim$ 10 Å. The Landau criterion of

$$v_c = \frac{\epsilon}{P}$$

is obviously not satisfied, needing an ion of far too large a mass (see appendix 1); this is overcome in both theories so far by allowing a long creation time i.e. the necessary energy is gained from the electric field. A more serious objection is the basic postulate of Huang and Olinto, and implicitly assumed by Di Castro,

that a critical ion velocity must be exceeded for vortex ring production; the expression $6\pi Rv = n\kappa$ remains empirical.

(c) Jones has refined the vortex ring model to take into account the image vortices in the ion when the ring is being formed. He considers the ion beam as a low density gas, with a Boltzmann energy distribution, and an energy spread comparable with the drift velocity. He then draws an analogy between the ion-vortex ring system, and the electron-phonon system for excess carriers in CdS described by Smith (1962) with the inverted population approach by Pippard (1963). Here, stimulated emission of phonons is possible in an electron gas when the electron drift velocity approaches the acoustic velocity, building up an acoustic wave.

For the ion-vortex ring case, an ion of initial and final momenta mv_1 and mv_2 produces an excitation of energy ε and momentum P ,conservation of energy and momentum gives

$$\frac{\varepsilon}{P} = \tfrac{1}{2}\frac{(v_1^2 + v_2^2)}{v_1 - v_2} = \tfrac{1}{2}(v_1 + v_2)$$

For emission, $v_1 > v_2$, and the process is only possible for

$$\frac{\varepsilon}{P} \geq \left(\frac{\varepsilon}{P}\right)_{min}$$

If we then assume the Landau criterion holds (i.e. $v \geq v_c = \left(\frac{\varepsilon}{P}\right)_{min}$ for the production of excitations) and that there is a unique velocity at which free vortices can be produced, then for an 'n' vortex to be formed

$$\left(\frac{\varepsilon}{P}\right)_{n\ min} = (v_c)_n$$

where $(v_c)_n = n(v_c)_1$

and $(v_c)_1$ is the first critical velocity. For low velocities ($v < v_c$) absorption of free vortex rings is preferred; there are more empty energy states corresponding to higher velocities than there are to lower velocities. The density of free vortex rings being negligibly low, this process is unimportant. When $v > v_c$, emission of vortex rings is energetically favourable, and the density of states is such that there are plenty of empty states at lower velocities. When $v > 2v_c$, emission of n = 1 and n = 2 vortex rings are both energetically favourable; but the population of states is such that the more energetic rings are preferred i.e. only n = 2 vortex rings are formed and shed by the ion. This gives the mechanism for the appearance of successive discontinuities, instead of an overall smeared fall in the mobility with field. This process considers the ion system as a whole transferring energy to the vortex system, both being in thermal equilibrium. The drop in mobility is given by

$$\frac{\Delta\mu}{\mu} = \frac{\dot{N}'}{N} \cdot \frac{P}{eE}$$

where $\dot{N}'$ is the rate of production of vortices with momentum P, N the number of ions in a field E. This is similar to equation (15) in Di Castro's theory, except Di Castro applied it to each individual ion and not the whole ion system.

The next part of the paper considers the microscopic details

of vortex ring production by individual ions. As shown in appendix I, an ion of mass 100 M_{He} needs a minimum velocity of 100 m/sec to create a vortex ring obeying the free vortex ring $\varepsilon - P$ relationship. Jones suggests that the critical velocity is lowered when image vortices are considered in the ion; the vortex ring when nucleated close to the ion is compressed from its equilibrium radius when free from the ion's influence. His argument is that rings are nucleated near the rear stagnation point of the ion, expand by drawing energy from the superfluid potential flow past the ion, and are shed when the vortex tangential velocity at the ion surface is zero. This gives two criteria for a critical velocity v_c: (1) as the free vortex velocity v_r is in the same direction as the ion motion u, shedding occurs when $v_r \leq u$, i.e. $v_c = v_r = u$.; (2) The other criterion, of zero tangential velocity, considers the tangential velocity round the ion due to the motion of the ion through the fluid, and the velocity fields of the vortex and its image; i.e. the vortex is shed when its velocity field counters that due to the potential flow of the ion. A full three dimensional analysis being formidable, he arrives at an approximate criterion

$$\pi R v = n \kappa$$

which has the same format as the Huang-Olinto postulate.

Jones then tries to fit this theory to the temperature dependence of the critical velocity, found by Bruschi et al. The effect of normal fluid ρ_n on a vortex core is to produce a dissipative force

proportional to the length of vortex core, ρ_n, and the relative velocity between the normal fluid and the vortex. For a free vortex ring, a dissipative force reduces its energy, and therefore radius, while accelerating its motion. He goes on to say that for a vortex to be shed, while under the influence of such a force, it must be nucleated with a larger energy (lower velocity) than in the case where the force is absent. As the force increases, the vortex ring radius close to the ion will increase more rapidly, so it leaves the ion earlier in its trajectory, and gives a lower critical velocity. As the force on the vortex ring is equivalent to a velocity, he expects

$$v_c(\rho_n) = v_c(o)\ (1 - c\rho_n)$$

where c is a constant, and is of the form found by Bruschi et al for temperatures between 1.2°K and 1.4°K. Above 1.4°K, to the λ point, the ion drags normal fluid with it due to viscosity, setting up a counterflow of superfluid. Vortices are formed at a constant superfluid velocity v*, so the critical velocities now go as

$$v_c = \frac{\rho_s}{\rho_n} \cdot \frac{1}{\beta} \cdot v^*$$

where β is a constant describing the increase in ρ_n due to electrostrictive and van de Waals forces round the ion.

Summary of Theories, and General Criticism

1. Circulation $n > 1$

All those theories have depended on the formation of vortex rings with circulation $n\kappa$ at a velocity $(v_c)_n = n(v_c)_1$. There has

been no evidence from other experiments of vorticity with $n > 1$; and by considering the velocity field near the core of a vortex

$$v_s = \frac{n\kappa}{2\pi r}$$

if we define a core radius by $r = a_n$ at a critical value of v_s = constant for all n (which could be the roton creation velocity) then we see that $a_n = \frac{n\kappa}{2\pi(v_s)_c} = na_1$ where a_1 is the core radius for unit circulation. If we take $a_1 \sim 1$ Å than for $n = 5$, $a_n \sim 5$ Å; this would seem large with respect to the ion radius of ~ 10 Å. Without a full quantum description of the ring or the core it is difficult to imagine the nucleation of such an entity, which would be dominated by the core.

It is found at high fields that the ion is trapped by a vortex ring at a velocity $v_g \sim 30$ m/sec. This ring always has unit circulation, while the theories say the ion should be nucleating rings with $n = 6$ or more. Huang and Olinto explain this by their stability criterion. For $E < E_g$, where E_g is the field corresponding to the ion velocity v_g, the ion forms an $n = 1$ ring, sheds it and accelerates and forms $n = 2$ ring etc., until it is in equilibrium with the applied field. The vortex rings have been shed as the viscous forces on the ion plus vortex ring complex do not balance the electric field force. But for $E > E_g$, the ion accelerates to form an $n = 1$ ring, and the complex can then adjust its velocity to satisfy zero net force on the complex; this is impossible for fields $E < E_g$.

It is obvious that if the ions already had a velocity greater than the first critical velocity needed to form an n = 1 ring when they entered the field $E > E_g$, they would accelerate to form an n = 2 ring; if this complex could find an equilibrium velocity in the field, it would become a stable entity, and should be capable of detection. No sign has been seen of them. From the theory, the electric field E_{g2} for stability of an n = 2 ion-ring complex is greater than that E_{g1} for an n = 1 ion ring complex. Therefore for fields $>E_{g1}$, but $<E_{g2}$, the ion should form rings with higher n and reach a limiting velocity around 42 m/sec. Again this has remained undetected.

Jones suggests that at ion drift velocities around v_g, vortex rings with $n \sim 5,6$ are being formed and shed, while n = 1 rings are also nucleated; but unable to move against the potential flow around the sphere in order to be shed, they are swept back to be trapped in the ions flow pattern, in a stable situation analogous to the classical case. As the complex gains energy from the field, the vortex ring grows and traps the ion in the core.

The formation and trapping of vortices behind two dimensional bodies is known to be stable classically; (here, at higher flow velocities the vortices are shed, forming the von Karmen vortex sheet); it is probably also stable for three dimensional bodies. We therefore expect the formation of a vortex ring by an ion to resemble the formation in a classical case; we need to know how the ring is first nucleated, and its subsequent history. Jones cannot

preclude the formation of rings with any value of n, and therefore he should consider all possible trajectories.

2. Criterion for Vortex Shedding (Production of Free Vortices)

The existence of mobility discontinuities at a critical velocity is because, in all three theories, there is a critical ion velocity at which the ion forms and sheds vortex rings. This critical velocity is empirically given by

$$k \cdot R_{ion} v_c = n\kappa$$

where k is a constant.

It is this condition that precludes forming and shedding vortex rings at velocities less than v_c. Huang and Olinto, taking $k = 6\pi$, assuming (1) that there is a long creation time to avoid the Landau criterion and get enough energy to form the vortex ring, and (2) that only one vortex ring is created by the ion at each critical velocity while attaining its equilibrium velocity, arrive at an expression for the measured drift velocity which depends on the drift length of the cell measuring the velocity. Goodstein et al (1968) have carried out a differential measurement of the ion mobility in two cells of different lengths. Their results did not agree with prediction, and showed no length dependence at all. They had difficulty in getting a discontinuity, but the Huang Olinto theory also predicts a high ion velocity cell length dependence independent of the mobility discontinuities being smeared out, which was not verified. However, this high field behaviour depends on the expression used for the

ion velocity as a function of field; and their formula (equation (6))

$$v_\infty = v_o \ (1 - e^{-E/E_o})$$

is only a crude approximation.

Goodstein's experiment did not exclude theories without the Huang-Olinto length dependence, i.e. the multiple creation idea by Di Castro and Jones.

Di Castro says an ion can shed a vortex ring when the ion velocity exceeds the vortex ring velocity. This process is obviously true for any ion velocity, so he assumes that an ion can only create free vortex rings of a certain size, depending on the ion radius. This is implicitly assuming a criterion similar to Huang and Olinto, and will then give a critical velocity, when the free velocity of the fixed radius vortex ring is less than the ion velocity. He considers the time taken to form a ring, and arrives at a time $\sim 10^4$ times greater than the thermal relaxation time; thus there is no need to consider satisfying the Landau criterion, or worry about the ion velocity's thermal fluctuations. The ion creates vortex rings of a fixed size continuously during its motion across the measuring length, instead of just the one in the Huang Olinto theory.

The n th discontinuity is due to forming vortex rings of the same size as are formed at n = 1, but with circulation $n\kappa$. For all ion velocities v_i, for $(v_c)_n \leq v_i \leq (v_c)_{n+1}$ vortices with circulation $n\kappa$ are formed. No justification for this postulate is given; and it is difficult to understand why the ion should not form

fixed size vortex rings, but with perhaps different n, and therefore velocity, at any ion velocity $v_i > (v_c)_1$.

3. Criteria for Periodicity of v_c

Di Castro then has three unexplained postulates; (1) the ion can only form a fixed radius vortex ring (with any value of n) (2) The ring is shed when $v_i \geq (v_r)_n = (v_c)_n$ (3) Only n rings are formed for $(v_c)_n \leq v_i \leq (v_c)_{n+1}$.

The third postulate is implied in his analysis; as the electric field increases between two critical velocities, the vortex ring production rate increases to balance the energy gain with loss of momentum to keep a constant ion mobility. If at a critical velocity $(v_c)_{n+1}$,(n+1) rings were not formed,then the ring production rate would have to show a sudden increase to give the additional loss of momentum. But if (n+1) rings were formed, (with impulse $(n+1)\ P_1$) then the same ring production rate would give an additional loss of ion momentum $\frac{(n+1)P_1}{n\ P_1}$ to give the (n+1) discontinuity. So assuming a vortex ring production rate proportional to the electric field, and increasing smoothly, as Di Castro does, he implies postulate (3) above to give the successive discontinuities. He gives no explanation for the critical ion velocity v_g when the ion forms and binds to a n = 1 vortex ring.

Postulate (1) may be critized on the grounds that although the ion can only form vortex rings of a critical size, this must be considered as an upper or lower bound on the possible size; if it could

form smaller rings, with velocity $v_r > (v_r)_c$ where $(v_r)_c$ is the velocity of the ring formed in Di Castro's postulate, then there is a critical ion velocity $v_i > (v_i)_c$ at which they would be shed. Similarly for higher energy, slower vortex rings would give $v_i < (v_i)_c$. Thus a continuous ring spectrum, perhaps bounded by $(v_r)_c$, would smear out the first discontinuity. Periodic discontinuities, involving $n > 1$, depend on postulate (3), which in the absence of any reason why n rings are favoured over any other value of $n < n_c$ rings, must be considered to be ~~shaky~~ dubious.

Jones implies the same three postulates as Di Castro, and tries to justify (1) and (2) from a microscopic theory of ring nucleation by an ion, and postulate (3) by considering the ion system and vortex system as a whole. He considers that the free vortex ring $\varepsilon - P$ relationship is modified close to an ion due to image vortices, and that at a critical velocity $(v_c)_n$ vortex rings with energy ε and momentum P can be produced, satisfying Landau's criterion

$$(v_c)_n = \left(\frac{\varepsilon}{P}\right)_{\min_1 n}$$

where $\left(\frac{\varepsilon}{P}\right)_{\min_1}$ refers to the modified vortex ring dispersion relationship. Then, for ion velocities $v_i > (v_c)_1$ the ion system, which has a Boltzmann distribution in velocity space, can emit vortex rings. For $(v_c)_n \leq v_i \leq (v_c)_{n+1}$, the ion is allowed to emit vortex rings with any value of n. But he says the relative occupation of states by the ions will favour rings with the highest value of n being

emitted and these rings will be those with the highest energy. The ions themselves therefore will occupy the lowest possible energy states after the emission of vortex rings. The number of ions in the different initial states will be governed by the classical Boltzmann distribution, because the density of ions in the beam is low. The transition probability for the emission of a ring does not depend therefore on the number of ions in these states. On statistical grounds there will be no reason therefore for the system to show a preferential emission of the vortex rings with large circulation $n\kappa$. The assumption that the transition probabilities were different can be ruled out, because this would have given a dependence of the size of the discontinutiy on the ion density, and this was not observed experimentally. Jones, therefore, cannot account for the periodicity of the discontinuities by his explanation of postulate (3). Such a postulate still remains a necessary part of the theory of the discontinuities. This may be shown by taking Jones' equation for the conservation of momentum of an ion-ring system, and writing it for nth discontinuity of constant size as

$$\frac{\Delta\mu}{\mu} = \frac{N'}{N} \cdot \frac{P_n}{eE}$$

where P_n is the momentum (impulse) of the vortices formed by the ion.

As the field increases between two critical velocities, the rate of production of vortices $\dot{N}'$ must be proportional to the field E to keep $\Delta\mu$ constant. So the above equation may be written

$$\frac{\Delta\mu}{\mu} = A \cdot P_n$$

where A is a constant ($A = \frac{\dot{N}'}{NeE}$)

The only way $\frac{\Delta\mu}{\mu}$ can change at a discontinuity is for P_n to change - for a classical vortex ring $P_n = nP_1$ where P_1 is the impulse to form a ring with n = 1.

Thus $$\frac{\Delta\mu}{\mu} = AnP_1 = n \cdot x \text{ constant}$$

If we allow the production of vortices per unit field to increase at a discontinuity, then we need not keep the postulate (3); but instead find an explanation for the vortex production rate depending on ion velocity.

Jones is uncertain in his microscopic theory of nucleation as to whether the critical ion velocity occurs when the vortex ring is just nucleated ($(v_c)_n = (\frac{\varepsilon}{P})_{min_1 n}$) or when the vortex ring is shed; his explanation of the temperature dependence of $(v_c)_1$ implies that the ion can nucleate vortex rings of any size and the effect of the normal fluid is to pick out the higher energy ones and let them leave the ion at lower velocities as ρ_n increases. When $\rho_n = 0$, (at T = 0) he does not say what happens to these higher energy ones that can presumably still be nucleated. The lower energy ones, having a higher

velocity than the ones that expand round the ion and are shed, will simply annihilate with their image in the ion. The momentum lost by the ion is due to the energy gained by the ring from the electric field via the potential flow past the ion as it grows; the nucleation of the ring in the first place involves nucleating the image with an equal and opposite impulse. We would thus expect that the critical velocity does not depend on the criterion $v_c \geq (\frac{\varepsilon}{P})_{min}$, but instead depends on the growth of a ring round the ion, leading to a criterion relating the ion radius and the critical velocity. Without the benefit of a proper theoretical discussion on this process, we would expect a lower bound on the energy of a nucleated ring for it to grow and be shed; but a ring with a higher energy would be expected to be shed at a lower velocity; a critical velocity might be observed if there is an upper limit on the energy of a nucleated ring, but otherwise we expect shedding of rings at all velocities, and thus no discontinuities.

Summary

We may summarize the above arguments by saying if and only if the three postulates given above are all true will periodic discontinuities exist; no reasonable explanation has yet been given to prove their validity. We do not doubt that ions can produce vortex rings, presumably by nucleation and growth, although even the process of nucleation is unknown (perhaps a proto - ring or roton suggested by Donnelly and Roberts, 1969), but only that the ion size determines a unique size

of vortex ring (postulate (1) before).

Another vortex ring production theory is by Donnelly and Roberts (1969) who suggest that a roton captured in the ion's velocity field has a probability of diffusing over a barrier in momentum space to form a ring; the probability of an ion nucleating a ring is large only for large ion velocities i.e. at $v_i = v_g$. They define a function $\frac{N_i}{N}$ which is the fraction of ions which do not form rings in unit time; and a plot of $\frac{N_i}{N}$ against the ion velocity shows it decreases sharply from unity only at high velocities. Experimentally, the decrease fits the theory, and the critical ion velocity for forming vortex rings ($\frac{N_i}{N} \simeq e^{-1}$) agrees for experiment and theory ($0.4 \lesssim T \lesssim 1.5^{\circ}K$). Although this theory applies to the high ion velocity formation of vortex rings, it also strongly implies that rings will not be formed at lower ion velocities; certainly not by the same fluctuation mechanism.

II. Vibrating Ion Theory

Because the ion structure is deformable, it is assumed that it can be made to vibrate at certain frequencies, according to the mode of the spherical harmonic which is excited. For certain assumptions about the ion structure, the vibrational frequency ν may be calculated, and hence the excitation energy $h\nu$. It is found that $\nu \simeq 10^{10}$, 10^{11} c/s, so $h\nu \sim kT$ where $T \sim 1^{\circ}K$.

Cope and Gribbon describe the motion of an ion by an analogy with a Frank-Hertz type experiment. When the ion has enough energy so that in an inelastic collision with a quasiparticle the ion loses some of its forward momentum, a vibrational state can be excited in the ion. The repetition of this process throughout the path of the ion gives an apparent decrease in the ion mobility.

There are a number of collision processes that could occur with quasiparticles; the ion could collide with a roton, with the roton losing its thermal energy $\sim\frac{1}{2}$ kT and the ion losing some of its kinetic energy;or it could absorb a roton, emitting a phonon;or the converse, absorbing a phonon and emitting a roton. If there is a long interaction time during the collision, energy can be gained from the field. The actual collision which is considered will give critical ion velocities which depend on the ion's effective mass; more important,the ratio of positive to negative ion masses and vibrational frequencies varies according to the process, assuming the experimental critical velocities. Cope and Gribbon eventually decide that the most likely collision is roton absorption with phonon emission. This will give the periodicity of the discontinuities at the experimental critical velocities if the positive ion mass $\simeq 80\ M_{He}$ and the negative ion mass $\simeq 160\ M_{He}$. This requires the vibrational frequencies of the two ions to be equal. The collision process chosen is just the instrument for providing the discontinuities - perhaps more than one type of collision might occur but only one

is dominant. Choosing the roton absorption, the following picture emerges. For $v_i > (v_c)$, an ion can be excited in a collision, losing kinetic energy $\frac{1}{2} mv_c^2$ - i.e. the ion velocity is reduced by the critical velocity necessary for excitation v_c. The time between collisions is inversely proportional to the ion velocity (giving a constant mobility with field between discontinuities) and an exciting collision occurs once in every 150 elastic (non-exciting) roton collisions, giving the magnitude of $\Delta\mu/\mu$. After exciting a vibrational state, the ion emits a phonon in a time $\sim 10^{-10}$ secs, and accelerates to its equilibrium velocity. A long interaction time $\sim 10^{-9}$ secs is assumed to allow for the ion's thermal fluctuations in its velocity.

When $(v_c)_2 \leq v_i \leq (v_c)_3$, the ion can excite its second vibrational state in an inelastic collision, reducing its velocity by v_c, so now $(v_c)_1 \leq v_i \leq (v_c)_2$. While the ion is accelerating again it has a finite probability of exciting its first vibrational state, and so losing more velocity v_c. This produces the second discontinuity. For a second discontinuity to appear, the second vibrational state must have a much larger probability of excitation then the first when $v_i > (v_c)_2$, and after this has been excited, the first vibrational state must then be excited. This postulate is similar to the vortex ring theory, when only n vortex rings are produced at the nth discontinuity. But here we have additional postulates, that after the nth vibrational state has been excited,

so must the (n-1)th etc ; and also that the frequency of excitation of the nth vibrational state at $(v_c)_n$ is the same as the frequency of excitation of the (n-1)th vibration state at $(v_c)_{n-1}$. Only then will the size of the discontinuity be constant with n. It is much more likely that vibrational states are excited randomly, giving a continuous decrease in mobility with increasing ion velocity.

This is a general criticism of any excitation process, and independent of the actual inelastic collision mechanism; the excitation probabilities must have very stringent requirements to satisfy before discontinuities can become observable.

F. Experimental Results

A basic criticism of published data is the drawing of empirical discontinuous lines through experimental points with no error bars, to emphasis the discontinuous nature of the phenomenon. The lines, corresponding to constant mobility levels, minimize the error in one velocity range of the measured mobility. Drawn in this way, most points with an error of ±2% (a typical stated maximum relative error in one velocity measuring run) lie on the lines. To fit points for ion velocities just greater than a critical velocity, the drop in mobility is not sudden, but falls gradually to the new level. Discontinuities are sharper for higher temperatures. (See Careri et al 1964, their Figs 3 and 5).

If we allow an error of ±3% in the measured mobility (∿ half the drop in mobility at a discontinuity) then continuous lines may be drawn through the points; thus we can only claim experimental evidence for the discontinuities for errors in the mobility less than ∿3%.

Careri et al discuss their errors for measuring the absolute value of the mobility. This is composed of the uncertainty in both the applied electric field and the value of the velocity, and also the value of the absolute temperature. The temperature was kept constant to 10^{-3}°K, giving an accuracy of 0.5% in the mobility with this temperature fluctuations. The drift velocity depends on the electrode spacing, known to 1.5%, and the cut off frequency

Careri's
0.5%, of ~~their~~ square wave, and do not allow for any error in calculating the value of the cut off frequency from their graph. The applied electric field depends again on the electrode spacing, known to 1.5% as before, and the amplitude of the square wave - measured on a voltmeter to ~1%. They quote a total systematic error of 4.5%, for an absolute value of the mobility.

What is more important is the relative error between points taken in one run; then the electrode spacing does not affect the result. This is easily seen from the triode operating equation, which leads to the ratio between two mobilities at the same temperature in different electric fields given by

$$\frac{\mu_1}{\mu_c} = \frac{(f_c)_1}{(f_c)_2} \cdot \frac{V_2}{V_1}$$

where f_c is the cut off frequency in an electric field produced by a square wave of amplitude V. It is this relative error that is important when discussing discontinuities. Careri et al estimate a relative error of ~2%, made up of 0.5% from keeping the temperature constant, 0.5% from knowing the absolute value of the frequency of their pulse generator, and 1% from the square wave amplitude. Again they ignore the error in actually calculating the value of f_c from their graphs.

Goodstein (1968) quotes a scatter of ~2-3% in relative values of the mobility using a triode cell; 1.5% for a temperature fluctuation of 10^{-3}°K, ~1% from extrapolating the current-frequency to zero current, and ~0.5% for the square wave amplitude.

Bruschi et al (1968) discuss the effect of cleanliness in the cell, especially the electrodes. Clean electrodes give a good linear relationship between the current and frequency, leading to a well defined cut off frequency. If the electrodes are not clean, a high frequency current tail appears near the cut off frequency, which is therefore not well defined. They discarded these results. No criteria of cleanliness is given, apart from the production of tails. All the electrodes were gold plated to try to avoid contamination. Even allowing for the best possible estimate of f_c, the error will be about 1%; even if a proper statistical analysis is made of each individual current/frequency reading to get the best straight line for an estimate of f_c, this is only relevant if a number of different runs are made to get an estimate of the error in f_c; and reproducibility is limited by temperature fluctuations which will determine a lower bound on the estimate of around 1%. Thus in a series of readings for different mobilities there is still an error of $\sim$1% for f_c, about 1.5% for temperature fluctuations, and $\sim$0.5% for the square wave amplitude, giving a total of 3%. Obviously accuracy is now limited by the temperature; and in theory this could be better controlled - it is fairly common practice to control to 10^{-6}°K. However there is heat being produced in the cell, both by the passage of the ions, and due to the radioactive source. If the potential difference between two electrodes is 100 volts, and there is an ion current of 10^{-12} amps,

there is 10^{-10} watts of joule heating being dissipated. A larger source of heat comes from the radioactive source $\sim 5.10^{-6}$ watts. This is negligible compared with a normal heat leak of a few milliwatts into the helium bath, but could cause thermal disturbances in the ion cell ; Careri has explained anomalous results (metastability) by such thermal upsets.

Assuming a total error of around 3%, then all the published data on discontinuities can be fitted by continuous curves i.e. all points lie within their errors on this curve. This means that a proper statistical analysis,considering the mean square deviations from a curve, will be unable to distinguish between a continuous or discontinuous theory, when the deviations are properly weighted by their experimental error of 3%. If we assume a discontinuous mobility theory, then the results can be analysed to give the discontinuity i.e. the critical velocity. This is basically what Careri et al and Bruschi et al have done, without proving the existence of the discontinuities first. For each run they get a value for v_c, assuming its existence, and then get the best value of v_c, i.e. their analysis gives a spread in v_c of 5-10%. A similar uncertainty in v_c for classical liquids is reported by Bruschi et al (1970).

Cope reported discontinuities of up to 10%, with no estimated error in each mobility measurement. His estimated error in v_c is $\sim$5%; this is due to the non sharpness of the discontinuities, and

thus in estimating a critical velocity by extrapolating the fall in the mobility back to the first constant level. The estimate of v_c thus depends on the number of readings taken in the vicinity of the critical velocity.

Cope measured the current by reading a meter on the electrometer; this has been found to be in error by at least 5% . The voltage square wave was obtained from an Advance H1 square wave generator. We estimate that the frequency of his square wave may have been measurable to an accuracy of ∿6%, while his output voltage may have been measurable to ∿5%. We conclude that the error in his relative mobility measurements may have been about 6%.

G. Summary

Mobility discontinuities have their basis in experimental results; the theories are phenomenological attempts to explain the results. We have tried to show that no existing theory gives a satisfactory explanation, without raising even more debatable postulates; this in itself does not negate their existence, but throws the emphasis back to analysing the experimental results. Here we have two clear cut divisions; a specific negative from Schwartz, and an implied negative from Rayfield and Reif, and a very well behaved, but unexplained, phenomenon from Careri et al. Bruschi et al (1970) have also reported discontinuities in classical liquids, agreeing with Henson's reported discontinuities in liquid N_2 and Ar . In liquid helium, discontinuities have only been seen with a triode cell; but even with this it is not always possible to find them - an Italian group in Padua did not have discontinuities with the same design of apparatus as a different group in Rome, who did have discontinuities. Then the situation reversed. Goodstein had great difficulty in measuring a discontinuity while testing the Huang-Olinto theory. Cope found discontinuities with $\frac{\Delta\mu}{\mu}$ of the order 7% to 10%, while our work, using a different cell with the same geometry, and more sophisticated electronics, has shown no reasonable sign of sudden changes in mobility.

We have also tried to show that in the absence of a theory for discontinuities, the accuracy of the experiments cannot

distinguish between the existence of discontinuities or their absence in an unequivocal way.

This can only be done by finding a theory that could account for the gross velocity-field dependence, and using this to see if there is a statistically significant deviation from it at the critical velocities.

Fig 4.6 Current versus frequency curve showing two possible straight line fits

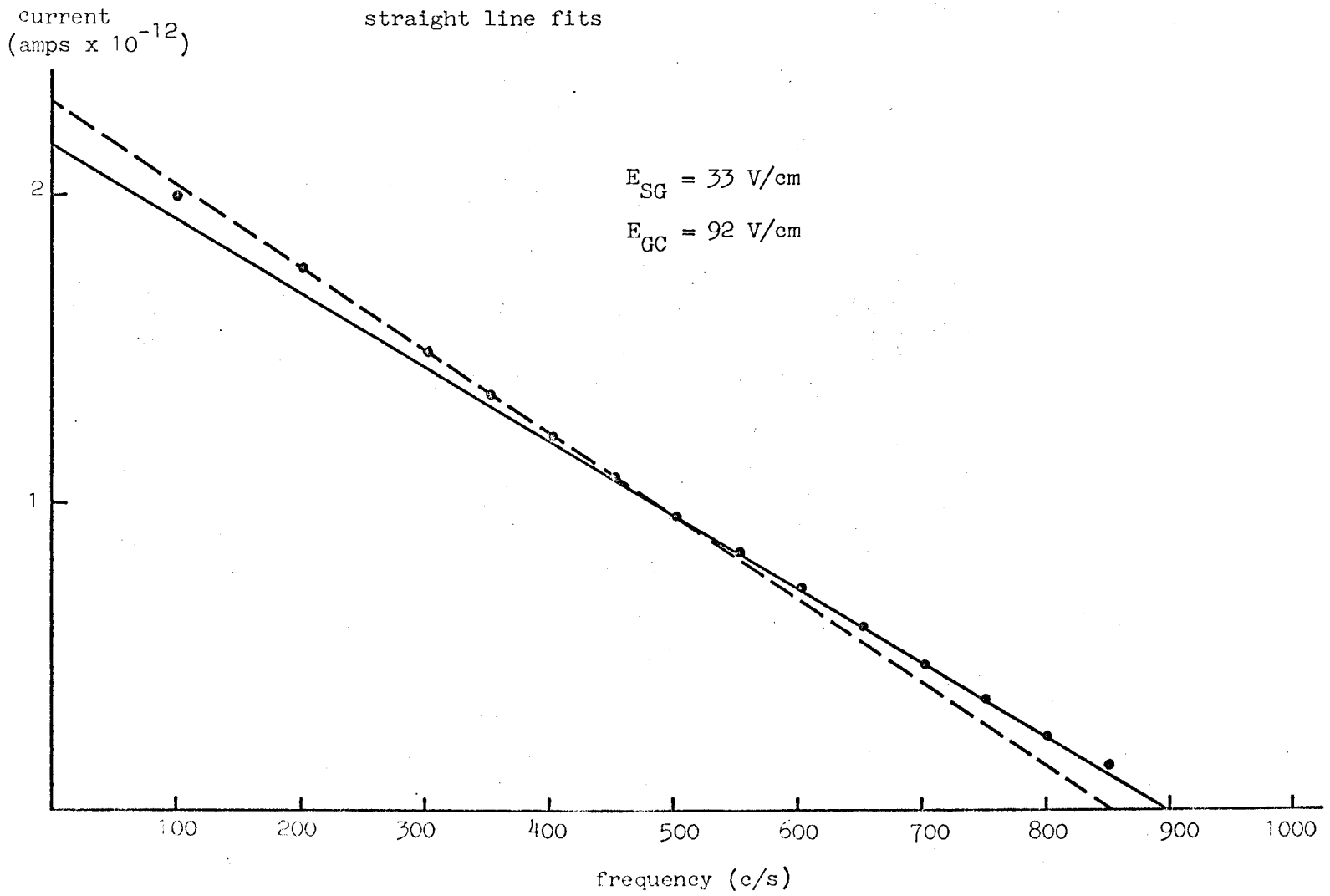

II RESULTS

A. Velocity Measurement

We used the triode square wave method, where the ion velocity is calculated from the cut-off frequency in a plot of current against frequency. The runs were taken for a number of different grids (mesh sizes 60, 110, 250 and 500 lpi) and electrode spacings (2 - 8 mm) at various temperatures (0.9-1°K). Within the accuracy of knowing the absolute temperature (about 10^{-2}°K) and the grid spacings, the mobility values were consistent with previous measurements.

It was found that the greatest error in our results arose from the current-frequency graphs in finding the cut off frequency f_c. The current was read every 25 or 50 cycles for a constant square wave voltage, with the lowest frequency used of 20 c/s, determined by the square wave amplifier time constants. This put a limit on the lowest fields used, of about 20 v/cm, to get enough points to draw a reasonable line - the lowest cut off frequency would be about 100-150 c/s. It was found that for low fields a good straight line could be drawn through all points, but as the field increased there would sometimes be a systematic high frequency current increase giving the effect of two lines; see Fig (6). We concentrated the measurements in the temperature range 0.9°K to 1°K, and with source-grid fields described by Cope to give the maximum discontinuity size. The low field mobility for positive ions would then vary from

7 to 14 cm^2/volt sec. Within these limits there was no systematic dependence for the onset of nonlinearity in the I-f curves on either the square wave frequency or field. In a typical run at a fixed temperature and source-grid field, the low square wave field graphs gave straight lines through all the points. There would then be a transition period with the low frequency points on one line and the high frequency points on another line with a higher cut off frequency. For higher fields the high frequency points constituted the main part of the whole graph. Where there were two possible lines, the frequency where they joined stayed nearly constant, or showed a small decrease, as the square wave field increased. This transition frequency was around 300 - 500 c/s. When velocities were measured up to the vortex ring creation velocity, it was found that the high frequency part of the graph gave consistent velocities. Later work, giving a continuous plot of current against frequency on an X-Y recorder, confirmed that for high square wave fields, the low frequency part (up to ~300 c/s) of the curve was anomalous, in that it showed a large deviation from the best straight line drawn through the rest of the curve. For low square wave fields there was no anomaly, and good straight lines were obtained.

Our results were obtained by considering the whole graph for low fields and the major high frequency part for high fields. For the transition range (commonly around the value expected for

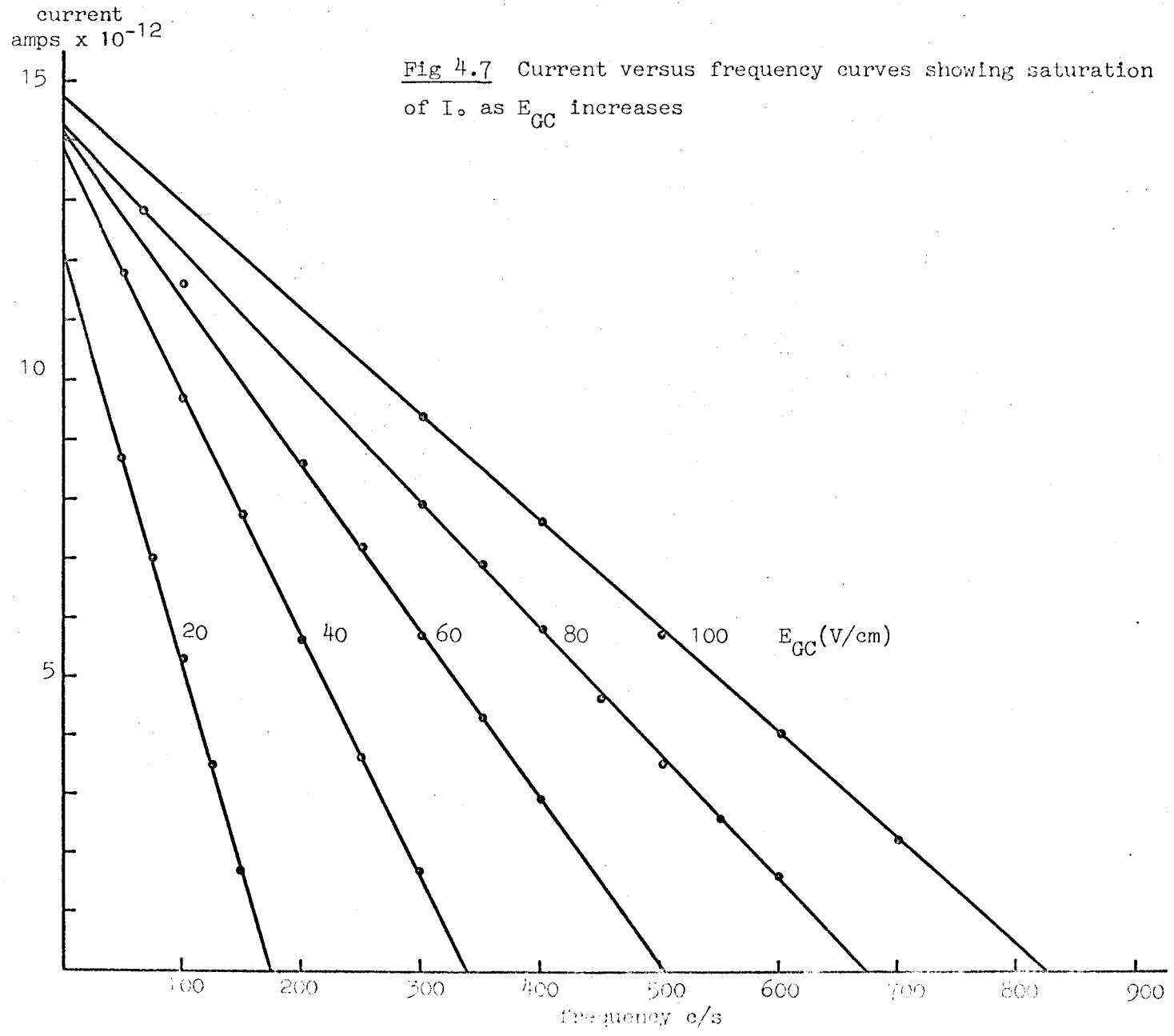

Fig 4.7 Current versus frequency curves showing saturation of I_o as E_{GC} increases

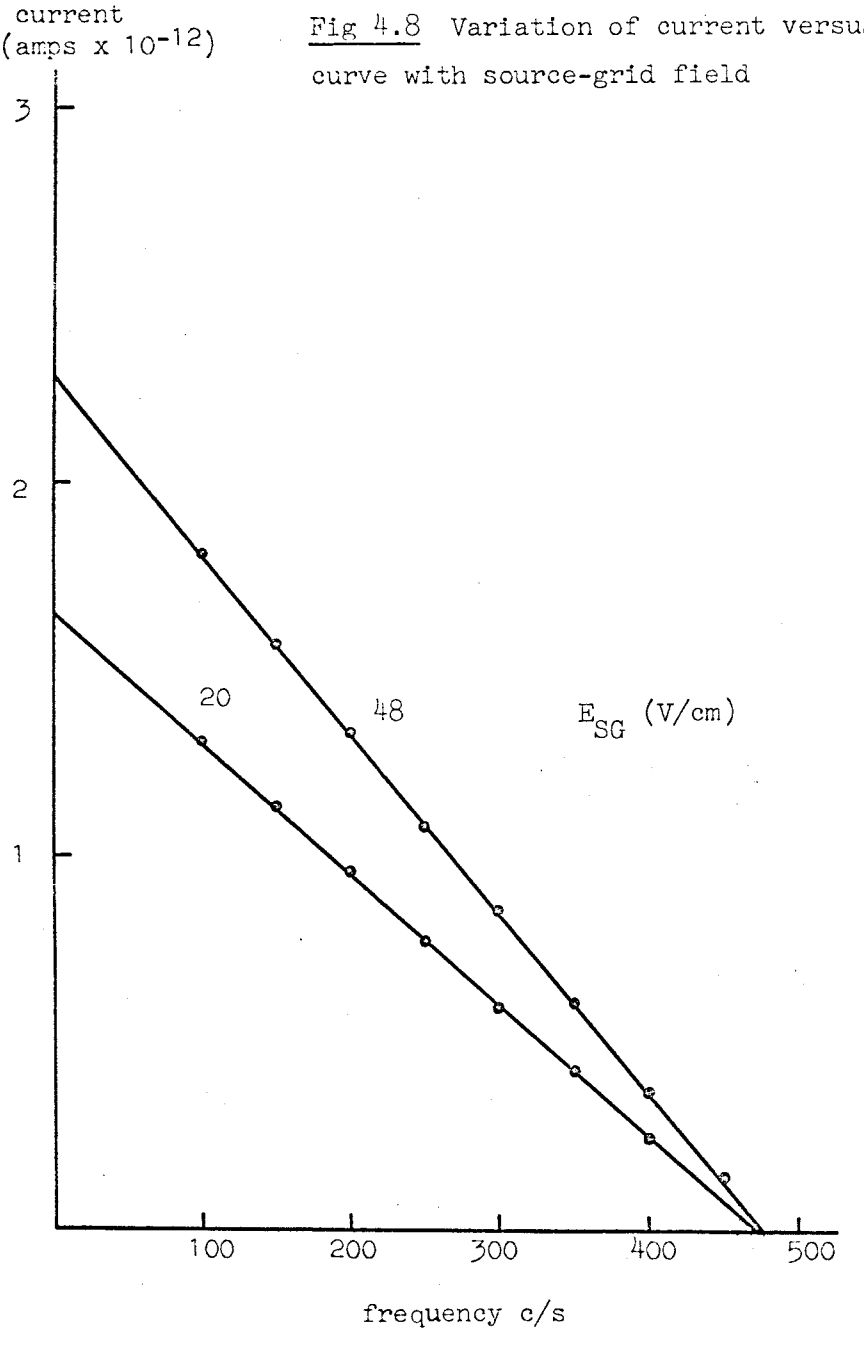

Fig 4.8 Variation of current versus frequency curve with source-grid field

the first discontinuity) both lines would be considered; there was no systematic dependence of the resulting mobility values consistent with the existence of two types of ion present with different mobilities corresponding to a discontinuity. The difference in cut off frequency between the two possible lines would be about 5%. It was this uncertainty in the linearity of the lines which gave the greatest error in the results. Extrapolating the current back to zero frequency should give a value $I_o/2$, where I_o is the expected current for equivalent fields in the D.C. case. I_o varies with the square wave voltage Fig (7), in such a way that for low source grid fields (~50 V/cm) I_o reached a maximum value, and there after decreased slowly. Higher source grid fields (~200 V/cm) gave I_o saturating at a constant value for high square wave fields. We show later this is the expected behaviour from considering the D.C. characteristics of the cell. This effect means that the slopes of the lines in the current-frequency graphs decrease as the square wave voltage increases. Increasing the source-grid field, and thus I_o, gives less variation in the slope when varying the square wave voltage, while also giving an overall increase in the slope with a sharper cut off at zero current Fig (8). The cut off frequency is independent of the source grid field, if a variation in the zero of current at high frequencies is allowed for, for a constant square wave field. Runs were performed for increasing and decreasing values of the square wave field, with

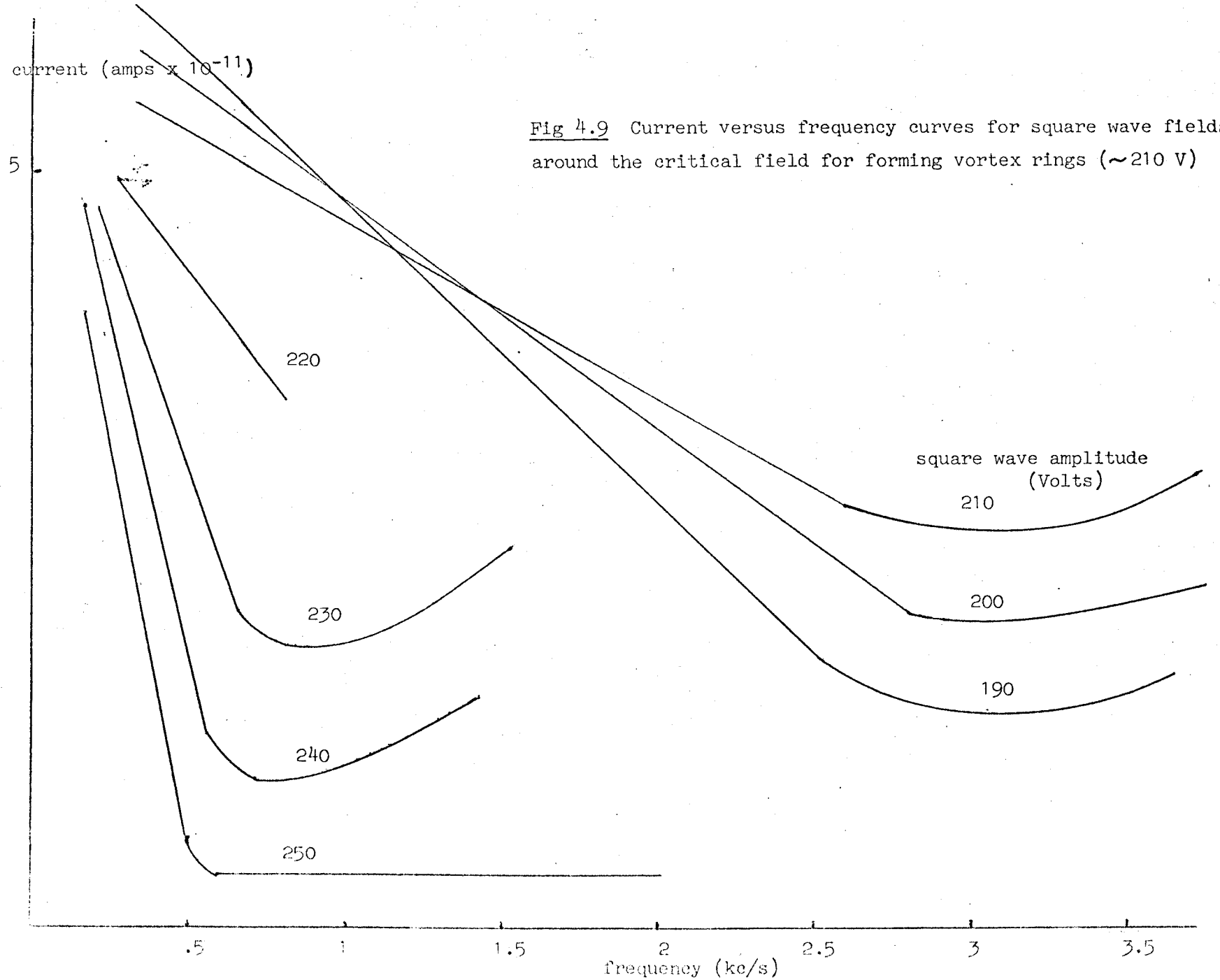

Fig 4.9 Current versus frequency curves for square wave fields around the critical field for forming vortex rings (~210 V)

reproducible results to 1% or better.

When high square wave fields were used, corresponding to velocities near the ion's maximum velocity and low energy vortex rings, the current-frequency curves showed a change. The current decreased linearly for low frequencies and then tailed off to a very high minimum current around the transit time frequency. For higher frequencies the current increased (Fig 9). For higher fields the current minimum decreased to zero, and a straight line was again seen, corresponding to a pure vortex ring current. This behaviour suggests a variable number of ions forming vortex rings around the ions maximum velocity.

We estimate the numerical error in our results as follows. In the low field measurements, looking for discontinuities, the greatest error in our results comes from estimating the cut off frequency. The current could be read to 4 decimal places, but there was a fluctuation that reduced the accuracy to around 1%. The frequency was accurate to 1 c/s, i.e. better than 1% most of the time. When looking for discontinuities we are only interested in relative values, so the combined error from the graph would result in the estimate of f_c being known to about 5 c/s i.e. ~1% for a good straight line. For readings which did not fall on a single line within this error, the two extreme values of f_c found by drawing limiting lines through the points could vary up to 10%; more commonly by about 5%. This method of analysis is subjective, but was used

as the number of readings with this uncertainty was fairly small, and being in the middle of a range of values would act as a check on the relative accuracy of the run; otherwise they could be discarded. The temperature was controlled to 10^{-3}°K, giving an error of around 1%, and the square wave amplitude known absolutely to ∿.5%, and relatively to better than .2%. We would thus put a lower estimate of ∿2.5% for our relative accuracy, with some points having considerably more error.

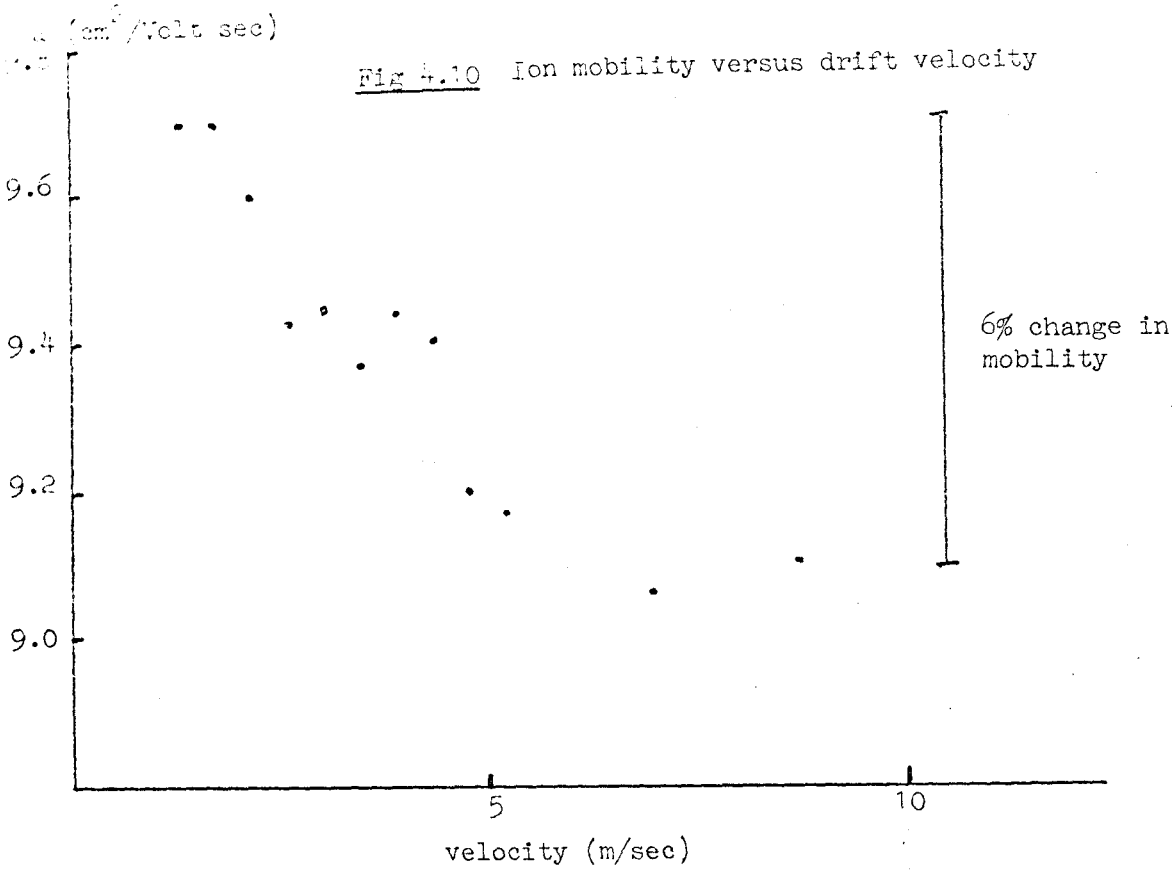

Fig 4.10 Ion mobility versus drift velocity

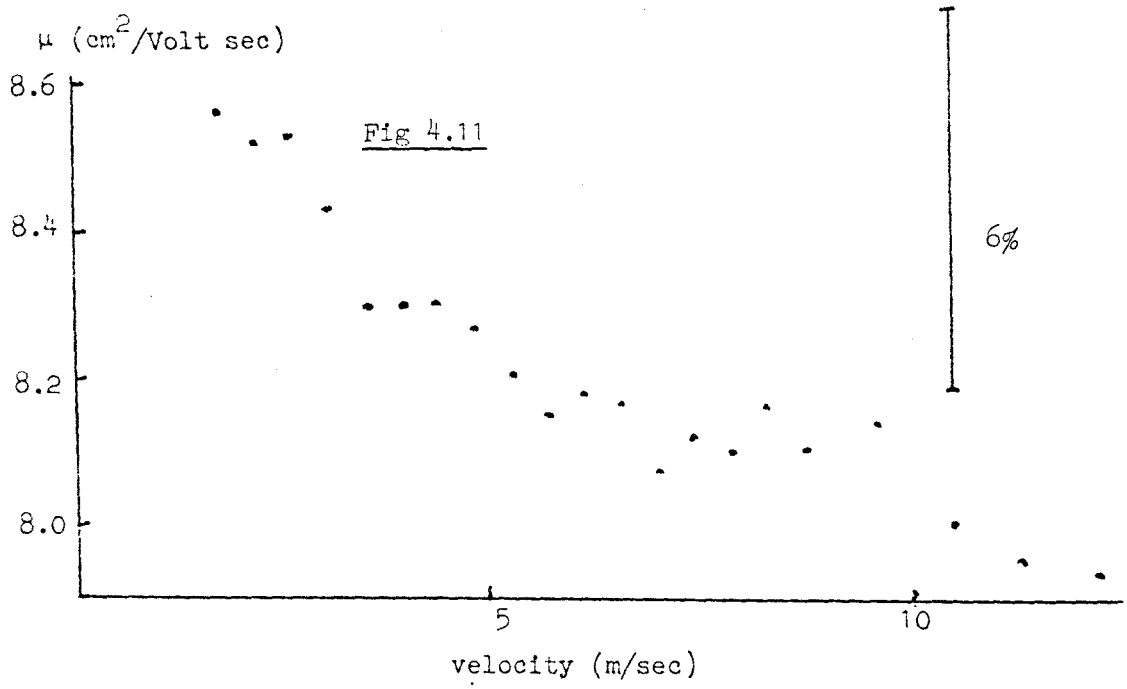

Fig 4.11

Fig 4.12

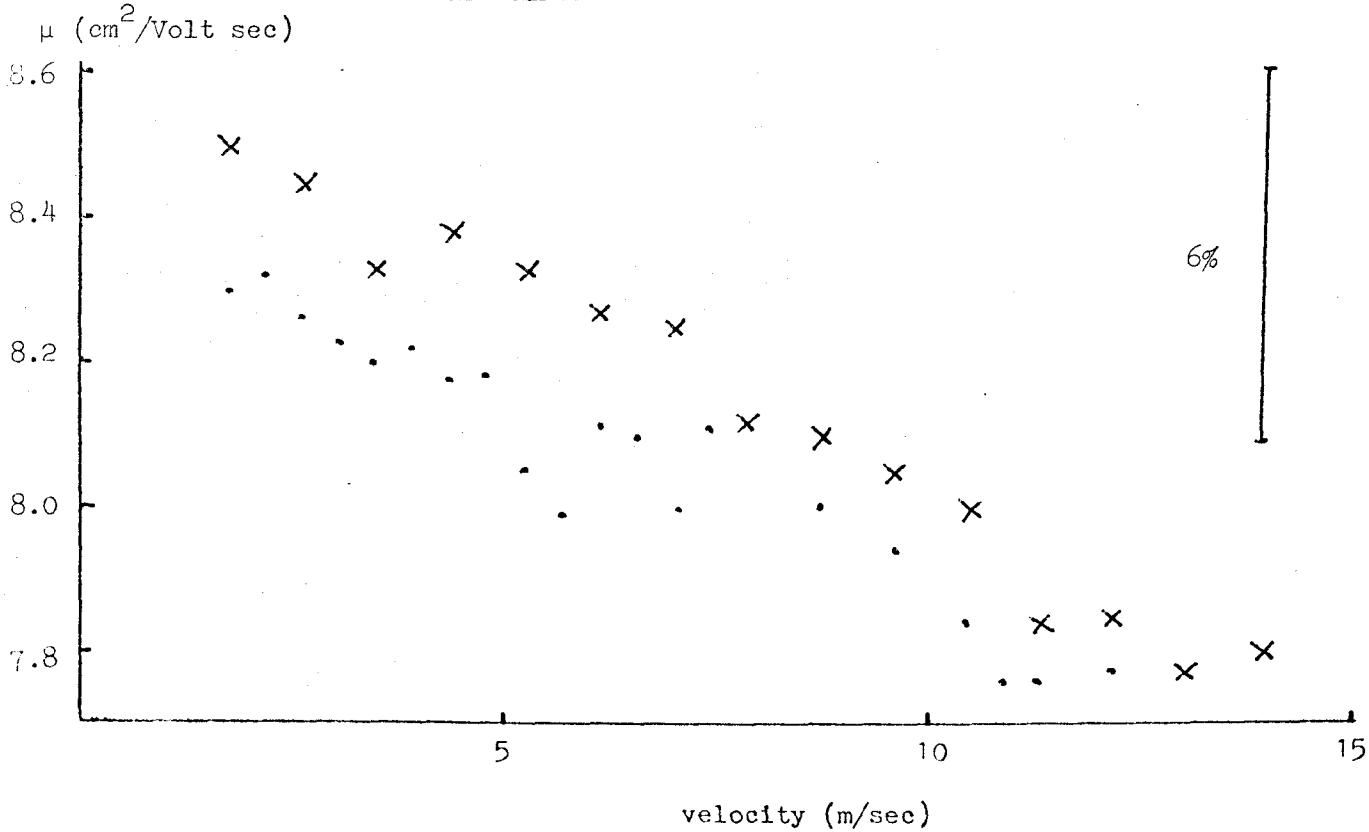

Fig 4.13

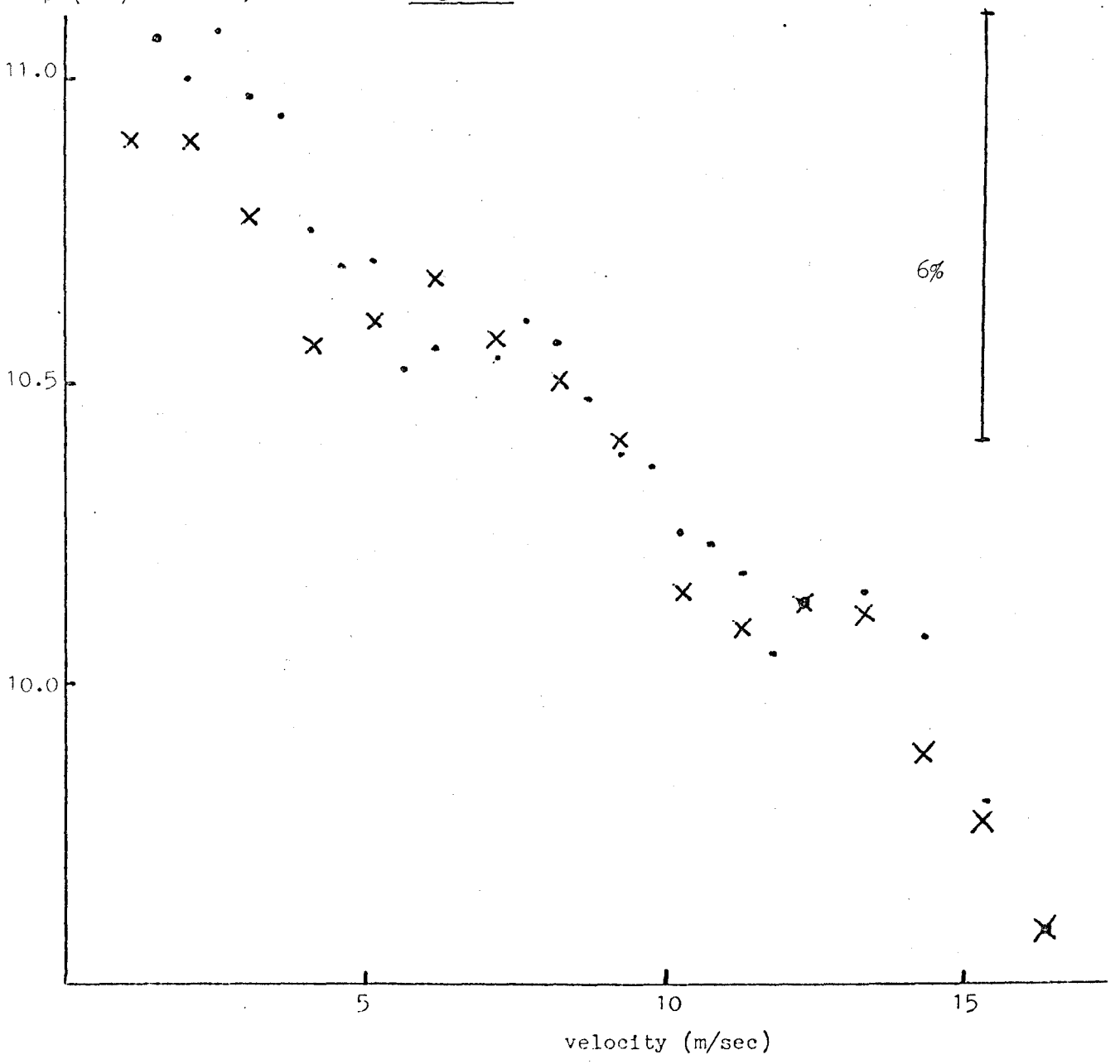

Fig 4.14

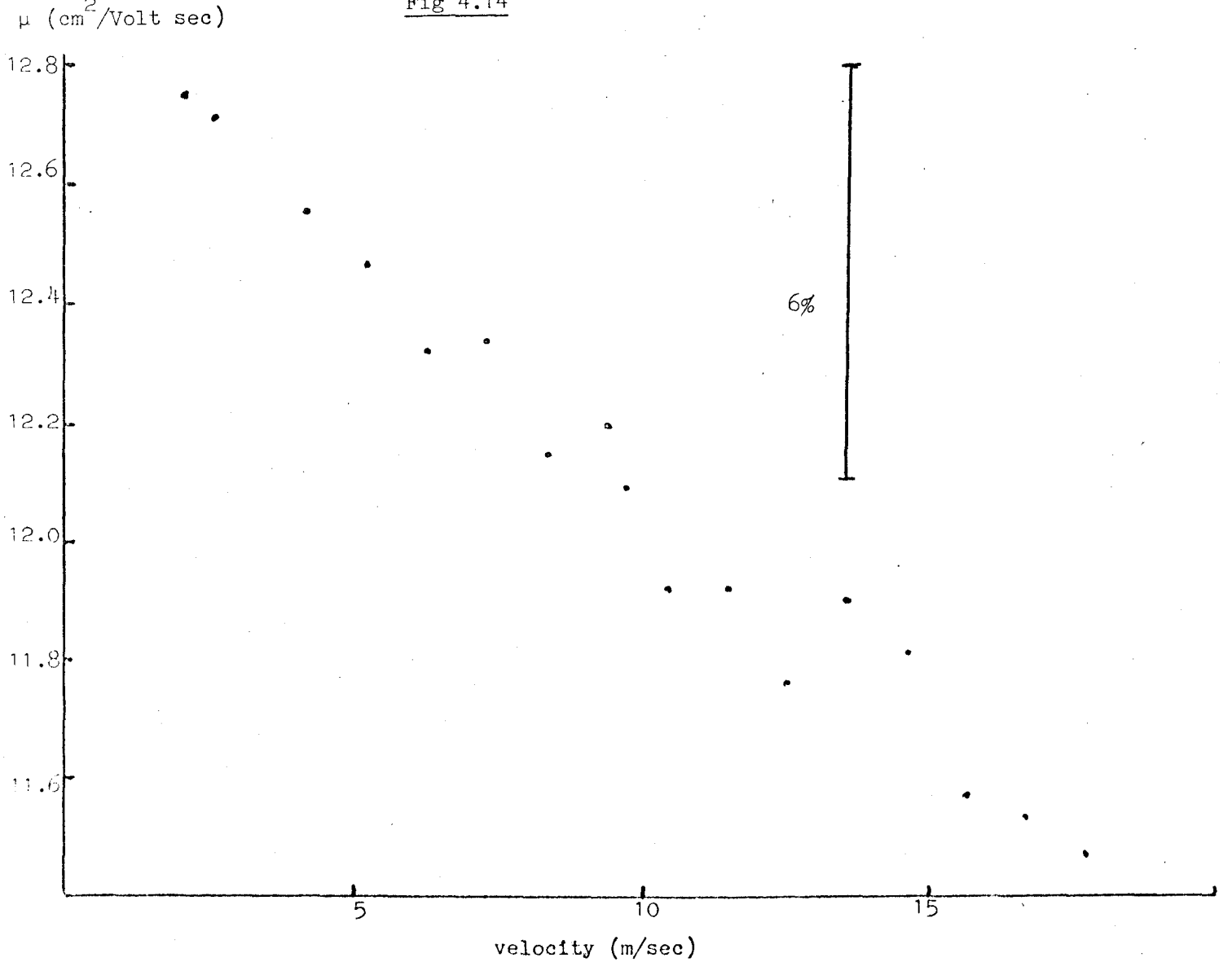
μ (cm²/Volt sec)
12.8
12.6
12.4
12.2
12.0
11.8
11.6
6%
5
10
15
velocity (m/sec)

Fig 4.15

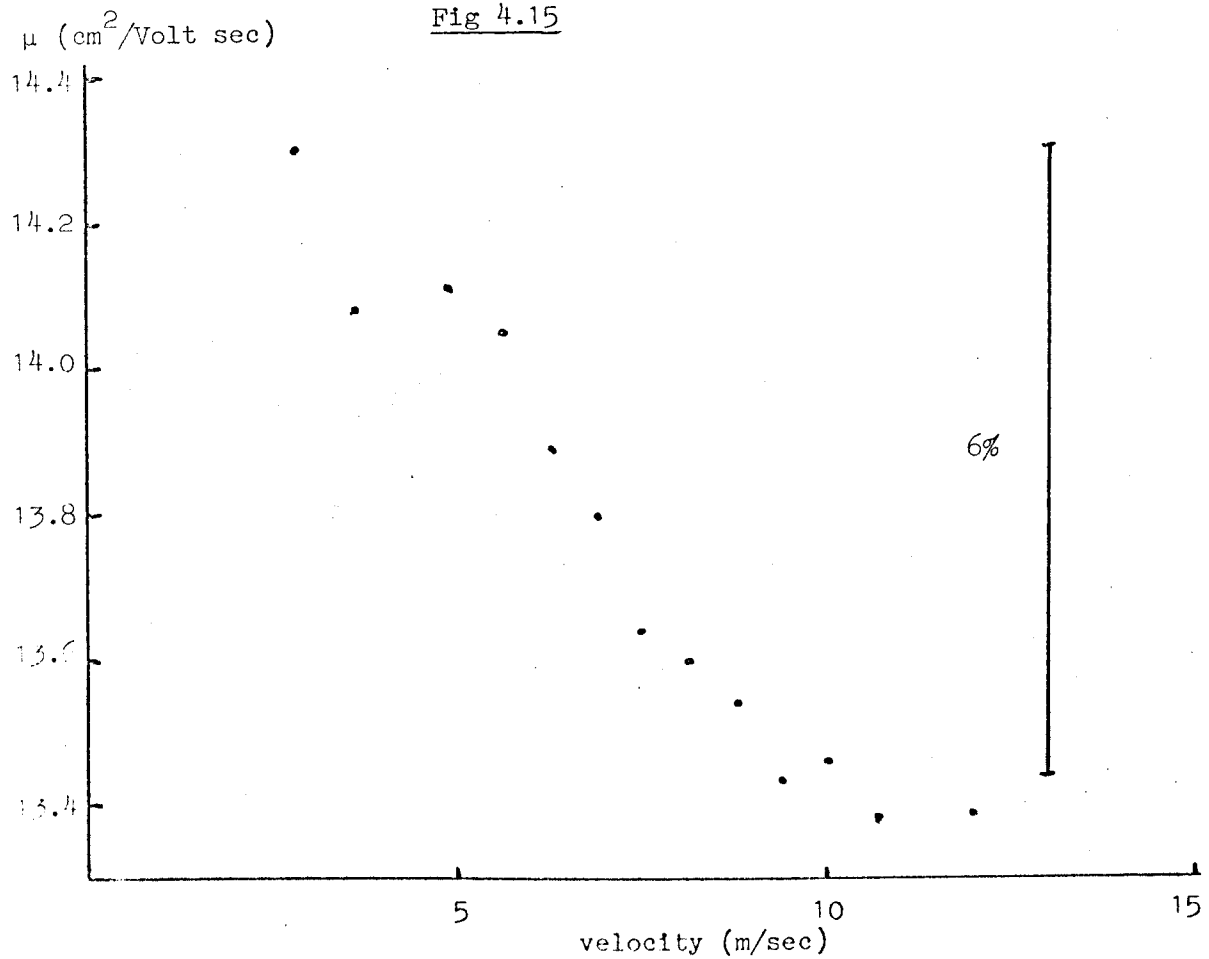

Fig 4.16

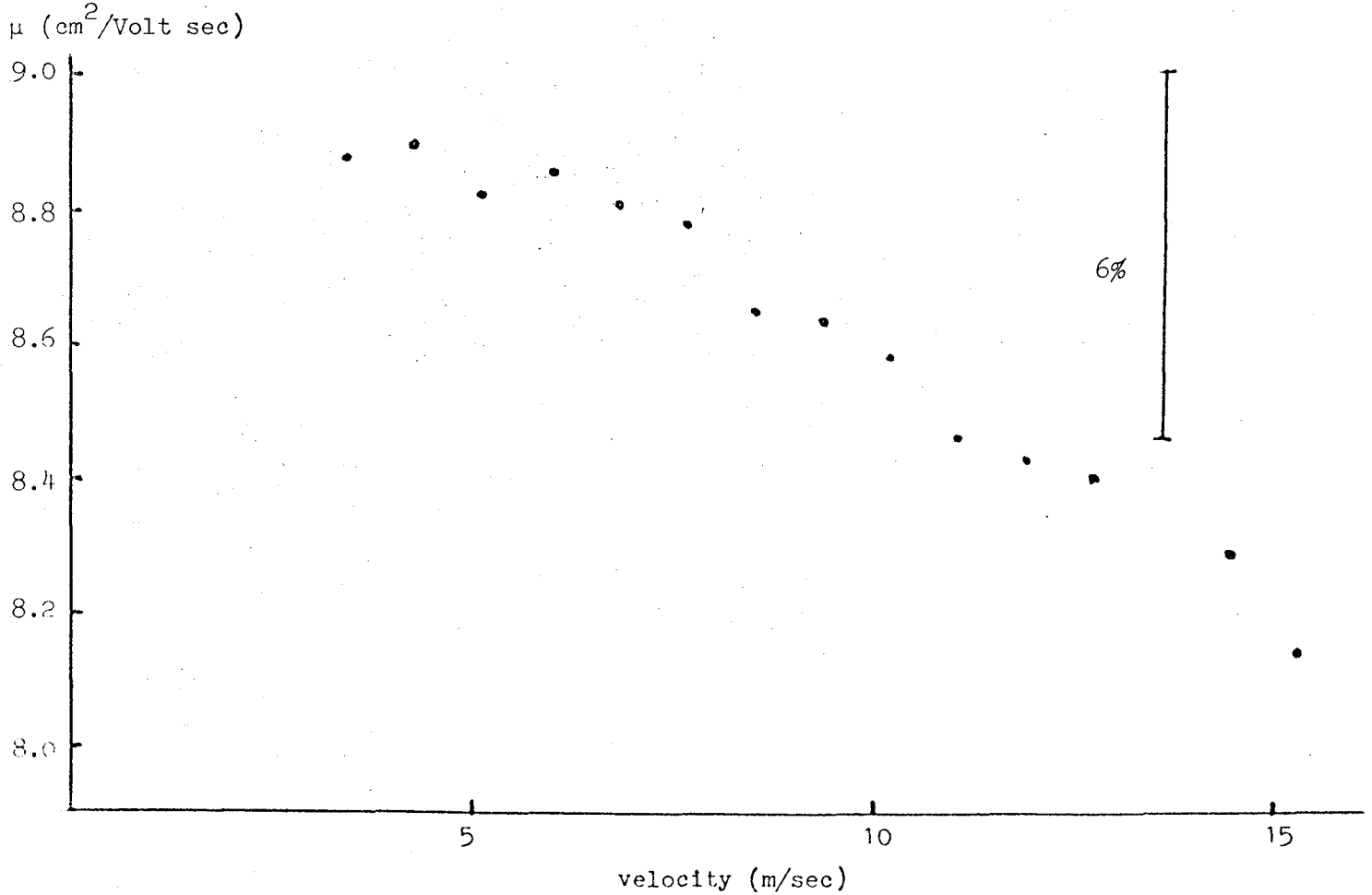

Fig 4.17

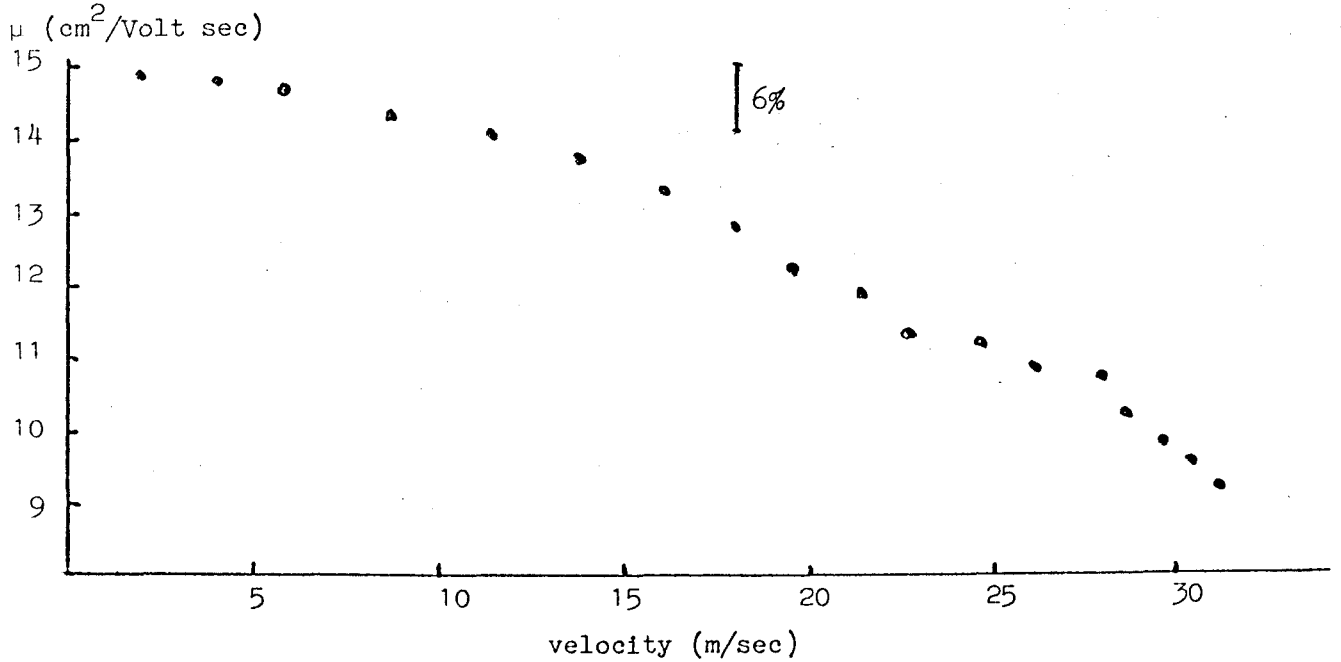

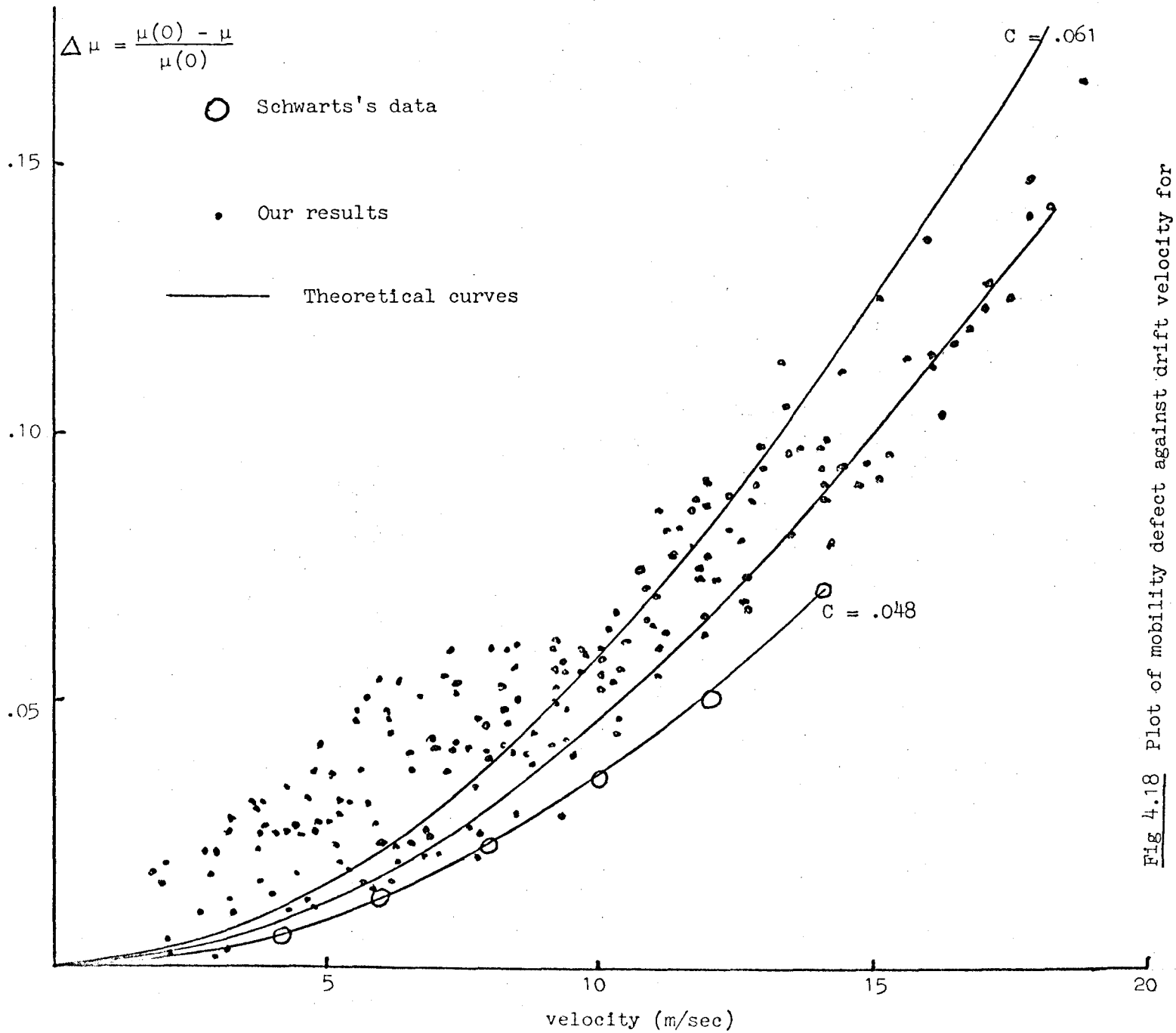

Fig 4.18 Plot of mobility defect against drift velocity for positive ions

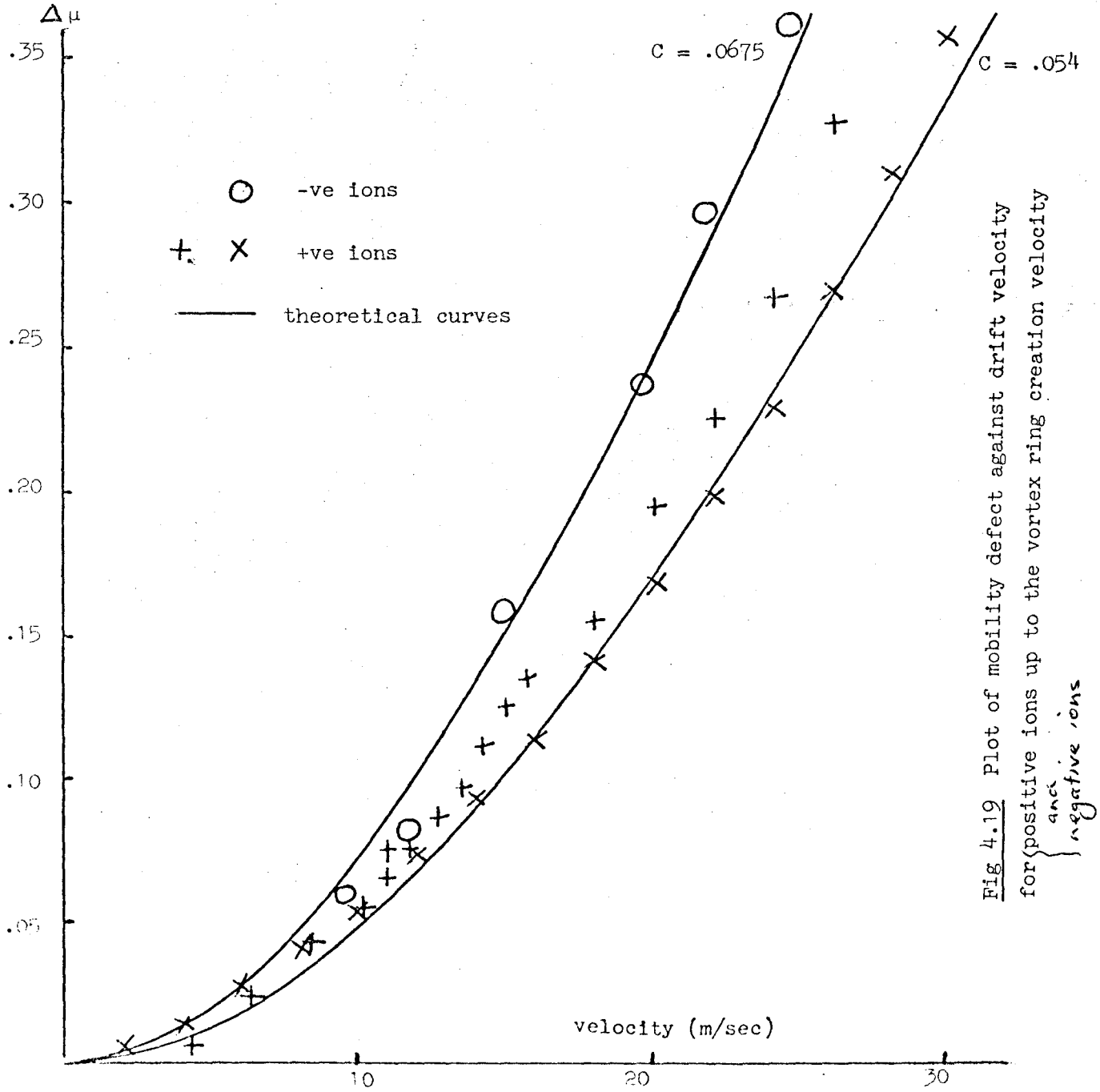

Fig 4.19 Plot of mobility defect against drift velocity for {positive ions and negative ions} up to the vortex ring creation velocity

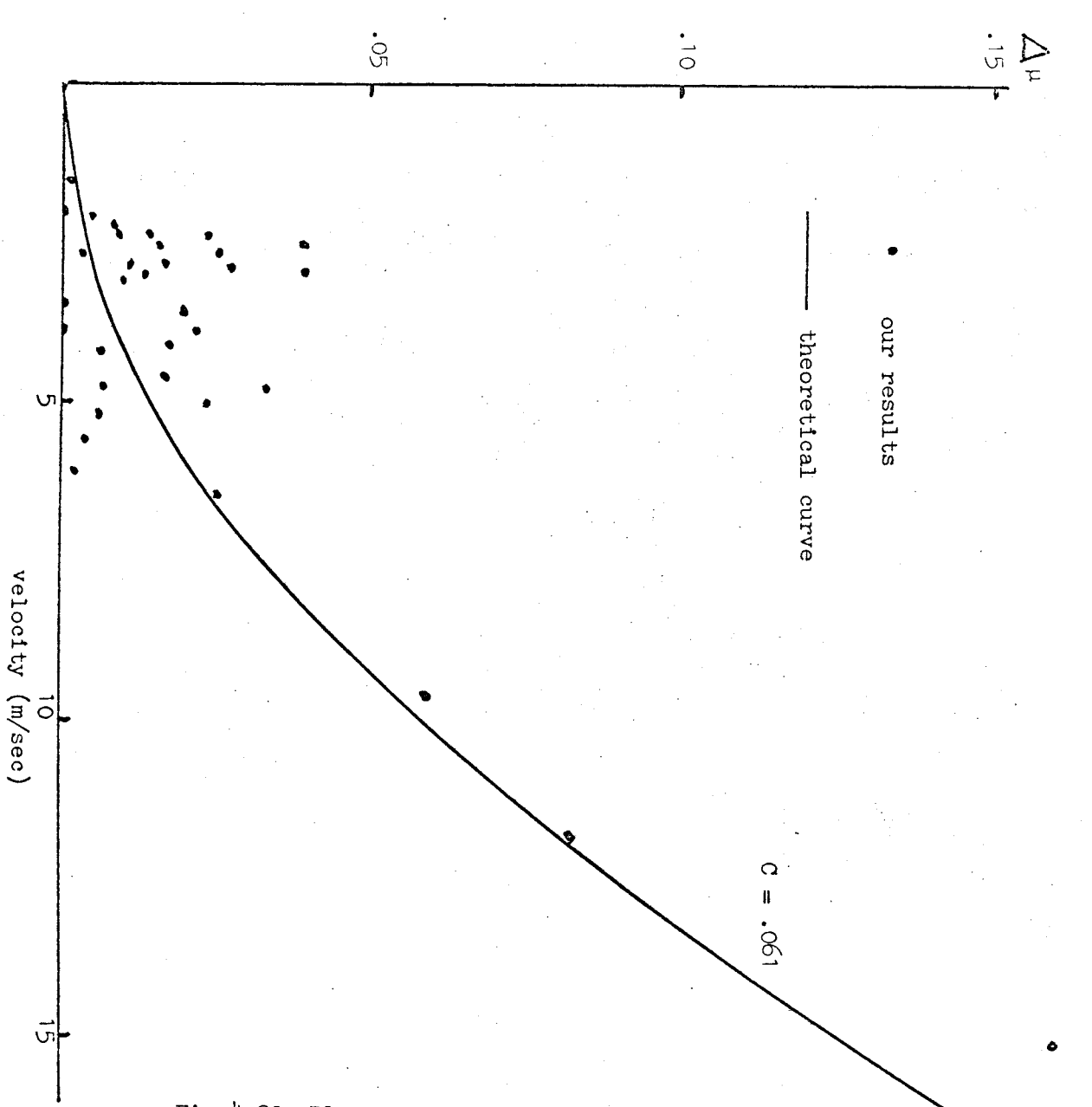

Fig 4.20 Plot of mobility defect for negative ions at low velocities

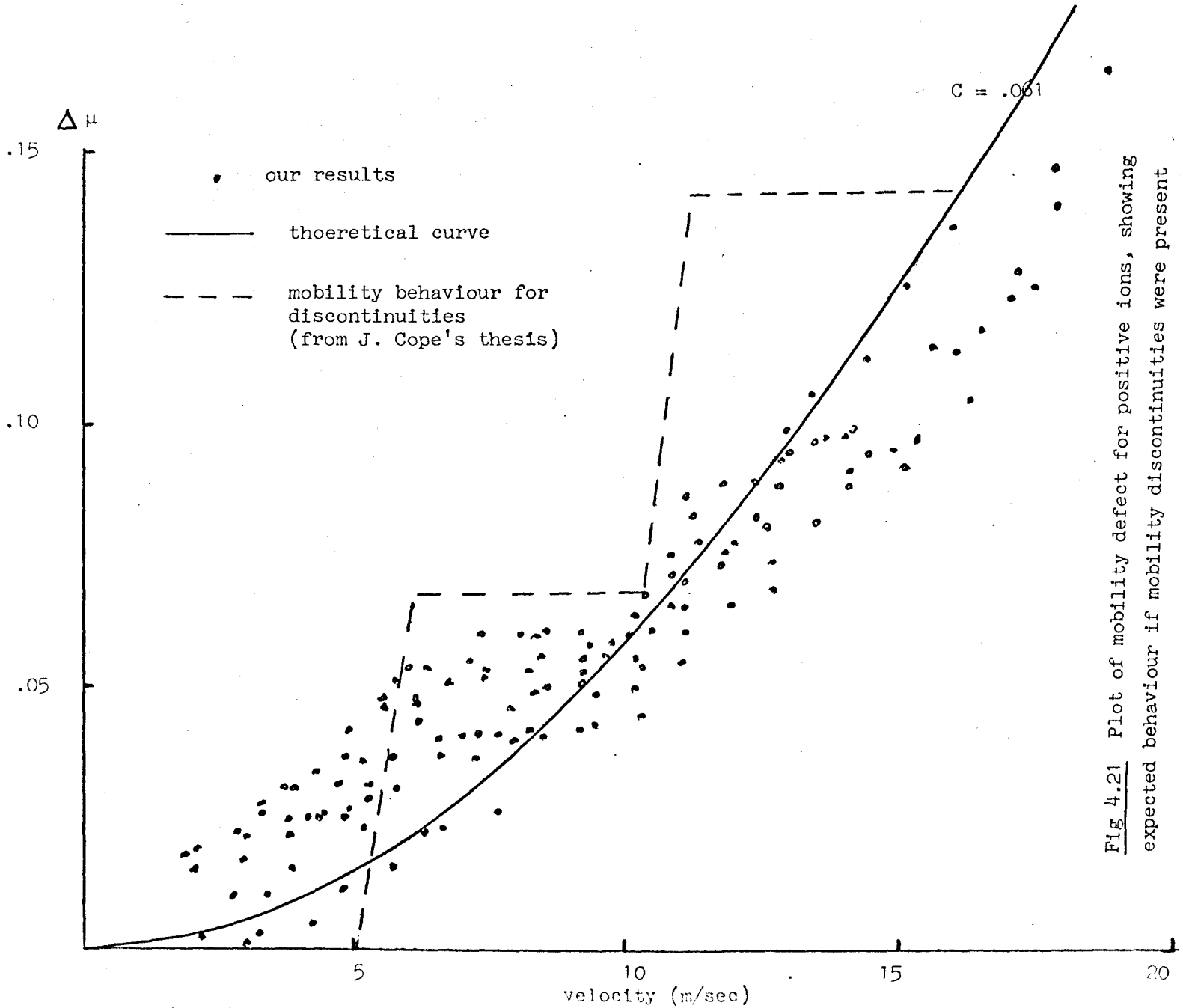

Fig 4.21 Plot of mobility defect for positive ions, showing expected behaviour if mobility discontinuities were present

Fig 4.22 Comparison with data from Schwartz (Fig 4.3) and our theory for mobility defect as a function of drift velocity (for positive ions)

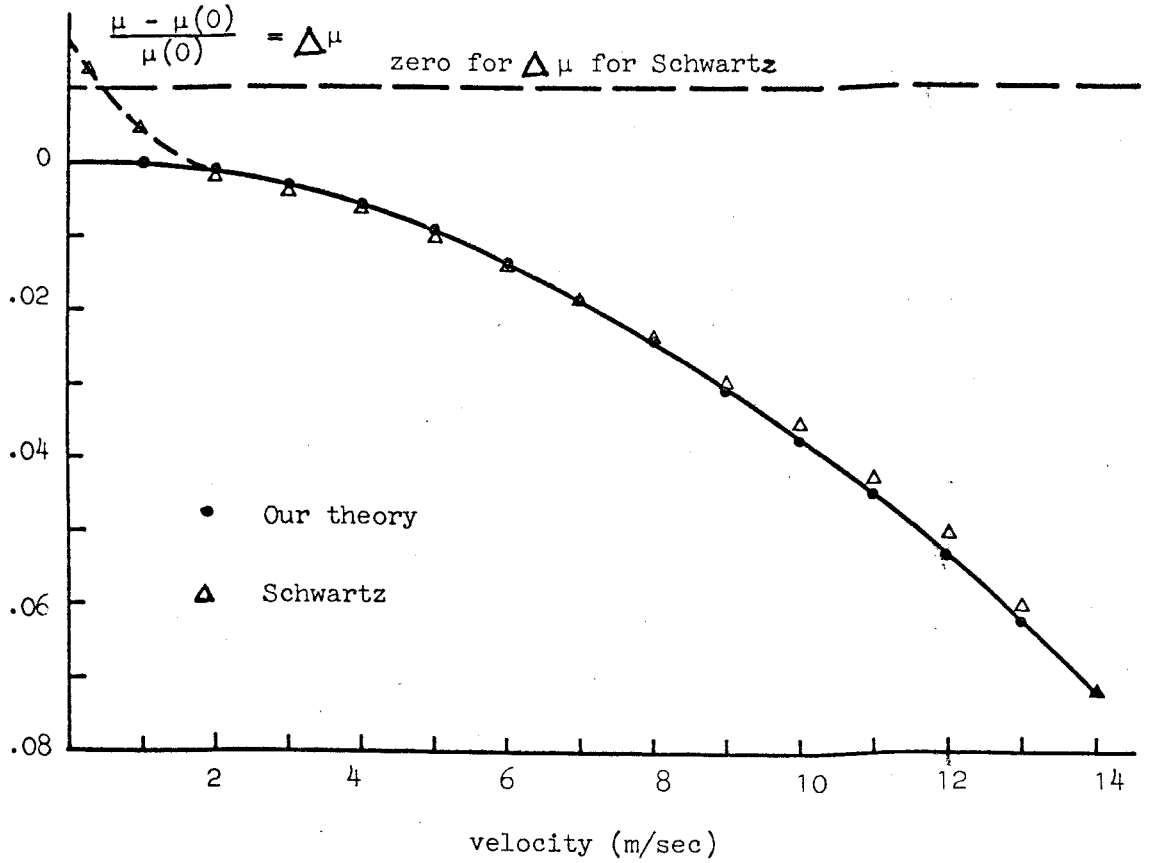

B. Representation of Results

Figs 10 - 17 show plots of mobility against velocity for various temperatures. None show a convincing discontinuity of a 6% fall in mobility. When the error in each individual point is considered, it can be seen that a continuous curve may be drawn through the results.

Figs 18 - 22 show plots of a reduced mobility, $\Delta\mu$, against velocity, where $\Delta\mu = \frac{\mu_o - \mu}{\mu_o}$, and μ_o is the zero field mobility. The continuous lines are theoretical curves, explained later. The experimental points in Fig 18 are from twelve different runs where we expected to see the second discontinuity. Results from other runs where only the first discontinuity was expected also fall within the existing spread of points.

Fig 19 shows points taken from runs reaching the vortex ring creation velocity, for both positive and negative ions. Fig 20 is similar to Fig 18 but for negative ions. If the discontinuities reported by Cope were present, they should show up as in Fig 21, which is for discontinuities of 6% for positive ions, taken from his thesis.

The value of representing the mobility in this way is that it emphasises the drop in ion mobility with increasing field; the theory given later gives $\Delta\mu$ as a weak function of temperature, but if discontinuities were present they would show as a distribution around the expected mobility discontinuity values in Fig 21 independent of

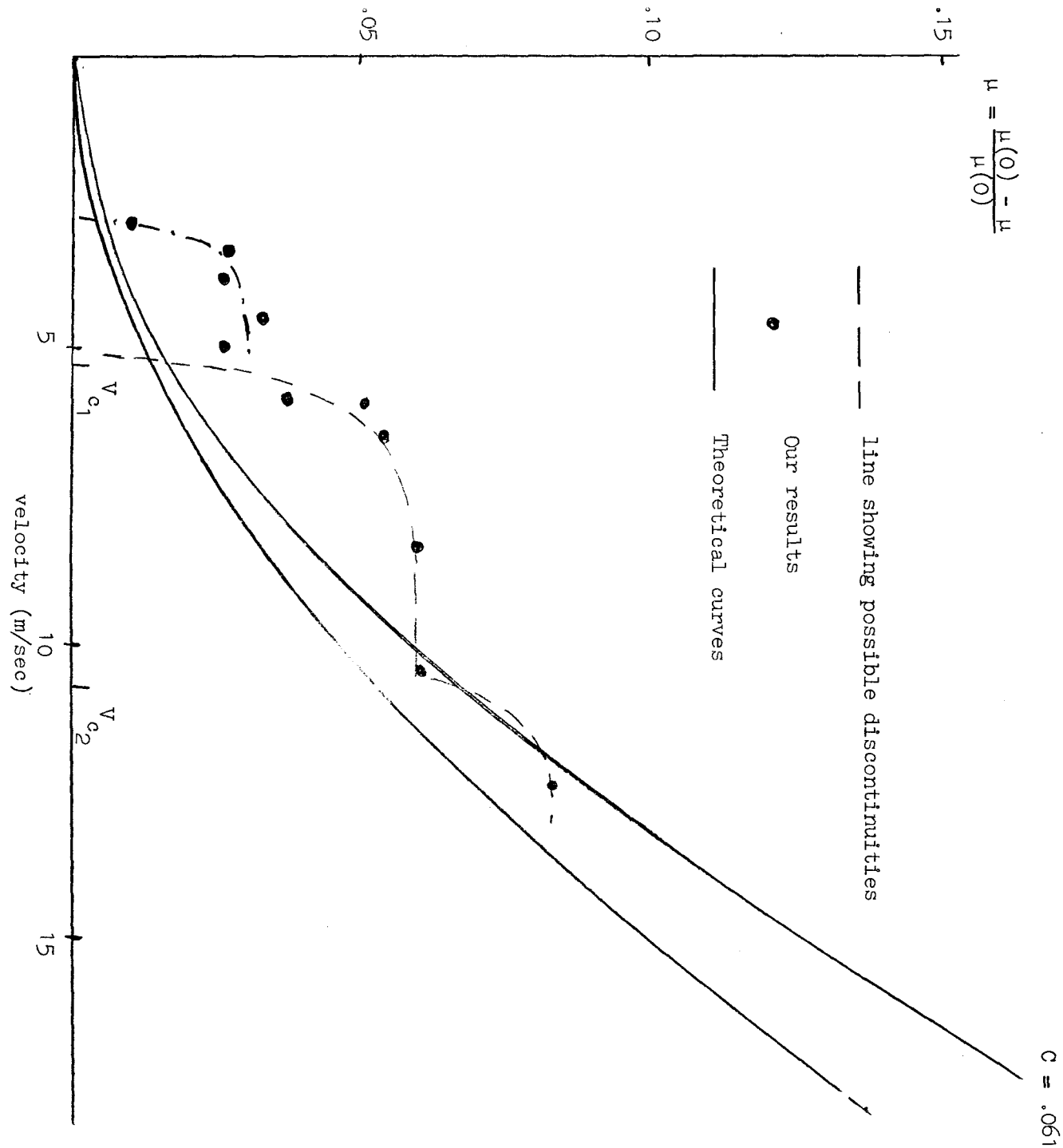

Fig 4.23 Plot of mobility defect against drift velocity for one run where discontinuities could be present

temperature. Instead, the mobility would appear to be a continuous decreasing function of velocity; and this leads to the main criticism of this form of representation - what value to take for μ_o. Theories for discontinuities assume the mobility is constant, independent of field, for ion velocities less than the critical velocity for the first discontinuity; μ_o would then be obtained from Figs 10 - 17 by taking an average of the mobility for these velocities. If the mobility is a continuous function of the field, then μ_o is obtained by extrapolating μ to zero velocity, according to the functional dependence of μ on E.

In practice, we have chosen μ_o for each run to give the best agreement with theory at high fields (high velocities); with the large scatter in results this can be rather subjective, but does not alter the underlying pattern of no discontinuities. It can be argued that some runs might show discontinuities, and others that did not would mask the effect on the plot; it is possible with one run on Fig 18 to see a first discontinuity of about 3% but this is hidden in the general scatter. This is shown separately in Fig 23. We were looking for evidence of the periodic nature of the discontinuities, which should have shown up as at least one point being on the third mobility discontinuity level in Fig 21.

The scatter in the points is due to a slight temperature dependence of the function $\Delta\mu$ (all results were taken in the temperature range 0.9°K to 1°K), the error in the mobility μ, and also in choosing a value

for μ_o. If the error in μ is 2%, then $\Delta\mu$ will vary by $\sim\pm.02$ units (.01 units $\equiv$ 1% in $\Delta\mu$).

Fig 19 shows that up to the vortex ring creation velocity, the points lie within experimental error on a theoretical curve, for both positive and negative ions. The theoretical curves are drawn with one adjustable constant, which describes the temperature dependence of $\Delta\mu$, and also the different behaviour between the two signs of ions.

The low field behaviour for positive ions, which has been adjusted for the best fit at higher fields in Fig 18, shows an excess scatter of low mobility points for low fields. The maximum deviation from a theoretical curve is about .03 units, corresponding to an error of 3% in μ. There is no sign of a systematic deviation expected for a discontinuity, but the general distribution of points at low fields suggests a smeared out discontinuity.

There is a greater scatter for the negative ion behaviour (Fig 20). One run, going up to 6 m/sec, shows a mobility constant to 1%; while others have a deviation up to .04 units i.e. 4% error in μ.

Fig 18 also shows the positive ion results obtained by Schwartz (1970) at a temperature 1.14°K. As this is a higher temperature than our results, we expect them to follow a different theoretical curve; which they do to within .5%. His negative ion mobilities show a constant mobility to about 8 m/sec, and then begin to fall.

In order to fit our data at high velocities to the theoretical curves, it has been necessary to give some experimental points a

negative $\Delta\mu$ at the lowest velocities. These are not shown, but all lie within .02 units of the axis. When fitting the data from Schwartz it was necessary to shift his zero mobility by about 0.1 units to get the theoretical curve to fit his points; this leaves a small fall in mobility (below the axis in our plot) for velocities below about 1.5 m/sec. While this is not significant with our results, the greater quoted accuracy of Schwartz means these points lie outside his experimental error. Fig 22 shows Schwartz's experimental points (plotted as our $-\Delta\mu$), our theoretical curve, and the change in the value for μ_o. The mobility behaviour for positive ion velocities below $\sim$1.5 m/sec is reminiscent of the mobility behaviour for ions in liquid nitrogen (Chapter 6), which is attributed to liquid motion. However, Schwartz's data for negative ions do not show a similar effect, although they would be expected to if this was a real phenomenon.

C. Theoretical Curves

The theoretical curves in Fig 18-22 were obtained by considering the change in the roton excitation spectrum due to the potential flow past the ion.

The normal kinetic theory expression for the low field ion mobility μ, gives

$$\mu \propto \frac{1}{N_r}$$

where N_r is the roton density. This is calculated from the dispersion relationship

$$\varepsilon(p) = \Delta + \frac{(p - p_o)^2}{2m^*}$$

and

$$n(p) = \frac{1}{h^3} \left(e^{\frac{\varepsilon(p)}{\kappa T}} - 1\right)^{-1}$$

so

$$N_r = \frac{1}{h^3} \int \left(e^{\frac{\varepsilon(p)}{\kappa T}} - 1\right)^{-1} d^3p$$

This is the roton density in a frame of reference moving with the superfluid. If we change to a frame of reference moving at velocity v_s with respect to the superfluid, the roton dispersion relationship is changed to

$$\varepsilon^*(p) = \Delta + \frac{(p-p_o)^2}{2m^*} - p.v_s$$

which changes the roton density to

$$N_r(v_s) = \frac{1}{h^3} \int \left(e^{\frac{\varepsilon^*(p)}{\kappa T}} - 1\right)^{-1} d^3p$$

This gives for the ratio $N_r(o)/N_r(v_s)$ (Appendix II)

$$\frac{N_r(o)}{N_r(v_s)} = \frac{\frac{p_o v_s}{\kappa T}}{\sinh \frac{p_o v_s}{\kappa T}}$$

When the ions are moving through the helium the potential flow of the superfluid round the ion will set up a varying superfluid velocity field. If we denote this velocity field by $\bar{v}_s$, we get for the ratio of mobilities when the ions are stationary $\mu(o)$ (zero superfluid velocity field around the ion) and moving with velocity v_D, $\mu(\bar{v}_s)$

$$\frac{\mu(o)}{\mu(\bar{v}_s)} = \frac{N_r(\bar{v}_s)}{N_r(o)} = \frac{\sinh(\frac{p_o \bar{v}_s}{\kappa T})}{(\frac{p_o \bar{v}_s}{\kappa T})}$$

i.e.

$$\mu(\bar{v}_s) = \frac{\mu(o)\ (\frac{p_o \bar{v}_s}{\kappa T})}{\sinh(\frac{p_o \bar{v}_s}{\kappa T})}$$

we relate the ion drift velocity v_D to the superfluid velocity field $\bar{v}_s$ by $\beta\, v_D = \bar{v}_s$ where β is a constant

so $$\mu(\bar{v}_s) = \mu(o)\, \frac{cv_D}{\sinh(cv_D)}$$

where $c = \frac{p_o \beta}{\kappa T}$

This gives for our reduced mobility

$$\Delta\mu = \frac{\mu(o) - \mu(\bar{v}_s)}{\mu(o)}$$

$$= 1 - \frac{cv_D}{\sinh\, cv_D}$$

which is the theoretical curve in Figs 18-22.

Physically, the theory says that due to the superfluid velocity field, the roton spectrum is changed to allow a greater density of rotons near the ion, compared with the roton density at infinity. This excess roton density increases the rate of momentum loss by the ion, giving a fall in mobility. The increase in roton density is similar to the theory proposed for a model of a vortex line by Chester et al (1968), where the condensate wave function shows a large depletion of particles near the vortex core, and that of Glaberson et al (1968) who examined the effect of the superfluid velocity field near a vortex core.

The constant β describes the excess roton distribution round the ion and the resulting loss of momentum, in order to identify the macroscopic drift velocity with a rapidly varying microscopic superfluid velocity field; i.e. the actual roton distribution can be averaged to a value which corresponds to a uniform flow of superfluid, of velocity βv_D.

The temperature dependence of $\Delta\mu$ comes from $c \alpha \frac{\beta}{T}$, where we would like β to be temperature independent. The only adjustable constant in this theory is β, relating the ion drift velocity to the average superfluid velocity field around the ion. Assuming potential flow around the ion at rest in a fluid moving at velocity U_o, then the fluid velocity at the two poles along the axis of the ion is zero, rising to a maximum of $\frac{3}{2} U_o$ round the equator of the ion.

At a point distance r from the ion, of radius R, angle θ to the axis, the fluid velocity v is ~~related to~~ a function of the fluid velocity at infinity U_o ~~by~~

$$v^2 = U_o^2(1 + \tfrac{1}{2}(\tfrac{R}{r})^3)^2 \sin^2\theta + U_o^2(1-(\tfrac{R}{r})^3)^2 \cos^2\theta$$

If we consider a reference frame where the ion is stationary, then we can identify U_o with v_D; the superfluid velocity field around the ion v_s is then identified with v. For an ion of radius ~10 A moving at 30 m/sec, v_s is a strongly varying function with distance well outside the limits for two fluid hydrodynamics to be normally considered valid. The same trouble occurs when considering the superfluid velocity field near a vortex core. We note this point, and then ignore it, in order to look at the agreement with experiment and whether it helps explain discontinuities.

The actual roton distribution varies as v_s i.e. from 0 to $\frac{3}{2} v_D$, for a stationary sphere, and $-v_D$ to $+\frac{1}{2}v_D$ relative to the flow at infinity. Negative velocities imply a decrease in roton density compared with the equilibrium density at infinity (for rotons polarized against the flow) so to get an average increase in density we can put limits on the value of β, i.e. $0 \lesssim \beta \lesssim \frac{1}{2}$. Our results give, for positive ions, $\beta = 0.40 \pm .01$, which we take to show that the superfluid velocity field giving the excess roton density can be identified with the ion drift velocity.

The excess roton density can be thought to arise due to a lowering of the roton energy gap Δ, to $\Delta - pv_s$. The rotons have

less energy than the equilibrium density at infinity, and are trapped close to the ion; thus the Landau criterion for producing excitations is not violated - the rotons are not emitted by the ion. The maximum lowering of the roton energy gap is about $2^{\circ}K$, when the ion begins to form vortex rings. The rings could be formed from these trapped rotons, as envisaged by Donnelly and Roberts (1969). We would then have a consistent picture describing the complete velocity field characteristic for ions.

D. Discussion

We will discuss our results with reference to the theory proposed in the previous section, and try to interpret the meaning of β in terms of physical process occuring around the ion boundary. Fig 18 shows Schwartz's data, fitted to our theoretical curve for $\Delta\mu$, using $c = 4.8 \times 10^{-4}$ for $T = 1.14^{\circ}K$. Two other theoretical curves are drawn for $c = 5.4 \times 10^{-4}$ and $c = 6.1 \times 10^{-4}$, corresponding to $T = 1^{\circ}K$ and $0.9^{\circ}K$ respectively, the temperature range in which our data was taken. Our data is not accurate enough to detect a possible temperature or velocity variation of β. The high field results (Fig 19) show that negative ions follow a curve $c = 6.75 \times 10^{-4}$; with the same value of β as for positive ions this corresponds to a temperature of $.81^{\circ}K$; and for the actual temperature, we get $\beta_{-} = .49$, where $\beta_{+} = .40$. A slight dependence of β on the ion radius is expected, as although the roton density should scale exactly as the ion radii, the total number of excess rotons depends on integrating the density over the perturbed volume around the ion; and we have made no explicit allowance for the mean free path of the quasiparticles responsible for the increased momentum loss rate by the ion.

At high ion velocities, the superfluid velocity field around the ion should resemble a retarded dipole flow (Takken, 1970) with a possible variation in β, due both to changing the excess roton distribution, and also a deviation from an 'equilibrium' distribution due to a finite relaxation time for changing the quasiparticle

number density. This last point is the mechanism giving attenuation in first and second sound; and has been expressed in terms of 'coefficients of second viscosity' by Khalatnikov (see eg. Wilks). Elastic collisions between quasiparticles result in a rapid energy and momentum transfer, giving respectively the thermal conductivity and the viscosity of the fluid, but the creation and annihilation of quasiparticles occurs during inelastic collisions, which is a much slower process. Landau and Khalatnikov considered various processes, and the one determining a change in roton numbers is a collision between a roton and a high energy phonon giving two rotons; the relaxation time for this is about 10^{-8} secs at 1°K.

Thus, if we allow the superfluid velocity field around the ion to create the excess roton density by inelastic collisions, in a similar way as the quasiparticle number density changes in a first or second sound wave, then there is a characteristic time for a change in the roton density, much greater than any fluctuations in the ions drift velocity due to its thermal energy.

It may be possible for the ion to build up a boundary layer of normal fluid around itself in this way, in which case we would expect an enhancement in the superfluid velocity field, a counterflow mechanism due to the ions motion; the actual roton distribution would depend on the time retardation of the dipole flow and the roton relaxation time which is temperature dependent. The circulation around a flow line that is fixed initially on the ion surface, could at a

critical velocity or due to fluctuations, become equal to $\frac{h}{m}$ when the flow line eventually leaves the ion, and forms a vortex ring (Takken).

We could also try and explain the temperature dependence of the zero field mobility for negative ions, $\mu(o) \propto \exp\left(\frac{\Delta}{kT}\right)$, where $\frac{\Delta}{k} \sim 7.6^{\circ}K$ by a change in the dispersion relation parameters due to the boundary conditions on the bubble surface.

These ideas are all speculative, and covered in our theory by a blanket constant c. If we allowed these effects to change c by a certain amount at a critical velocity, we could then build up a theory explaining discontinuities; as our results show no sign of discontinuities apart from a scattered deviation from theory at low velocities, this is not worthwhile.

Our theory gives a gross dependence of the variation of mobility with electric field, or drift velocity. Results which showed discontinuities would still be expected to follow this overall relation, the discontinuities being perturbations on the smoothed mobility dependence. We can then put limits on the size of possible discontinuities, in relation to a given (periodic) critical velocity. For both positive and negative ions, at their maximum velocity where they form vortex rings, the drop in mobility from the zero field value is $\Delta\mu \simeq 36\%$. For positive ions, the vortex ring creation velocity is about 30 m/sec at $T \sim 1^{\circ}K$, and reported critical velocities are multiples of 5.2 m/sec. This gives a maximum of 6 mobility levels,

and the average mobility drop between each level cannot exceed 6% - the reported size. For negative ions, with a maximum velocity of about 26 m/sec and a critical velocity about 2.4 m/sec, we expect the average mobility drop to be between 3% and 4%, about that reported by Bruschi et al (1968).

Depending on how the zero field mobility is defined, discontinuities may be fitted in various ways. If $\mu(o)_d$ is defined, for data showing discontinuities, as the first mobility level for velocities less than the first critical velocity, and $\mu(o)_t$ for our theory where the theoretical curve gives a zero $\Delta\mu$ for zero velocity, then the discontinuities give mobility values always less than the theoretical value. By increasing $\mu(o)_d$ or decreasing $\mu(o)_t$ then the theoretical curve can be made to pass through discontinuities so some mobilities are less, and some greater than the theoretical mobility - this is just shifting the $\Delta\mu$ axis for the theory with respect to the $\Delta\mu$ axis for discontinuities; we have already shown how $\mu(o)$ can vary by up to 2% depending on how mobility curves are extrapolated to zero field.

Schwartz showed no drop in mobility for negative ions below a velocity of $\sim$8 m/sec. The original data from Careri et al (1964) also showed a nearly constant mobility, with only one discontinuity (i.e. a 4% fall in mobility) up to about 12 m/sec. Above this, the mobility fell sharply. The high field data follows our theoretical curve. Our results showed more scatter than with positive ions, but

one run showed only a 1% variation in mobility up to 6 m/sec.

The temperature dependence predicted by the theory, and seen over a small range 0.9 K to 1.1°K, is a decreasing fall in mobility with increasing temperature; because of the unknown temperature dependence of β (relating the ion drift velocity and the superfluid velocity field) we cannot predict the exact temperature dependence outside this range.

E. Summary

The experimental results agree within their limits of accuracy with a theory that does not suggest discontinuities. The error in the relative mobility values is estimated to be 3%, due mainly to the non linearity of the current-frequency graphs determining the cut off frequency and hence the ion velocity. This was true for positive and negative ions, and a number of different grids, all of which were gold plated and thoroughly cleaned before use.

The theory predicts a drop in mobility with velocity, fitting both our results, and the more accurate published data of Schwartz. The theory contains one adjustable parameter, which relates the ion drift velocity to the superfluid velocity field around the ion producing an excess roton density distribution, and relates the macroscopically observable ion velocity to the microscopic processes of momentum loss by the ion. When this parameter is fixed, the theory describes the temperature dependence over a small range due to the intrinsic temperature dependence of c.

$$c = \frac{p_o \beta}{\kappa T}$$

where $v_s = \beta v_D$

and β is temperature independent.

CHAPTER 5

D.C. CHARACTERISTICS

I. INTRODUCTION

This work was started to check the operation of the triode cell, and in particular the influence of the grid, with regard to our velocity measurements; it was suspected that a space charge was set up near the grid, causing non-linearity in the current-frequency characteristics. We also wanted to test field penetration through the grid. Later work at high fields showed interesting behaviour of vortex rings, in that there was a sharp peak in the collected current at a critical electric field for negative ions, but not for positive ions. We also looked for effects due to negative conductance, caused by the velocity field relationship having a negative differential mobility for the vortex ring regions.

Any velocity measurement arrangement involves the ion beam being transmitted through a grid, usually with a change in electric field at the grid. This means the electric field in the vicinity of the grid (in a plane parallel to the grid) is modulated in strength, to a degree depending on the grid mesh size and on the values of the two fields. One effect of this field modulation is to decrease the transmission coefficient of an ion beam, for an increase in the incident field; and a smaller effect is to change the effective fields between electrodes, due to a change in the effective potential of the grid.

Bruschi, Mazzoldi and Santini (1968) have reported a method of measuring a critical velocity for a mobility discontinuity in a triode cell, by keeping a constant frequency square wave between the grid and collector, and varying the square wave amplitude. A plot of current against field showed a change in slope at a critical field, corresponding to a critical ion velocity, which they identified as the onset of a mobility drop. We did not find a similar effect; the shape of the current against field curve was the same as that obtained from pure D.C. experiments, as would be expected. Bruschi could give no explanation of his effect, or justification for regarding it as a critical field (and therefore velocity) for a discontinuity, but it implies that mobility discontinuities may affect the D.C. current characteristics.

Fig 5.1 Potential distribution in a triode along two lines.

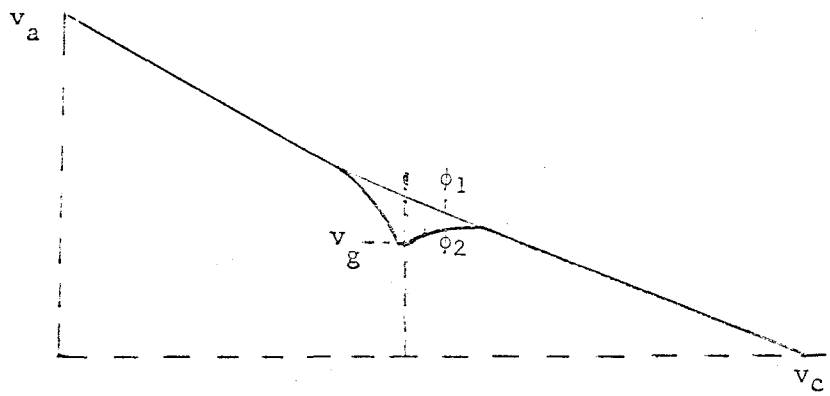

Fig 5.2 Potential distribution for effective zero field between the grid and cathode.

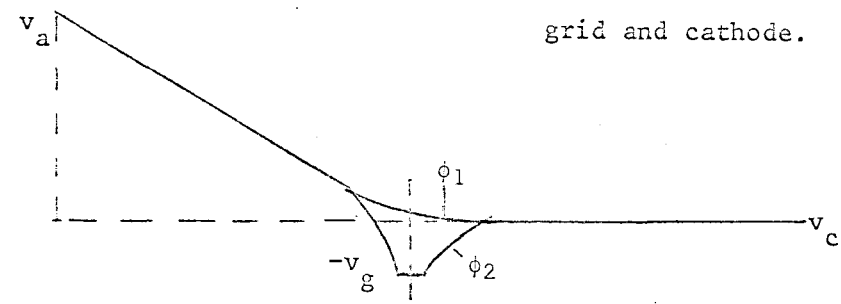

II. AN 'IDEAL' GRID

a. Theory

This is a brief summary from Verster (1963). Consider a grid situated between two plane electrodes, with potentials v_g, v_a and v_c respectively. Then the potential distribution along the axis will depend whether the path passes through a grid space (ϕ_1) or a grid wire (ϕ_2). Fig 1 shows the distribution for the two cases. The potential is modulated in a plane parallel to the grid, and may be represented by a Fourier series; then the component with the same period as the grid will decay with distance from the grid x as exp $(-2\pi x/\ell)$, where ℓ is the distance between two grid wires. At large distances from the grid the modulation is small, and an average potential in a plane x = constant is a well defined function of x only. By letting the cathode potential float, a suitable adjustment of v_a and v_g can be made to give average zero field between the grid and cathode, at distances far from the grid ($>>\ell$) (Fig 2). The penetration factor D is then defined as

$$D = -\left(\frac{v_g}{v_a}\right)_{E_c = 0}$$

where v_a is the anode potential, and v_g the small negative applied grid potential. We see the effective potential of the grid at large distances is not v_g, but may be defined as

$$v_{eff} = \frac{v_g + Dv_a}{1 + 2D}$$

when $v_c = 0$.

Fig 5.3 Intersection of equipotentials (ϕ) with a plane perpendicular to the grid.

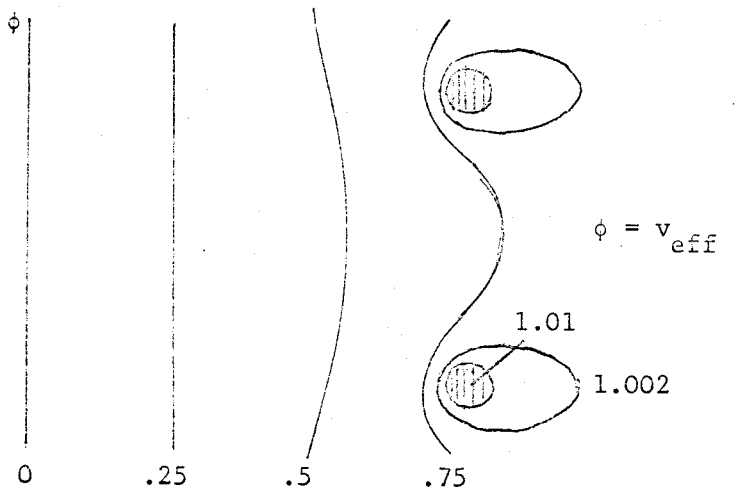

Fig 5.4

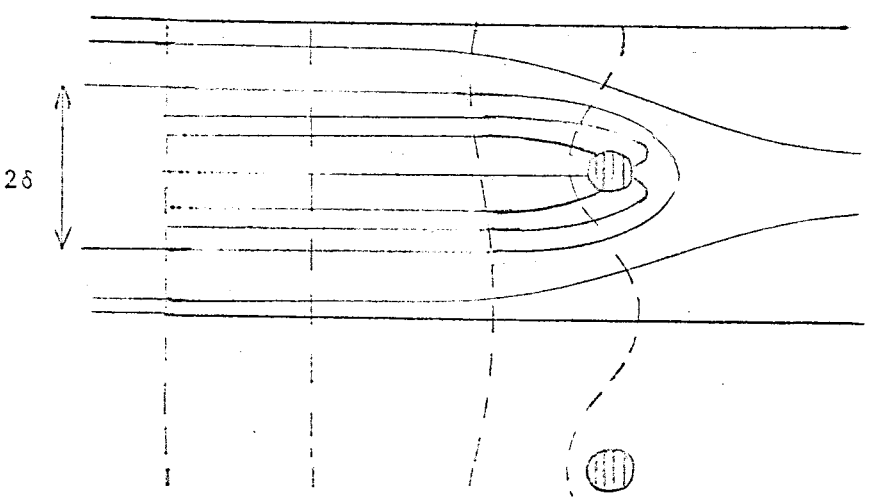

Lines of force (path taken by ion) around the grid wires.

Fig 5.5

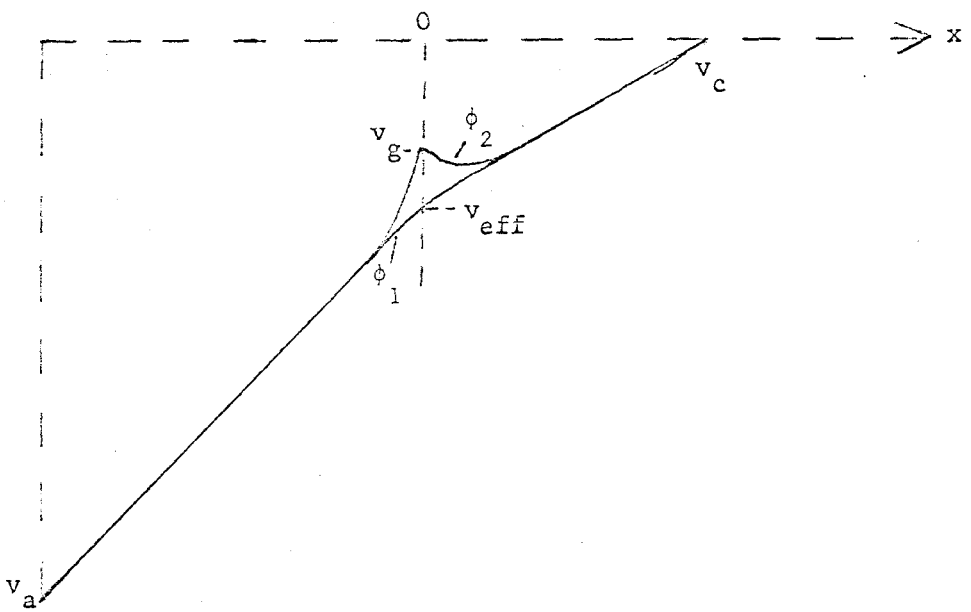

Coordinate system used for evaluating the Transmission coefficient 5.2(b).

Values of D for a grid of known dimensions may be found from Versters) results. Table I gives the values for our grids.

Verster also shows plots of the potential distribution around the grid wires (Fig 3). The lines are equipotentials, where ϕ=0, 0.25. 0.5, 0.75, 0.98 and 1.002 x v_{eff}; to the left of the grid there is a constant field, and to the right zero field, where $\phi=v_{eff}$. The grid potential is 1.01 x v_{eff}.

b. Transmission coefficient

Using the above theory we derive an expression for the transmission coefficient.

Fig 4 shows schematic field lines for the potential distribution in Fig 3, and Fig 5 the potential distribution for potentials equal to v_a, v_g and v_c = 0.

The field lines are drawn orthogonal to the equipotentials, and are the paths followed by ions. We see how the potential distortion at the grid causes an effective capture width 2δ downstream (the ions are assumed to travel from left to right) by making all field lines within this width end on the grid. When v_a is increased, keeping v_g and v_c constant, the potential distortion changes to increase the capture width.

We consider the two dimensional distribution in Fig 4, and relate this to the hydrodynamic flow of a source strength K in a uniform stream, velocity at infinity u_∞. There is a stagnation

point at a distance r_o from the source, where

$$r_o = \frac{K}{2\pi u_\infty}.$$

The streamline which passes through the stagnation point divides the flow into two parts; only the inner flow is accessible to streamlines from the source. The width of this bounding streamline tends asymptotically to a width at infinity of

$$2y = \frac{K}{u_\infty} = 2\pi r_o.$$

We make the identification

$$2\delta = 2y$$

and the stagnation point r_o will correspond to some distance from the grid wire: we take this to be where the potential in a line passing through the grid wire (ϕ_2) reaches a minimum between the grid and cathode, such that the field at that point is zero. If the distance between the grid and cathode is d, and the spacing between the grid wires is ℓ, then using the axes in Fig 5 we have for the potential at a distance x from the grid

$$v_x = v_{eff}\left(1 - \frac{x}{d}\right) + (v_g - v_{eff})\, e^{\frac{-2\pi x}{\ell}}.$$

Thus

$$\frac{dv_x}{dx} = -\frac{v_{eff}}{d} - \frac{2\pi}{\ell}(v_g - v_{eff})\, e^{\frac{-2\pi x}{\ell}}$$

which is zero at

$$x_o = \frac{\ell}{2\pi} \ln\left(\frac{2\pi d(v_{eff} - v_g)}{\ell\, v_{eff}}\right).$$

Using

$$v_{eff} = \frac{v_g + Dv_a}{1 + 2D}$$

we get

$$2\pi x_o = \ell \ln \left(\frac{2\pi d \, D\left(\frac{v_a}{v_g} - 2\right)}{\ell \left(1 + D\frac{v_a}{v_g}\right)} \right)$$

Identifying r_o with x_c, we get

$$2\delta = 2\pi x_o$$

The transmission coefficient is the ratio of the width of the ion beam not captured, to the total width

i.e. $$T \propto \left(\frac{\ell - 2\delta}{\ell}\right)$$

$$= 1 - \ell n \left(\frac{2\pi dD\left(\frac{v_a}{v_g} - 2\right)}{\ell\left(1 + D\frac{v_a}{v_g}\right)} \right)$$

This decreases as v_a increases. Puting in our values for D, d, ℓ, v_a and v_g makes T = 0 at $\frac{v_a}{v_g} = 5$ (well within the range of our results), which is not seen experimentally. This is due to the crude approximation used, but it does give qualitatively the expected behaviour. This is the best we can do without an analytic expression for the potential distribution around the grid. It does suggest however that a zero field could exist behind the grid wires, with our dimensions for $\frac{v_a}{v_g} \geq 3$; ions could be held here, increasing the field distortion.

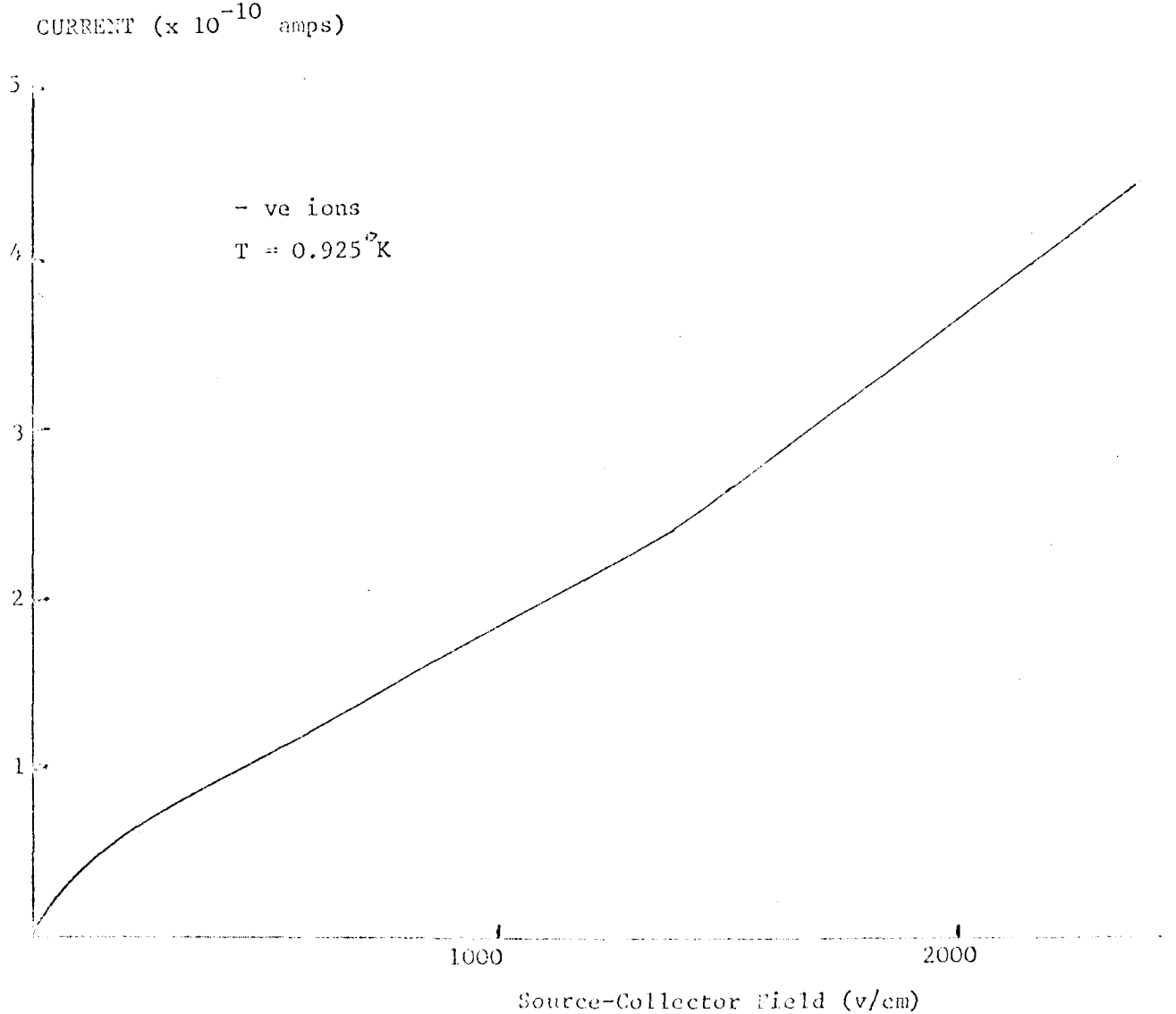

Fig 5.6 Diode Characteristic

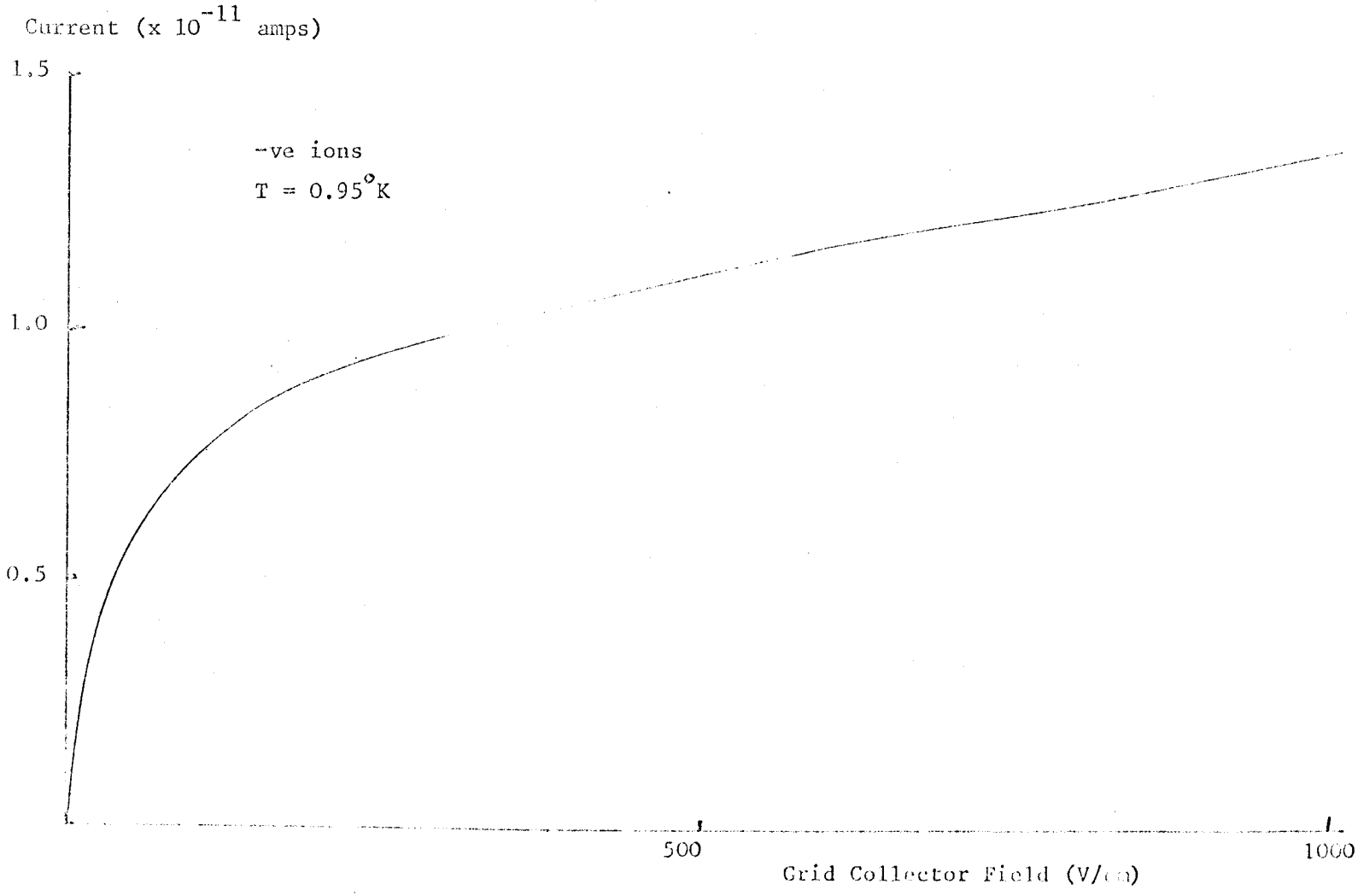

Fig 5.7 Triode characteristic for E_{gc} = constant (= 40 V/cm)

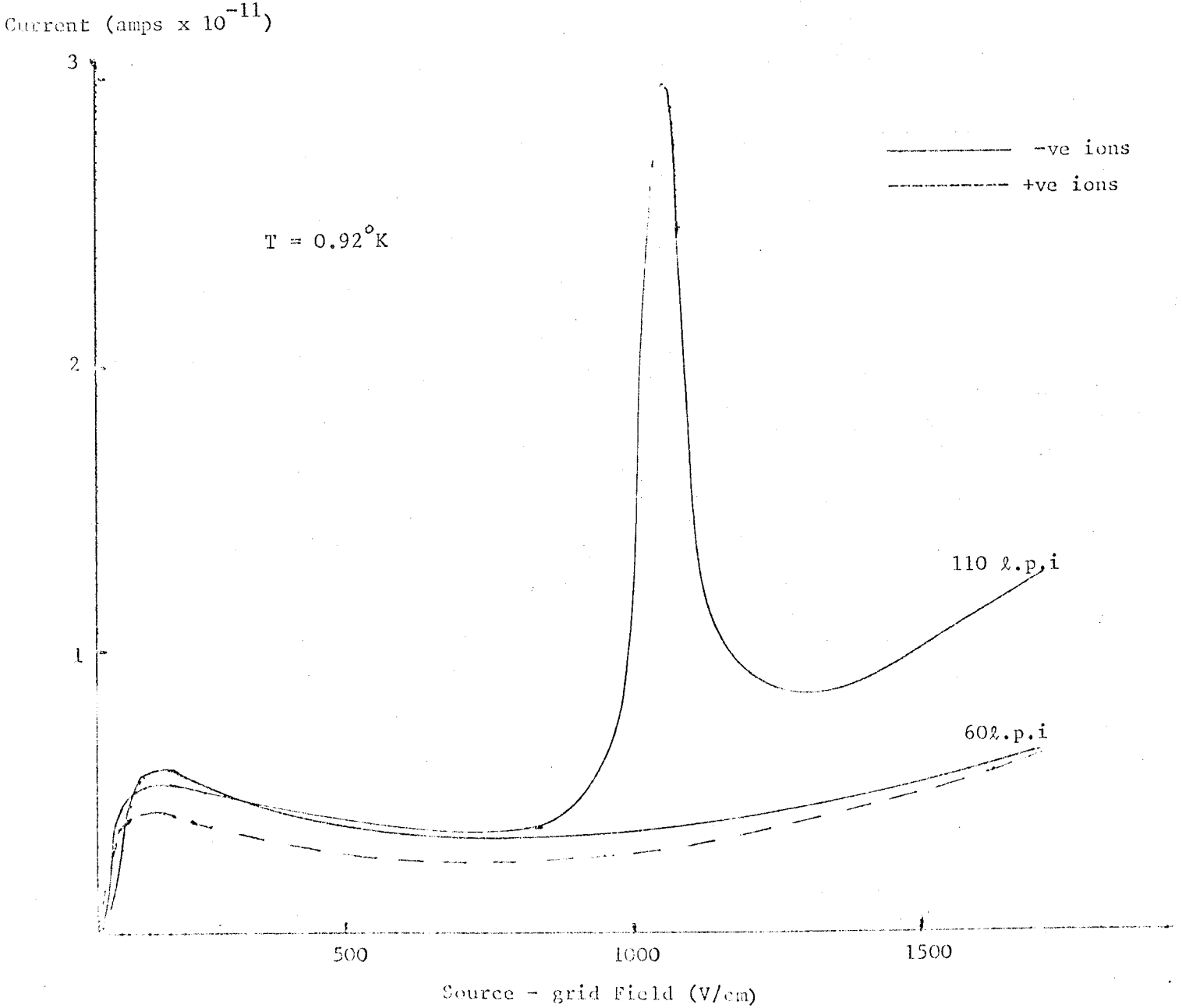

Fig 5.8 Triode characteristic for E_{GC} = constant (= 30 V/cm) showing the different high field behaviour for different grid sizes and sign of ionic change.

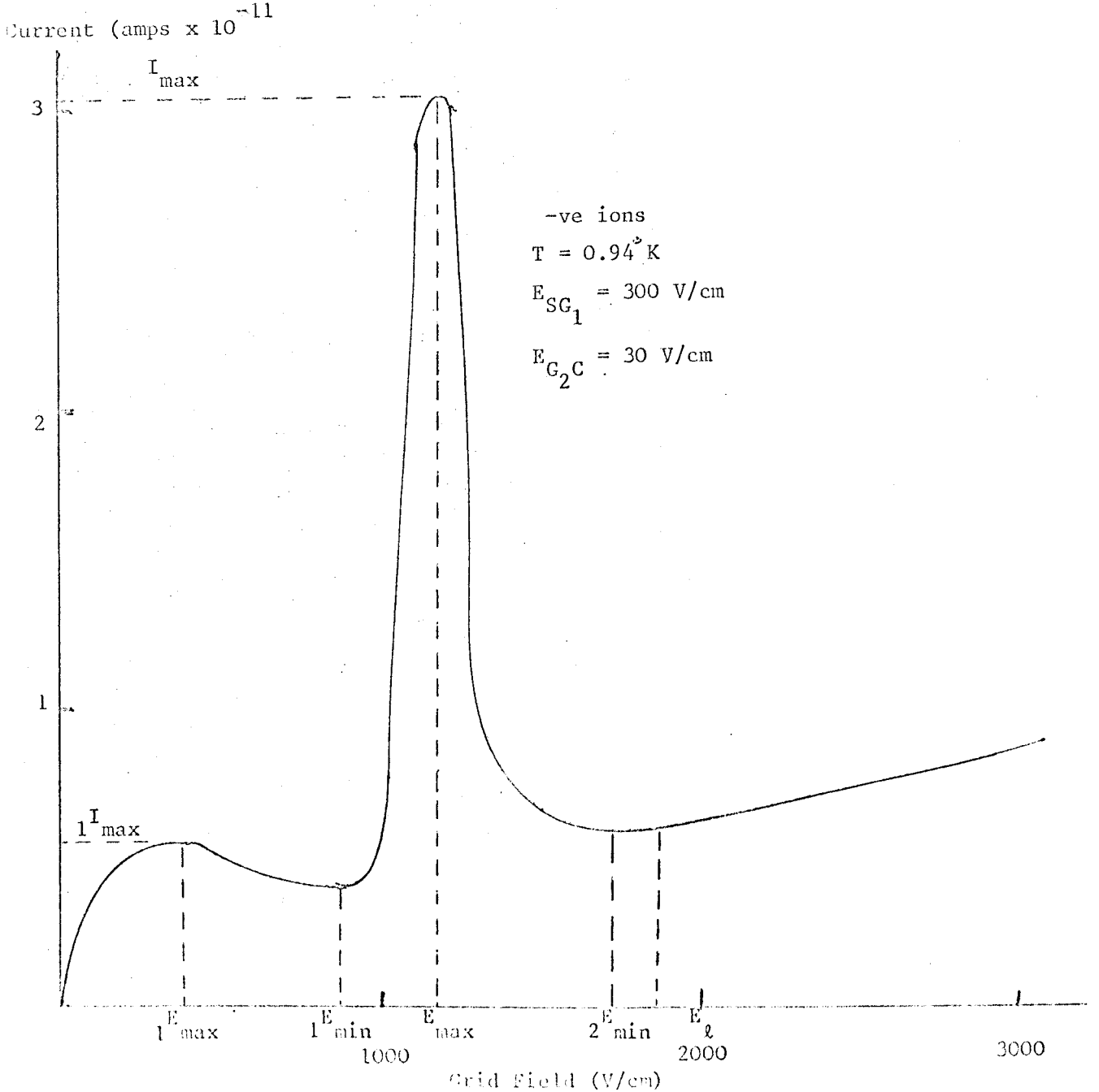

Fig 5.9 Tetrode characteristic

Defining various characteristic fields and currents.

Fig 5.10 Tetrode characteristics for various constant grid fields. (grid-collector field ≡ extracting field).

III. RESULTS

a. Introduction

A number of runs were taken using cells of different geometries, under various conditions of temperature and pressure, with grids of different mesh sizes. Different electrode configurations were examined, diodes with no grid, triodes and tetrodes with one and two grids respectively. The grids were placed between the source and collector electrodes.

A diode characteristic is shown in Fig 6. This shows an increasing current with field. To eliminate source effects, Fig 7 shows a triode characteristic with the source-grid field constant. Fig 8 shows a triode characteristic with the grid-collector field constant; this shows the vortex ring current peak for negative ions, but not for positive ions. Again to eliminate source effects Fig 9 shows a tetrode characteristic with the source-first grid field and the second grid-collector field constant. This is qualitatively the same as Fig 8. Fig 10 shows a tetrode characteristic for varying the second grid-collector field; this is qualitatively similar to Fig 7 showing an increasing current for all fields; for both positive and negative ions.

We can summarize the behaviour by saying (1) for varying the field from the collector to the nearest electrode (grid or source) the current rises with field for all fields, (2) for varying the field between any other two electrodes, the high field (vortex ring) current has a complex field dependence.

Fig 5.11 Tetrode characteristic

a) Total current incident on second grid (I_T)

b) Current drawn by second grid (I_G)

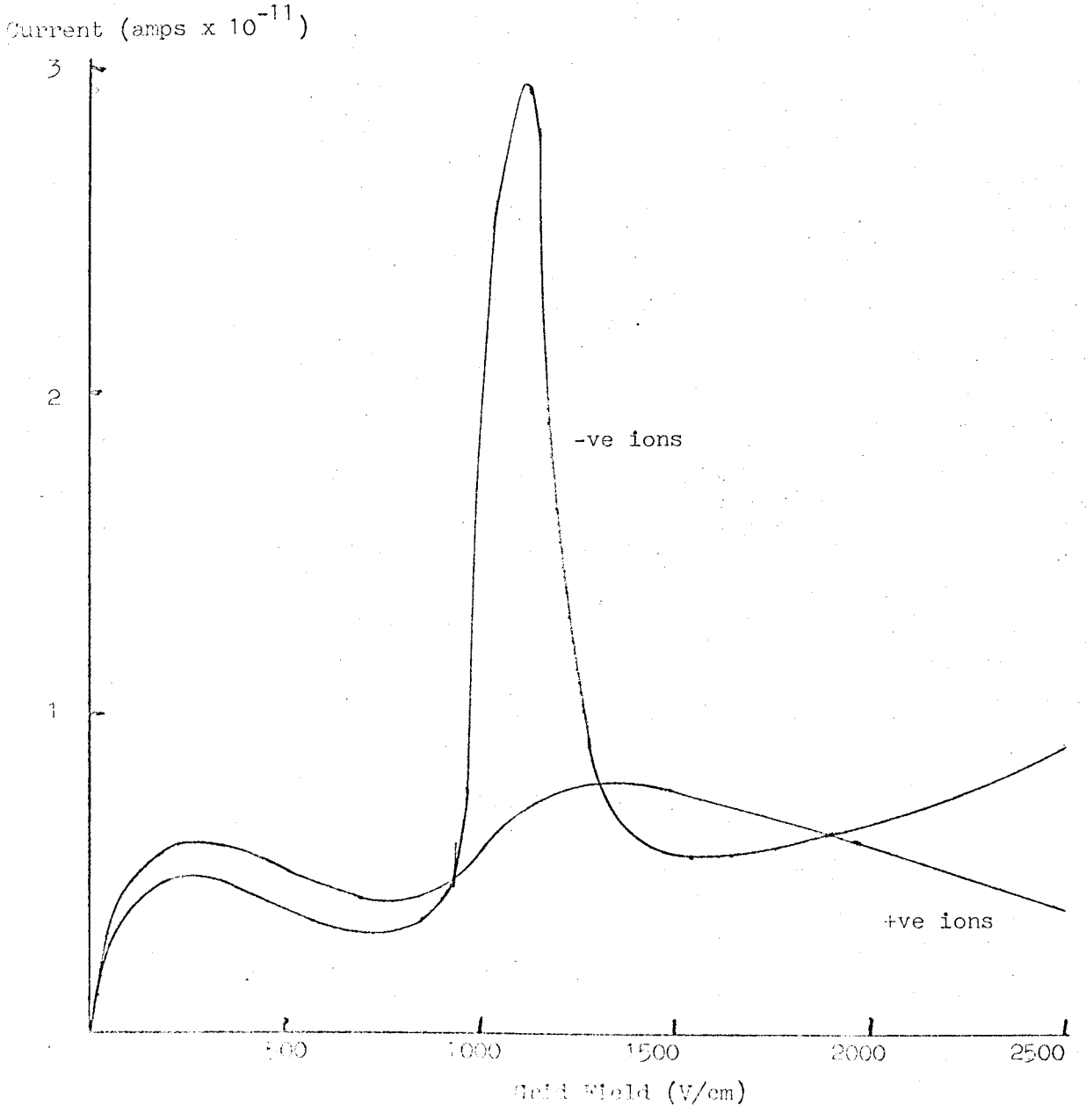

Fig 5.12 Tetrode characteristic
Current reaching the collector I_C, where $I_C = I_T - I_G$,
taken from Fig 5.11

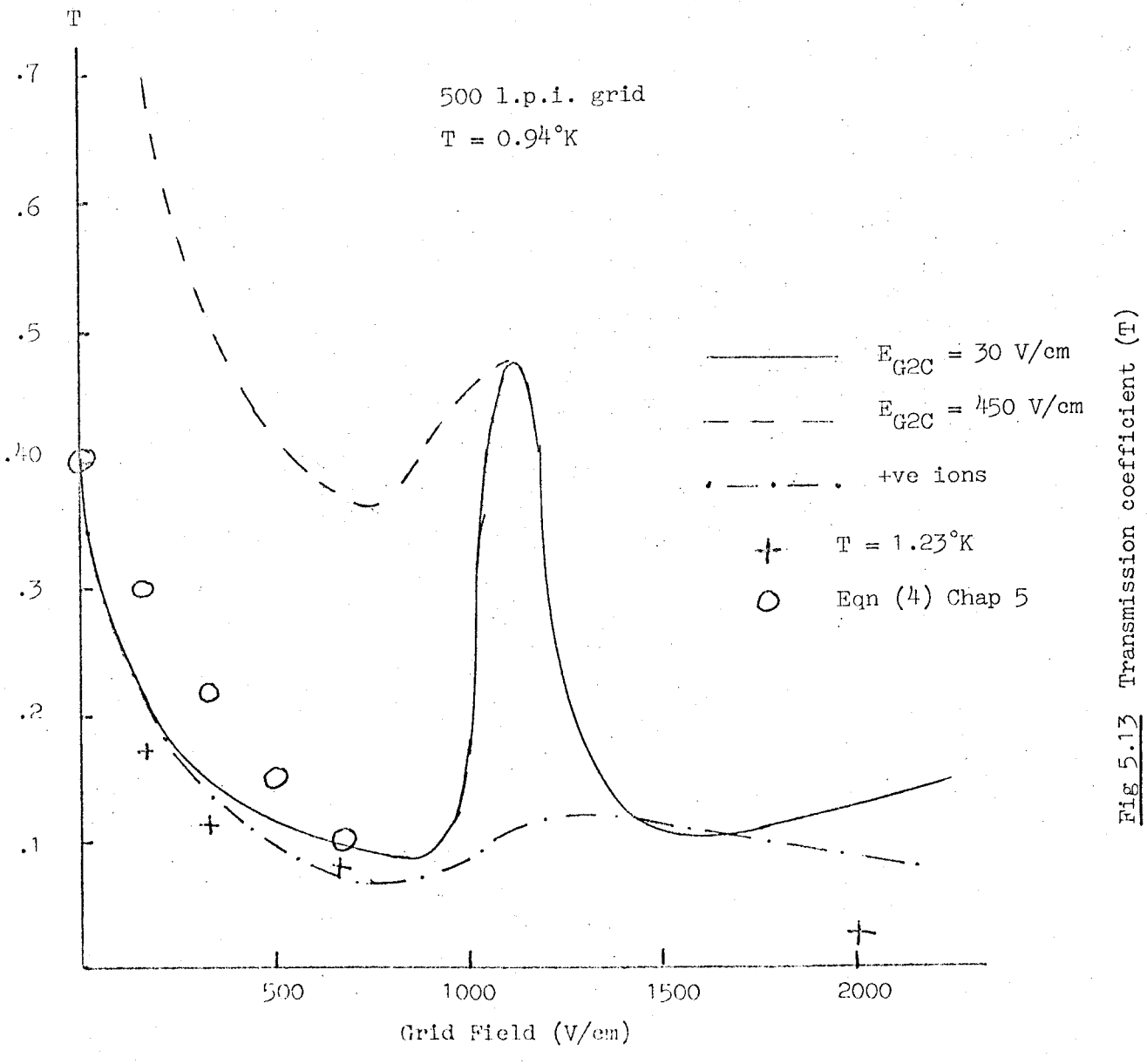

Fig 5.13 Transmission coefficient (T)

In a triode or tetrode, the current measured is the current passing between the last grid and collector; from point (1) above we would expect that the current between any two electrodes to increase monotonically with field, so the variation in measured current in point (2) would be due to the grid. This is seen in Fig (11), which shows the current in a tetrode collected on the second grid, when the field between the two grids was varied; in Fig 11a the field between the second grid and the collector electrode was opposite in sign to that between the two grids, so this gives the total current I_T between the two grids: in Fig 11b the field between the second grid and collector was the same sign as the field between the two grids, so the current passed on to the collector electrode, with current I_G collected by the grid.

The fields and dimensions for Figs 9 and 11 were the same. Fig 12 is taken from Fig 10, and is a plot of $I_T - I_G$, against field i.e. the incident current transmitted by the grid; this is precisely Fig 9 showing that the current reaching the collector I_C is the difference between the current incident on the grid I_T and the current drawn by the grid, I_G

$$\text{i.e.} \quad I_C = I_T - I_G$$

We can thus define a transmission coefficient for a grid, for varying the incident field, as

$$T_i = \frac{I_C}{I_T}$$

This is shown in Fig 13 for various values of the grid collector field E_{G_2C}. We expect T_I to vary with E_{G_2C} as from Fig 9. I_C varies with E_{G_2C}, whereas I_T should be independent of E_{G_2C}; this is because the current drawn by the grid decreases as the extracting field E_{G_2C} increases.

In general, when a characteristic was being taken in a cell, the fields that were kept constant were small fields, below the vortex ring formation field. This was for convenience, and no basic change in the characteristics was seen when the fields were above this critical field.

For the triode, it would be possible to construct a 3 dimensional model for the complete current-field characteristics; (I v E_{SG} v E_{GC}) for one temperature and pressure; for the tetrode we would need a 4D model. As the grid was also found to affect the characteristics, we have at least 5 variables (if we discount the electrode spacings) to give a complete account of the current variation in a triode for one type of ion. Our results will thus only pick out the interesting variations, with an indication of how they vary with the other parameters.

Most of our measurements were of the current reaching the collector i.e. after being transmitted by a grid with a field dependent transmission coefficient. As the ion current from the source is also field dependent, we can have no absolute measurement of how the current density varies with field. This can be seen as follows.

Consider a source of ions (either the radioactive source, or a grid) producing (or transmitting) ions at a rate $\dot{N}$ per sec over an area A. If they move in an electric field at a velocity v, in time t they move a distance ℓ. Then the total charge Q_T in volume V after time t is given by

$$Q_T = \dot{N}et$$

$$V = Avt$$

thus the charge density ρ is given by

$$\rho = \frac{Q_T}{V} = \frac{\dot{N}e}{Av}$$

and the current I is

$$I = \rho vA = \dot{N}e$$

which is independent of v, and therefore of the electric field. Therefore our variation in current with electric field is due to the field dependence of $\dot{N}$; for a grid this corresponds to the field dependence of T_i.

If we could keep the charge density constant, we expect to see a current vary with field as the ion velocity v(E)

$$I = \rho A.v(E)$$

and thus have a region of negative differential conductivity for the vortex ring region, assuming the current density was small enough to avoid field distortion.

We shall discuss our results in detail under two headings; low field and high field results, the boundary being approximately

the field needed to create vortex rings. The experimental results were taken over the whole range in field for any one run.

b. Low Field Results

As we have shown, the current field characteristics do not depend on the intrinsic field dependence of the ion velocity; although the grid transmission coefficient may depend on the ion velocity. Fig 13 shows that the low field value of T_i depends only on the fields on each side of the grid; for a constant extracting field (E_{G_2C}), the transmission coefficient varies with incident field ($E_{G_1G_2}$) in the same way for positive and negative ions, and at different temperatures. We take this to mean that T_i is independent of the field dependence of the ion velocity, and only varies with field according to a theory similar to the one in section 2 b. This theory was an electrostatic analogy, depending only on the potential distribution around the electrodes; assuming the charged particles follow the force lines, then their velocity, and thus their field dependence, is immaterial. If, however, the ion takes a long time to reach an equilibrium velocity in a given electric field (as when bound to a vortex ring) then they will not necessarily follow the force lines around the grid where these are rapidly varying with position, and there will be deviations from the 'theoretical' transmission coefficient, as seen at high fields.

We can obviously define another transmission coefficient T_x

for when the incident field is constant and the extracting field is varied. This will give a curve like Fig 11 a, taken for a tetrode. Here the source-first grid field E_{SG_1} was kept constant, a reverse field kept between the second grid and collector, and the current was measured on the second grid for varying the field between the grids. Figs 10 and 7 are similar in that only the grid collector field was varied, so the current incident on the grid was constant. These curves are fitted approximately by

$$I = I_o(1 - e^{-E/E_1} + cE)$$

where the constant c is to allow for the steady current increase at high fields. Current characteristics in classical fluids have been fitted by similar equations (Secker and Lewis 1965, Januszajtis 1963). I_o is found by extrapolating the linear high field part of the curve to zero field.

The low field part of the curves in Figs 11 a and b may be fitted by

$$I_T = I_o(1 - e^{-E/E_1}) \qquad (1)$$

$$I_G = I_o(1 - e^{-E/E_o}) \qquad (2)$$

where I_T is the total current reaching the second grid in a tetrode and I_G is the current drawn by the grid.

Then the current reaching the collector is

$$I_C = I_T - I_G$$

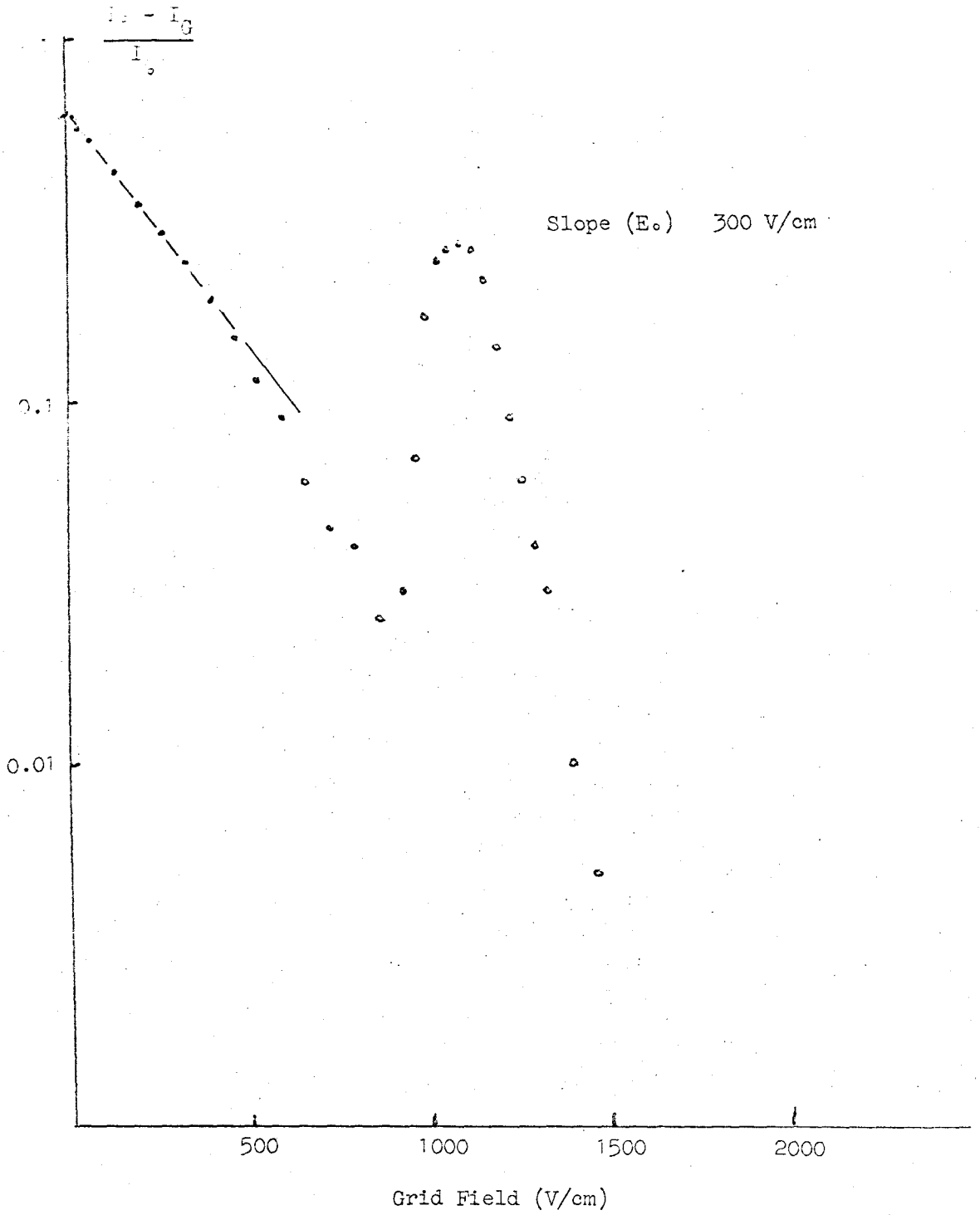

Fig 5.14 Plot of $I_G = I_o (1 - e^{-E/E_o})$ from Fig 5.11

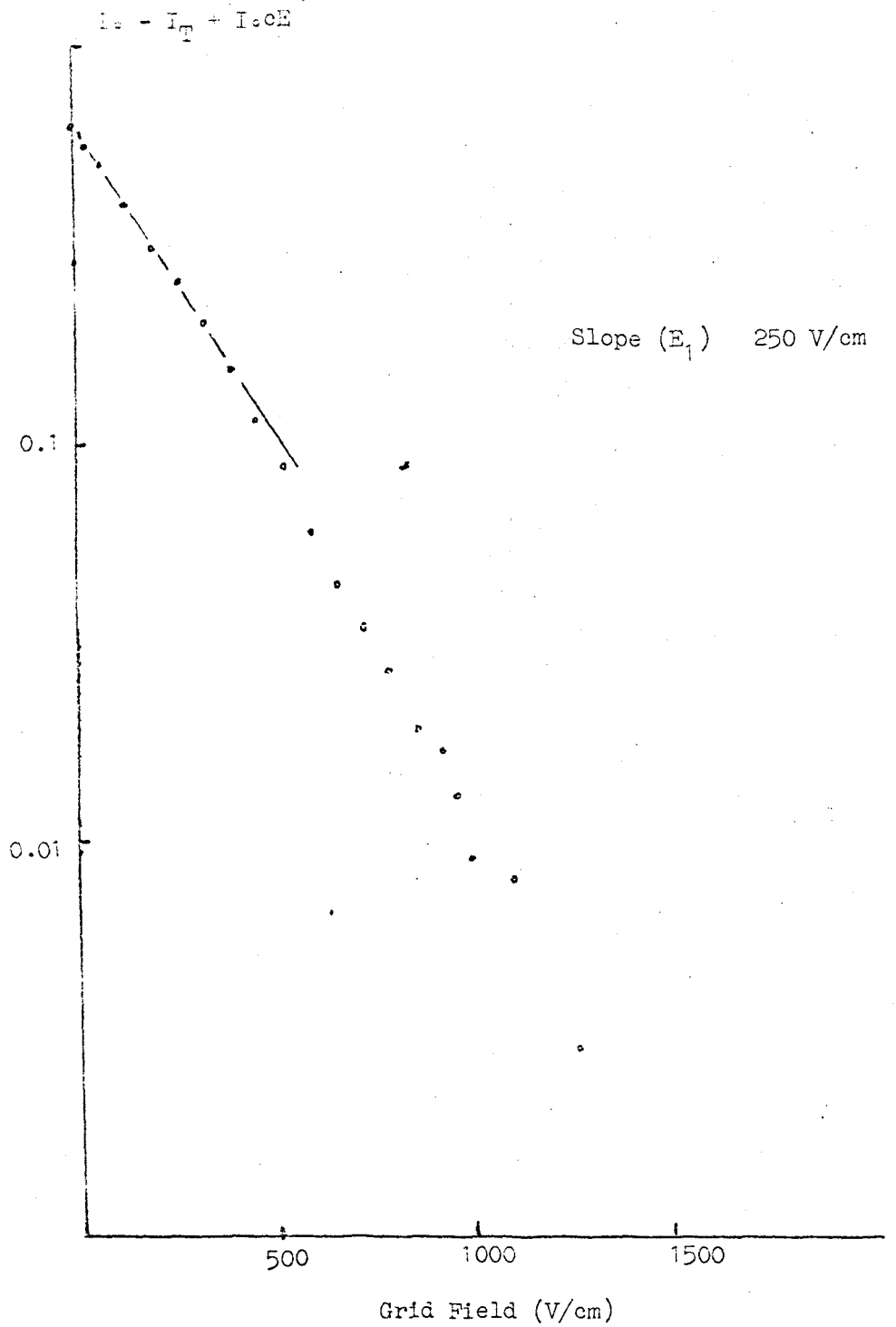

Fig 5.15 Plot of $I_T = I_o (1 - e^{-E/E_1} + cE)$ where $E = E_{G1G2}$ (Grid Field) from Fig 5.11

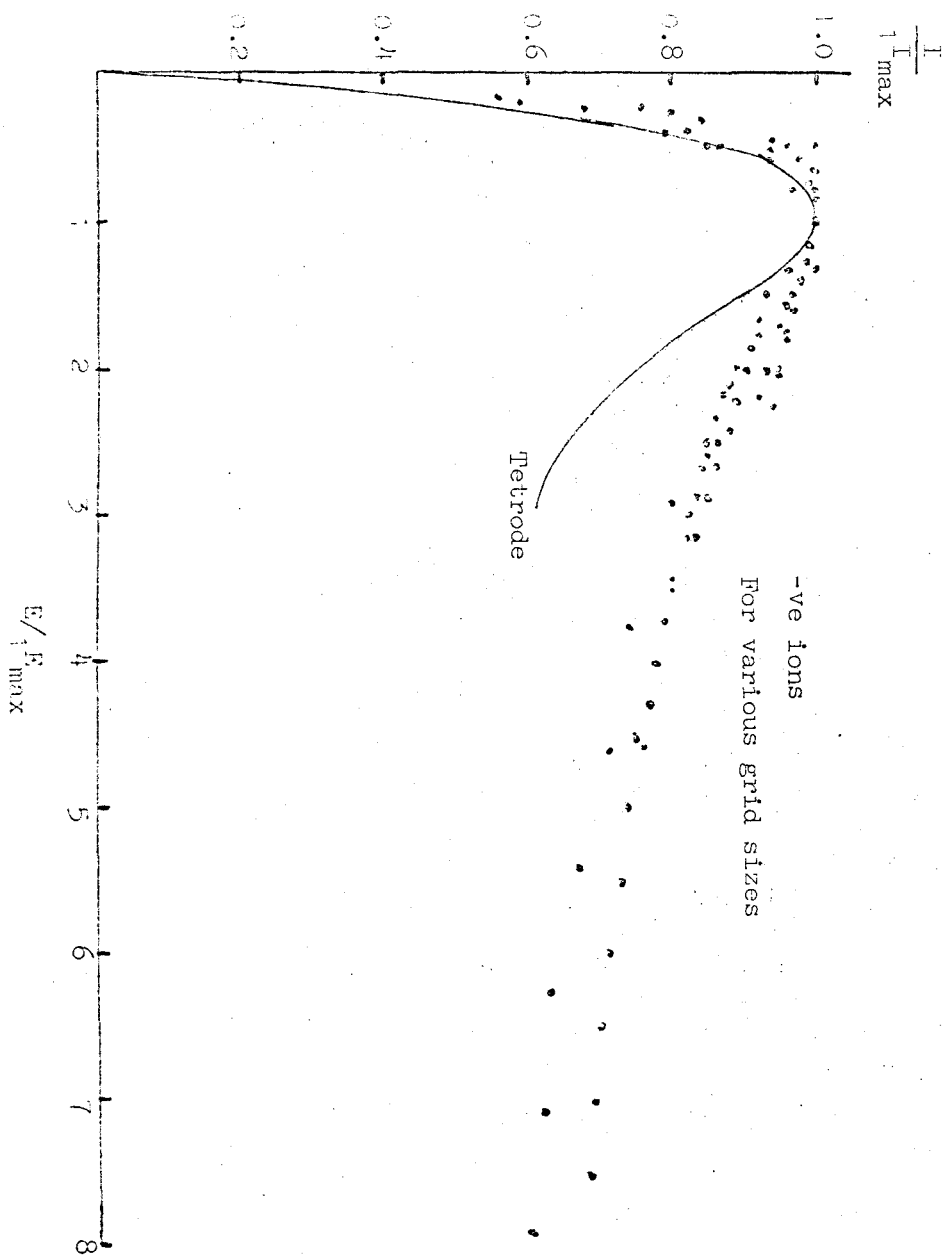

Fig 5.16 Plot of $\frac{I}{{}_1I_{max}}$ versus $\frac{E}{{}_1E_{max}}$ (defined in Fig 5.9)

for Triodes. For fields E up to ${}_1E_{min}$

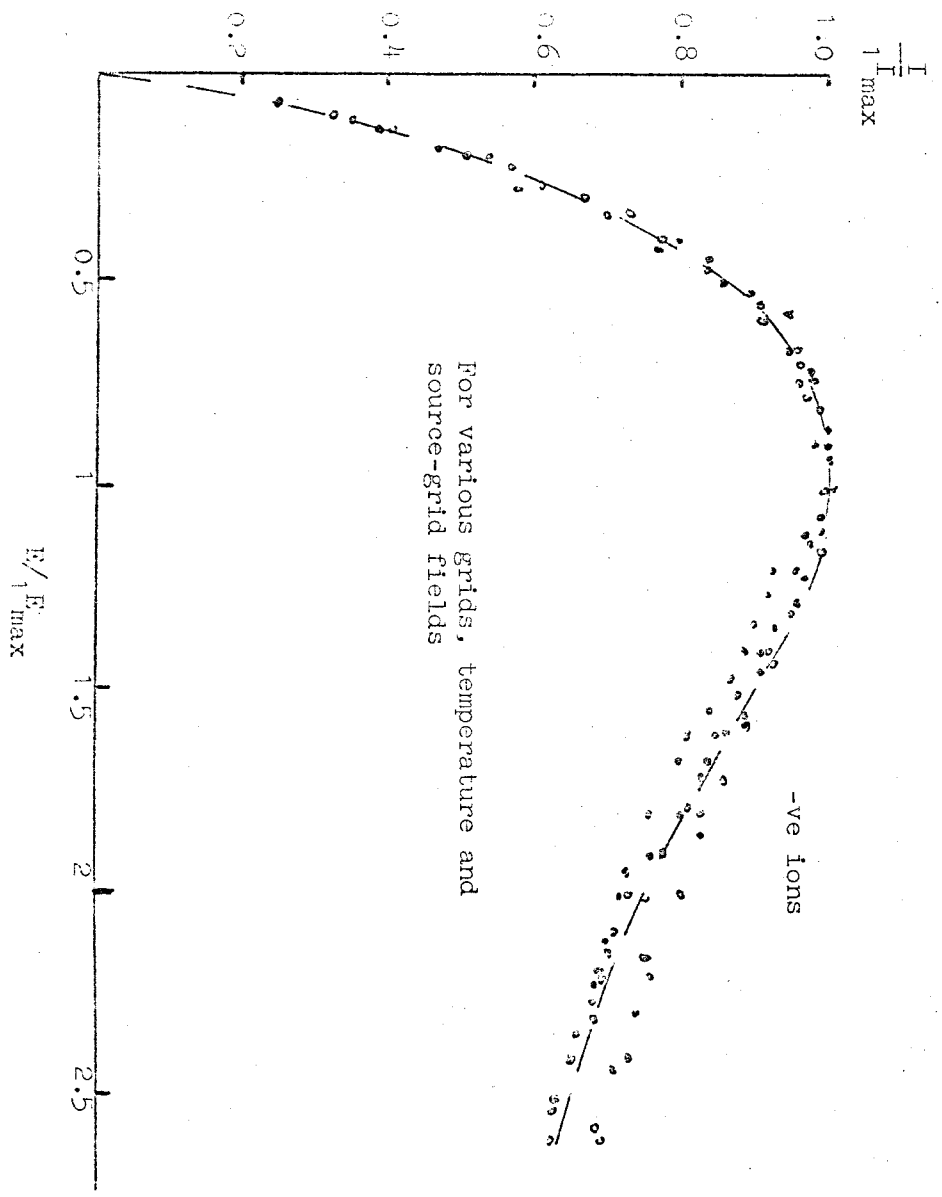

Fig 5.17 Plot of $\frac{I}{I_{1max}}$ versus $\frac{E}{E_{1max}}$ for Tetrodes

$$= I_o(e^{-E/E_o} - e^{-E/E_1}) \qquad (3)$$

where E_1 and E_o are constants, describing the transmission coefficients of the grids, and E is the field between the two grids.

The transmission coefficient will then be

$$T_i = \frac{I_C}{I_T} = \frac{e^{-E/E_o} - e^{-E/E_1}}{1 - e^{-E/E_1}} \qquad (4)$$

Figs 14 and 15 show a log-linear plot of $(I_o - I_G)$ and $(I_o - I_T)$ against field, showing the degree of approximation to which they fit the expressions (1) and (2). Equation (4) is plotted in Fig 13 using values for E_1 and E_o from Figs 14 and 15.

It was found that the collector current followed equation (3) for triodes and tetrodes. The current rises from zero at zero field to a maximum, and then decreases slowly until high field (vortex rings) effects become important. The field ($_1E_{max}$) where the current was a maximum ($_1I_{max}$) varied considerably according to grid, temperature, other electrode fields, and also time; but it was found that a plot of $I/_1I_{max}$ against $E/_1E_{max}$ gave a universal plot. These are shown in Figs 16 and 17 for triodes and tetrodes. The significance of these plots is difficult to analyse, as they depend on the field dependence of the grid transmission coefficient as well as the source field dependence, and these are not known analytically; our approximations are not good enough to derive this relationship.

We may summarise the results by saying that the characteristics depend only on the field dependence of the grid transmission coefficients and the source, and not on the ion velocity. Our results show continuous curves at all fields. Thus the effect reported by Bruschi et al (1968) when measuring an ion critical velocity by a change in slope of an effective D.C. characteristic is of doubtful significance; to make sure the curves were not frequency dependent we carried out runs varying the square wave field for a constant low frequency, and obtained similar curves to our D.C. ones. If under certain conditions there is a discontinuous change in the slope, it must be due to the transmission coefficient changing; in which case discontinuities are related to the conditions around the grid.

c. High Field

When the electric field is high enough to produce vortex rings, the grid transmission coefficient T_i changes from its low field behaviour. The most remarkable phenomenon is seen for negatively charged vortex rings at low temperatures, where there is a large peak in T_i, Fig 13. T_x shows no abnormal change from its low field value, having a continual slow increase towards saturation. This variation in T_i is clearly seen in Fig 12 for the current reaching the collector. Figs 11 a and b show that the change in T_i is due to less current being drawn by the grid, and not due to a high field behaviour of charge carriers with a negative

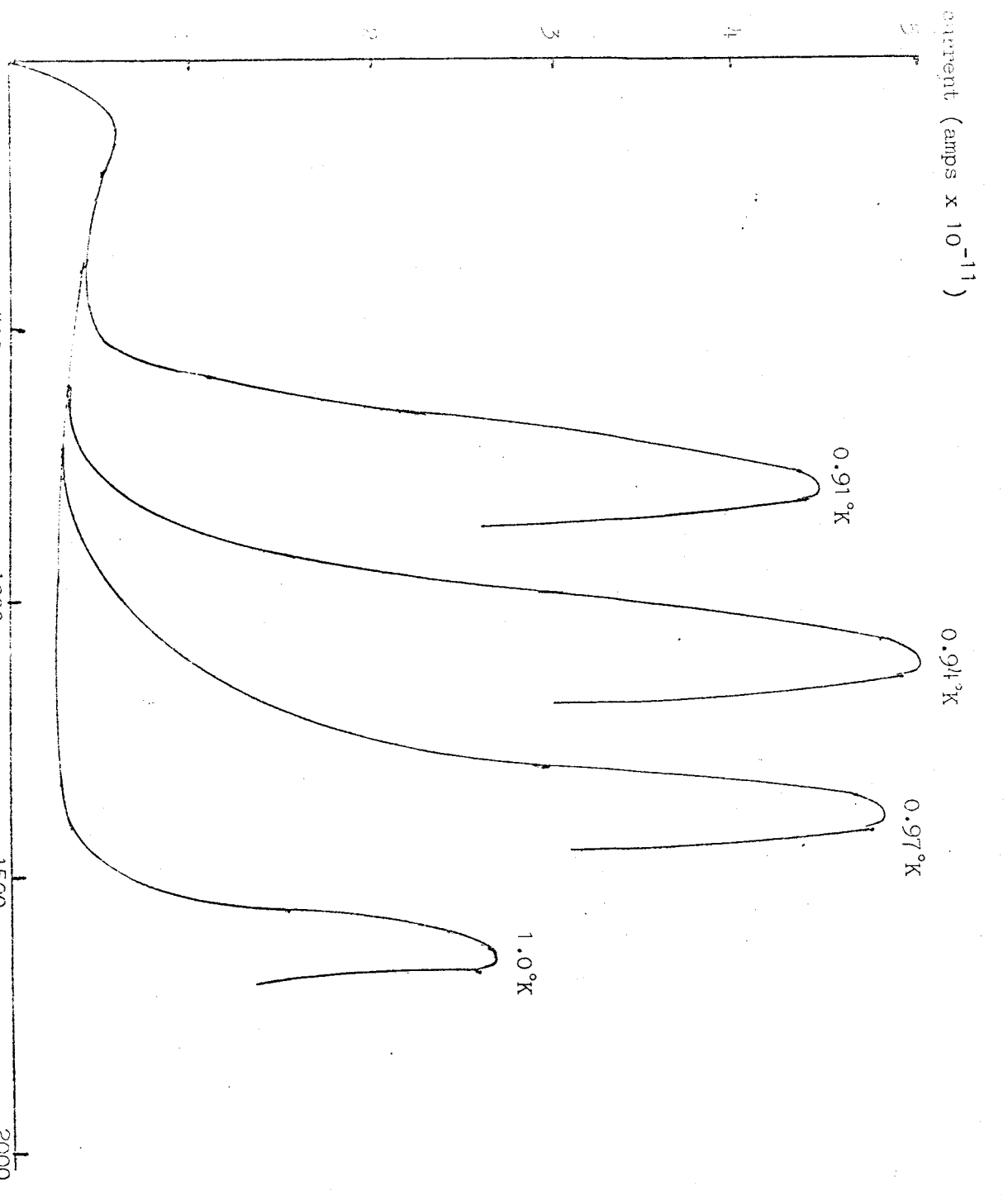

Fig 5.18 Variation of negative ion peak with temperature (Triode)

differential mobility.

Fig 11 a shows that I_T is nearly constant at high fields, so the variation in T_i is given to a good approximation by the variation of I_C with field. This was how most of our results were taken.

The difference in the behaviour of T_i between positive and negative charged vortex rings shows that T_i is now determined by the properties of the vortex rings; for low fields (bare ions) T_i was independent of the ion properties (eg velocity).

(i) Negatively charged vortex rings

It was found that the current peak Fig 12 had its maximum value at an electric field that was temperature and pressure dependent; the amplitude of the current maximum depended on temperature and pressure; and the existence of the peak depended on the grid mesh size.

Fig 8 shows two current characteristics taken in a triode under the same conditions of temperature and fields,one for a 601pi mesh and the other for a 1101pi grid; there is no current peak for the 601pi grid. Grid meshes of 2501pi and 5001pi also showed peaks, similar to the 1101pi grid.

Fig 18 shows how the current peak varies with temperature at the saturated vapour pressure (in a triode, grid 5001pi). The same behaviour is shown for other grids giving peaks, and also for higher pressures. We see that the peak decreases sharply in

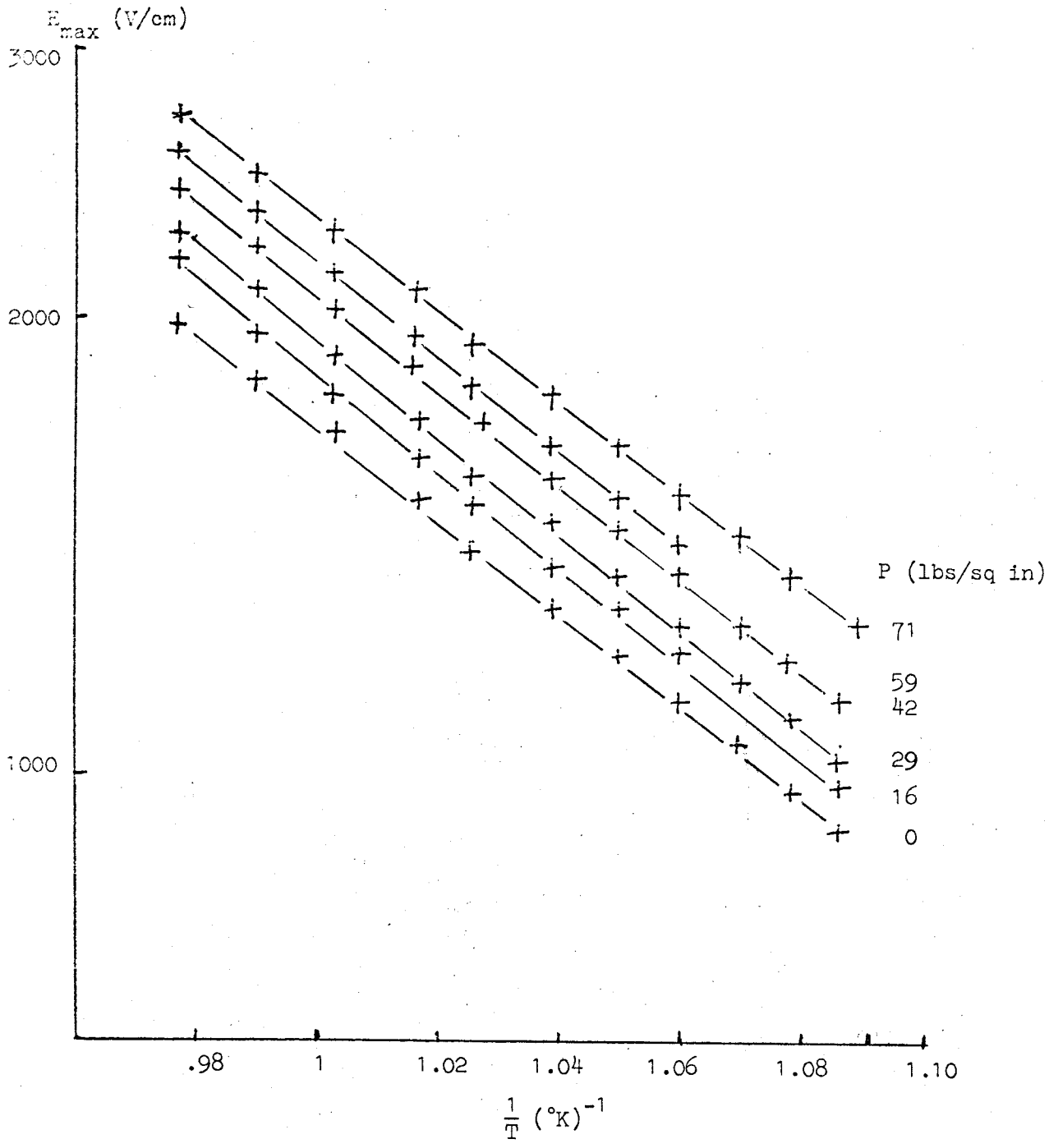

Fig 5.19 Plot of E_{max} versus $\frac{1}{T}$ for constant pressure

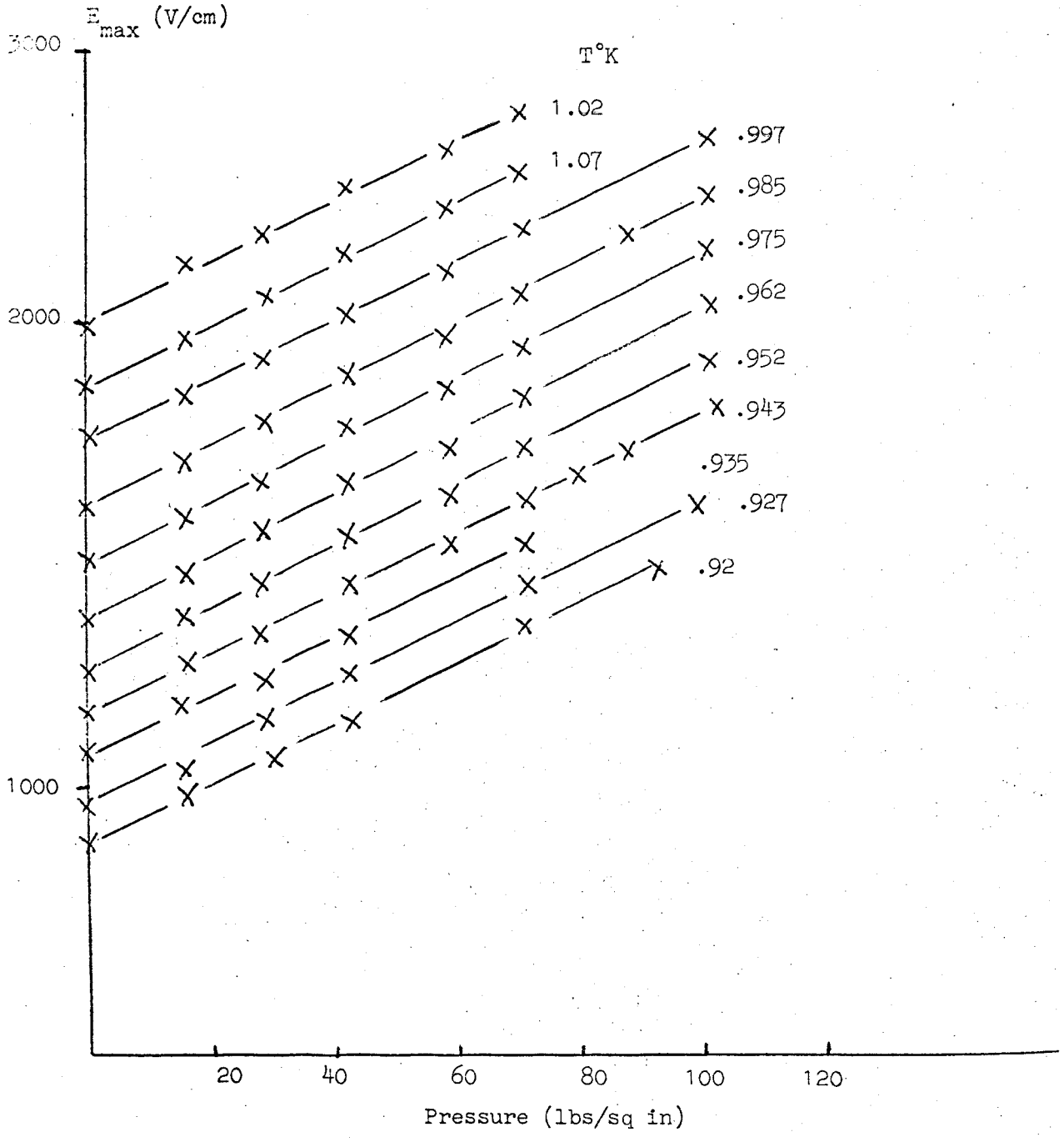

Fig 5.20 Plot of E_{max} versus pressure for constant temperature

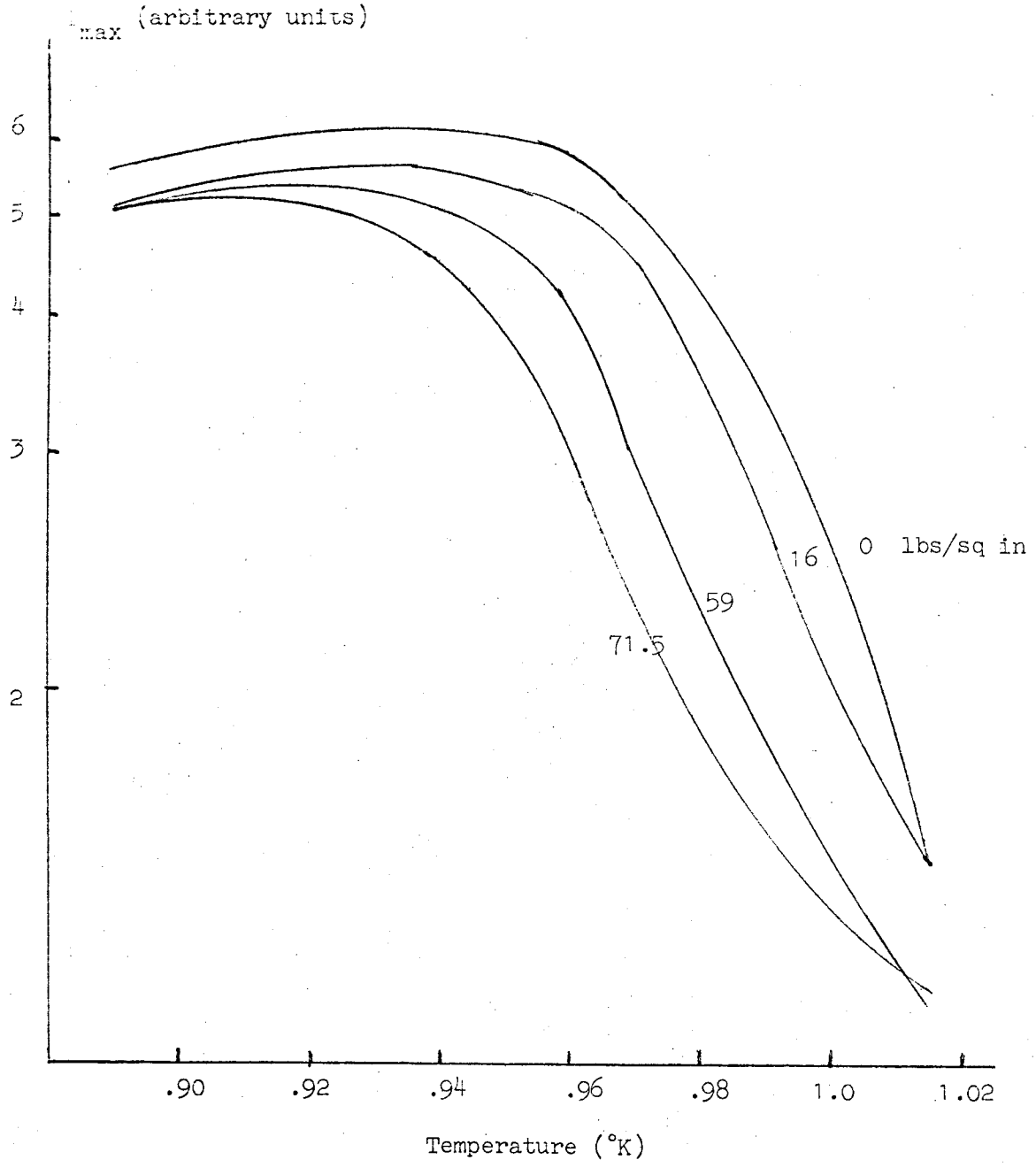

Fig 5.21 Plot of $\ln(I_{max})$ versus temperature for constant pressure

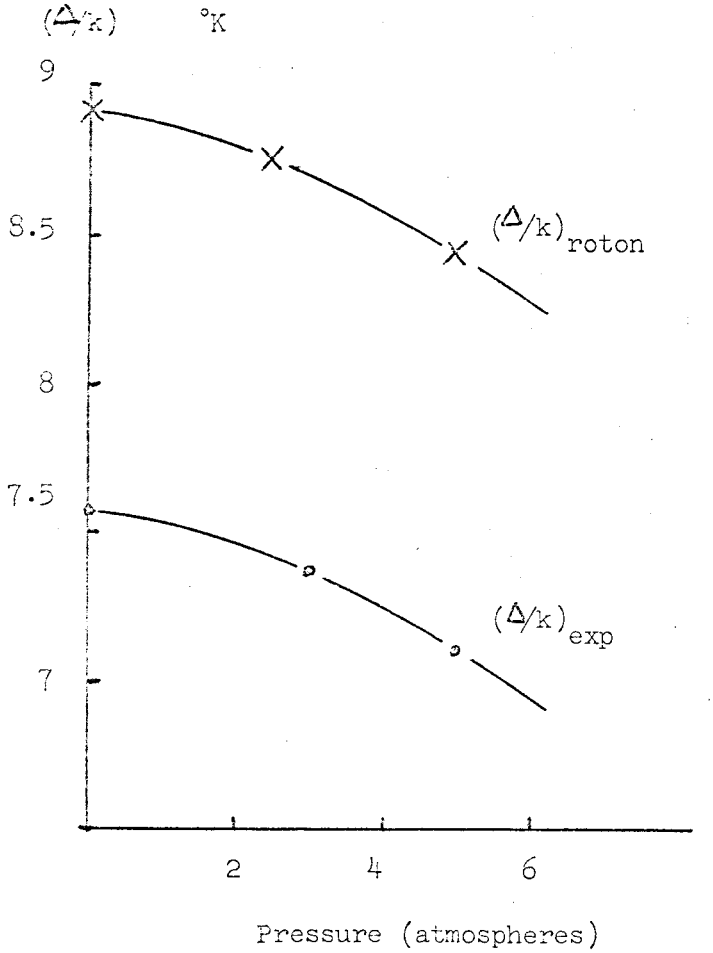

Fig 5.22 Plot of $(\Delta/k)_{exp}$ versus pressure compared with $(\Delta/k)_{roton}$ (from Wilks)

amplitude to zero at a temperature around 1 K. Fig 19 shows how the field (E_{max}) at the current maximum (I_{max}) varies with temperature at various pressures; Fig 20 shows the variation in E_{max} with pressure for constant temperature, and Fig 21 the variation in I_{max} with temperature for constant pressure.

Properties of E_{max} 1. Temperature Dependence

The variation of E_{max} with temperature in Fig 19 may be described by

$$E_{max} \propto \exp\left(-\frac{\Delta}{kT}\right)$$

where $\frac{\Delta}{k}$ varies with pressure. At saturated vapour pressure, we get $\frac{\Delta}{k} = 7.58 \pm .20^{\circ}K$. Fig 22 shows how these values of $(\frac{\Delta}{k})$ vary with pressure, and compares them with the known variation of $(\frac{\Delta}{k})$ for the roton energy gap with pressure (Wilks 1967). It is seen that they vary in the same way, but with our values being lower by a constant difference of about 1.3 K. We can compare our temperature dependence with the known temperature dependence of the low field bare ion mobilities which are of the form

$$\mu \propto \exp\left(\frac{\Delta}{kT}\right)$$

where $\frac{\Delta}{k} = 8.8^{\circ}K$ for positive ions

$\frac{\Delta}{k} = 8.1^{\circ}K$ or $7.97^{\circ}K$ for free negative ions

$\frac{\Delta}{k} = 6.1^{\circ}K$ for negative ions trapped in vortex lines.

at the saturated vapour pressure. Our value falls between those

for free and trapped negative ions. (The significance of this is uncertain, as the difference between $(\frac{\Delta}{k})$ for positive and negative ions is also unexplained.)

2. Vortex ring velocity at E_{max}

The temperature dependence of the frictional force $\alpha(T)$ on a charged vortex ring $\alpha(T)$, described earlier, is

$$\alpha(T) \propto e^{-\Delta/kT}$$

where $\frac{\Delta}{k} = 8.6$ K and Δ is the roton energy gap. Taking from Huang and Olinto (1965) the semiempirical formula for $\alpha(T)$, which is expected to hold for temperature above about 0.7 K,

$$\alpha(T) = \exp\ (13.9 - \frac{\Delta}{kT}) \text{ eV/cm}$$

we get, over our temperature range,

$$\frac{eE_{max}}{\alpha\ (T)} = \text{const} = 10 \pm 0.1$$

From the equation of motion for a vortex ring (Appendix 3) this means the vortex ring incident as the grid has a constant velocity (and therefore radius) at E_{max} independent of the temperature.

3. Pressure dependence

Fig 20 shows that the variation of $E_{max}(P)$ with pressure P is described by

$$\ln(\frac{E_{max}(P)}{E_o}) = a\ P$$

where E_o is the value of E_{max} at the saturated vapour pressure, and 'a' is a constant. We find $a = 61.5 \pm 0.5 \times 10^{-3}$ at $T = .99^{\circ}K$ and $a = 64.7 \times 10^{-3}$ at $T = 0.92^{\circ}K$ for our pressure range. The

highest pressures obtained were about 7 atmospheres.

We can try and relate the pressure dependence of E_{max} to the roton number density. Then

$$N_r \alpha p_o^2 m_r^{\frac{1}{2}} e^{-\Delta/kT}$$

where $p_o = p_o^* (1+.0029\ P) = p_o^*(1+bP)$

$m_r = m_r^* (1-.0217\ P) = m_r^*(1-cP)$

$\Delta = \Delta^* (1-.0075\ P) = \Delta^* (1-aP)$

are the pressure dependent terms, with a linear interpolation between vapour pressure and the melting point giving the values of the coefficients (from Donnelly, 1967).

We then get to a good approximation

$$\ln\left(\frac{N_r(P)}{N_r(o)}\right) = \left(2b - \frac{c}{2} + \frac{\Delta^* a}{kT}\right) P \ .$$

Using $\Delta^* = 8.7^{\circ}K$, we get for the coefficient of P on the right hand side

$$\ln\left(\frac{N_r(P)}{N_r(o)}\right) = 60.6 \times 10^{-3} \ . \ P$$

and using $\Delta^* = 7.38^{\circ}K$

$$\ln\left(\frac{N_r(P)}{N_r(o)}\right) = 50.6 \times 10^{-3} \ . \ P$$

where the variation in Δ^* with pressure accounts for $\sim$80% of the magnitude of the coefficient.

Using values of N_r at 0 and 5 atmospheres at $T = 1^{\circ}K$ from Donnelly (1967), we get

$$\ln\left(\frac{N_r(P)}{N_r(o)}\right) = 59.7 \times 10^{-3} \ . \ P$$

and at $T = 0.9^{\circ}K$

$$\ell n\left(\frac{N_r(P)}{N_r(o)}\right) = 67.2 \times 10^{-3} \cdot P$$

Our values of 'a' agree well with these figures, and apart from the discrepancy in the value of $\frac{\Delta}{k}$ for the temperature dependence, it appears that this phenomenon is related to the roton number density. We can definitely say that E_{max} is not connected with the low field free ion mobility $\mu-$; for increasing pressure, $\mu-$ increases to a maximum at about 5 atmospheres and then decreases, so at pressures less than 5 atmospheres $\frac{1}{\mu-}$ would be a decreasing function; to fit the temperature dependence, $E_{max} \propto \frac{1}{\mu-}$, but for the pressure dependence $E_{max} \propto \mu-$.

The pressure dependence of $\alpha(T)$, the frictional force on a vortex ring, may be estimated from the theory by Rayfield and Reif (1964). Here, the force is proportional to the momentum-transfer cross section between vortex lines and rotons σ_r, and hence the momentum density of rotons

$$\rho_r \propto P_o^4 \, e^{-\Delta/kT}$$

$$\alpha(P) \propto \rho_r \cdot \sigma_r$$

Assuming a pressure independent cross section, we get, using the interpolation formulae as before, that

$$\ell n\left(\frac{\alpha(P)}{\alpha(o)}\right) \simeq \left(4b + \frac{\Delta^* a}{kT}\right) P$$

$$\simeq 66.6 \times 10^{-3} \, P \text{ for } \Delta^* = 7.6^{\circ}K$$

$$\simeq 79.2 \times 10^{-3} \, P \text{ for } \Delta^* = 8.7^{\circ}K$$

at $T = 1^{\circ}K$.

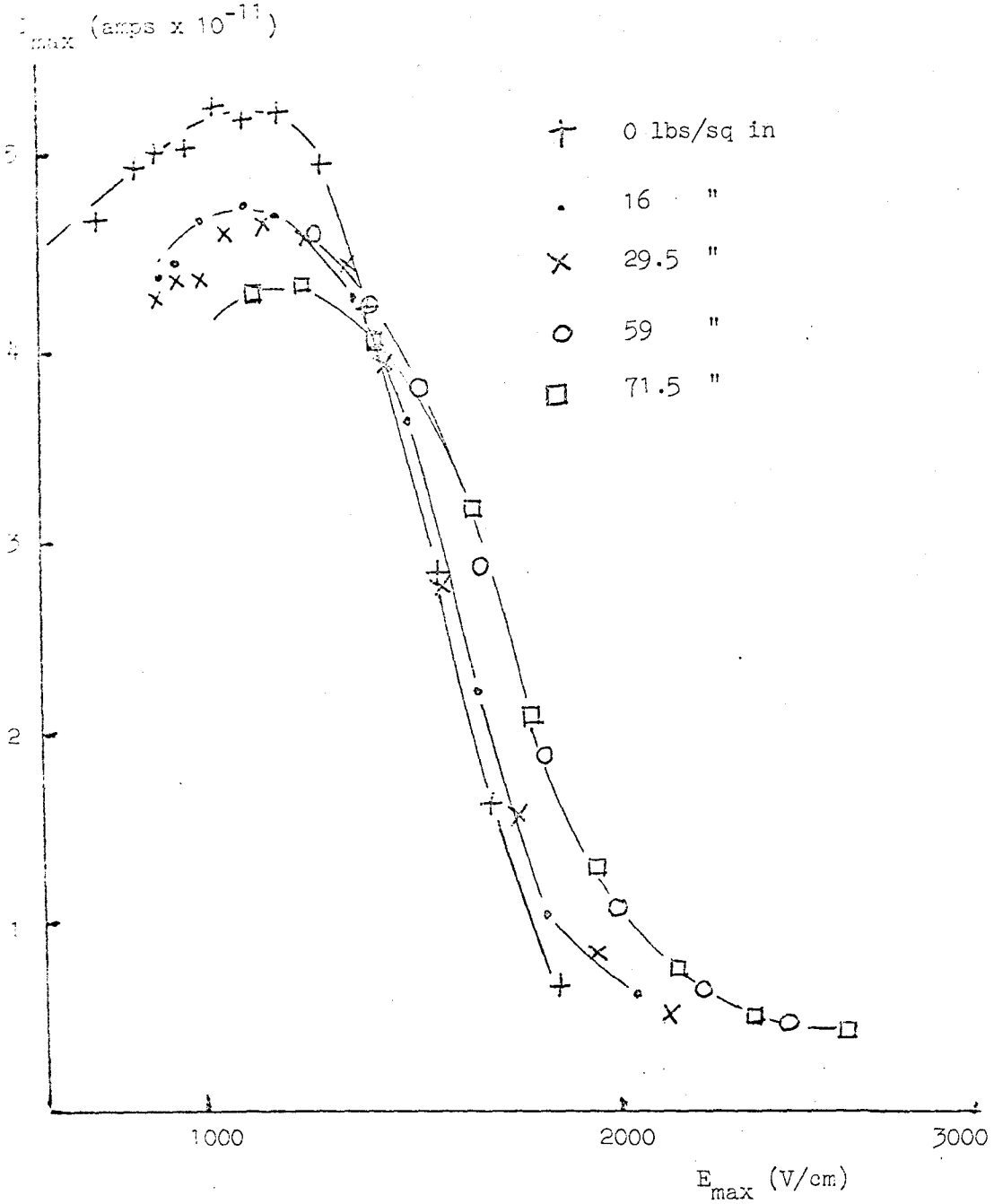

Fig 5.23 Plot of I_{max} versus E_{max} for constant pressure

Thus over our temperature and pressure range, we have a reasonable agreement with

$$\frac{eE_{max}}{\alpha(T,P)} = \text{const} \simeq 10$$

This implies that at E_{max_1} the vortex rings incident on the grid have a velocity and therefore size and energy that is independent of the temperature and pressure. E_{max} is unchanged by the fields in the other parts of the cell (including the extracting field from the grid) and the grid mesh size (except the 601pi grid).

4. Properties of I_{max}

Fig 21 shows the peak amplitude (I_{max}) as a function of temperature. The overall shape is very similar to the ion-vortex line capture cross section curves measured by Springett (1967), but are concentrated at a lower temperature. A more revealing plot is shown in Fig 23, of peak amplitude as a function of the incident electric field (E_{max}). There is a small shift to higher fields at higher pressures, but it keeps the characteristic of a well defined cut off, which is described by

$$I_{max} = I_o \, e^{-E_{max}/E_o}$$

$E_o(P)$ varies with pressure P, being

$$E_o(0) = 202 \pm 5 \text{ v/cm}$$

$$E_o(5) = 332 \pm 5 \text{ v/cm}$$

and

$$E_o(P) = E_o(0) \; (1 + 0.13 \, P)$$

where P is in atmospheres.

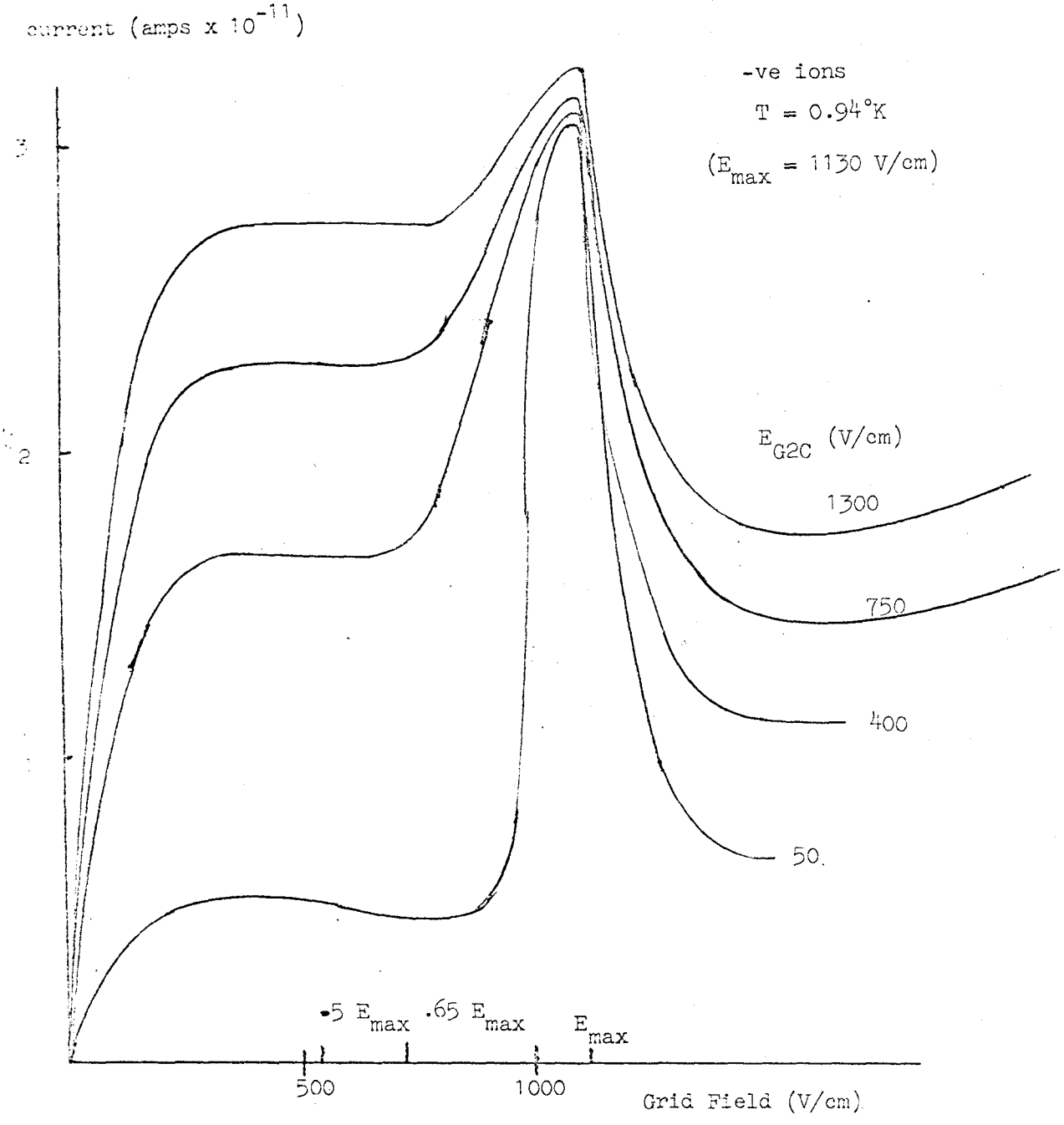

Fig 5.24 Tetrode characteristic. for various constant extracting fields (E_{G2C})

5. Peak shape

The shape of the peak depends on the grid mesh size, temperature, pressure and extracting field. Fig 24 shows a number of characteristics taken in a tetrode, the current plotted against the field between the grids $E_{G_1G_2}$ for a number of different constant extracting fields E_{G_2C}.

The field where we expect vortex rings to be created E_{vr} is calculated from Appendix 3 (using the Huang-Olinto theory) as

$$E_{vr} = 6.5 \frac{\alpha(T)}{e}$$

and from knowing the field at the current maximum

$$E_{max} = 10 \frac{\alpha(T)}{e}$$

we get

$$E_{vr} = 0.65 E_{max}$$

This was checked by velocity measurements in the grid space; the transition from bare ions to a vortex ring current is not well defined, but indicates

$$E_{vr} \simeq 0.5 E_{max}$$

We can explain this discrepancy by considering the derivation of the Huang-Olinto criterion; they assume that the ion is captured by a vortex ring at a velocity of 5 m/sec, and use a value for $\eta(R)$ appropriate to a vortex ring of that velocity. It is more likely that the ion is captured by a faster moving vortex ring, which would have a lower value of $\eta(R)$, and thus a lower critical field than that described by the Huang-Olinto theory.

Fig 5.25 Variation of $_1E_{min}$ with extracting field; one of the parameters describing the shape of the negative ion peak

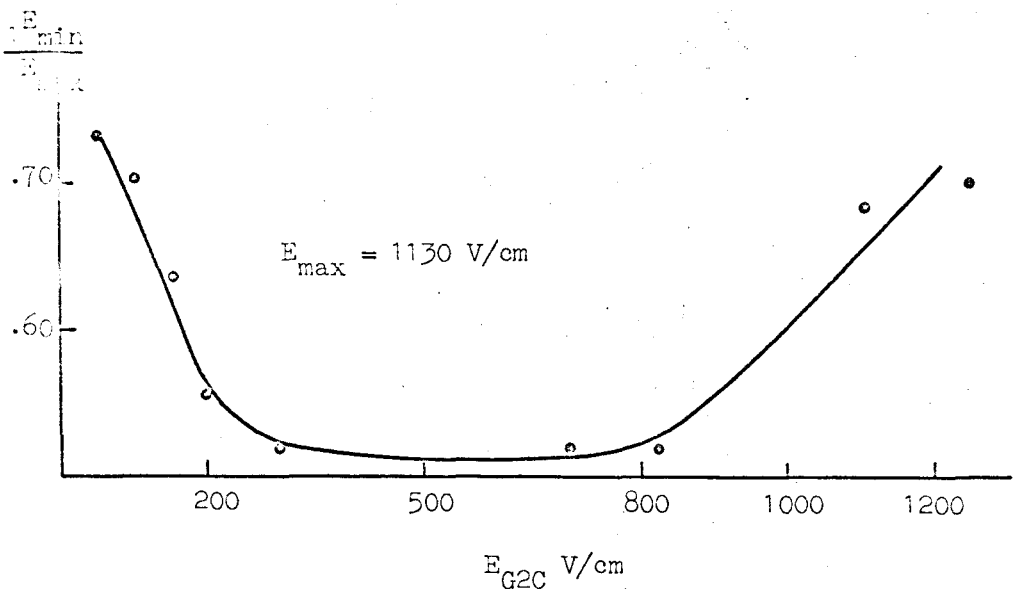

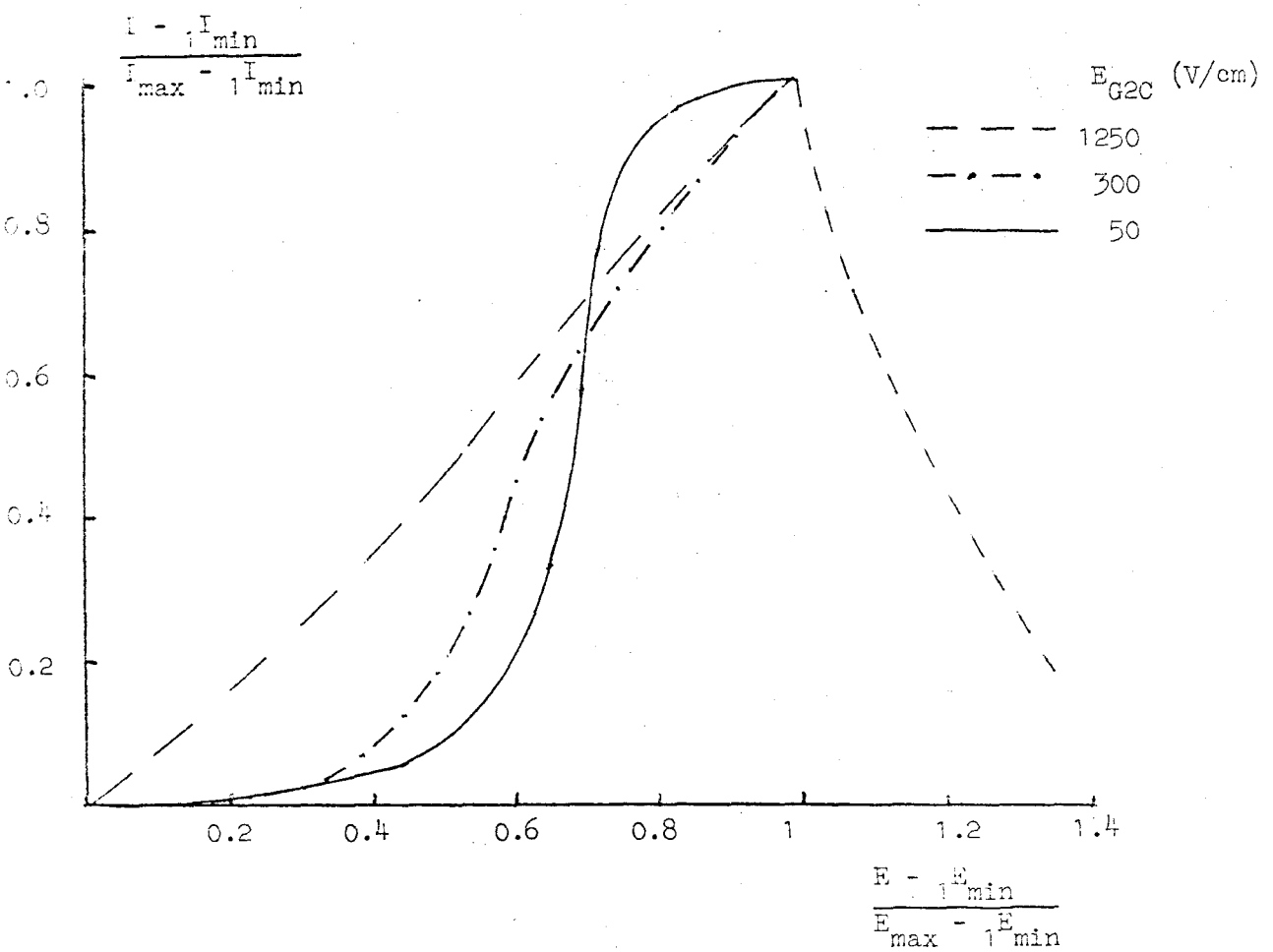

Fig 5.26 Plot of $\frac{I - {}_1I_{min}}{I_{max} - {}_1I_{min}}$ versus $\frac{E - {}_1E_{min}}{E_{max} - {}_1E_{min}}$ to show variation in peak shape in Fig 5.24

Our estimate of E_{vr} depends on the boundary conditions for the field being the same for velocity measurements and the D.C. case; any charge accumulation at one of the grids could alter the field sufficiently to give a non-uniform field through the rest of the grid space, giving an effective or average field for vortex ring formation which is reached for different potentials on the grids for A.C. and D.C. methods. Due to this uncertainty in E_{vr}, we cannot say that one definite part of the D.C. characteristic is due to the onset of production of vortex rings; the current minimum seen before the rise to the peak occurs at a field $_1E_{min}$ which is a complex function of the other fields in the cell - Fig 25 shows the variation of $_1E_{min}/E_{max}$ with extracting field E_{G_2C}. This is expected to be a complex region, as the low field bare ion current depends on the properties of the vortex rings; $_1E_{min}$ will then depend on which current is dominant for a given field distribution.

Fig 26 shows a normalised plot of peak current against field for various extracting fields; there is a steady decrease in curvature for increasing extracting field. The fall in current after the peak is exponential, to a current minimum at a field $_2E_{min}$. The rate of fall depends slightly on the extracting field E_{G_2C}; the value of $_2E_{min}$ is independent of E_{G_2C}, but has a small dependence, in a tetrode, on the source grid field E_{SG_1}. For fields

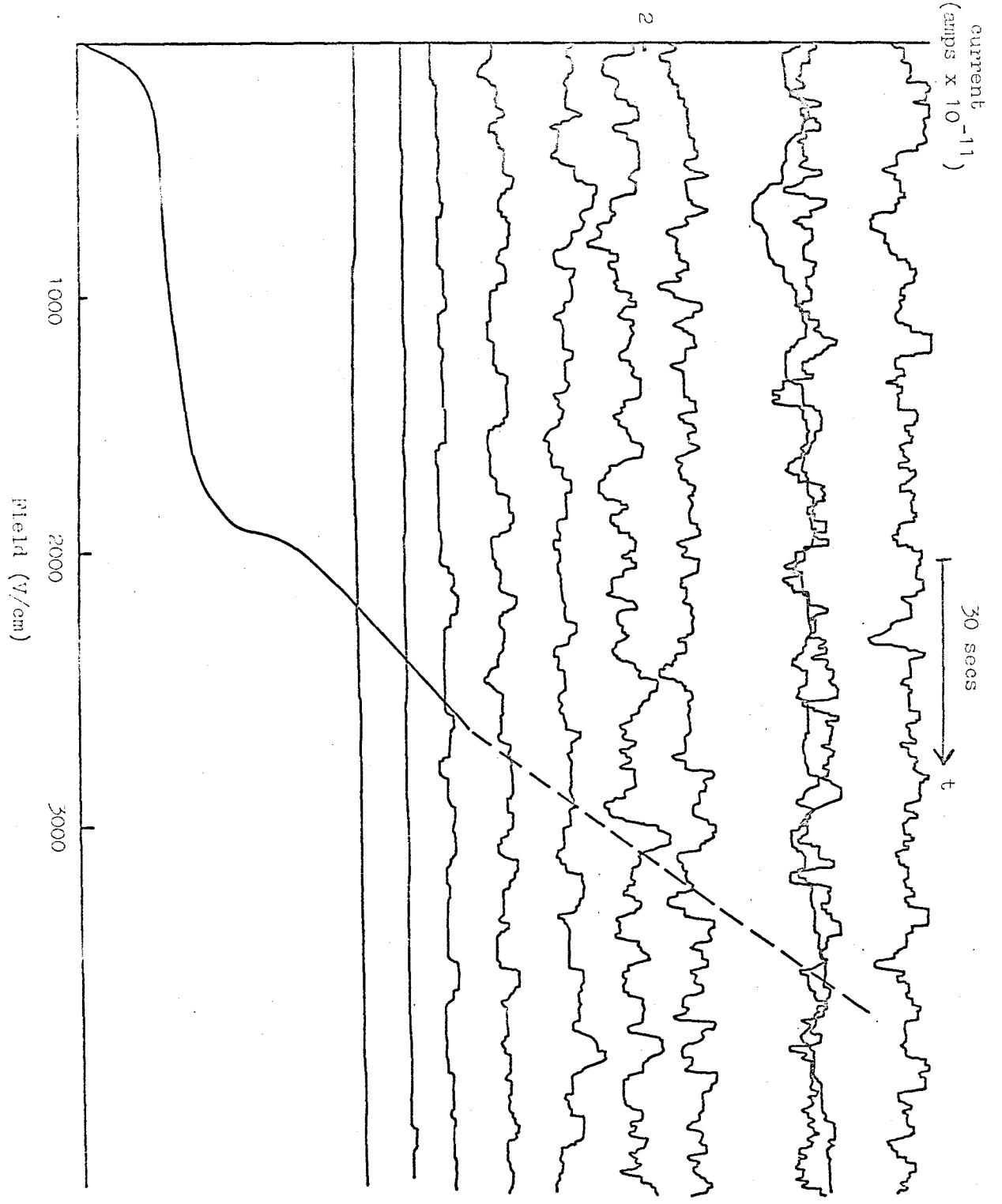

Fig 5.27 Showing current noise when electric field is greater than E_{max}

higher than $_2E_{min}$, the current rises linearly with an increasing amplitude of current 'noise', as shown in Fig 27. The linear rise in current is shown by the dotted line. The current noise is indicated by the 'noisy' lines of current against time; the field at which each 'noisy' current line was taken was the field where the current crosses the dotted line.

(ii) Positively charged vortex rings

The main differences between the behaviour of positively and negatively charge vortex rings may be seen from Figs 12 and 13. For fine grid meshes, such as 500 lpi mesh, there was a small positive current rise through a broad maximum followed by a constant decrease at high fields. The high field positive currents were noise free. This was in contrast to the behaviour of negative ions which showed a 'noisy' increase in current beyond the current minimum at the highest fields.

IV. COMPARISON OF HIGH FIELD RESULTS WITH SECOND SOUND ATTENUATION

An interesting correlation can be made between the field E_{max} at the current peak maximum, and the field E_α found by Bruschi et al (1966) for the onset of second sound attenuation by vortex rings. A brief summary of their results, is that when measuring vortex ring velocities by a triode technique they found a minimum in the drift velocity, at a certain field. Close to this field at a field E_α they found an extra attenuation of second sound proportional to the ion density, and a 'persistence' of drift velocity, seen by a current being collected through a region of zero field. Later velocity measurements by a pulse technique (Bruschi and Santini 1970) have shown that there is no minimum in the vortex ring drift velocity; the high energy vortex rings take a long time to reverse their direction of motion in a triode, of the order of the square wave frequency, which leads to the anomalous velocity effect first reported. The extra attenuation of second sound is due to the vortex line density, of the vortex rings bound to the ions; Hall and Vinen (1956) have shown in rotating helium experiments that there is an extra attenuation coefficient proportional to the density of vortex line. Using their value of the attenuation coefficient and line density, Bruschi et al with an ion density of $\sim 10^6$ ions/cc need rings with radius $\sim 10^6$ Å near the field E_α to give the required vortex line

density. The later velocity measurements by Bruschi, Mazzi and Santini (1970) have been taken to confirm that the vortex ring velocity (and therefore radius) agreed with this requirement (Santini, private communication, 1970). (However, using the theory in Appendix (3), $R_{v\ ring} \sim 4.10^3$ Å at E_α).

The amplitude and temperature dependence of E_α^- for negative ions agree well with our E_{max}; E_α^- is given by

$$E_\alpha^- = A.e^{\Delta/kT}$$

where
$$\frac{\Delta}{k} = 7.69 \pm .13^\circ K$$
$$A = 4.024.10^6 \text{ v/cm} .$$

Our values for E_{max} are

$$\frac{\Delta}{k} = 7.58 \pm .20^\circ K$$
$$A = (3.5 \pm .8) \times 10^6 \text{ v/cm}$$

which agree within the limits of accuracy. Most of our error comes from not knowing the absolute temperature to within $\sim 10^{-2}{}^\circ K$.

The pressure dependence of E_α^- is different from that of E_{max}^-. The variation in E_α^- with pressure can be expressed as

$$E_\alpha^-(P) = E_\alpha(0)\ (1+aP)$$

where $a = 0.12 \pm .01$ atmos^{-1}

A similar expression for E_{max}^- gives

$$a = .072 \pm .003$$

This implies the agreement between E_{max}^- and E_α^- at the vapour pressure is fortuitous. Bruschi et al found a similar attenuation for positive ions, but at higher fields at a fixed temperature.

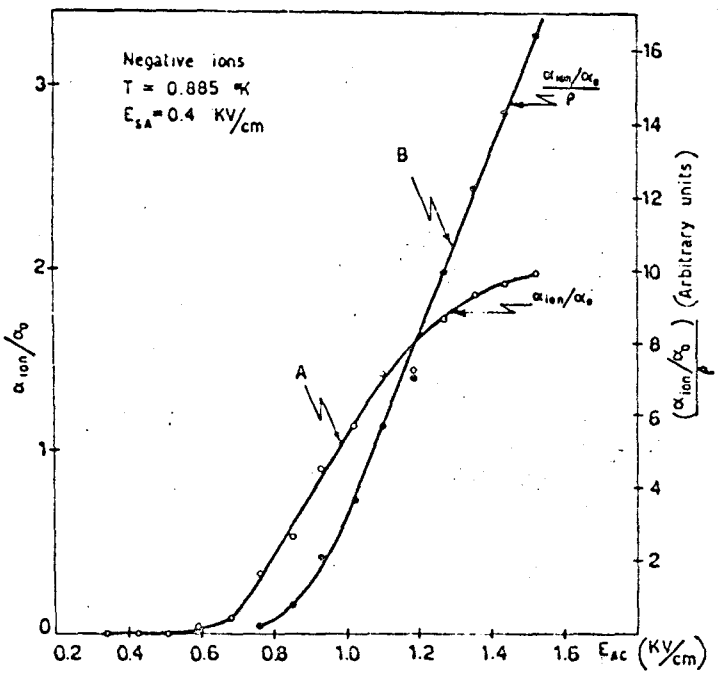

FIG. 5. This figure contains a direct comparison of the plot versus the electric field E of: (a) the extra attenuation coefficient α_{ion} relative to α_0; (b) the ratio of the relative extra attenuation coefficient α_{ion}/α_0 and the charge density ρ.

Fig 5.28 Plot from Bruschi et al (1966) of extra second sound attenuation per unit charge versus the electric field

Secondary effects, like the persistence of drift velocity, were less marked for positive ions.

The significance of the apparent equality of E_α^- and E_{max}^- is difficult to explain mainly due to the uncertainty in the meaning of E_α^-. E_α^- is defined as the onset of second sound attenuation; a plot of the ratio of the relative extra attenuation coefficient and the charge density $(\frac{\alpha_{ion}}{\alpha_o} \cdot \frac{1}{\rho})$ against electric field in Fig 5 of the paper by Bruschi et al (our Fig 28) show that at high fields ($>E_\alpha^-$) the coefficient is a linear function of field, which can be extrapolated to zero attenuation at a field we call $E_o > E_\alpha^-$. For fields less than E_o, the attenuation coefficient approaches the zero attenuation axis as an asymptotic curve. The intersection of this curve with the axis gives E_α^-. Now in theory we would expect an extra second sound attenuation whenever vortex rings were present; only at a certain field (and therefore size of ring, and hence density of vortex line) would the equipment be capable of resolving this extra attenuation. If indeed the extra attenuation coefficient is proportional to the total length of vortex line present, as assumed by Bruschi, then the function $\frac{\alpha_{ion}}{\alpha_o} \cdot \frac{1}{\rho}$ should be proportional to the vortex ring radius R. This is related to the vortex ring velocity v by

$$R = \frac{K}{4\pi v}(\eta - \tfrac{1}{4})$$

and the vortex ring velocity is related to the electric field E by (Appendix 3)

$$v = \frac{A.eE.e^{-eE/\alpha(T)}}{\alpha(T)}$$

where A is a constant and $\alpha(T)$ is the frictional force on a vortex ring. Thus we get

$$\frac{\alpha_{ion}}{\alpha_o} \cdot \frac{1}{\rho} \propto \frac{e^{eE/\alpha(T)}}{eE/\alpha(T)}$$

which increases exponentially for large E, compared with the linear dependence found by Bruschi et al. Thus the status of regarding E_α^- as a well defined field cannot be based on a theory requiring second sound attenuation to be proportional to the size of the vortex rings. Similarly, the linear dependence of the attenuation coefficient or electric field cannot depend on this theory; although for fields around E_α^- this may be true - we cannot tell from the accuracy of the published figure.

On Fig 28 we have defined another two fields: E_o, the intersection of the linear part of the curve with the axis; and E_1, for the onset of the linear part of the curve. Using their formula to find E_α^- ($=Ae^{-\Delta/kT}$, where A and Δ/k have been quoted earlier) we find

$$E_\alpha^- \simeq 670 \text{ v/cm}$$

$$E_o \simeq 890 \pm 10 \text{ v/cm}$$

$$E_1 \simeq 950 \pm 10 \text{ v/cm}$$

giving

$$\frac{E_o}{E_\alpha^-} = 1.33 \pm .02$$

$$\frac{E_1}{E_\alpha^-} = 1.42 \pm .02$$

We find from our D.C. characteristics that the field at the current minimum $_2E_{min}$ and the field for the onset on the linear increase in current E_ℓ (Fig 9) are related to E_{max} by

$$\frac{_2E_{min}}{E_{max}} = 1.33 \pm .05$$

and

$$\frac{E_\ell}{E_{max}} = 1.42 \pm .05$$

The large errors are because these two fields are not always well defined. We do not have a systematic dependence of $_2E_{min}$ or E_ℓ on grid size, temperature or extracting field, but a number of results from different conditions give the same ratios as above.

We could then make a correspondence between our D.C. characteristics and the extra second sound attenuation per unit charge density found by Bruschi et al. At a field $E_{max}(\equiv E_\alpha)$ the current falls exponentially, corresponding to the onset of second sound attenuation. The current goes through a minimum (at a field $_2E_{min} \equiv E_o$) and then shows a linear increase above a field E_ℓ $(\equiv E_1)$ corresponding to the linear increase in the attenuation coefficient. As shown by Hall and Vinen, the extra attenuation coefficient is linearly proportional to the vortex line density, so the linear increase of the attenuation coefficient with electric field found by Bruschi cannot be explained by the increasing size of vortex rings with electric field. This

is approximately exponential.

V. DISCUSSION OF HIGH FIELD RESULTS

a. Formation of vorticity

We suggest that at E_{max} the superfluid around the grid undergoes a transition to a turbulent state, consisting of an array of vortex lines formed by the vortex rings.

The formation of vorticity is suggested by hysteresis effects seen in the D.C. characteristics for negative ions. If the field is gradually increased from zero to a value well above E^{-}_{max}, we get the normal graph of current against field; when the field is now gradually decreased the current plot around the peak is not reproduced. Changing the field from a value greater than E^{-}_{max} to E^{-}_{max}, the current increases very slowly, taking a time of the order of a few minutes to reach a current value about 50% of the original value. When the field is increased from zero to E^{-}_{max}, the time taken to reach I_{max} is of the order of the response time of the electrometer i.e. $\sim$ 10 secs. When the field has exceeded E^{-}_{max}, it must be brought back to zero, and left for a time of the order of a minute before the current plot is reproducible otherwise the current peak is lowered. This behaviour strongly suggests that vorticity is being formed in the superfluid; the decay time is similar to that found for vorticity by Hall and Vinen in heat current measurements of second sound attenuation, while the build up time for vorticity is of the order of a few seconds (Wilks, 1967).

By considering the total energy of a collection of vortex rings, and the energy of a vortex line with the same total length of vorticity as the rings, we can get an approximate critical ring size where it is energetically favourable for the vorticity to exist as a line, or a number of vortex lines, rather than rings.

The energy of unit length of vortex line is (Atkins 1959)

$$E_\ell = \int_a^b \tfrac{1}{2}\rho_s v^2 . \, 2\pi r . dr$$

$$= \pi\rho_s \kappa^2 \ell n(\frac{b}{a})$$

where ρ_s is the superfluid density, κ the circulation, 'a' the vortex core size, and b the average separation between vortex lines. To the same approximation, the energy of a vortex ring of radius R is

$$E_r = 2\pi^2 R\rho_s \kappa^2 \ell n(\frac{R}{a}) .$$

For a total of N rings of radius R, the total length of vorticity L is $2\pi R.N$. The total energy of length L of vortex line is

$$E_L = 2\pi RN . \pi\rho_s \kappa^2 \ell n(\frac{b}{a})$$

and the total energy of the vortex ring system is

$$E_R = N . 2\pi^2 R\rho_s \kappa^2 \ell n(\frac{R}{a})$$

$$\frac{E_L}{E_R} = \frac{\ell n(\frac{b}{a})}{\ell n(\frac{R}{a})} .$$

We see when $b < R$ the vortex line system has a lower total energy than the ring system. This transition occurs (for a vortex ring (i.e. ion) density of 10^6 ions/cc) when there is an average

separation of $\sim 10^{-2}$ cms between the vortex rings. When the vortex ring radius is greater than this value, we satisfy the condition for the existence of a lower energy state of a mass of vortex line. This transition is the same as regarding the rings as interacting with each other, and therefore losing their individual identity. The radius of 10^{-2} cms is that quoted by Bruschi needed for a vortex ring in an electric field E_α to give the observed attenuation coefficient.

This transition radius obviously depends on the ion density, in contradistinction to our results for $\bar{E}_{max}$, and the results of Bruschi for E_α which showed these fields were independent of the ion density. The important point is that $\bar{E}_{max}$ is only defined when the ion beam is transmitted through a grid which has a mesh size greater than a certain value (the experiments by Bruschi all used grids, but of an unknown mesh size, so we cannot state the same for E_α). This strongly suggests that the grid is responsible for the existence of the field $\bar{E}_{max}$; while the properties of $\bar{E}_{max}$ depend on the phenomenon which has been created. We therefore suggest that the grid acts in such a way as to nucleate a transition to an orderly turbulent state of an array of vortex lines.

To explain the difference in behaviour between positive and negative ions, we suggest that for fields less than E_{max}, vortex rings are being captured on the grid wires. As the field increases to E_{max}, the amount of vorticity captured by the grid from vortex

rings increases until it forms an array of vortex lines close to the grid. This transition will occur when it is energetically favourable for the small pieces of vorticity to coagulate to a line; if the length of line is of the order of the grid mesh size, there is then a criterion for a critical mesh size for the existence of the current peaks. The attachment of vortices to fine wires was shown to be possible by Vinen (1960) who measured the circulation of a vortex attached to a wire. Measurements of a circulation equal to a fraction of a quantum $\frac{h}{m}$ were attributed to a partial attachment of a line, and these were less stable than values of a single quantum $\frac{h}{m}$ (full attachment) as would be expected. He also showed that when a line was fully attached to a wire, it was stable to large amplitude vibrations; this implies a reasonably large binding energy, making it likely a vortex ring could be captured by a grid wire.

If ions were trapped by such vorticity, they would eventually be collected by the grid wires, in a time depending on the ion mobility, the length of vortex line and the effective field felt by the ion. This means at any one time there will be an excess number of trapped ions present to provide a repelling field for the other (free) ions. As the amount of vorticity captured by the grid increases, so does the number of ions and hence the repelling field. This would give the sharp rise in the negative ion current for fields less than E^{-}_{max} due to the reduction of the current drawn by the grid. As positive ions have a much higher escape probability

from vorticity, they will be trapped for a much shorter time and thus produce a smaller repelling field. This will give a smaller reduction in the grid current, and a smaller current rise.

b. Influence of the extracting field

The difference in the D.C. characteristics between varying the incident and extracting fields is because the incident field determines the amount of vorticity incident on the grid, and therefore the amount of vorticity captured by the grid. The extracting field will not change the amount of vorticity captured by the grid, but will affect the amount of charge that can be captured by the vorticity. The change in the shape of the negative ion peak with extracting field (Fig 26) is due to the increase of the low field current with extracting field, and a nearly constant current I^-_{max} at E^-_{max}, independent of the extracting field Fig 10. This implies the number of ions released by the grid at E^-_{max} depends mainly on the escape probability of the ions trapped in the grid vorticity. At E^-_{max} the main influence of the extracting field is to alter the escape probability slighty. Positive ions do not show the same 'current saturation' at E^+_{max} (which is not well defined), but I^+_{max} increases with extracting field in the same way as the current at a lower field for bare ions. The behaviour of I_{max} can be considered from the view put forward in section 3(a), where the current depends on the rate of production of ions at the grid. For low fields we expect this to be field

dependent because of the field dependence of the transmission coefficient, as discussed in section 3(b). This is also true for high fields i.e. vortex rings incident on the grid, except at E^-_{max} (Fig 10). At E^-_{max} , the rate of production of ions is independent of the extracting field, except at very low fields ($\sim$10 V/cm). This field independence is seen in Fig 13 where the transmission coefficient of a grid at E^-_{max} is independent of the extracting field; this follows naturally from the independence of I_{max} on the extracting field.

The field dependence of the transmission coefficient arises because of the field distortion around the grid, as discussed in section 2. If this coefficient is independent of the extracting field at E^-_{max} ,it implies no field penetration and thus the grid can be regarded as a planar conducting electrode instead of a discrete array of conducting wires. This means that mobile charge must be trapped in the grid mesh so that it can rearrange itself to cancel out the extracting field penetration. This will happen if, at E^-_{max}, there is vorticity in a continuous distribution between the grid wires to trap the negative ions. The potential distribution through the apparatus will be given as in section 2, Fig 5, but with $V_{eff} = V_g$

The main effect of changing the extracting field at E_{max} will be to vary the ion escape probability. There have been no experimental results published on the field dependence of the escape

probability P but if we assume P is related to the capture cross section σ by

$$\sigma = \sigma_o e^{-Pt}$$

where t is a characteristic time, we get

$$P \propto - \ell n\, \sigma .$$

Results by Tanner (1966) indicate the field dependence of σ is given by

$$\sigma \propto \frac{1}{E}$$

and therefore $P \propto \ell n\, E$. This could explain the small increase of I_{max} with large extracting fields. The influence of the incident field on the escape probability will be discussed later.

c. High Field ($>E_{max}$) behaviour

When the field is increased above E_{max}, the vorticity breaks away from the grid, forming a 'quasi' turbulent region of vortex lines. This turbulence has been 'injected' by the grid into the fluid, and is not due to a transition to turbulence by the whole fluid (i.e. a free turbulence); heat flow measurements suggest a much higher energy is needed for this transition than is supplied by the ions. The fall in current could be because the vorticity around the grid is reduced, thus reducing the trapped ion repelling field, and increasing the grid current. The linear increase in current for very high fields arises because the grid current does not increase as fast as the total current. For $E > E_{max}$, the grid current is an increasing function of the electric field, implying there is no fundamental significance

of the field $_2E_{min}$.

The 'quasi' turbulent region will have an equilibrium length of vortex line; the existing vorticity will decay with time due to quasiparticle collisions, and vorticity from the grid will be supplied continually to the region. If we assume that the turbulent region consists of a homogenous and isotropic array of vortex lines, then the equilibrium length of line will be that given by Vinen (1957) (Chapter 1) for mutual friction in a heat current. As the only mechanism for producing vorticity is from the vortex rings formed by the ions, this puts an upper limit to the amount of line formed per unit time. The classical expressions for vortex ring motion in Appendix 3, show that the length of line formed by ions does not give a high enough vortex line density to produce the experimental values of the extra second sound attenuation coefficient for fields near E_α; we therefore assume this vorticity has a slower decay time than the rate at which it is being produced by the ions, allowing an equilibrium density to be built up. Also,if this vorticity was concentrated in a small volume near the grid instead of being distributed throughout the cell between the electrodes, this would give a higher line density. As the electric field is increased, the volume occupied by the turbulence spreads throughout the cell. It is confined to the region occupied by the ions, because the vortex lines will be preferentially pinned to the grid wires, preventing it escaping

and also only in this region is extra vorticity being added. For electric fields greater than $_2E_{min}$, the distance travelled by a vortex ring while decaying in a zero field region is of the order of the spacing between the electrodes (i.e. $\sim$1 cm). The behaviour of the current with field will then depend on the vortex ring - vortex line interaction. Schwarz (1968) has shown that charged vortex rings propagating in rotating helium (i.e. across an array of vortex lines) can lose their charge to the lines, the interaction being described by an effective capture width. Thus in our case we expect most of the current to reach the collector by being trapped on vorticity.

d. Behaviour of I_{max}

The dependence of I_{max} on E_{max}, temperature, and pressure, in Figs 21 and 23 is similar to the temperature dependence of the negative ion-vortex line capture cross section σ (Springett 1967). Because the current behaviour up to I_{max} is due to the grid current being reduced by a repelling field set up by ions trapped in vorticity on the grid, the behaviour of I_{max} with temperature and field will depend on the capture cross section of the grid vorticity and the incident charged vortex rings (σ_g). For a large cross section the repelling field will be high, and there will be a large I_{max}. As σ_g decreases, so will the repelling field, and thus the grid current will increase, lowering I_{max}.

The exponential decrease of I_{max} with field (Fig 23) is

due to a decrease in σ_g. This could arise either from a decrease in the ring capture cross section, or an increase in the ion escape probability; by analogy with Springett's results we choose to discuss the latter.

If the behaviour of σ_g depends on the ion escape probability, then the only difference between the results of Springett and ours is the electric field felt by the vortex lines. From the theory of the escape probability by Donnelly(1964),if the ion has a potential energy u(r) due to it replacing the rotating superfluid near a vortex core, the escape probability P is given by

$$P \propto e^{\frac{-u(r)}{kT}}$$

Applying an electric field E along the x axis will reduce the potential barrier by

$$u(E) = eEx$$

giving an escape probability

$$P \propto e^{-\frac{(u(r) - eEx)}{kT}}$$

The potential energy u(r) is proportional to the superfluid density ρ_s, and this describes the temperature dependence. Springett represents his results for the steep fall in σ at high temperatures by

$$\sigma = \sigma_o e^{-Pt}$$

where P is the escape probability, depending on the temperature and pressure through ρ_s and the electric field E through $u_T = u(r) - eEx$ as above. Taking from his results a point

where $\sigma = \frac{1}{2}\sigma_o$ we get $u_T \doteq 43^\circ K$, for effectively zero applied field (20 V/cm). From our results, I_{max} falls to half its value at a field of 1500 V/cm and a temperature $\sim 1^\circ K$. Using the value of $u(r) = 43^\circ K$ at $1.7^\circ K$ we get $u(r) = .53^\circ K$ at $1^\circ K$ at the saturated vapour pressure. If we take $x = 50$ Å for the minimum in the potential barrier (Donnelly 1967) we get $u(E) \doteq 10^\circ K$. Thus $u_T \doteq 43^\circ K$, and we get a good agreement with Springett for the value of the escape probability, at zero pressure. $u(r)$ is a strong function of pressure through the pressure dependence of the negative ion radius as well as the superfluid density, which gives the strong pressure dependence in σ seen by Springett. Our results do not show the same pressure dependence, so the agreement at vapour pressure could be fortuitous.

Douglass (1968) has reported an anomalous decrease in the ion-vortex line capture cross section below $1.1^\circ K$, which he found to be due to an increase in the escape probability with falling temperature; the theory by Donnelly, found to hold for temperatures above $1.2^\circ K$, predicts a decrease in escape probability with falling temperature. Douglass has not published any details on his findings, but we will give a brief discussion of the effect on our results. If at low temperatures ($\sim 0.9^\circ K$) the escape probability is high, then we cannot use the idea of a space charge round the grid wires setting up a repelling field. Instead, we must say that

the current peak is due to an enhanced escape of ions from the grid region, which would otherwise have been captured. We would then expect the same phenomenon for positive ions, which always have a much higher escape probability than negative ions. As this is not seen, we say that our results are not easily explained by an increase in escape probability at low temperatures. However, if we take our results in Fig 23 to show that I_{max} is a function of the electric field rather than the temperature, as long as the mean lifetime of an ion trapped to a vortex line is greater than a certain critical value, our explanation does not depend on a temperature variation of the mean lifetime (and therefore escape probability). Douglass's results show a mean lifetime varying from $\sim$10 secs at 0.9°K to $\sim$1 min at 1.1°K. We expect that the time for which a negative ion is trapped by vorticity near the grid to be much smaller than this; and if this time is nearly constant with temperature then the variation in escape probability will only depend on the field. Similarly, we could explain the lack of the pressure dependence if we say the increased escape probability under pressure is negligible compared with the actual lifetime of the ion on the grid vorticity before it is captured by the grid. The dependence on the electric field is because this gives a preferred direction for the ions to escape; thermal or pressure dependent escape of the ions will be symmetric about the vortex line, with a high probability of recapture by another vortex line.

e. Criticism and Conclusion

While the existence of the current peak for negative vortex rings is a grid dependent phenomenon (because of the difference in behaviour with different mesh sizes and also electric fields) the well defined and grid independent behaviour of the current around E_{max} shows the physical processes giving the current maximum are due to the properties of vortex rings, vortex lines and charged ions. Without knowing the exact potential distribution around the grid wires, we can only suggest a likely hypothesis, based on the growth of vorticity (seen by second sound attentuation experiments,) and the behaviour of the ion-vortex line capture cross section and escape probability predicted by Donnelly.

This hypothesis depends on vorticity being captured by the grid, and this vorticity capturing ions to form a repelling field and lowering the grid current. The fall in I_{max} with increasing field is due to the field dependence of the ion escape probability from a vortex line. The fall in current with increasing field above E_{max} is due to vorticity breaking away from the grid and spreading out between the electrodes.

We have not been able to find a criterion either for a critical grid mesh size for the existence of the current peak, or for a critical field (E_{max}) for the current maximum, where we suggest the vorticity begins to propagate through the apparatus.

The basic mechanism which we suggest for the increase in current at the peak is the setting up of a repelling field around the grid wires by trapped charge, and thus changing the transmission coefficient. In principle this must be correct, as we can see the reduction in the grid current (Fig 11). However it could be argued that the transmission coefficient should show a change for vortex rings compared with bare ions; in section (2) b we suggested that bare ions could follow the field lines close to the grid, and the transmission coefficient depended on how many lines ended on a grid wire. Vortex rings would not necessarily follow the field lines in a region where they were varying rapidly with position, due to the time taken for a vortex ring to reach its equilibrium velocity in a given electric field, but would be 'scattered' by the field lines. For high energy vortex rings we would expect a small scattering, and thus the effective transmission coefficient should be nearly equal to the geometrical coefficient; to counteract this, the high potentials needed to create the vortex rings would increase the field distortion around the grid. In principle it should be possible to calculate the effect of a given field distribution on the scattering of vortex rings, knowing the vortex ring dispersion relationship ($E \propto p^{\frac{1}{2}}$); but it would be complicated by the fact that the region of field distortion is of the same magnitude as the distance travelled by the ion while changing its velocity. Rayfield and Reif (1964) have considered the case of small angle deflection of

vortex rings at low temperatures by an electric field perpendicular to the direction of motion; the deflection angle observed for rings was four times that expected for a classical particle (obeying $E \propto p^2$). This small angle result cannot be used in our case, which is for large angle scattering.

In summary, the difference between positive and negative ions suggests that as the positive vortex ring transmission coefficient shows only a small change from the bare ion case, there must be another mechanism to give the enhanced negative ion current, through an increase in the negative ion vortex ring transmission coefficient; and the most likely mechanism is the repelling field around the grid wires which we have suggested.

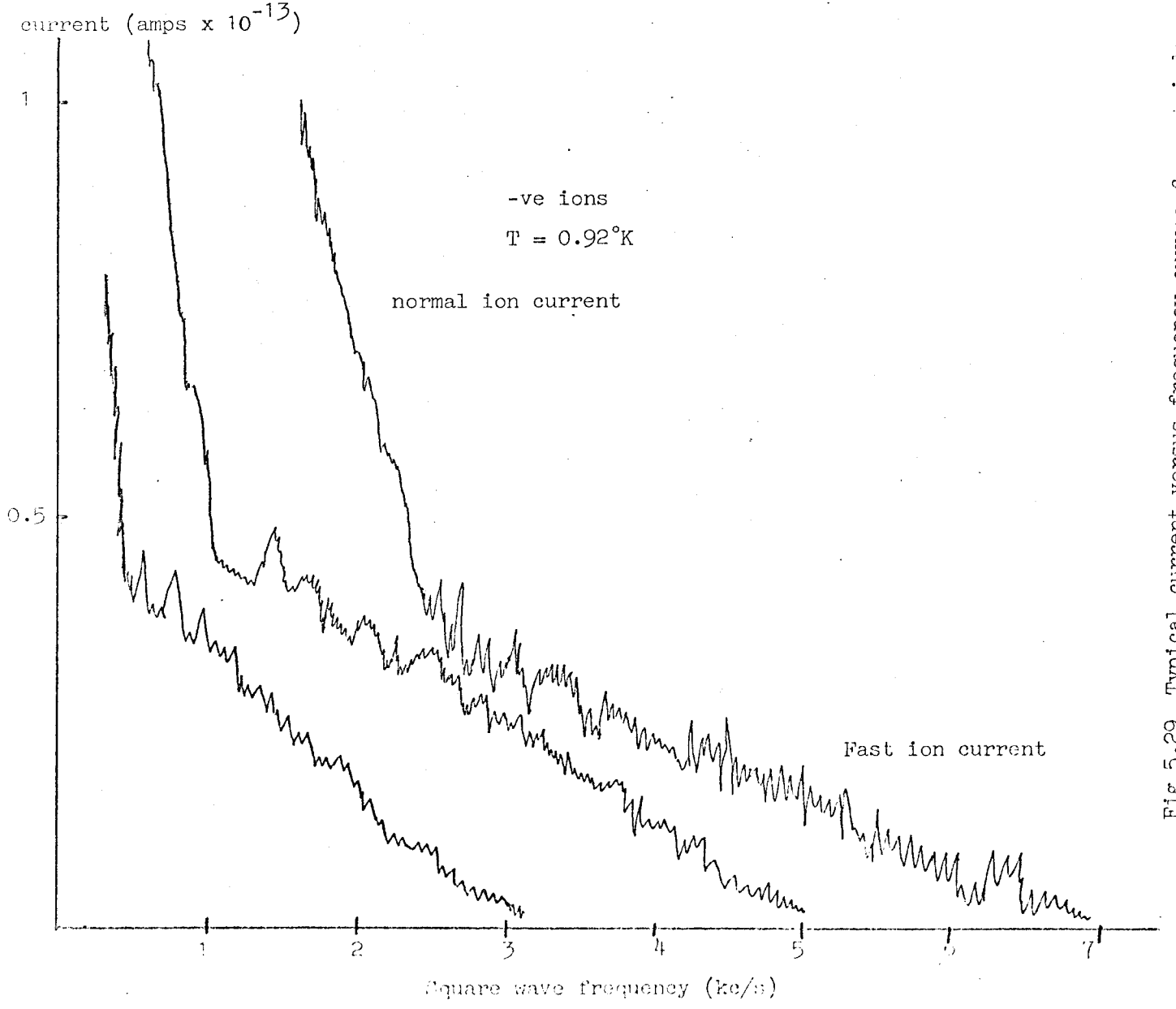

Fig 5.29 Typical current versus frequency curves for a triode, showing the 'fast ion' component

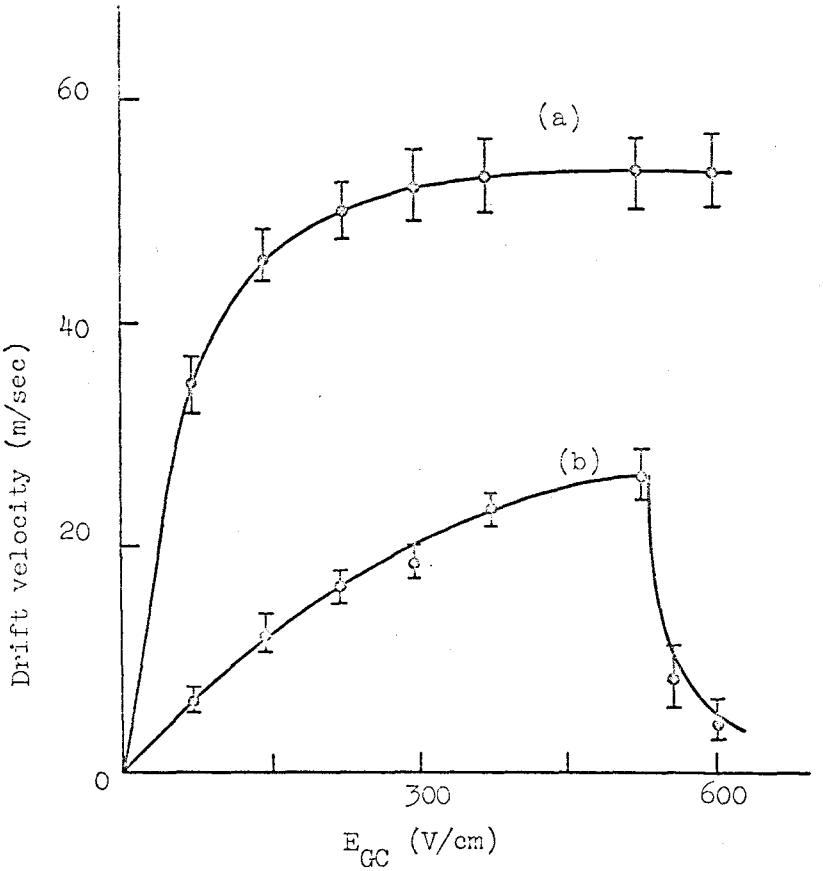

Fig 5.30 Ion drift velocity in m/sec versus electric field E_{GC} in V/cm. Curves for T = 0.92°K. Curve (a), fast ion current; (b) normal ions, forming vortex rings

VI. 'FAST ION' PHENOMENA

a. Introduction

For field conditions in a triode or tetrode that gave a negative ion vortex ring peak, we measured the velocity of the ions in the grid-collector space, using the square wave method. (This is equivalent to the velocity measurements in Chapter 4, but with high source-grid (incident) fields).

Fig 29 shows the current-frequency curves obtained for various square wave amplitudes, with the incident field equal to E_{max}. The high frequency 'tail' on each curve is attributed to a higher mobility charge carrier than the normal negative ion. For each curve we can define two velocities, one for a frequency where the two lines meet (which is the normal ion velocity) and the other at a frequency where the current reaches zero (the fast ion velocity).

These two velocities are shown in Fig 30 as a function of the electric field. The normal ion velocity shows the expected field behaviour i.e. forming vortex rings and showing a decreasing velocity above a critical field. The fast ion velocity saturates at high fields, at a velocity of $\sim$54m/sec.

The same phenomenon was seen by D.T. Meldrum, carrying out work for an honours project, using our apparatus. These results were obtained over a period of about 2 months, with a Po^{210} source providing the ions and have been previously reported (Doake and Gribbon (1969)). After this time the source had become too weak to

give a reasonable current, and an Am^{241} source did not give the fast ion current, with the same cell dimensions. We have a total of three runs which show a well defined fast ion current, and a number of other runs which show a high frequency tail, but without the same well defined behaviour. These last results are for both sources, and a number of different electrode configurations. When we were unable to obtain a fast ion current, we tried the effect of infra red radiation ($\sim$ 2μ wavelength) and a heat current ($\sim$ m watts) without repeating the previous results. A small magnetic field ($\sim$200 gauss) also had no effect.

Effects due to the source have been described by Rayfield (1968) and Surko and Reif (1968). Rayfield found a Po^{210} source produced vortex rings, and Surko and Reif found a neutral excitation also from Po^{210}; both of these effects were found at low temperatures ($\sim$ 0.7°K) and were negligible at 1°K. Thus the significance of our results is hard to evaluate, but by analogy with mobility discontinuities (which show a fluctuating existence) and the fact that these three runs show a well defined behaviour, we will give a discussion of possible explanations.

b. Fast ions models

1. Ion trapping in grid vorticity

We explained the current peak seen under D.C. conditions by the trapping of ions in turbulence around the grid. When measuring velocities, this turbulence could act as an effective ion source

closer to the collector than the grid, giving an enhanced velocity. We would still expect these ions to form vortex rings at a critical field around that where the normal ions form rings, and show a fall in velocity at high fields. This is not seen.

2. High energy vortex rings

The fast ion current could be due to vortex rings penetrating the grid, and having enough energy to reach the collector before decaying. From the calculations in Appendix 3 we expect a vortex ring formed in a field around E_{max} to travel a distance a fraction of a millimetre in zero field; for fields higher than E_{max} this distance increases exponentially. Thus the magnitude of the fast current should increase as the incident field on the grid is increased. Our results show two conflicting types of behaviour; (1) the fast ion current is a constant fraction ($\sim$5%) of the D.C. current (i.e. shows a peak at E_{max}) and (2) the fast ion current rises slowly as E is increased beyond E_{max}. In the first case the magnitude of the fast current is $\sim$10% of the total zero frequency current. We would expect a much higher proportion at high fields. In the second case the proportion of fast ion current saturated at about 65% at high fields.

The behaviour of high energy vortex rings in an oscillating square wave field is difficult to analyse rigorously. However as this seems a likely explanation of the phenomenon we will make an approximate calculation for the decay of a vortex ring in a square wave field.

We assume first that the vortex ring has enough energy to reach the collector in zero field; this implies that a fast ion current will be seen only at the lowest temperatures we could obtain, in approximate agreement with results. We use the equations of motion for a vortex ring, defined in Appendix (3) but now modified to allow for a finite field in the space where they decay. This means that the term $\alpha(T)$ describing the frictional force on the vortex ring is replaced by an effective force F given by

$$F = \alpha(T) \pm \frac{eE}{\eta(R)}$$

where the two signs allow for the effect of the forward and reverse square wave field, of magnitude E. If the initial vortex ring velocity is v_1 then its velocity v_2 after the forward square wave period (time t) is

$$\frac{1}{v_2^2} = \frac{1}{v_1^2} - \frac{Ft}{A}$$

(where $A = \frac{\kappa^3 \rho (n-\frac{1}{4})}{8\pi}$ = const. see Appendix 3)

and $$F = \alpha(T) - \frac{eE}{\eta(R)}$$

The velocity v_3 after the subsequent reverse square wave period will be

$$\frac{1}{v_3^2} = \frac{1}{v_2^2} - \frac{F^1 t}{A}$$

where $F^1 = \alpha(T) + \frac{eE}{\eta(R)}$

Therefore the change in vortex ring velocity after 1 complete square wave cycle is given by

$$\frac{1}{v_3^2} = \frac{1}{v_1^2} - \frac{t}{A}(F + F^1)$$

$$= \frac{1}{v_1^2} - \frac{2t.\alpha(T)}{A}$$

which is just the change in vortex ring velocity when decaying in a zero field region in the same time of 2t. Thus the square wave frequency will have no effect on the current.

If on the other hand the ring does not reach the collector while decaying in zero field, then it will have an average velocity during the forward half of the square wave, made up of the average velocity of the decaying ring, and the velocity of the bare ion in the square wave field. If the vortex ring decay time is much shorter than the square wave period (low frequencies) then the current- frequency graph will be similar to that for normal ions, but with an average velocity for the ions; from Appendix (3) the average velocity for the decay of a ring is twice the rings initial velocity, which is usually small ($\sim$30cm/sec) for source grid fields around E_{max}. Therefore the current-frequency graphs would be cut off at a frequency corresponding to the normal ion velocity. For incident fields around E_{max} the decay time of a vortex ring is $\sim 10^{-6}$ secs; therefore we expect a negligible distortion on the current frequency graphs (which show a cut off $\sim$7 kc/s.

3. Ion trapping in decaying turbulence

We explained the D.C. characteristics by vorticity being built up at the grid, which then breaks away and fills the measuring

space. This 'quasi' turbulence interacts with the charged vortex rings which penetrate the grid, by capturing the ion (Section 5(d)). The motion of the ions will now be determined by the form of the turbulence.

The general form for the decay of turbulence is a flow of energy from large eddies to smaller ones, and hence dissipated as heat through viscosity (Batchelor, 1953). We therefore expect our 'quasi' turbulence to decay in the same way as vortex rings i.e. a decrease in size with an increase in velocity. The smallest ring will have a radius $\sim$ 5Å, and a velocity $\sim$54 m/sec (using the classical equations of motion). If an ion can be trapped by this form of turbulence and form a stable entity in an electric field less than that needed for an ion to create a vortex ring, this would give a limiting ion velocity of $\sim$54 m/sec. The structure of this kind of charge carrier would presumably be different from a normal charged vortex ring, which has a ring radius much greater than the negative ion radius.

Rayfield (1968) has shown that negative ions under pressure can create and bind to vortex rings at velocities up to $\sim$54 m/sec; increasing pressure lowers the negative ion radius, and the critical velocity for vortex ring creation is inversely proportional to the ion radius. The values for the negative ion radius under pressure found in this way agree with those found by Springett (1967) by negative ion trapping on vortex lines. The ion radius when the

critical velocity is 54 m/sec is ∿11Å. At higher pressures (lower ion radius) the ion velocity is limited by roton creation instead of producing vortex rings. Rayfield also showed that vortex rings produced by the source were stable entities in electric fields much less than that needed to create vortex rings by the bare ion.

We can have three models for the negative ion fast current; (1) a bare ion with a radius less than ∿11Å, (2) an ion trapped to a very small vortex ring, or (3) an extension of (2) but with the vorticity in a different flow pattern round the ion, compared with a normal vortex ring.

The first model would give the observed velocity-field dependence i.e. the velocity would be limited by roton creation at high fields, without forming vortex rings. It is difficult to explain why the ion radius should be so small at the vapour pressure where we see the fast ion current. Theoretical estimates for excited electron states in the bubble increase the ion radius (Fowler and Dexter 1968).

If the ion was bound to a small vortex ring as in model (2), we still need an ion radius ∿11Å (Rayfield 1968) to explain the trapping. The relative sizes of the required vortex ring (∿5Å) and the ion (∿ 11Å) suggest that the ion is not bound to the vortex core, as for larger vortex rings. It seems likely that the vorticity has a different distribution around the ion, perhaps forming a 'skin' over the bubble surface (model 3). This skin would alter the

boundary condition on the bubble surface, which could change the equilibrium bubble radius. This can arise from changing either the well depth of the electron, increasing the surface tension, or considering the total ion energy to contain an extra term describing the energy of the vorticity around the ion; or a combination of all three.

We can explain the observed velocity field dependence for model (2) by saying that the small ring $\sim$5Å radius is the smallest ring that can exist before it finally loses its energy by degrading to quasiparticles. This final decay could be inhibited by the presence of the ion, giving the charged entity a lifetime comparable with the square wave frequencies we used (i.e. $\sim 10^{-3}$ secs). At low fields the entity will dissociate during its flight across the measuring space, giving an effective average velocity of less than 54 m/sec, composed of fast ion moving at 54 m/sec and then a normal ion with a much lower velocity. In high fields the entity will reach the collector before breaking up, giving a velocity $\sim$54 m/sec.

The velocity-field dependence for model (3) could be because the vorticity around the ion is unable to grow to form a normal vortex ring, and the ion velocity is limited by roton creation at high fields.

We suggest in section (c) following that a fast ion is formed only by excited bubble states, interacting with vorticity to give a changed entity corresponding to model (3).

c. Photoejection evidence for fast ions

We suggest that the photoejection experiments by Northby and Sanders (1967) and Zipfel and Sanders (1968) may provide evidence for a fast ion state.

Using a triode mobility cell operating at just above the cut-off frequency, they measured a current when 'fast carriers' were produced by the incident light. The spectra were obtained at different wavelengths by normalizing the measured current to the incident light intensity. Their interpretation of the experiment was simply the photoionization of an electron (from a bound state to the continium) which gave the high mobility current. This leads to a well depth of 0.55 eV at zero pressure, increasing rapidly to $\sim$1.05 eV at 15 atmospheres.

This value of the well depth disagrees in magnitude and pressure dependence with theoretical estimates of 1.0 to 1.2 eV (Jortner, Keştner, Rice and Cohen (1965), Burdick (1965), Miyakawa and Dexter (1970)), and experimental values of the barrier to electron injection into liquid helium of $\sim$1.1eV (Sommer (1964) and Woolf and Rayfield (1965)). Miyakawa and Dexter have reanalysed the experiments, and concluded that the large peak in the photo excitation spectrum is not a transition to the continuum as assumed by Sanders et al, but a transition from a 1s to a 2p state, based on a well depth of 0.95 eV at zero pressure.

The difficulty is to explain how the excitation (and not ionization) of a bubble can influence the ion mobility, to give a current reading in the experiment. In the operation of the experimental cell, the source grid field was above the critical field for producing vortex rings, i.e. similar to the condition when we measured a fast ion current. Miyakawa and Dexter suggest that the current flow in the measuring space in the triode cell is limited by trapping on vortex lines, and that when an ion is excited it gives up $\sim$0.2 eV in heat while relaxing to its new equilibrium radius (Fowler and Dexter 1968) which thermally dissociates the ion from the vortex line.

We can criticise this explanation on the grounds that our results do not show that the bare negative ion mobility is affected by vortex line trapping (for source grid fields around E_{max}) as required. Also an excited bubble state has a much larger equilibrium radius ($\sim$28Å, Fowler and Dexter) than an unexcited bubble, and should therefore be more strongly bound to a vortex line. Instead we suggest that the measuring space is a region of decaying vorticity (section b(3)) which can interact with an excited ion to form a fast ion entity, already described.

d. Conclusion

The fact that photoejection spectra can only be obtained when there is a region of decaying vorticity (probably in the form of vortex rings) implies that the excited bubble state only has

a long lifetime ($>10^{-3}$ secs) when it can interact with vorticity. The entity formed by the interaction must have a high mobility to explain the operation of the triode cell in the photoejection experiments.

The difficulty in identifying the fast carrier in the photoejection experiments with our fast ions is that the only similarity in the experimental conditions is the field conditions under which they are seen. The photoejection experiments were carried out at 1.3°K, and ours at $\sim$0.95°K; and we had no obvious means of obtaining excited bubble states.

If we explain a fast ion current in both cases by an interaction with vorticity (as in b(3)) then we must assume that an unexcited bubble cannot form a fast ion, or at least has a much smaller probability than an excited bubble, otherwise the triode cell in the photoejection experiment would not have shown the observed behaviour (when a current was measured at a frequency above the cut-off for a normal ion current).

One possible mechanism for obtaining excited bubble states in our apparatus is by a vortex ring decaying to give its energy to the ion. This is analogous to the results of Cunsolo and Maraviglia (1968) who have shown that a negatively charged vortex ring decays at a liquid-vapour surface transferring all its energy to the electron which is ejected into the vapour. (This was not seen by Surko and Reif (1968) however). A vortex ring

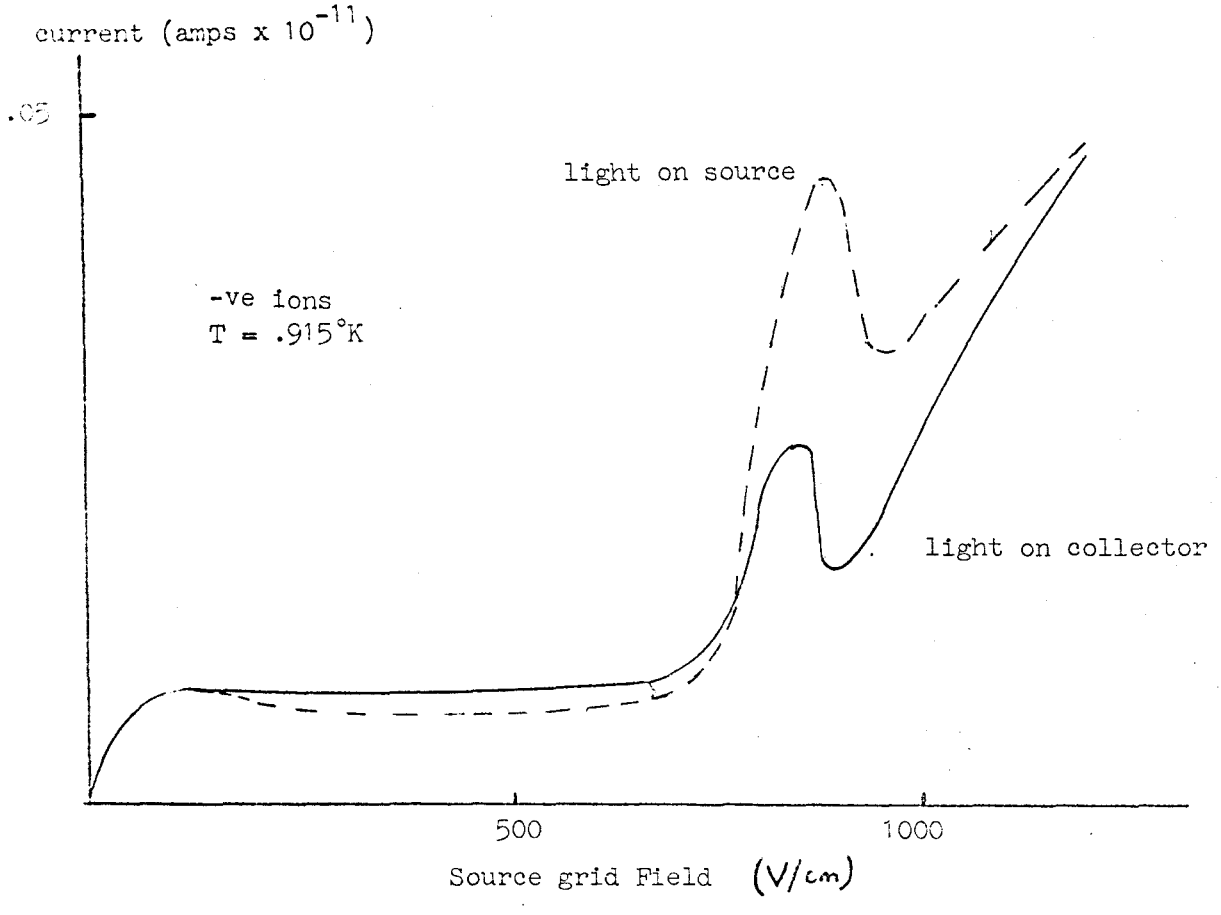

Fig 5.31 D.C. characteristic showing the effect of shining a light into the ion cell

with a velocity less than $\sim$2m/sec has an energy greater than $\sim$0.5 eV, which is the energy needed to form an excited bubble state. This process is unlikely, as the ring is expected to decay by interacting with the normal fluid.

Another mechanism in our apparatus would be simply that stray radiation of the correct wavelength was creeping into the experimental cell. We tried to test this hypothesis by shining a tungsten light (maximum intensity at a wavelength $\sim 2\mu$) into the experimental cell. This rather crude light source produced a lot of heating (raising the helium bath temperature) and the currents were too noisy to detect a fast ion component in the velocity measurements. However there was a noticeable difference between the D.C. characteristics for shining the light on the source grid space and the grid-collector space, for electric fields around E_{max}. Fig 31 shows a large reduction in the current for fields $\sim E_{max}$ when the light is incident on the grid collector space. This is consistent with our previous explanation for the D.C. characteristic (section V) if excited bubble states are formed which interact with vorticity producing high mobility charge carriers, which will lower the retarding field around the grid mesh allowing more current to be collected by the grid.

In summary, it appears that there is evidence for an interaction between an excited bubble state and vorticity, such that a high

mobility charge carrier is formed with a lower limit on the lifetime being $\sim 10^{-3}$ secs. Our experimental results show a limiting drift velocity of $\sim$54 m/sec, implying a small bubble of radius less than 11Å (in contradistinction to a 'bare' excited ion radius $\sim$28Å (Fowler and Dexter)).

VII. NEGATIVE CONDUCTANCE

a. Introduction

The velocity field characteristics for charge carriers in superfluid helium show a negative differential mobility $(\frac{\partial v}{\partial E})$ when vortex rings are formed. An analogous negative differential mobility in semiconductors is responsible for negative differential conductivity effects, including the Gunn effect (high frequency current oscillations for a D.C. applied voltage).

In a material that exhibits a negative differential conductivity (n.d.c.)(i.e. has a region where the current decreases with increasing field) the specimen is electrically unstable above a threshold applied field, and breaks up into two domains of different conductivity, carrying the same current density.

As the current density is the same in each domain, one of them must have most of the available voltage dropped across it and is called the high field domain, while the other domain can carry the same current at a lower field. The Gunn oscillations are due to the periodic propagation of these domains through the specimen.

This domain formation only occurs for high charge densities. For low charge densities an internal space charge is built up in the specimen, and the increase in carrier density compensates for the decrease in drift velocity. This does not lead to an external negative D.C. conductivity when the boundary conditions (the electric fields at the two electrodes) are taken into account (Shockley 1954).

b. High Field Domain Formation

A stable high field domain is formed by the growth of a fluctuation in the electric field, in a time shorter than the time taken to propagate between electrodes. This leads to a criterion on the charge density and specimen length for the appearance of a domain.

Following the analysis given by Pamplin (1970), if we assume that the current density is due to a fixed number density of electrons n, then the current density at any point x at a time t is given by

$$J = nev - eD \frac{\partial n}{\partial x} + \varepsilon_o \frac{\partial E}{\partial t}$$

which is the sum of the drift, diffusion and displacement contributions respectively.

Using Poisson's equation

$$\frac{\partial E}{\partial x} = \frac{ne}{\varepsilon_o}$$

and solving these two equations by a small signal theory we get propagation of electric waves according to

$$E \doteq E_o + \Delta E \exp(i\kappa(x-vt)). \exp(-t/\tau)$$

where the wavelength of the disturbance is $\frac{1}{\kappa}$, v the velocity of propagation, and τ is the differential dielectric relaxation time, given by

$$\tau = \frac{\varepsilon_o}{ne} .(\frac{\partial v}{\partial E})^{-1}$$

Normally (positive conductivity) any electric field fluctuations

will decay with a time period

$$\frac{\varepsilon_o}{ne\mu}$$

but under n.d.c. conditions $(\frac{\partial v}{\partial E})$ is negative, and thus τ is the time constant for the growth of a fluctuation. To get a fully developed domain, τ must be less than the transit time of the perturbation between the electrodes (distance apart ℓ) and therefore

$$\tau < \frac{\ell}{v}$$

This gives a relationship between the charge density and specimen length

$$n\ell > \frac{\varepsilon_o v}{e} (\frac{\partial v}{\partial E})^{-1}$$

for the propagation of high field domains.

c. Relevance to Liquid Helium

Because of the intrinsic negative differential mobility of charge carriers in liquid helium, we would expect to see effects due to negative differential conductivity. Using the equation of motion for a vortex ring (Appendix 3), we get

$$v(\frac{\partial v}{\partial E})^{-1} \sim \frac{\alpha(T)}{e}$$

at high fields. Therefore the critical $n\ell$ product is given by

$$n\ell > \frac{\varepsilon_o \alpha (T)}{e^2}$$

At temperatures around $1^{\circ}K$, $\alpha(T) \sim 100$ eV/cm, and for a drift distances $\sim$1cm

$$n > 10^8 \text{ ions/cc}$$

For charge densities greater than this, high field domains should be formed giving an oscillating current for D.C. applied voltages.

The frequency of oscillation will depend on the transit time of the domain.

This ion density was greater than those we could obtain ($\sim 10^6$ ions/cc) and it was not possible to construct a cell $\sim$100 cm in length. However, $n\ell$ is very temperature dependent through $\alpha(T)$, it should be possible to see domain formation at lower temperatures ($\sim 0.6^{\circ}K$ for an ion density 10^6 ions/cc and a cell 1 cm long) or alternatively by using higher charge densities. This effect is independent of the sign of the ionic charge.

Gamota (private communication, 1970) has observed at low temperatures the change in the shape of a pulse of vortex rings drifting across a zero field space of 3 cm, due to the negative differential mobility of the vortex rings. The leading edge of the pulse feels a field due to the rest of the charge in the pulse, which slows it down. Similarly the field at the trailing edge is decreased, speeding up the vortex rings and giving a charge bunching effect.

Negative conductance effects were studied as it was thought they could explain the high field D.C. characteristics.

CHAPTER 6

ION MOTION IN LIQUID NITROGEN

I. INTRODUCTION

This work was done to try to find the mobility discontinuities reported by Henson (1964) in liquid nitrogen and argon, similar to those found in liquid helium (see Chapter 4). The existing theories for the discontinuities were valid only for a superfluid and no theory had been proposed for a 'classical' liquid. Since the completion of our work, there have been reports by Bruschi, Mazzi and Santini (1970) of discontinuities in four liquids, HeI, N_2, Ar, and C Cl_4, and by Henson (1970) of discontinuities in HeI. These results will be discussed later (III,10), in relation to our results.

We used the same velocity measuring method in liquid nitrogen as in liquid helium (i.e. the triode square wave method) but with modifications to allow for the much lower mobility of the nitrogen ion ($\sim 10^{-3}$ cm^2/volt.sec compared with ~ 10 cm^2/volt.sec for He). This meant using high voltage ($\sim$400 V) low frequency ($\sim$1 c/s) square waves and a short drift space distance (1 mm); to reduce the capacitive pick up on the collector (Chapter 4), three extra guard grids were placed in front of the collector. To find the effect of these grids, we took D.C. characteristics for this electrode configuration (called the multiple grid case) as well as for a normal triode arrangement.

The results are discussed for first the D.C. case, and then for the A.C. velocity measurements. There was no basic difference in the general D.C. field behaviour between the results for positive and negative ions; the velocity measurements are all for positive ions. This was because of the uncertainty in the character of the negative ion; oxygen impurities, which are present to 1 ppm in the liquid nitrogen are about a hundred times more efficient in trapping electrons (forming O^-) than nitrogen molecules. But if the structure of the ion is a cluster of nitrogen molecules bound to the negative charge by polarization forces, then the structure should be independent of the parent charge carrier (to a first approximation) and we would not expect a large difference in behaviour between negative ions formed by O^- or N^-. But because of this uncertainty we have worked with positive ions only.

Fig 6.1 D.C. characteristic for a triode for constant grid-collector field

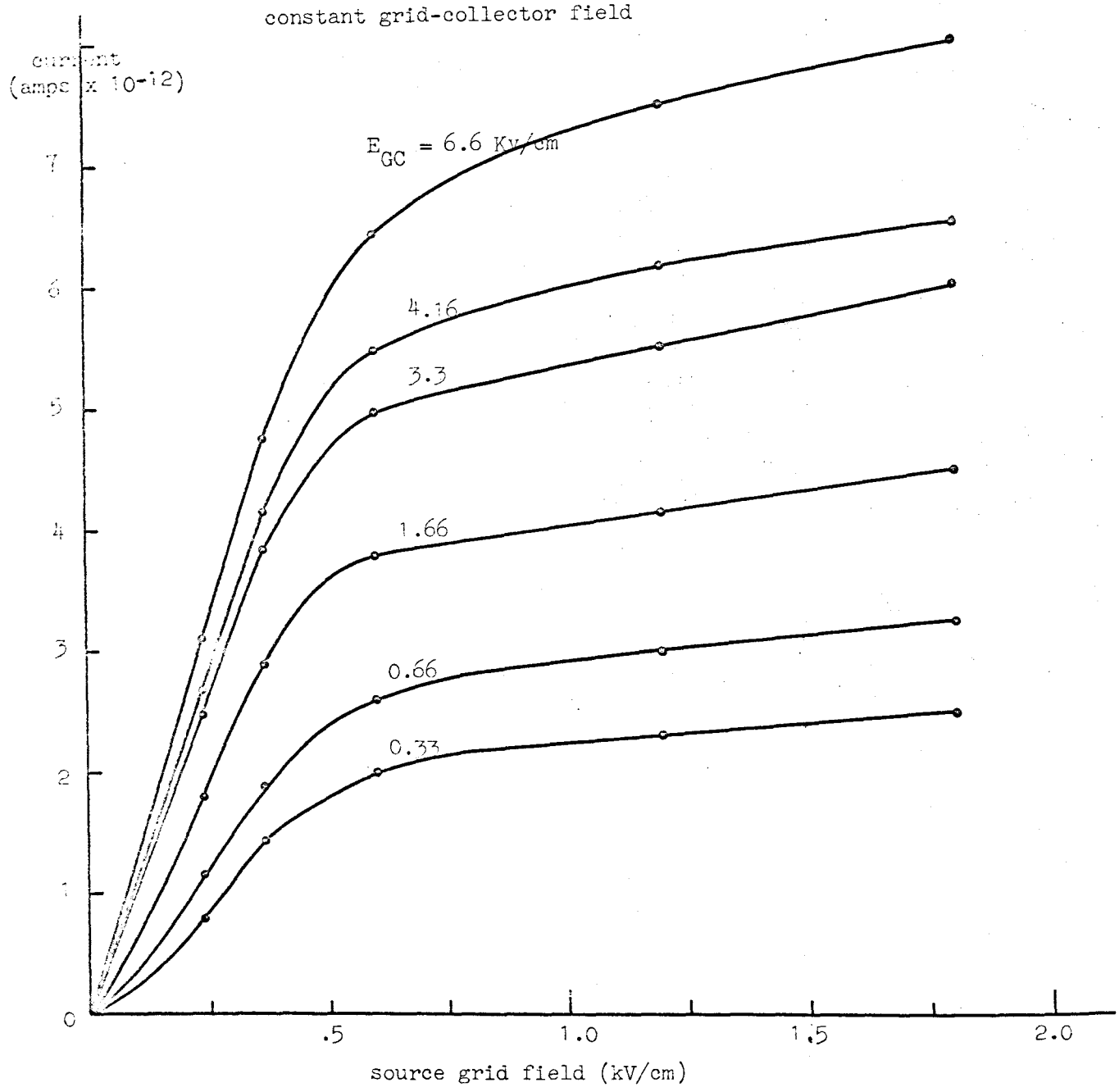

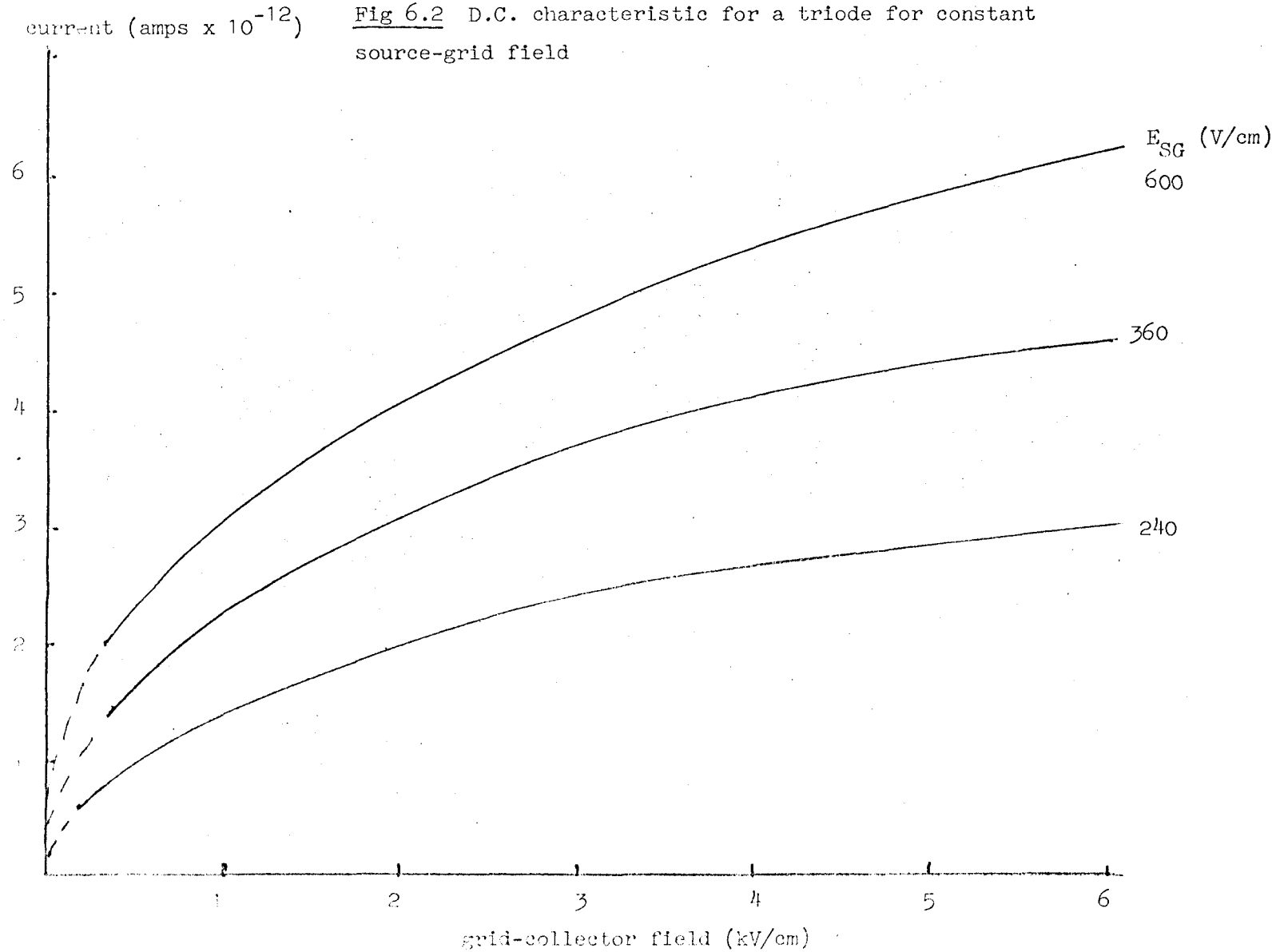

Fig 6.2 D.C. characteristic for a triode for constant source-grid field

II. D.C. CHARACTERISTICS

a. Triode

Figs 1 and 2 show the current behaviour for (1) varying the source-grid field E_{SG}, for various constant grid collector fields E_{GC} and (2) for varying E_{GC} for various constant values of E_{SG}. The points for Fig 1 were taken from Fig 2.

The source grid distance was 2 mm, the grid-collector distance 3 mm, and the grid had a mesh of 60 lpi.

These curves are similar to those found by Dey and Lewis (1968) for ion mobility in liquid argon, and Secker and Lewis (1965) in n-hexane. They are also similar to those we found in liquid helium for bare ions (i.e. for fields below the vortex ring creation field , see Figs 7 and 8, Chapter 5).

An empirical formula due to Januszajtis (1963) fits the curves in Fig 2

by $$I = I_o(1 - \exp(-\frac{E}{E_o}) + cE)$$

as found to describe the corresponding helium characteristics (Chapter 5, section 3(b), and Figs 7 and 10).

The nitrogen characteristic in Fig 1 differs from the corresponding helium characteristic (Chapter 5, Fig 8) by showing a continual increase in current with field E_{SG}, instead of having a maximum value and then decreasing. This is probably due to the field dependence of ion production at the source being different.

Fig 6.3 D.C. characteristic for a multiple grid cell

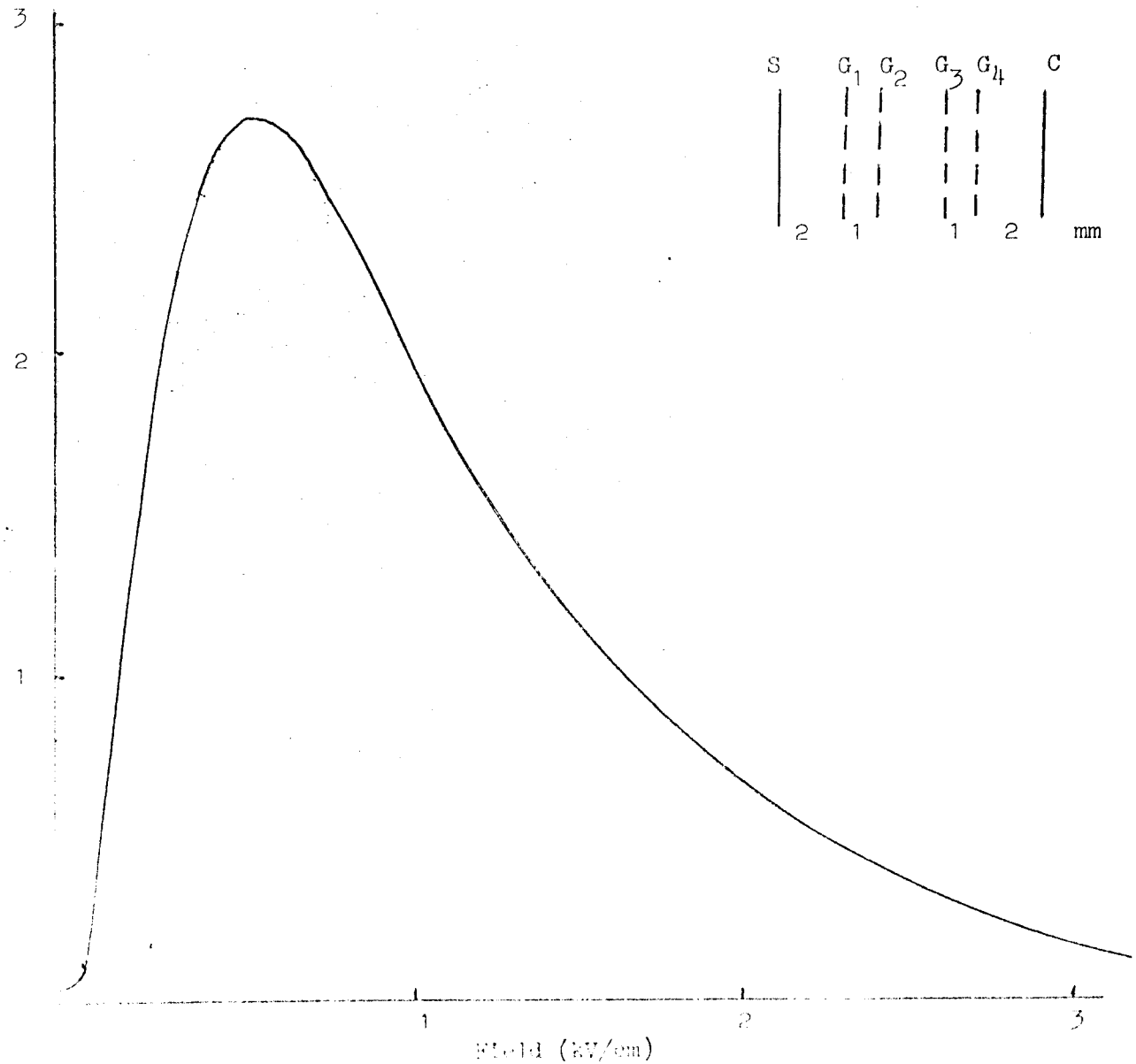

b. Multiple Grid

The multiple grid arrangement is shown in the insert in Figure 3, which also shows the relation between the ion current and the field $E_{G_1G_2}$ between grids G_1 and G_2. The curve does depend slightly, but not substantially, both on the field E_{SG_1} between source and G_1 and on the field E_{G_2C} between G_2 and the collector.

The curve is similar to that found for low grid fields in the tetrode cell in liquid helium at about 1 K, e.g., in Figure 5.9 for fields below $_1E_{min}$, or in other words for fields below the threshold for the creation of vortex rings.

The similarity with helium can also be seen by comparing Figure 3 and Figure 5.17. From the similarity, we can assume with some confidence that the effect of the grid on the transmission of an ion beam is a property of the grid itself, and does not depend on the properties of the ion or the nature of the host liquid. This latter aspect has already been discussed in detail in Chapter 5, Section II,a.

Fig 6.4 Typical current versus frequency curve

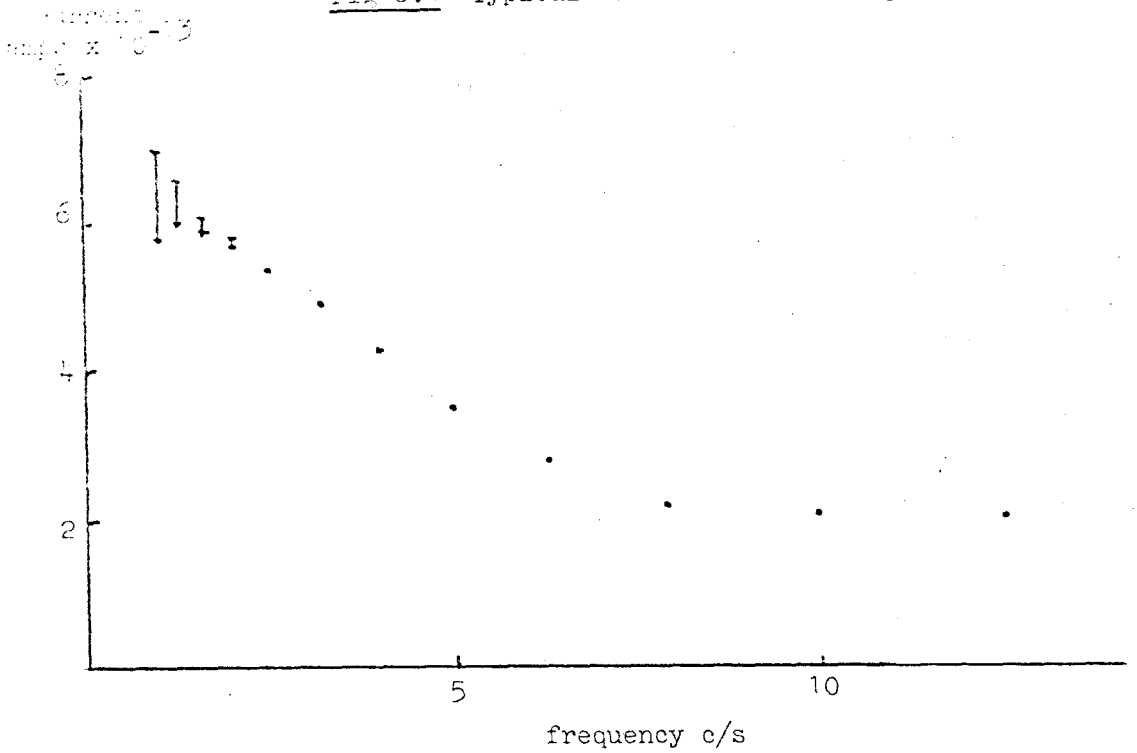

Fig 6.5 Schematic current versus frequency curve, defining I_o, I_∞, f_r and f_o

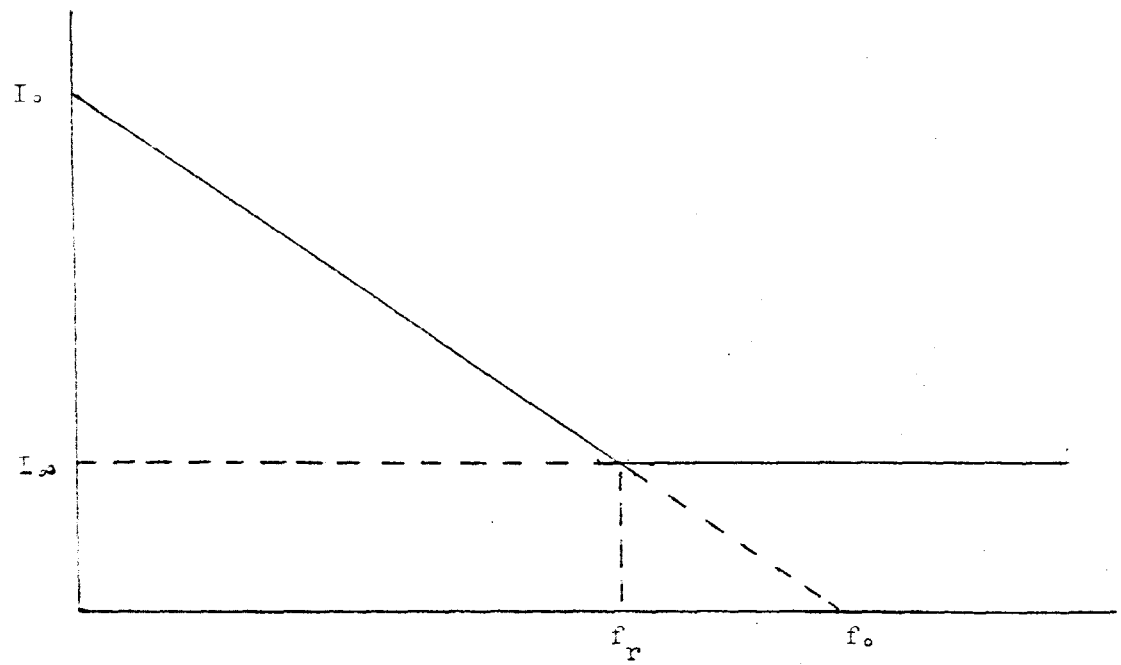

III. A.C. RESULTS

1. Introduction

We used the grid configuation shown in the inset in Fig 3, but with the spacing between G_2 and G_3 being 5 mm. The square wave was applied between the grids G_1 and G_2 i.e. G_2 acted as the collector in an equivalent triode cell. Despite having three guard grids, there was still a large pick up in the electrometer when the square wave reversed its polarity for the lowest frequencies used (~1 c/s). The effect of this on the current-frequency plot can be seen in Fig 4 , where at the lowest frequencies we have plotted the two extreme readings of the electrometer. At higher frequencies, the electrometer time constant averages the pick up to zero, and the current readings are steady. Straight lines can always be drawn through all the points, but the accuracy of reading a frequency intercept is limited by the spread in current values at the low frequency end.

The velocity measurements were all made at atmospheric pressure, with no special precautions taken against introducing impurities into the liquid; results in helium, and in nitrogen and argon by Bruschi et al (1970) indicate that impurities play only a minor role in the mobility behaviour of the ions.

We describe the results of five runs , taken for different values of the source grid field; in three of the runs (A-C) the forward and reverse square wave field was the same, and in two

(D,E) the grid biases were such that the reverse field was three times that of the forward field.

2. Interpretation of the Current-Frequency Curves

We found that straight lines could be drawn through the individual points on a given current-frequency curve, as expected for the triode method, but the high frequency cut off current was not zero. This high frequency result is unexpected, as in helium, at low fields, the current is cut off at I = 0. A typical current-frequency graph is shown diagramatically in Fig 5. For square wave frequencies up to f_r, the graph is a straight line of current against frequency. For higher frequencies, the current tends to a constant value I_∞, commonly non-zero for (relatively) low square wave amplitudes (small fields). I_o is the extrapolated current for zero frequency. f_o is the frequency for extrapolating the straight line portion of the curve to I = 0, and f_r is the frequency when the current becomes independent of frequency (at I_∞).

Two mobilities can be defined, corresponding to the two cut off frequencies f_o and f_r;

$$\mu_o = \frac{2f_o d}{E}$$

$$\mu_r = \frac{2f_r d}{E}$$

where d is the spacing between the grids G_1 and G_2 (about 1 mm) and E is the field between G_1 and G_2 produced by the square wave. The significance of these two values will be discussed later.

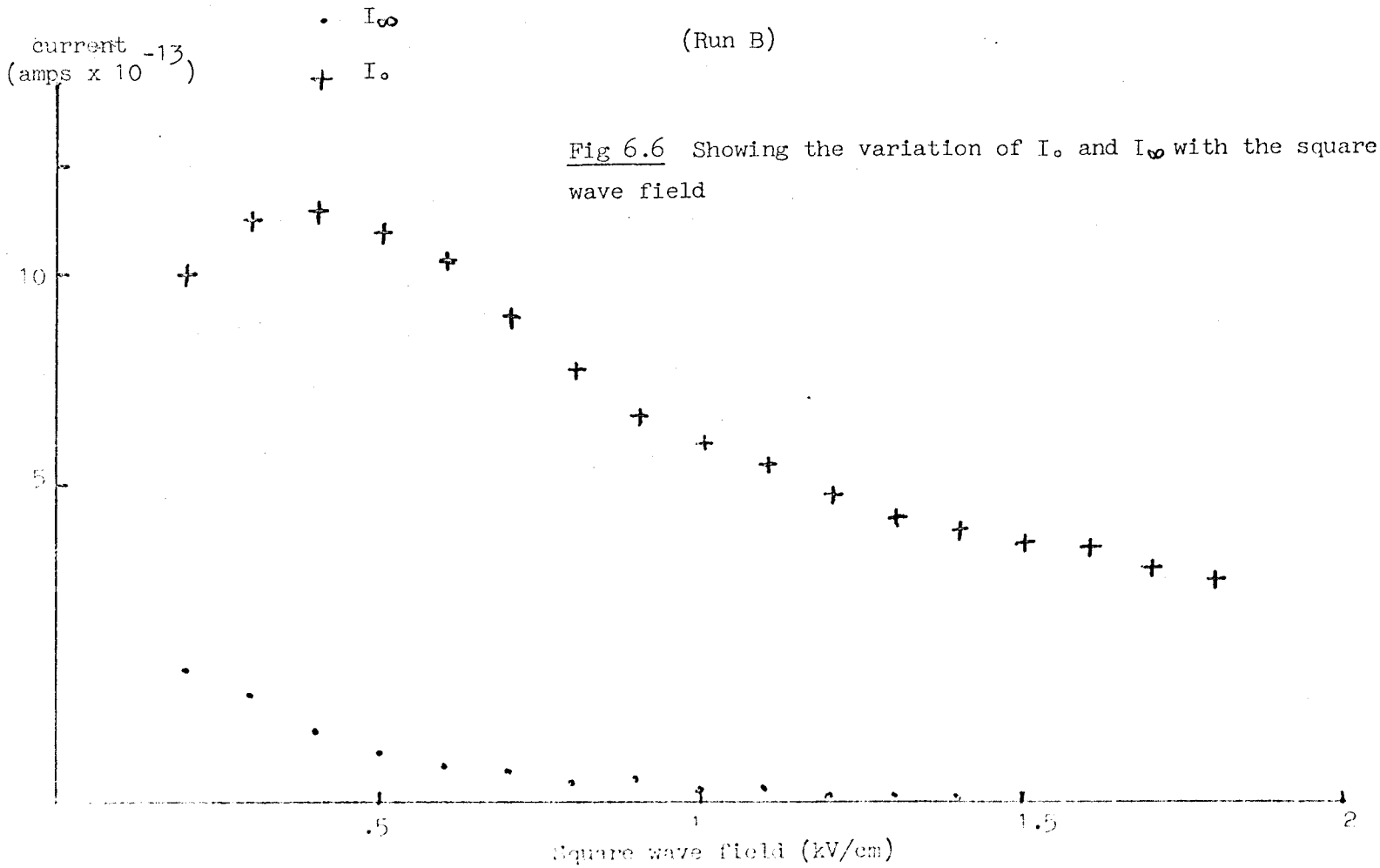

Fig 6.6 Showing the variation of I_o and I_∞ with the square wave field

Fig 6.7 Comparing the variation of the D.C. current and 2 x I$_o$ with the square wave field

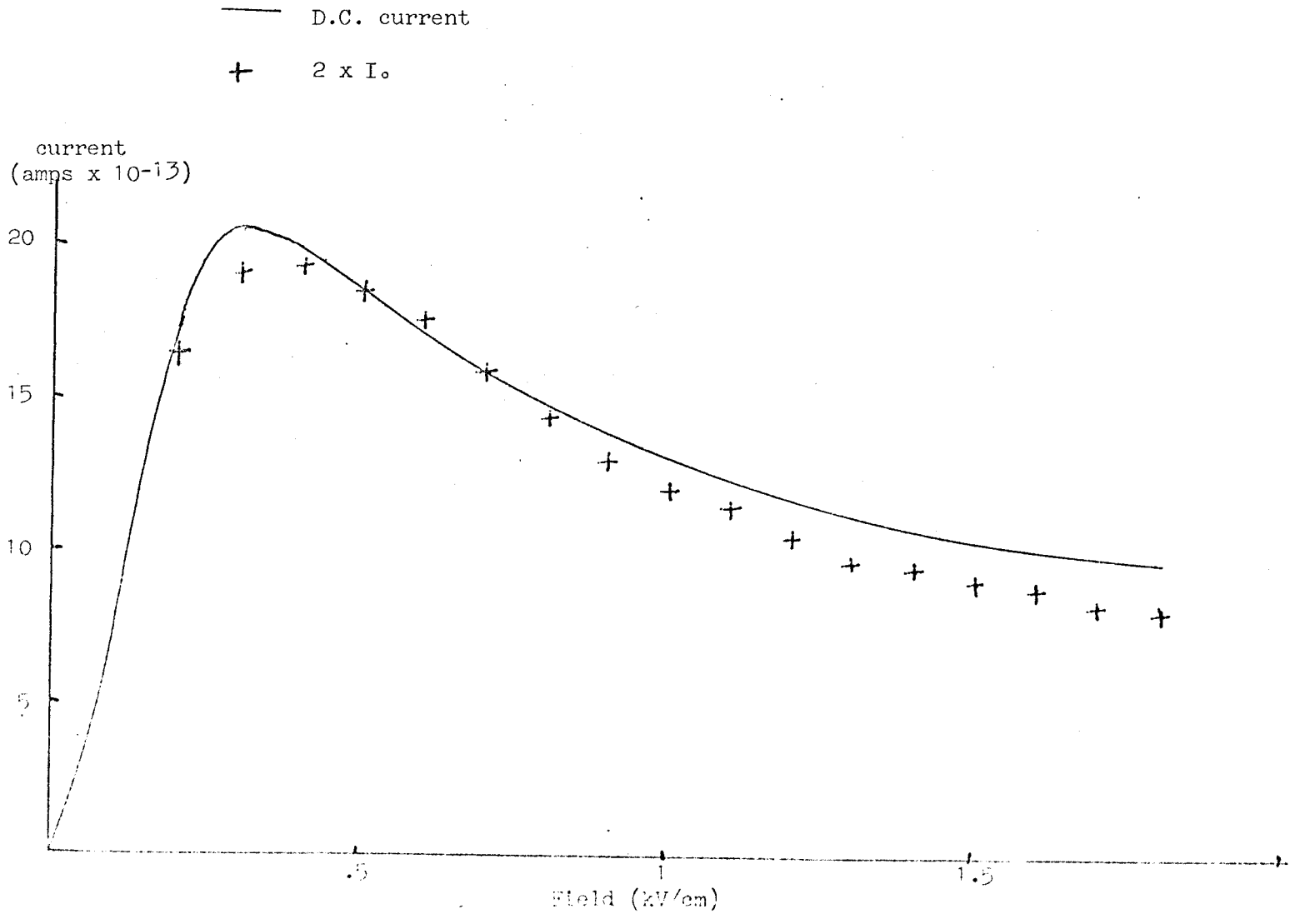

Fig 6.8 Showing the variation of I_o and I_∞ with the square wave field

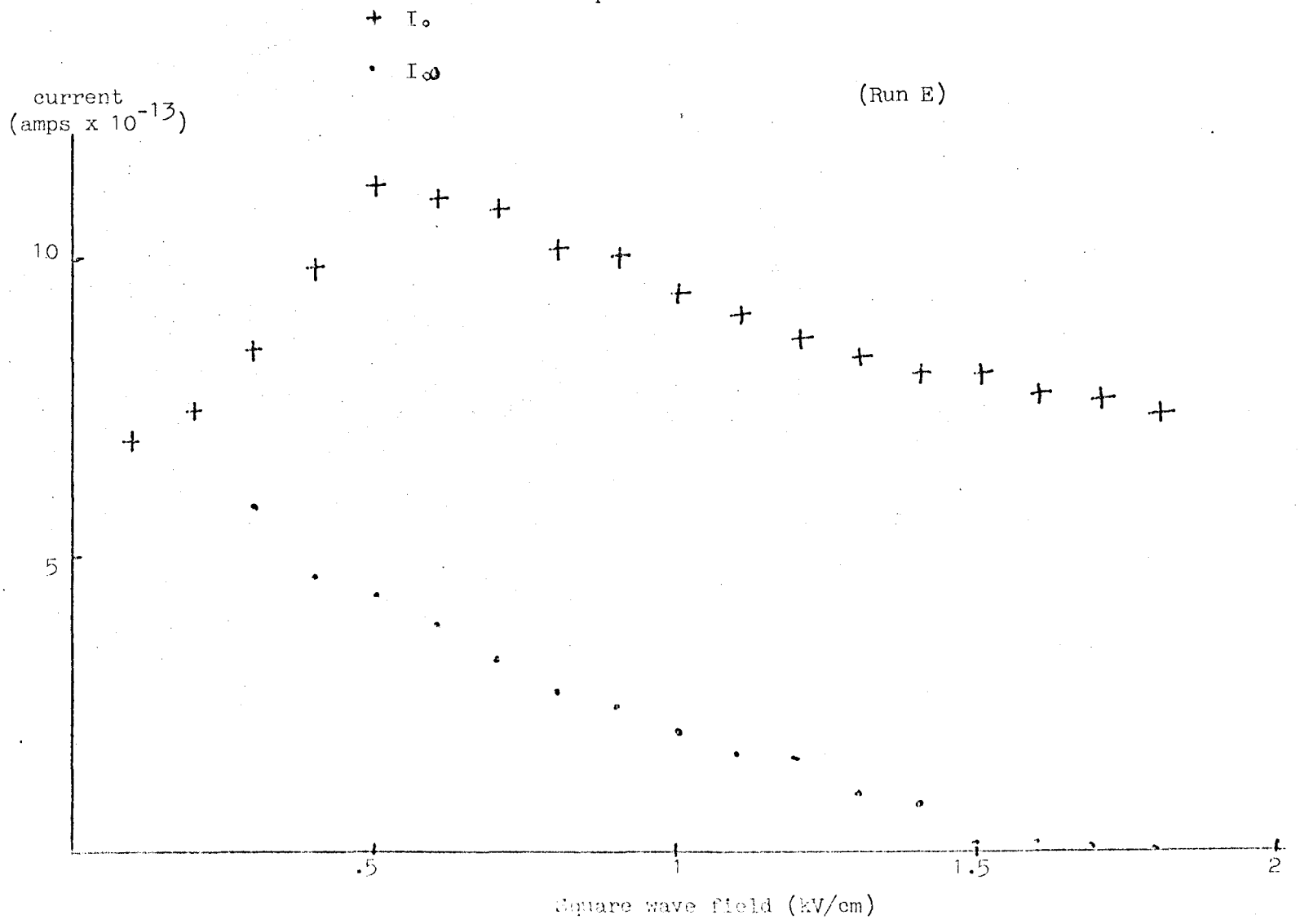

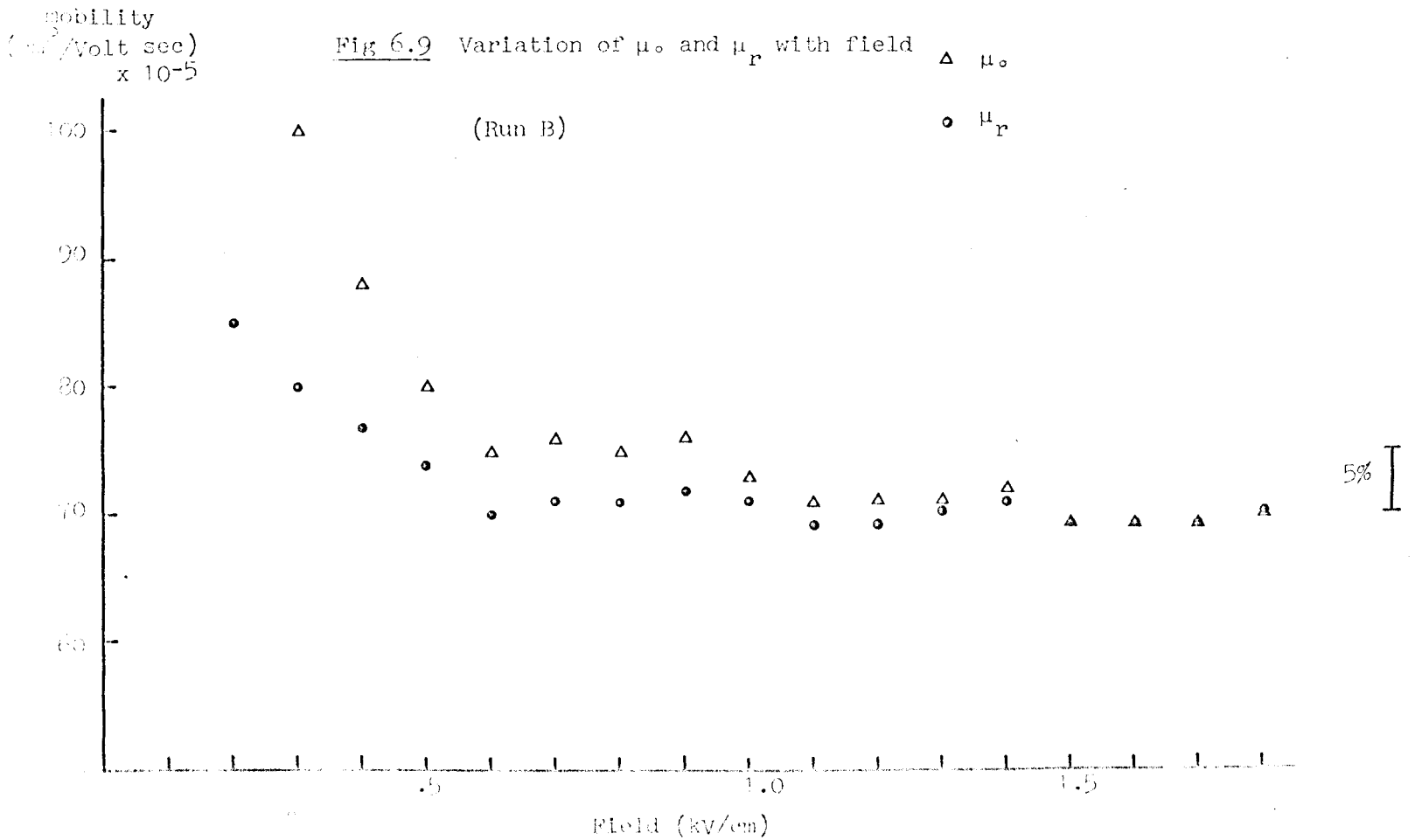

Fig 6.9 Variation of μ_o and μ_r with field

Fig 6.10 Variation of μ_o and μ_r with field

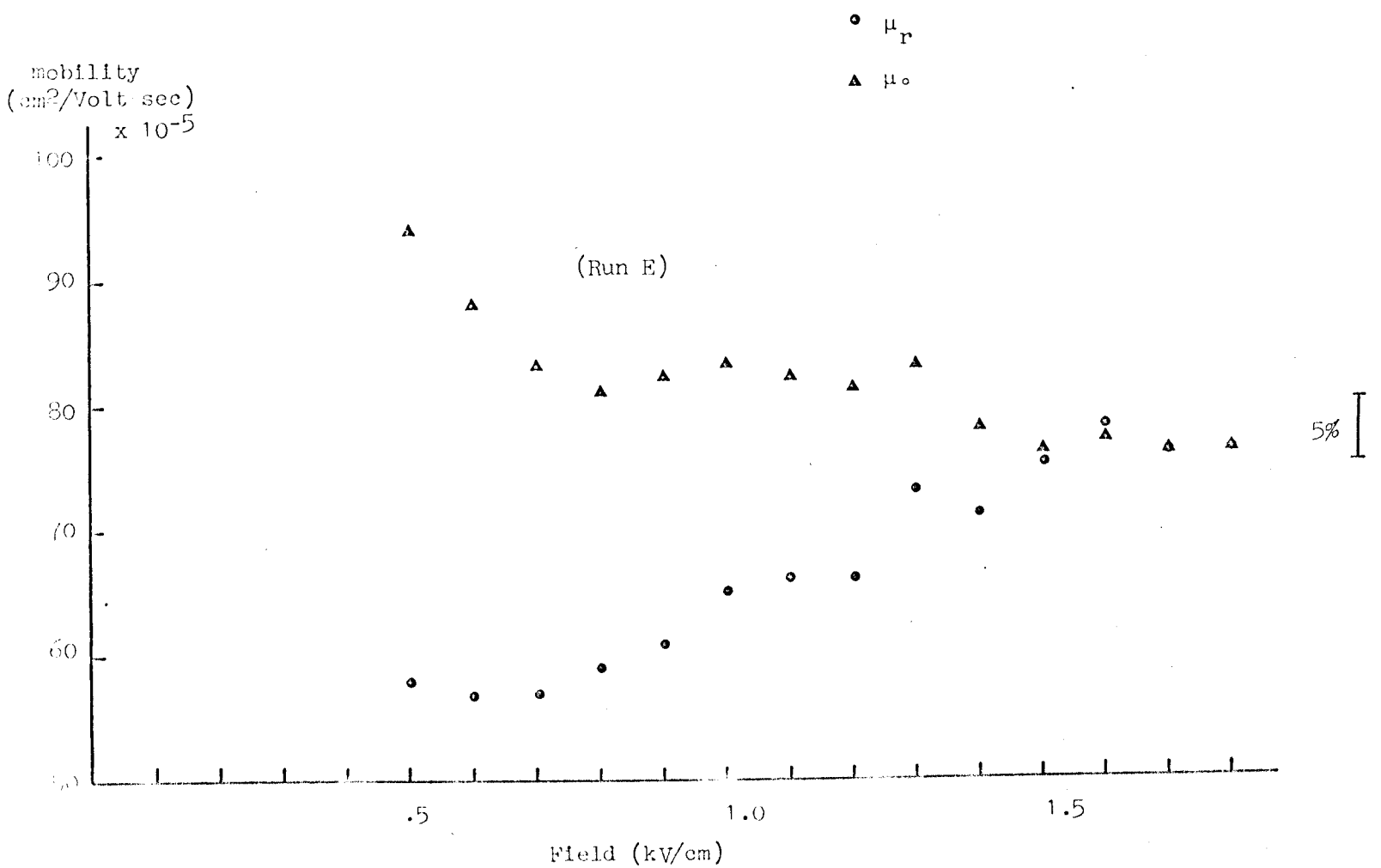

Fig 6.11 Variation of μ_o with field, from five runs

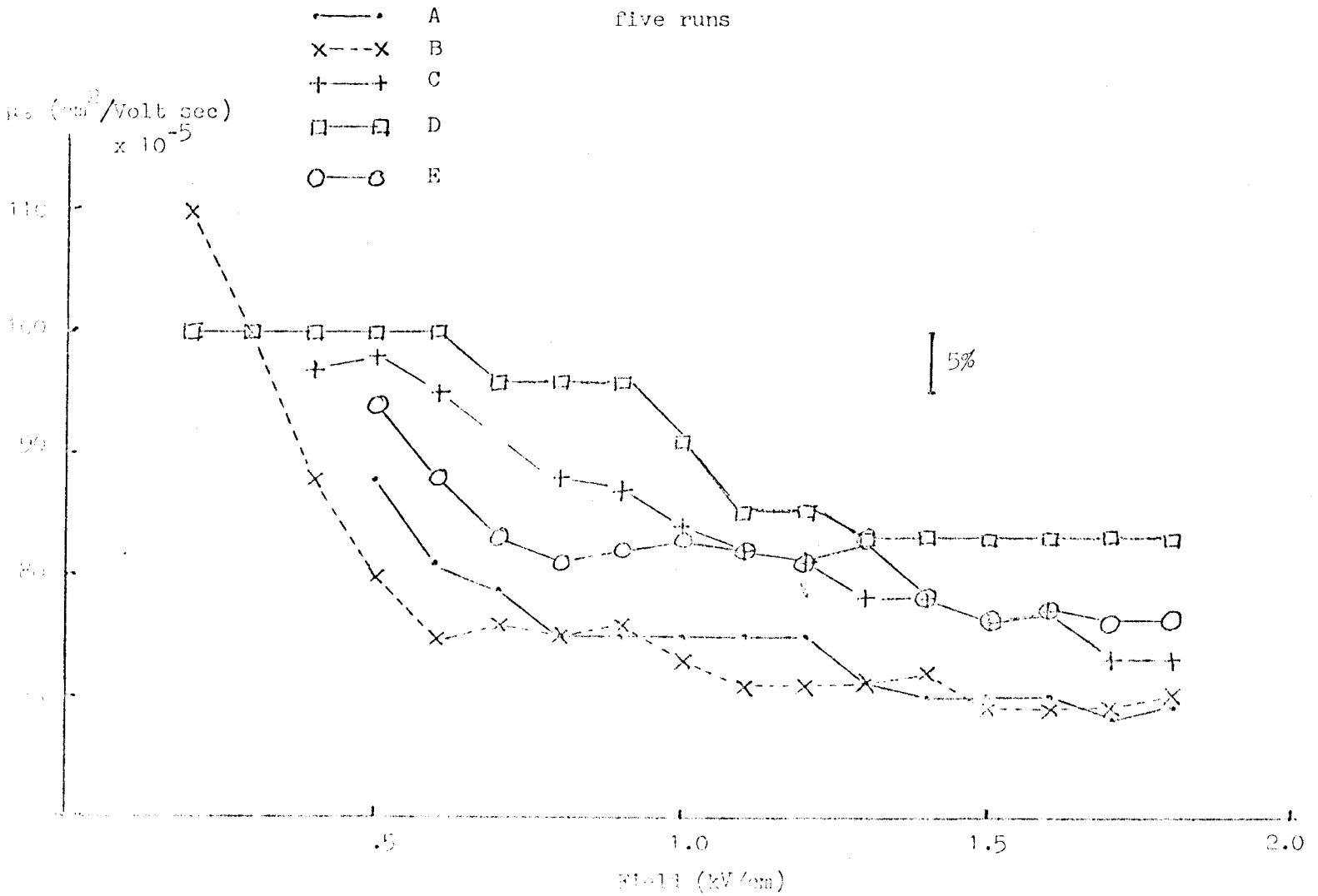

Fig 6.12 Variation of μ_r with field, from five runs

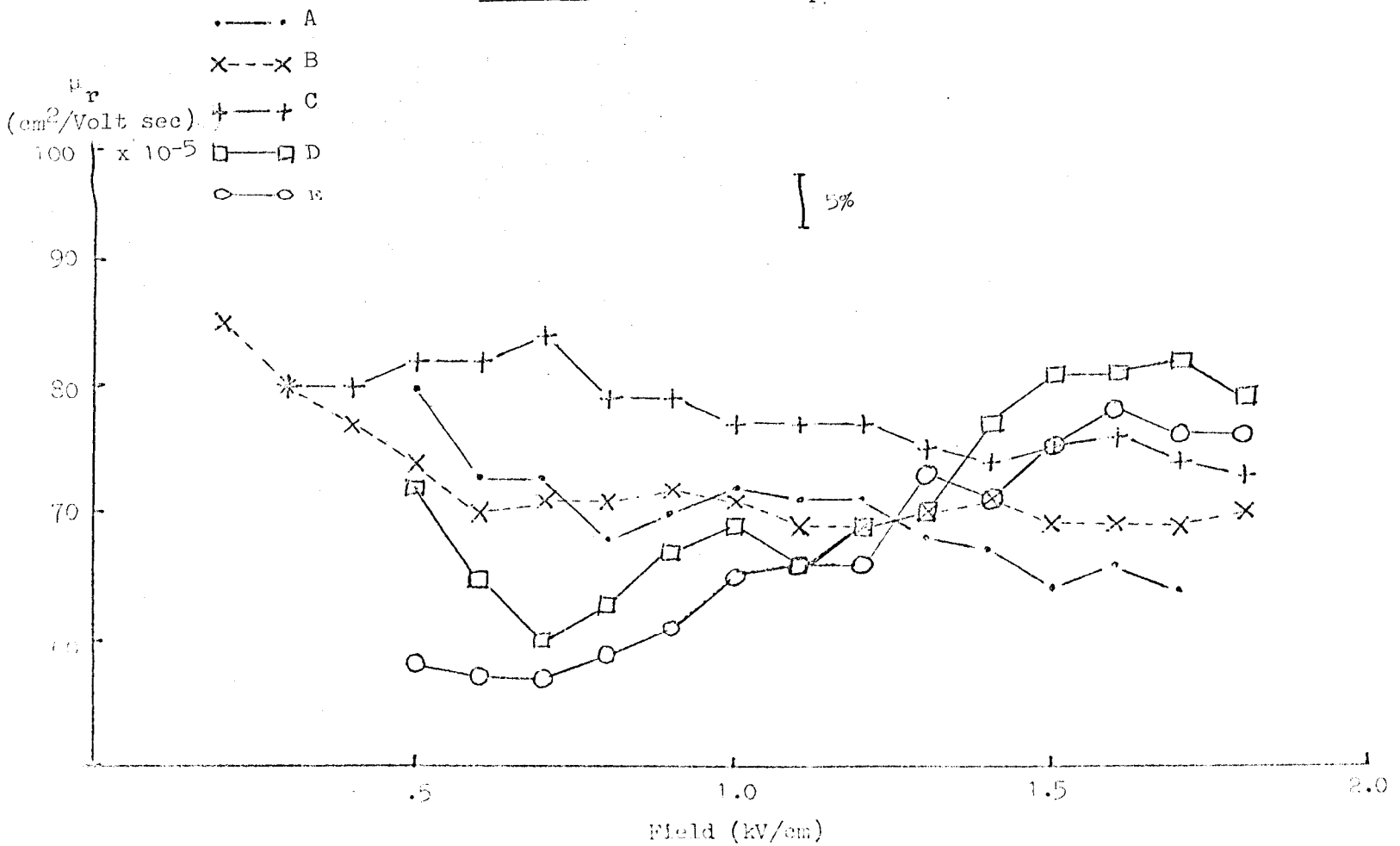

3. Comparison of I_o with D.C. Characteristic

To check that the triode method is operating properly, the current I_o from the current frequency curves is compared with the current obtained from the cell with D.C. voltages giving the same fields as in Run B when the cell is conducting a current (i.e. the square wave is giving a forward field). Fig 6 shows a plot of I_o against field ($E_{G_1G_2}$) for run B and Fig 7 a plot of the D.C. current (I_{DC}) against the field $E_{G_1G_2}$. From the triode operating equation (Chapter 3, equation (1)).

$$I_f = I_{D.C}(\tfrac{1}{2} - \frac{df}{V_D})$$

when $f = 0$ $\qquad I_o = \tfrac{1}{2} I_{D.C}$

Fig 7 also shows a plot of $2I_o$ against the field, agreeing well with $I_{D.C}$. We take this to mean that the current-frequency curves are reliable, and that I_∞ is therefore not a spurious current read by the apparatus, but has a distinct significance; this is also shown in Fig 6. For a comparison between the group of runs (A, B and C) and (D,E), Fig 8 shows a plot of I_o and I_∞ against field for run E. The behaviour of I_o is qualitatively the same as in run B (Fig 6), but I_∞ is more pronounced. This will be discussed later.

4. Mobility Results

We plot the values of both μ_o and μ_r as a function of field. Fig 9 is for Run B, and Fig 10 for Run E. Fig 11 shows the values for μ_o taken from five runs, and Fig 12 the values of μ_r for the

Fig 6.13 Variation of $\bar{\mu}_o$ and $\bar{\mu}_r$ with field

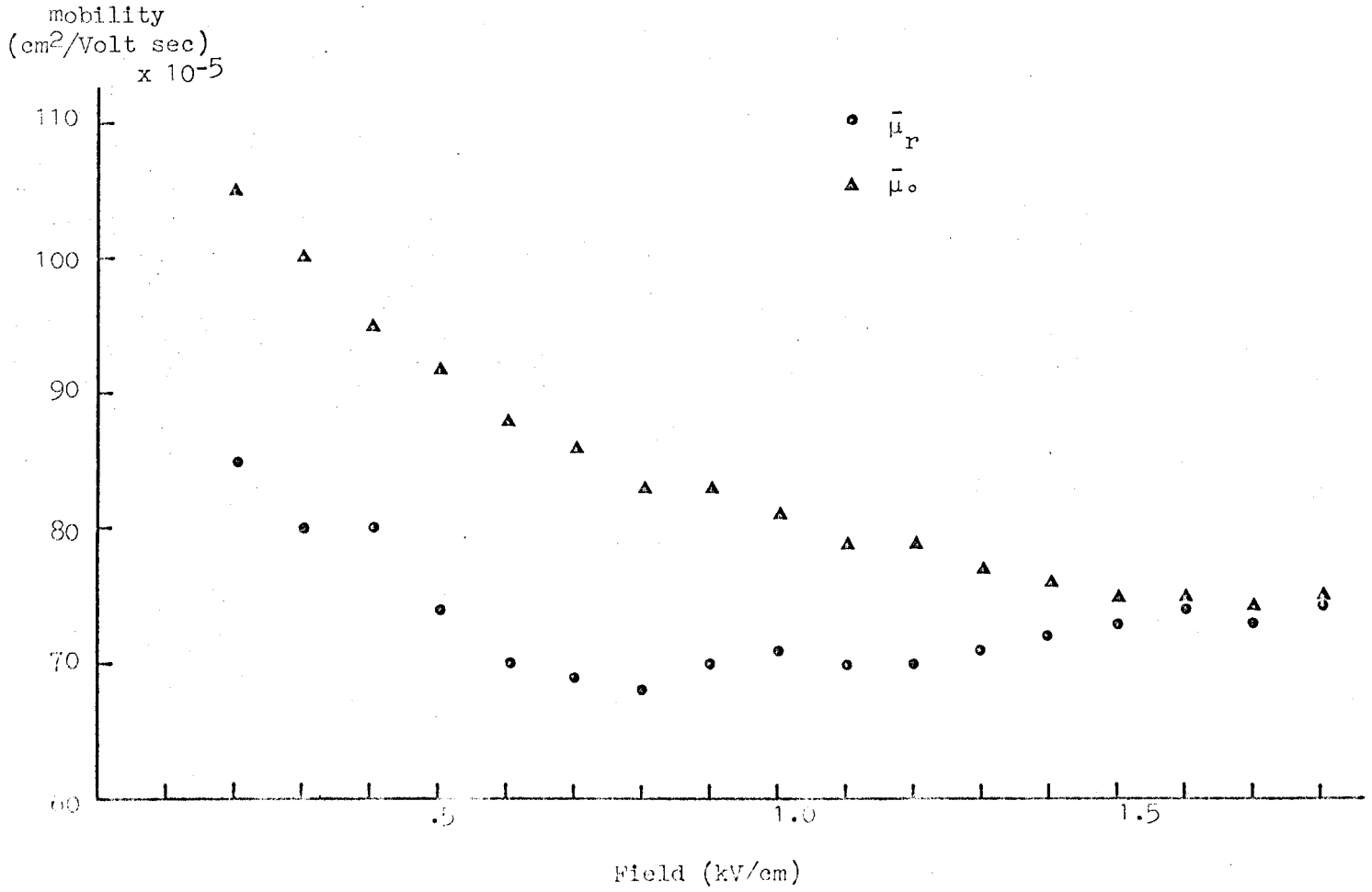

same five runs. Fig 13 shows the average values of μ_o and μ_r in a given field from these five runs. In Figs 9 and 10 the error bar gives the estimated error in each reading; as we are concerned only with the relative mobility values, this is composed mainly of the uncertainty in the values of f_r and f_o estimated from the current frequency graphs, and is about 5%. The absolute error is greater, due to the uncertainty in the electric field and the grid spacing; we estimate this to be around 10%. We do not know either the pressure or temperature dependence of the mobilities, but would by analogy with results in HeI (Swan 1960, Meyer et al, 1962) expect a very small temperature dependence; we therefore ignore any small temperature change due to the change in atmospheric pressure for different runs.

Fig 11 shows that the values of μ_o have a scatter of around 20%, but that there is the same behaviour in all five runs with the field. Fig 12 however shows that μ_r in runs D and E have a slight increase with field, while A, B and C show a slight decrease.

For a given field, the values of both μ_o and μ_r show a scatter of about 20% between different runs, although the behaviour in a single run is consistent with a lower relative error between different electric fields.

Fig 6.14 Plot of $(\mu_o - \mu_r)$ against field for five runs

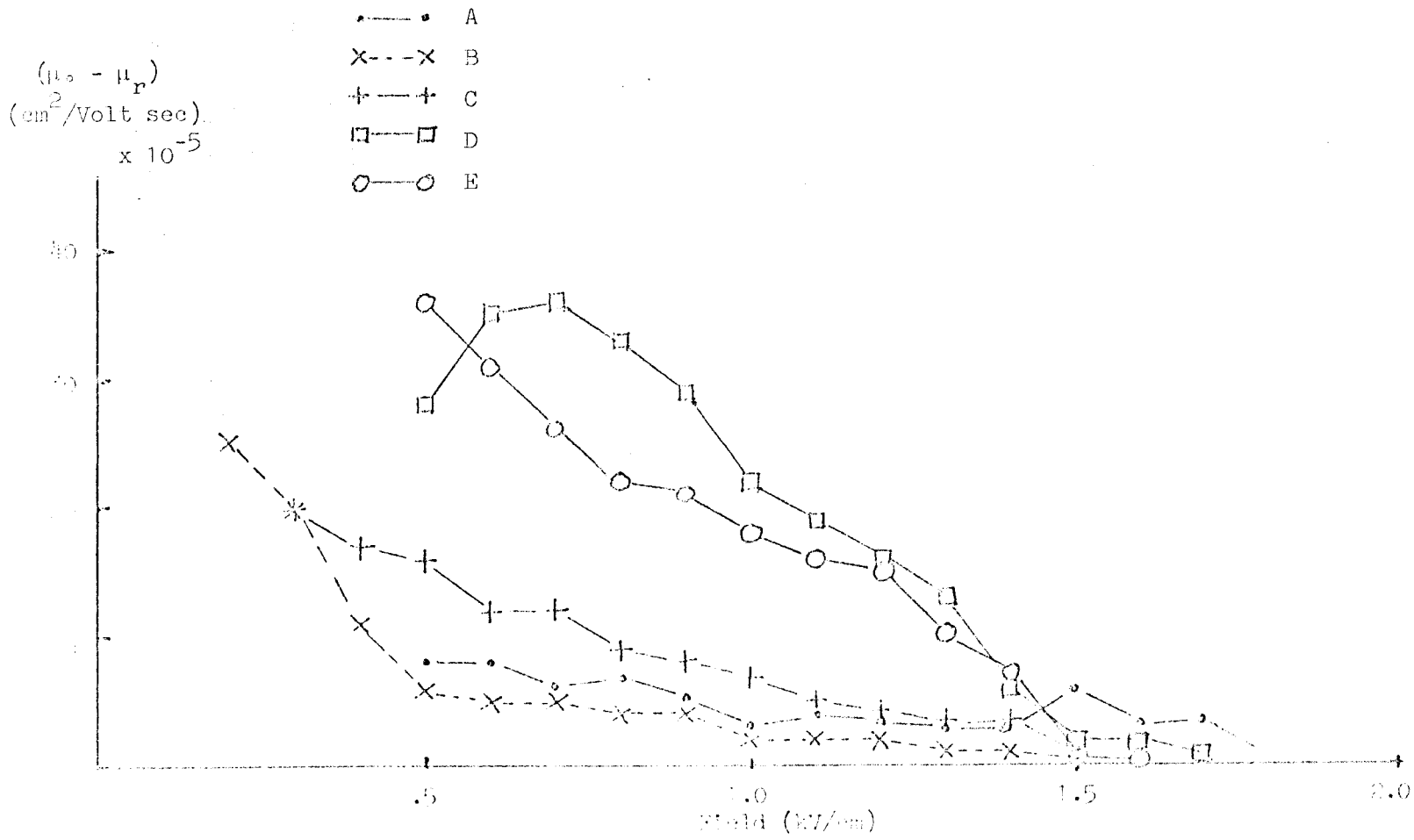

Because of this scatter between runs, the plot of the average values in Fig 13 is of doubtful significance. We plot in Fig 14 the values of $(\mu_o - \mu_r)$ for each run: we see that despite the different behaviour of μ_r between runs, the function $(\mu_o - \mu_r)$ has the same qualitative behaviour for each run, but with runs A, B and C grouped together (group 1), and D and E together (group 2). This will be discussed later.

5. Comparison with other Reported Results

The velocity measurement technique used by both Henson and Bruschi et al (1970) was a pulse technique i.e. the velocity was measuring by analysing the current pulse for ions moving in one direction only through the apparatus. There has not been a previous report of using the triode square wave method to measure ion velocities in liquid nitrogen (or any other classical liquid). The possibility of defining two mobilities is only easily possible in the triode method, as the zero of current is well known then; a pulse method would measure the time taken for the edge of the current pulse to fall to an equilibrium current value, which need not be zero. This would give a mobility value equivalent to our μ_o (the faster ion velocity).

Henson used field emission at a tungsten tip as an ion

source, obtaining currents of around 10^{-9} amps; he also used very high gating fields (~5000 V/cm). Bruschi et al using a radioactive source, worked with currents of the order 10^{-12} amps (the same magnitude as our currents). Henson's value for the low field positive ion mobility was 2.5×10^{-3} cm^2/volt sec. Our average value of μ_r was 7.1×10^{-4} cm^2/volt sec, and μ_o was about 10.5×10^{-4} cm^2/volt sec. This agrees well with Bruschi, but is a factor of 3 lower than Henson. It is suggested later this discrepancy is because of the much higher current used by Henson.

6. Liquid Motion

In classical liquids, the motion of ions under the influence of an electric field will cause liquid motion in the direction of the ion motion; the magnitude of the liquid motion depending on the viscosity of the liquid, the electrical energy input to the cell, and the cell configuration. This liquid motion will increase the ion velocity, and give an anomalously high mobility measurement.

Liquid motion in hexane has been directly observed by Gray and Lewis (1965), by injecting a small amount of dye into a cell through which a small current (~ 10^{-11} amps) was being passed.

The dye was seen to be carried past the collecting electrode, into a field free region of the cell, confirming the liquid was in motion, and the dye was not just attached to the ions. Liquid velocities of the same order as the ion velocities were observed (~1 cm/sec).

It has been shown that liquid motion caused by ionic conduction in an insulating liquid can create pressures of the order of a fraction of an atmosphere. This effect has been used to construct 'ion drag' pumps (Stuetzer, 1960) which are extremely rugged and simple.

Liquid motion has been used to explain ion mobility results in n-hexane (Secker and Lewis, 1965) and in liquid argon (Dey and Lewis, 1968), using a theory by Kopylov (1964) which relates the liquid velocity to the current and electric fields in the cell. Both sets of results above showed that: 1. their values for the mobility were higher than expected and that 2. the low field ion mobility decreased as the steady state cell current decreased.

In the theory by Kopylov, the liquid velocity v_e is given by

$$v_e = A_1 E \ln\left(\frac{A_2 I}{E}\right) \qquad (1)$$

where E is the electric field, I the current, and A_1 and A_2 are constants depending on the liquid properties and cell dimensions. This is expected to be valid for large values of $\beta = \frac{A_2 I}{2E}$; and for small values, the liquid velocity tends to

$$v_e = \pi A_1 A_2 I \qquad (2)$$

Kopylov gives v_e as an increasing function of $\frac{A_2 I}{2E}$.

To see the effect of liquid motion on measured mobility values, we can consider that the measured ion velocity v_o is in a frame that is stationary with respect to the liquid (moving with velocity v_e). Then the real ion velocity v_r (with respect to the liquid) is given by

$$v_r = v_o - v_e$$

i.e.
$$v_o = v_r + v_e \tag{3}$$

if we define the mobility to be $\mu = \frac{v}{E}$ where E is the applied electric field, then

$$\mu_o = \mu_r + \mu_e \tag{4}$$

This shows that the measured ion mobility is greater than the real mobility, by the liquid mobility; the mobilities are additive as the effect of the liquid motion is only to alter the reference frame (if the effect of the liquid motion was to provide a mechanism for additional momentum loss by the ion, we would get

$$\frac{1}{\mu_o} = \frac{1}{\mu_r} + \frac{1}{\mu_e}$$

as happens say in helium where there can be more than one type of scattering mechanism (rotons and phonons) where the mobility μ is given by

$$\frac{1}{\mu} = \frac{1}{\mu_{rot}} + \frac{1}{\mu_{ph}}$$

where μ_{rot} is the mobility expected from roton scattering and μ_{ph} the mobility from phonon scattering.)

This explains the high mobility values found by Secker and Lewis, and Dey and Lewis.

The variation of the low field mobility with current can be seen from equation (1): as the current increases, so does v_e, and thus μ_e and therefore the measured mobility increases. The theory by Kopylov agreed qualitatively with the results by Secker and Lewis, and Dey and Lewis, but not quantitatively. This is probably due to the interaction of the liquid velocity in different parts of the measuring cell.

7. Variation of Mobility with Field

Previous results of ion mobilities in liquids have been analysed by classical kinetic theory (see Swan, 1960), which has been shown to be applicable when the region of validity of the proper equations has been found.

If the energy gained by the ion from the electric field E in one mean free path λ is less than the ions thermal energy kT, then low field conditions apply; if the reverse is true, then high field equations must be used.

The criterion for low field conditions is

$$\left(\frac{M}{M_i} + \frac{M_i}{M}\right) eE\lambda << kT \qquad (5)$$

where M_i is the ion mass, and M the mass of the liquid molecule.

If the ion mean free path is less than the ion radius, for low field conditions the mobility is given by Stokes Law, i.e.

$$\mu = \frac{e}{6\pi\eta R} \qquad (6)$$

where η is the liquid viscosity, and R the ion radius. The mobility is then independent of the electric field.

We will show that our value of the ion mobility is consistent with the validity of low field conditions for the electric fields used in our apparatus.

Using equation (6), and $\mu_r = 7.1 \times 10^{-4}$ cm^2/volt sec we get R ~7A; this is reasonable, agreeing with the radius of the positive ion in liquid helium. It shows that polarization effects are important in determining the ion mobility, and are expressed through an effective mass for the nitrogen ion; we take this to be $M_i \simeq 40M$, by analogy with the helium ion. Putting this value in equation (5) shows that low field conditions apply when $\lambda \lesssim 20$ A; this is almost certainly true, as this is the expected ion mean free path in liquid helium when the roton density (providing the scattering centres) is around 10^{19}/cc. The density of scattering centres in liquid nitrogen is around 10^{22}/cc.

This means we can take the real ion mobility in liquid nitrogen to be independent of the field, and the field dependence of the measured ion mobility to show the field dependence of the liquid motion.

8. Analysis of Results

We suggest that the behaviour of our velocity measuring cell, as seen by the current-frequency graphs, is due to liquid motion.

The existence of I_∞ is because the liquid always carries some of the current through the cell to the collector at any square wave frequency; on the reverse half of the square wave

the ions have a smaller velocity relative to the cell than for the forward cycle, and therefore not all the ions will return to the grid. (The variation of I_∞ with the amplitude of the reverse square wave field will be discussed later). We make the identification of the real ion mobility (with respect to the liquid) to be our μ_r, and the measured ion mobility (with respect to the cell) as μ_o. This follows from regarding the liquid velocity to change the reference frame in which the velocity is measured; μ_r is given when the square wave current reaches the background current, and a continuation of the same line gives μ_o when the background current is zero. (as seen in the I-f curves Fig 4).

Therefore, according to equation (4)

$$\mu_o = \mu_r + \mu_e$$

where μ_e is obtained from equation (1)

$$\mu_e = \frac{V_e}{E} = A_1 \ln \frac{A_2 I}{E}$$

Thus

$$\mu_o - \mu_r = A_1 \ln \left(\frac{A_2 I}{E}\right) \qquad (7)$$

In the analysis of our results we have assumed a constant current I , and modify equation (7) to

$$\mu_o - \mu_r = c_1 \ln\left(\frac{c_2}{E}\right) \qquad (8)$$

where $c_1 = A_1$ and $c_2 = A_2 I$: both are assumed constant, independent of the field.

We fit this equation (8) to the results for $(\mu_o - \mu_r)$ shown in Fig 14 for (1) each individual run (2) the group A, B and C

TABLE I

Run	C_1 ($\times 10^5$) $cm^2/volt.sec$	C_2 ($\times 10^{-3}$) V/cm	correlation coefficient
A	6.2 ± 1.6	2.30 ± .07	.76
B	12.3 ± 1.2	1.26 ± .04	.94
C	11.8 ± 0.3	1.75 ± .01	.99
D	37.0 ± 5.0	1.70 ± .04	.91
E	30.3 ± 1.6	1.72 ± .02	.98
A+B+C	12.3 ± .9	1.50 ± .05	.89
D+E	34.5 ± 2.3	1.70 ± .03	.94
average	14.7 ± .2	1.97 ± .02	.99
Henson	54 ± 5	9.8 ± 0.2	
Bruschi	5.4	4.10 for $\mu_r = 7.10^{-4}$ $cm^2v^{-1}s^{-1}$ 1.7 for $\mu_r = 95.7 .10^{-5} cm^2v^{-1}s^{-1}$ 4.0 for $\mu_r = 81.10^{-5}$ $cm^2v^{-1}s^{-1}$	

(3) the group D and E (4) the average value of $(\mu_o - \mu_r)$ in Fig 13. We used a multiple linear regression analysis to obtain values for c_1 and c_2 with their standard error; the correlation coefficient gives an indication of the reliability of the results. Table 1 shows the results. We see that a good agreement is obtained between theory and experiment, with our results falling into two distinct groups as expected.

9. Discussion

We will discuss the values of c_1 and c_2 in table I with reference to the field conditions in our cell for each run, and show how they are consistent with the concept of liquid motion.

From Table I we see that c_2 is approximately constant for each run, but that c_1 shows a significant difference between the runs A, B and C and runs D and E. From equation (8), we see that c_1 has the dimensions of a mobility, while from equation (7) and (8) we see that c_2 is proportional to the current. The theory indicates that the liquid velocity should be proportional to the current; in the triode velocity measurements the time average of the current decreases with increasing square wave frequency, while the current magnitude in each frequency pulse is constant. We expect a characteristic time for the liquid to reach an equilibrium velocity for a given current; if this time if greater than the square wave frequency, then c_2 should be independent of the frequency dependent current, but be proportional to the equivalent D.C.

TABLE 2

Run	E_{SG} / E_F	E_R / E_F
A	E_{SG} = 900 v/cm (const) 3 → ½	1
B	.7 → .9 low field high field	1
C	1	1
D	½	3
E	½	3

$$\frac{E_{SG}}{E_F} = \frac{\text{field in source grid region}}{\text{field in measuring space when square wave on}}$$

$$\frac{E_R}{E_F} = \frac{\text{field in measuring space when square wave off}}{\text{field in measuring space when square wave on}}$$

Fig 6.15 Plot of μ_e and V_e against field. From theory by Kopylov, using our experimental parameters

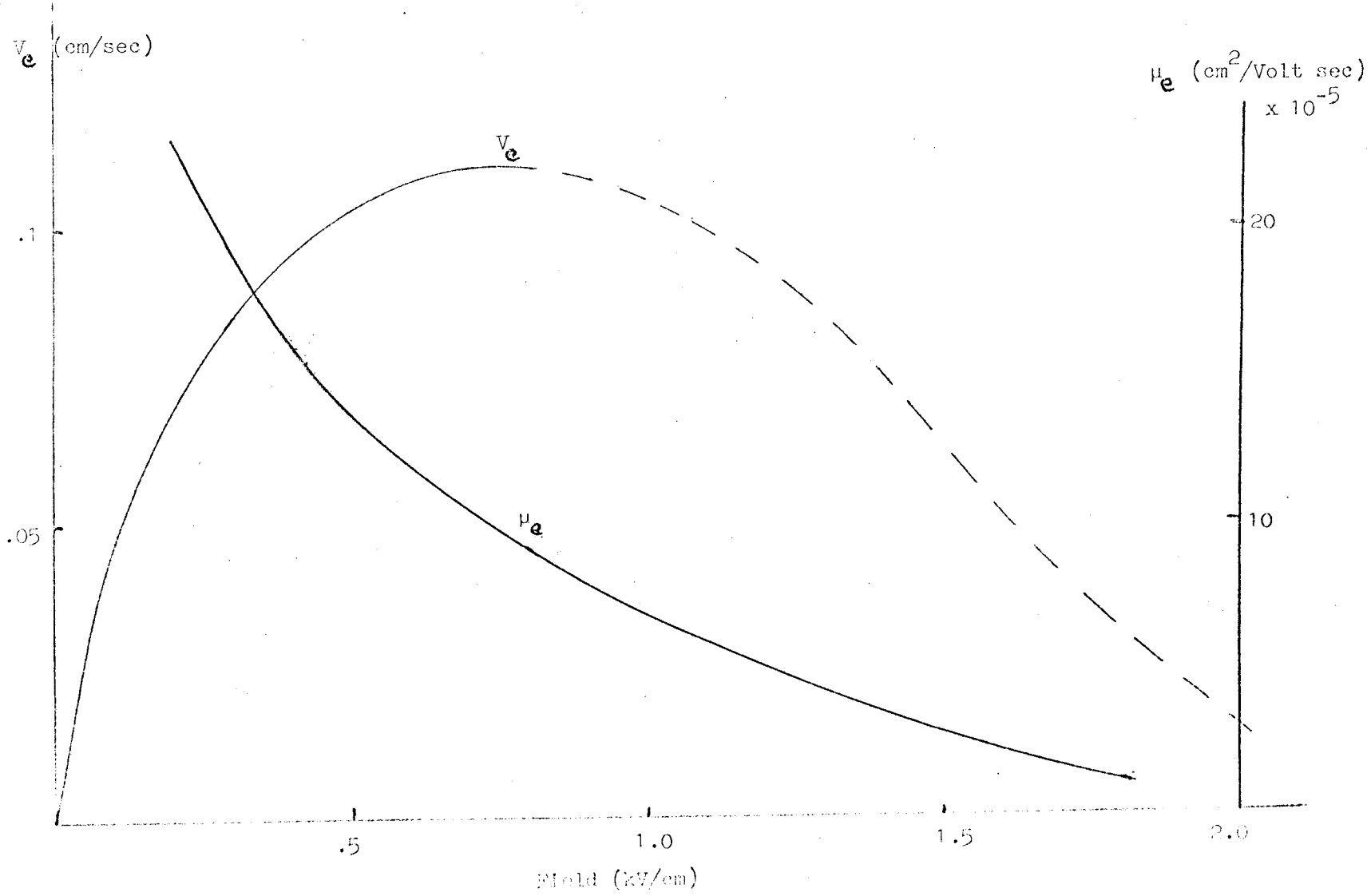

current. We take the small error in c_2 to show that this is true for each individual run, and the slight difference between each run to show a possible small dependence on the D.C. current.

Table 2 shows the ratio of the source-grid field to the square wave forward field E_{SG}/E_F (when ions are passing to the collector) and the ratio of the reverse and forward square wave fields E_R/E_F. The striking difference between the group (1) runs and group (2) is the value of E_R/E_F, being three times higher for group (2); this is compared with the higher values of c_1 (by a factor of about 3) for group (2) over group (1). A possible explanation lies in the field behaviour of liquid velocity and mobility. Fig 15 shows a plot of equation (1), of v_e against field, using our values of c_1 and c_2. Also shown in Fig 15 is $\mu_e = \frac{v_e}{E}$ as a function of the field. While the behaviour of μ_e is reasonable, we need to examine the behaviour of v_e to see whether equation (1) is valid for the whole field range. In section (6) it was said that equation (1) was valid for large values of a parameter $\beta = \frac{A_2 I}{2E}$ $(= \frac{c_2}{2E})$. This is true for small fields; with our value of c_2 ($\simeq$1700 V/cm), β reaches unity at a field E $\sim$850 V/cm. (Kopylov gives no criterion for a value of β for the validity of his equations). Fig 15 shows that v_e reaches a maximum value of $\sim$.11 cm/sec at a field $\sim$700 V/cm. For high fields (small β) we expect the liquid velocity to be given by equation (2). Using our values for c_1 and c_2, we get $v_e \sim 1$ cm/sec, which is higher than the low field (high β) velocity. This is in

contradiction to the results quoted by Kopylov, who gave v_e as an increasing function of β (i.e. v_e decreases as E increases). However physically we would expect v_e to rise from zero at zero field, and saturate at high fields. This would give an effective liquid mobility falling with increasing field, as shown in Fig 15. The liquid motion in the measuring space is affected first by the forward motion of the ions, and then in the reverse half of the square wave cycle the liquid motion will be reduced by the ions still in the measuring space travelling back to the grid. If the reverse field is higher than the forward field, the reduction in the liquid motion in the forward direction will be less than when the forward and reverse fields are equal, as the liquid mobility is lower. Also, the forward motion of the liquid occurs when a current is being passed i.e. for a time τ_f equal to half the square wave period

$$\tau_f = \frac{1}{2f}$$

The reverse motion is induced only for the time it takes to empty the measuring space i.e. the transit time τ_t. For square wave frequencies greater than the cut off frequency f_c, the ratio of τ_f to τ_r will depend on the ratio of the forward and reverse fields. Thus a high reverse square wave field will cause a smaller reduction in the liquid motion in the forward direction, and give a higher value of c_1, as found. This process does not depend strongly on the characteristic time taken to reach an equilibrium liquid velocity,

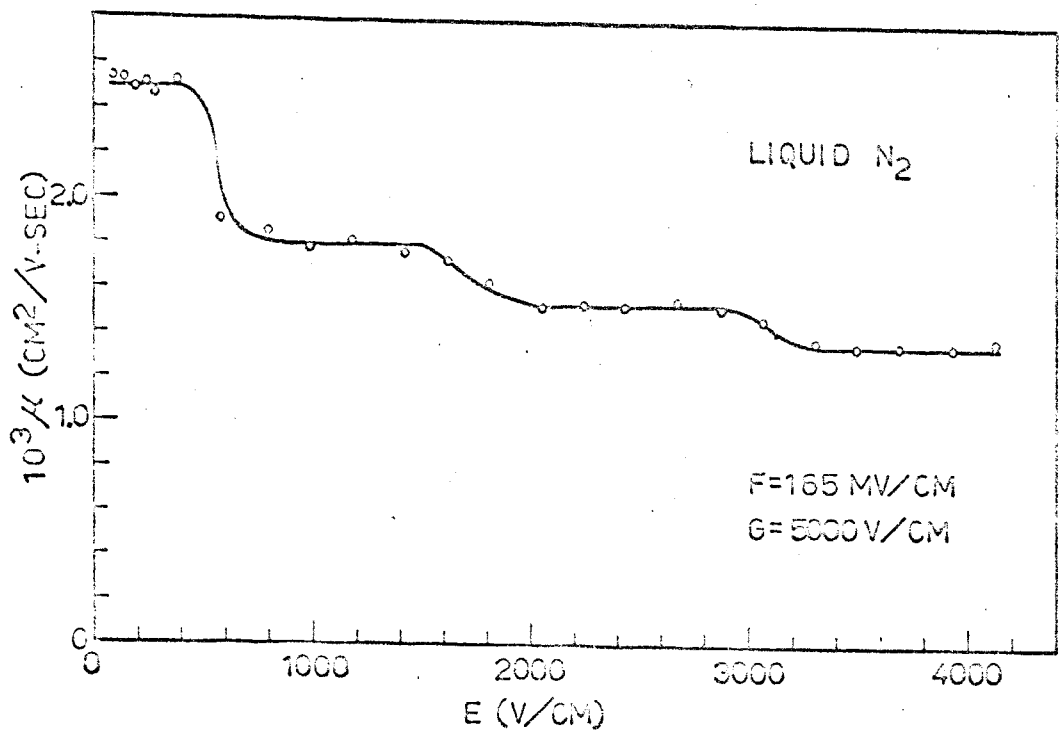

FIG. 15. Experimental data in liquid nitrogen presented as ion mobility versus applied field with $F=165$ MV/cm and $G=5000$ V/cm.

Fig 6.16 From Henson (1964)

as long as this time is greater than the square wave frequency; a quasi-equilibrium liquid velocity will be induced, being a time average over a number of square wave periods.

The liquid motion induced by the current in the source region is expected to continue into the measuring space, which will tend to negate the reverse current liquid motion.

The values for the liquid mobility we obtain, $\sim 3.10^{-4}$ cm^2/volt sec, compare well with those found in hexane; $\sim 6.10^{-4}$ cm^2/volt sec by Secker and Lewis, and $\sim 4.6 \times 10^{-4}$ cm^2/volt sec by Gray and Lewis.

Our analysis has concentrated on the difference between our measured mobility values ($\mu_o - \mu_r$); as μ_r should be independent of field, the slight field dependence seen in Fig 12 cannot be explained, except to question the validity of the definition of μ_r and μ_o from our current frequency graphs as the absolute mobility values.

10. Relation to Mobility Discontinuities

We will discuss first Hensons results for the positive ion mobility in liquid nitrogen, and then discuss the reported discontinuities in classical liquids.

Henson has plotted his nitrogen positive ion mobilities as a function of the electric field, and drawn a line connecting each experimental point (Henson 1964, Fig 15), our Fig 16. The result is a series of constant mobility levels, with changes to a new level at fields which have no simple relationship.

The change in mobility between levels decreases with increasing field. His zero field mobility is $\sim 2.5 \times 10^{-3}$ cm^2/volt sec.

We have analysed his results according to equation (1) and find values for c_1 and c_2 given in Table 1 (taking $\mu_r = 7.10^{-4}$ cm^2/volt sec). The value for c_1 is slightly greater than ours, as would be expected by his velocity measurement method; a pulse of ions in one direction only would give no reduction in the liquid motion, and higher source fields would tend to increase the liquid motion.

The much larger value of c_2 is because Henson works with currents of the order 10^{-10} amps while our currents are of the order 10^{-12} amps. The theory gives $c_2 \propto I$, which gives a rough agreement quantitatively (to a factor of about 5) and does suggest the increase in c_2 with current as observed. We therefore suggest that the overall field dependence of the mobility measured by Henson may be explained by liquid motion, in the same way as our results.

The results by Bruschi et al (1970) for the positive ion mobility in liquid nitrogen (under 1.8 atmosphere pressure) have been fitted to the theory, taking their overall field dependence from their fig 1. We take their mobility values to be our μ_c, when the value of c_1 is immediately obtained (Table 1), being the slope of the curve. The value of c_2 then depends on the value used for μ_r; in Table 1 we show the value of c_2 taking μ_r as 7×10^{-4} cm^2/volt sec (as with Henson), which is our result, and

also the value of μ_r taking c_2 as $1.7.10^3$ (which is our result, and expected to be the same for Bruschi, as the currents used and the cell geometries were similar to ours). This latter value of μ_r is in good agreement with the results quoted by Bruschi, for their low field values, but means that liquid motion gives a negative contribution to the mobility at high fields. Also shown in Table 1 is a value for μ_r for $c_2 = 4.10^3$, which agrees with the high field mobility values. The small value of c_1 is taken to mean that liquid motion has less effect in their cell; the variation of c_2 and μ_r is probably not significant because of the crudeness of the fit of their data to the theory and also because of an unknown pressure dependence in the ion mobility.

Bruschi et al reported mobility discontinuities in four classical liquids, with critical velocities that were reproducible to within 5%, except for nitrogen, where v_c varied from .8 cm/sec to 1.3 cm/sec. They do not report the size of the discontinuities, but extrapolating from their Figs 1 and 2, we get $\Delta\mu \sim 4.10^{-5}$ cm^2/volt sec for both liquid N_2 and C Cl_4, while $\frac{\Delta\mu}{\mu} \sim 4\%$ for N_2 and $\sim$20% for C Cl_4.

Henson has reported several distinct mobility levels in HeI, without determining either a critical velocity, the range of field over which the mobility level was constant, or describing how he determined a level. His low field mobility for positive ions was $\sim 6.47 \times 10^{-2}$ cm^2/volt sec while that found by Bruschi et al

was $3.5 \cdot 10^{-2}$ cm^2/volt sec. Henson used the same velocity measuring technique as in liquid nitrogen.

The discrepancy between the low field mobility results in HeI implies that Hensons measuring technique is causing liquid motion, similar to that in liquid nitrogen. The field needed to reach the first critical velocity is 5 kv/cm from Bruschi's results. Henson worked at field strength up to 7 kv/cm, so his results must either have been taken from separate runs; i.e. each run showed a constant mobility, which differed from run to run, or his mobility levels occurred for critical velocities much less than Bruschi's et al. Without knowing the field dependence of his mobility levels we cannot analyse his results for evidence of liquid motion. However he does report that his measuring technique could give as many as three different times of flight for a given applied field, with no criteria for which one he analysed.

Bruschi et al state that the presence of liquid motion can be seen as a dependence of the mobility on the current density, and as a continuous decrease of the mobility with electric field; they did not test for this, but worked at low current densities to avoid the effect. As their current densities were the same order as ours, we consider it likely that their results are affected by liquid motion.

Once the liquid is set into motion in a measuring cell, the resulting flow pattern could take a long time to decay, or to change

to another flow pattern. This would give a scatter in the measured mobility values; if the measurements are always taken in a systematic fashion (say for increasing field) then the appearance of discontinuities could occur in a regular way, due to the time taken between each individual measurement.

In any case, mobility discontinuities are intimately related to liquid motion. The ions reach an equilibrium drift velocity in an electric field in a fluid by losing momentum through scattering off the background fluid; the equilibrium velocity is given when the rate of momentum loss equals the force from the electric field. Thus the ions are transferring energy to the fluid. This energy is either dissipated through heating (through inelastic collisions) and thus depends on the thermal conductivity of the liquid, or the liquid gains the momentum lost by the ions (through elastic collisions) and depends on the viscosity of the liquid. If the liquid gains the momentum, there is a force exerted on the fluid in the direction of the ion motion; this gives a pressure gradient in the fluid as found and used in ion drag pumps (Stuetzer 1960), and thus an overall motion of the fluid in the direction of the ion motion. The magnitude of this motion will depend on the relative importance of the elastic and inelastic scattering probabilities, and the degree of correlation in the direction of the elastic collisions. A mobility discontinuity is due to an increased interaction with the fluid i.e. an increase in the rate of loss of

momentum by the ion, which is gained by the liquid. Both processes depend on the mechanism for energy and momentum transfer, which in turn depends on the ion velocity and thus the electric field. Using classical kinetic theory to analyse the ion mobility does not take into account the full interaction with background fluid, except through a collision cross section. Henson has explained his mobility levels by changing the cross section by discrete amounts, which suggests that a full analysis which considers the background fluid would be fruitful.

APPENDIX I

For an ion of mass M, with a dispersion relationship $E = \frac{P^2}{2M}$, to create an excitation with energy ε and momentum p, we get by considering conservation of energy and momentum

$$P = P' + p$$

$$E = E' + \varepsilon$$

that $$\frac{P}{M} = \frac{\varepsilon}{p} + \frac{p}{2M}$$

Therefore the ion needs a minimum velocity v_c to create the excitation, given by

$$v_c = \frac{\partial E}{\partial P} = \frac{P}{M}$$

$$v_{ion} \geq v_c = \frac{\varepsilon}{p} + \frac{p}{2M} \qquad (1)$$

which is the Landau criterion for the formation of an excitation.

If the excitation is a vortex ring, then

$$\varepsilon = \frac{(n\kappa)^2 \rho R \eta}{2}$$

$$p = n\kappa\rho\pi R^2$$

for $n = 1$

$$v_{ion} \geq \frac{\kappa\eta}{2\pi R} + \frac{\kappa\rho\pi R^2}{2M}$$

This connects the velocity and mass of the ion with the size of the vortex ring produced.

For a given ion mass, there is a minimum value of v_{ion}, given by

$$\frac{\partial v_{ion}}{\partial R} = 0$$

i.e. $$(v_{ion})_{min} = \frac{3\kappa\eta}{4\pi} \left(\frac{2\pi^2\rho}{\eta M}\right)^{1/3} \qquad (2)$$

when a vortex ring of radius R is produced, where R is given by

$$R^3 = \frac{\eta M}{2\pi^2 \rho}$$

Taking the mass of the ion to be $\sim 100\ M_{He}$, we get

$$(v_{ion})_{min} \sim 100 \text{ m/sec}$$

For an ion of infinite mass, the Landau criterion equation (1) reduces to

$$(v_{ion})_{min} = \left(\frac{\varepsilon}{p}\right)_{min}$$

For an ion to produce a vortex ring at a velocity of 5.2 m/sec, it needs a mass given by equation (2) as

$$M_{ion} = 3.10^6\ M_{He}$$

APPENDIX II

For a roton dispersion relation

$$\varepsilon(p) = \Delta + \frac{(p - p_o)^2}{2m^*} \qquad (1)$$

we use Bose statistics for the number density, giving

$$N_r(0) = \frac{1}{h^3} \int (e^{\frac{\varepsilon(p)}{kT}} - 1)^{-1} \, d^3p$$

$$= \frac{4\pi}{h^3} \int_o^\infty p^2 (e^{\frac{\varepsilon(p)}{kT}} - 1)^{-1} \, dp \quad . \qquad (2)$$

Changing the frame of reference to one moving at velocity v_s to the superfluid the dispersion relationship is changed to

$$\varepsilon^*(p) = \Delta + \frac{(p - p_o)^2}{2m^*} + p.v_s \qquad (3)$$

giving

$$N_r(v_s) = \frac{1}{h^3} \int_o^\infty (e^{\frac{\varepsilon^*(p)}{kT}} - 1)^{-1} \, d^3p \quad . \qquad (4)$$

As we are only interested in the small region close to the roton minimum in the dispersion curve, we approximate equation (2) to

$$N_r(0) = \frac{4\pi p_o^2}{h^3} \int_o^\infty e^{-\frac{\varepsilon(p)}{kT}} \, dp$$

i.e.

$$N_r(0) = \frac{4\pi p_o^2}{h^3} \, e^{\frac{\Delta}{kT}} \int_o^\infty e^{-\frac{(p-p_o)^2}{2m^*kT}} \, dp$$

The integral is evaluated by letting

$$x^2 = \frac{(p - p_o)^2}{2m^*kT}$$

when

$$dx = \frac{dp}{(2m^* kT)^{\frac{1}{2}}}$$

thus
$$N_r(0) = \frac{4\pi p_o^2}{h^3} e^{-\frac{\Delta}{kT}} (2m^*kT)^{\frac{1}{2}} \int_0^\infty e^{-x^2} dx .$$

The integral equals $(\pi)^{\frac{1}{2}}$, so

$$N_r(0) = \frac{4\pi p_o^2}{h^3} (2\pi m^* kT)^{\frac{1}{2}} e^{-\frac{\Delta}{kT}} .$$

To evaluate equation (4), equation (3) must be written in the more general form

$$\varepsilon^*(p) = \Delta + \frac{(p - p_v)^2}{2m^*} - pv_s \cos\theta$$

and
$$d^3p = p^2 \, dp \sin\theta \, d\theta \, d\phi$$

so
$$N_r(v_s) = \frac{1}{h^3} \iiint_{\theta=0}^{\pi} (e^{\frac{\varepsilon^*(p)}{kT}} - 1)^{-1} p^2 \sin\theta \, dp d\theta d\phi .$$

This can be approximated as before to

$$N_r(v_s) = \frac{1}{h^3} \iiint e^{-\frac{\varepsilon^*(p)}{kT}} p^2 \sin\theta \, dp d\theta d\phi$$

$$= \frac{1}{h^3} \iint e^{-\left(\Delta + \frac{(p-p_o)^2}{2m^*}\right)/kT} \left(\int_0^\pi e^{-pv\cos\theta} \sin\theta \, d\theta\right) x \, dp d\phi ,$$

We evaluate the last integral by letting

$$x = \frac{pv\cos\theta}{kT}$$

so
$$dx = -\frac{pv\sin\theta}{kT}$$

and the limits of integration are changed to

$$\theta = 0, \quad x = \frac{pv}{kT}$$

$$\theta = \pi , \quad x = -\frac{pv}{kT}$$

thus

$$\int_0^{\pi} e^{-pv\cos\theta}\sin\theta\,d\theta = -\frac{kT}{pv}\int_{\frac{pv}{kT}}^{-\frac{pv}{kT}} e^{-x}\,dx$$

$$= \frac{kT}{pv}\left(e^{\frac{pv}{kT}} - e^{-\frac{pv}{kT}}\right)$$

$$= 2\sinh\left(\frac{pv}{kT}\right) \Big/ \frac{pv}{kT}$$

If we make the approximation that we are only interested in values of p near p_o, we get

$$N_r(v_s) = \frac{4\pi}{h^3}\cdot\frac{kT}{p_o v}\cdot\sinh\left(\frac{p_o v}{kT}\right)\int p^2\, e^{\frac{-\left(\Delta + \frac{(p-p_o)^2}{2m^*}\right)}{kT}}\,dp$$

$$= \frac{\sinh\left(\frac{p_o v}{kT}\right)}{\left(\frac{p_o v}{kT}\right)}\cdot\frac{4\pi}{h^3}\int p^2\, e^{\frac{-\left(\Delta + \frac{(p-p_o)^2}{2m^*}\right)}{kT}}\,dp$$

$$= \frac{\sinh\left(\frac{p_o v}{kT}\right)}{\left(\frac{p_o v}{kT}\right)}\cdot N_r(0)$$

Thus

$$\frac{N_r(0)}{N_r(v_s)} = \frac{\frac{p_o v_s}{kT}}{\sinh\left(\frac{p_o v_s}{kT}\right)}$$

As we have used the same approximations in calculating $N_r(0)$ and $N_r(v_s)$ we expect the ratio to be a good estimate when the expression for $N_r(0)$ is valid.

The shape of the velocity field curve is then given by

$$\mu(v_D) = \frac{v_D}{E} = \frac{\mu_o C v}{\sinh Cv}$$

i.e. $v_D = \frac{1}{C} \sinh^{-1} (E\mu_o C)$

where $C = \frac{\beta p_o}{kT}$ and $v_s = \beta v_D$

APPENDIX III

Vortex ring motion

The equilibrium motion of a charged vortex ring in an electric field E is described by

$$eE = \alpha(T)\ (\eta - \tfrac{1}{4})$$

where $\alpha(T)$ is the frictional force on a vortex ring (Rayfield and Reif 1964).

Using the classical relationships

$$R = \frac{\kappa}{4\pi v}\ (\eta - \tfrac{1}{4})$$

$$\eta = \ln \frac{8R}{a_o}$$

where R is the vortex ring radius moving at velocity v with circulation κ, and a_o is the size of the vortex core, we get

$$eE = \alpha(T)\ \{\ln(\frac{2\kappa eE}{a.\pi v\alpha(T)}) - \tfrac{1}{4}\}$$

putting $$\frac{eE}{\alpha(T)} = x$$

then $$v = \frac{2\kappa}{\pi a_o e^{\frac{1}{4}}} .xe^{-x} \qquad (1) \quad \text{for } x > x_{min}$$

$$= 5.2 \times 10^4\ xe^{-x}$$

the value of x_{min} is the critical field E_c to form a vortex ring; this may be estimated from the Huang and Olinto stability criterion

$$eE_c = \alpha(T)\ (\eta - \tfrac{1}{4} - \ln(1 - \frac{v}{v_o}))$$

giving $$\frac{eE_c}{\alpha(T)} = 6.5$$

This is the result used when discussing the high field D.C. characteristics in Chapter 5.

Vortex ring decay

Imagine a charged vortex ring to enter a region with zero electric field. The only force acting on the ring will be the frictional force due to quasiparticle collisions $\alpha(T)$.

$$\therefore \quad F = \alpha(T)\ (\eta - \tfrac{1}{4}) = \frac{dP}{dt}$$

where P is the impulse of the ring, given by

$$P = \kappa\rho\pi R^2$$

using
$$v = \frac{\kappa}{4\pi R}\ (\eta - \tfrac{1}{4})$$

$$\varepsilon = \tfrac{1}{2}\kappa^2\rho R(\eta - \frac{7}{4})$$

we get
$$\varepsilon = \frac{\kappa^{3/2}\rho^{\frac{1}{2}}}{2\pi^{\frac{1}{2}}} \cdot P^{\frac{1}{2}} \cdot (\eta - \frac{7}{4})$$

and

$$v = \frac{\kappa^{3/2}\rho^{\frac{1}{2}}}{4\pi^{\frac{1}{2}}} \cdot P^{-\frac{1}{2}} \cdot (\eta - \tfrac{1}{4}) = A\,P^{-\frac{1}{2}}$$

The distance s travelled by the ring, while losing energy and therefore growing smaller and faster, is given by

$$\begin{aligned} s &= \int v\,dt \\ &= \int A\,P^{-\frac{1}{2}}dt \\ &= \int_{P_1}^{P_2} A\,P^{-\frac{1}{2}}\,\frac{dP}{F} \\ &= \frac{2A^2}{F}\left(\frac{1}{v_1} - \frac{1}{v_o}\right) \\ &= \frac{\kappa^3\rho(\eta - \frac{1}{4})}{8\pi\ \alpha(T)}\left(\frac{1}{v_1} - \frac{1}{v_o}\right) \qquad (2) \end{aligned}$$

where v_1 is the original ring velocity, and v_o the velocity when the ring disappears.

The time taken while travelling this distance is given by

$$\frac{dv}{dt} = F\frac{dv}{dP} = \frac{8\pi v^3 \alpha(T)}{\kappa^3 \eta\rho}$$

hence $$t = \frac{\kappa^3\rho(\eta - \frac{1}{4})}{16\pi\,\alpha(T)} \cdot \left(\frac{1}{v_1^2} - \frac{1}{v_o^2}\right) \qquad (3)$$

If $v_o >> v_1$, we get $s = 2v_1 t$

i.e. the average velocity of a vortex ring decaying is twice its original velocity $\bar{v} = 2v_1$

For the distance travelled by a vortex ring while decaying in zero field, assuming $v_o >> v_1$

$$s = \frac{\kappa^3\rho(\eta - \frac{1}{4})}{8\pi\,\alpha(T)} \cdot \frac{1}{v_1}$$

$$\simeq \frac{1}{6v_1} \text{ cms at } 1^\circ K$$

v_1 is given by equation (1)

$$v_1 = \frac{2\kappa}{\pi a_o e^{\frac{1}{4}}} \, xe^{-x} \quad \text{where } x = \frac{eE}{\alpha(T)}$$

$$s = \frac{\kappa^2\rho a_o(\eta - \frac{1}{4})e^{\frac{1}{4}}}{16\,\alpha(T)} \cdot \frac{e^x}{x}$$

$$= 3.10^{-6}\,\frac{e^x}{x} \text{ cms.}$$

SUMMARY

We were unable to obtain a convincing result that showed a mobility discontinuity reported by other authors, in either superfluid helium or liquid nitrogen.

In helium, we obtained an expression that described the dependence of the ion drift velocity on the electric field up to the vortex ring creation velocity. This expression results from the modification of the quasiparticle excitation spectrum (in particular the roton part for our temperature range around 1°K) due to the superfluid velocity flow around the ion increasing the local roton number density close to the ion surface, giving an increased rate of loss of ion momentum to the fluid.

We explained our mobility results in liquid nitrogen by suggesting that the liquid is set in motion, with a velocity in the direction of the ion motion; the dependence on the electric field was fitted to a theory by Kopylov.

We do not take our results as showing that mobility discontinuities do not exist; but do suggest that the time constants involved in liquid motion may cause the experimental results to show a kind of hysteresis. The concept of 'metastability' invoked by Careri to explain why he did not sometimes observe a discontinuity should instead be used to say that only when the liquid state changes from one macroscopic flow pattern to another will a

discontinuity be observed. This idea obviously predicts that the phenomenon will depend on the dimensions of the cell in which the ion velocity is being measured.

Our D.C. results showed that the effect of a grid on the ion beam can be explained in terms of a field dependent transmission coefficient for the grid, independent of the ion velocity (for bare ions). The transmission coefficient depends only on the grid structure, and the potentials on the other electrodes in the cell. This means we would not expect the D.C. characteristic to show any behaviour related to a mobility discontinuity (as in Fig 4.1).

The effect of the grid on a beam of charged vortex rings is complex, and depends on the interaction between the grid wires and the vortex rings, and the ions and vorticity. We explain our negative ion results by the grid capturing vortex rings, and this vorticity capturing other ions. A repelling field is set up around the grid wires which decreases the current captured by the grid. This gives the negative ion current peak. The vorticity around the grid grows for increasing ~~the~~ size of the incident vortex rings, until this vorticity can propagate throughout the rest of the cell.

The fast ion current suggests that the interaction between an excited negative ion bubble and a piece of elementary quantized vorticity forms an entity that can be accelerated to the Landau critical velocity. We use this charge carrier to explain why the photo ejection experiments of Sanders et al could measure a current.

FIGURES

Chapter 2

Fig 2.1	Drift velocity versus E

Chapter 3

Fig 3.1	Square wave generator
3.2	D.C. Biases
3.3	Diode Bridge
3.4	Nitrogen square wave generator
3.5	Block diagram circuit
3.6	Cryostat
3.7	Ion Cell

Chapter 4

Fig 4.1	'Square wave effect' (Bruschi et al)
4.2	Temperature dependence of v_c (Bruschi et al)
4.3	Ion mobilities (Schwartz)
4.4	Triode pulse waveforms (Square wave between S and G)
4.5	Triode pulse waveforms (Square wave between G and C)
4.6	I - f curves showing two lines
4.7	Variation of I - f curves with E_{SG}
4.8	I - f curves showing saturation of I_o
4.9	I - f curves around the vortex ring formation field
4.10-4.17	Mobility versus drift velocity
4.18-4.22	$\Delta\mu$ versus drift velocity
4.23	$\Delta\mu$ versus drift velocity showing possible discontinuity

Chapter 5

Fig 5.1-5.5	Field distortion due to grid mesh
5.6-5.8	Triode D.C. characteristics
5.9-5.10	Tetrode D.C. characteristics
5.11	I_T and I_G for -ve ions in tetrode
5.12	I_c
5.13	Transmission coefficient
5.14	$\ln I_G$

5.15 $\ln I_T$

5.16 $\frac{I}{I_{1\,max}}$ versus $\frac{E}{E_{1\,max}}$ triode

5.17 $\frac{I}{I_{1\,max}}$ versus $\frac{E}{E_{1\,max}}$

5.18 Temperature dependence of current peak

5.19 E_{max} versus $\frac{1}{T}$

5.20 E_{max} versus P

5.21 I_{max} versus T

5.22 $\frac{\Delta}{k}$ versus P

5.23 I_{max} versus E_{max}

5.24 Characteristic for varying extracting field

5.25 E_{min}/E_{max} versus $E_{G_2 c}$

5.26 $\frac{I - I_{1\,min}}{I_{max} - I_{1\,min}}$ versus $\frac{E - E_{1\,min}}{E_{max} - E_{1\,min}}$

5.27 Current noise

5.28 Second sound attenuation coefficient as a function of electric field (Bruschi et al)

5.29 I-f curves showing fast ion current

5.30 Drift velocity versus field, for fast and normal ions.

5.31 Effect of light on D.C. characteristics

Chapter 6

Fig 6.1 D.C. Triode

6.2 D.C. Triode

6.3 D.C. Multiple grid

6.4 Typcial I-f curve

6.5 Schematic I-f curve

6.6 I_∞ and I_o versus E. Run B

6.7 I_{DC} and 2 x I_o versus E

6.8 I_∞^{DC} and I_o versus E Run E

6.9 μ_∞^o and μ^o versus E Run B

6.10 μ_o^o and μ_r^r versus E Run E

6.11 μ_o versus E. Five runs
6.12 μ_r versus E. Five runs
6.13 $\overline{\mu_o}$ and $\overline{\mu_r}$ versus E
6.14 $(\mu_o - \mu_r)$ versus E Five runs
6.15 v_e and μ_e versus E
6.16 Ion mobilities measured by Henson

REFERENCES

K.R. Atkins (1959) Phys. Rev. 116, 1339
Liquid Helium, C.U.P.

G.K. Batchelor (1953) Homogeneous Turbulence, C.U.P.

D.F. Brewer and D.O. Edwards (1961) Phil. Mag.6, 1173

L. Bruschi, B. Maraviglia and P. Mazzoldi (1966) Phys. Rev. 143,84

L. Bruschi, P. Mazzoldi and M. Santini (1968) Phys. Rev. 167, 203

L. Bruschi, G. Mazzi and M. Santini (1970) Phys. Rev. Lett. 25, 330

B. Burdick (1965) Phys. Rev. Lett. 14, 11

C. Di Castro (1966) Nuovo Cimento 42B, 251

G. Careri, S. Cunsolo and P. Mazzoldi (1964) Phys. Rev. 136, A303

G. Careri, S. Cunsolo and M. Vincentini-Missoni (1964)
Phys. Rev. 136, A311

C.E. Chase (1966) Superfluid Helium Ed. J.F. Allen, Academic Press

G.V. Chester, R. Metz and L. Reatto (1968) Phys. Rev. 175, 275

J. Cope (1966) Ph.D. Thesis, unpublished.

J. Cope and P.W.F. Gribbon (1970) J. Phys.(C) 3, 460

S. Cunsolo (1961) Nuovo Cimento 21, 76

S. Cunsolo and P. Mazzoldi (1961) Nuovo Cimento 20, 949

S. Cunsolo and B. Maraviglia (1968) LT 11 1, 265

S. Cunsolo, B. Maraviglia, and M.V. Ricci (1968) Phys. Rev. Lett. 26A,
605

A.J. Dahm and T.M. Sanders (1965) Phys. Rev. Lett. 17, 126

T.H. Dey and T.J. Lewis (1968) Brit. J. App. Phys. (2) 1, 1019

C.S.M. Doake and P.W.F. Gribbon (1969) Phys. Rev. Lett. 30A, 251

R.J. Donnelly (1967) Experimental Superfluidity (University of Chicago Press)

R.J. Donnelly and P.H. Roberts (1969) Phys. Rev. Lett. 23, 1419

R.L. Douglass (1968) Phys. Rev. 174, 255

W. Beall Fowler and D.L. Dexter (1968) Phys. Rev. 176, 337

G. Gamota (1970) Journal de Physique; colloquium on liquid helium, Grenoble

D.L. Goodstein, V. Buontempo and M. Cerdonio (1968) Phys. Rev. 171, 181

W.I. Glaberson, D.M. Strayer and R.J. Donnelly (1968) Phys. Rev. Lett. 21, 1740

E. Gray and T.J. Lewis (1965) Brit. J. Appl. Phys. 16, 1049
(1969) Brit. J. Appl. Phys. (2) 2, 93

H.E. Hall and W.F. Vinen (1956) Proc. Roy. Soc. A238 204; A238 215

B.L. Henson (1964) Phys. Rev. 135, A1002
(1970) Phys. Rev. Lett. 24, 1327

K. Hiroike, N.R. Kestner, S.A. Rice and J. Jortner (1965) J. Chem. Phys. 43, 2625

K. Huang and A.C. Olinto (1965) Phys. Rev. 139, A1441

A. Januszajtis (1963) Acta Phys. Polon 24, 809

B.K. Jones (1969) Phys. Rev. 186, 168

J. Jortner, N.R. Kestner, S.A. Rice and M.H. Cohen (1965) J. Chem. Phys. 43, 2614

G.N. Kopylov (1964) Soviet Phys -Tech Phys. 8, 962

C.G. Kuper (1961) Proc. Intern. School of Physics Liquid Helium Ed. G. Careri, 414.

J.L. Levine and T.M. Sanders (1967) Phys. Rev. 154, 138

* P.L. Richards and P.W. Anderson (1965) Phys. Rev. Lett. 14, 540.

C.C. Lin (1963) Proc. Intern. School of Physics, Course XXI Ed. G. Careri

L. Meyer and F. Reif (1961) Phys. Rev. 123, 727

L. Meyer, H.T. Davis, S.A. Rice and R.J. Donnelly (1962) Phys. Rev. 126, 1927

T. Miyakawa and D.L. Dexter (1970) Phys. Rev. A1, 513

J.A. Northby and T.M. Sanders (1967) Phys. Rev. Lett. 18, 1184

B.R. Pamplin (1970) Contemp. Phys. 11, 1

A.B. Pippard (1963) Phil. Mag. 8, 161

L. Prandtl (1952) Fluid Dynamics

G.W. Rayfield and F. Reif (1964) Phys. Rev. 136, A1194

G.W. Rayfield (1968) Phys. Rev. 168, 222

F. Reif and C. Meyer (1960) Phys. Rev. 119, 1164

* K.W. Schwarz (1968) Phys. Rev. 165, 323
(1970) Phys. Rev. Lett. 24, 648

P.E. Secker and T.J. Lewis (1965) Brit. J. Appl. Phys. 16, 1649

W. Shockley (1954) Bell Syst. Tech. J. 33, 799

D.M. Sitton and E. Moss (1969) Phys. Rev. Lett. 23, 1090

R.W. Smith (1962) Phys. Rev. Lett. 9, 87

W.T. Sommer (1964) Phys. Rev. Lett. 12, 271

B.E. Springett (1967) Phys. Rev. 155, 139

O.M. Stuetzer (1960) J. Appl. Phys. 31, 136

C.M. Surko and F. Reif (1968) Phys. Rev. 175, 229

D.W. Swan (1960) Proc. Phys. Soc. 76, 36

E.H. Takken (1970) Phys. Rev. A1, 1220

D.J. Tanner (1966) Phys. Rev. 152, 121

A.M. Tyndall and C.F. Powell (1930) Proc. Roy. Soc. 129, 162

J.L. Verster (1963) Philips Rev. Rep. 18, 465

W.F. Vinen (1957) Proc. Roy. Soc. A240, 114; A240 128, A242, 493; A243, 400
(1960) Proc. Roy. Soc. 255, 218

G. Wannier (1953) Bell Syst. Tech. J. 32, 170

J. Wilks (1967) Prop. of Liquid and Solid Helium O.U.P.

M.A. Woolf and G.W. Rayfield (1965) Phys. Rev. Lett. 15, 235

C. Zipfel and T.M. Sanders (1968) LT 11 1, 296